

Hardware design, optimization and fabrication for a portable medical device to monitor chronic kidney disease

By

Anh Tran Tam Pham

*Thesis
Submitted to Flinders University
for the degree of Doctor of Philosophy*

Doctor of Philosophy

College of Science and Engineering

26/10/2023

CONTENTS

CONTENTS	I
ABSTRACT	VI
ABBREVIATION	VIII
DECLARATION	XI
ACKNOWLEDGEMENTS	XII
LIST OF FIGURES	XIV
LIST OF TABLES	XXII
PUBLICATIONS AND AWARDS RELATED TO THIS THESIS	XXIII
PUBLICATIONS	XXIII
AWARD.....	XXIII
FINANCIAL ACKNOWLEDGEMENT	XXIV
CHAPTER 1. INTRODUCTION	1
1.1. CHRONIC KIDNEY DISEASE BACKGROUND	1
1.2. CLINICAL CKD MONITORING METHODS	2
1.3. PRINCIPLE OF DEVELOPING POC DEVICES TO DETECT BIOMARKERS IN DISEASE MONITORING.....	4
1.4. THE METHODOLOGY AND THE RESEARCH QUESTION.....	6
1.4.1. <i>The methodology</i>	6
1.4.2. <i>The research questions</i>	9
1.5. THE THESIS OUTLINE	9
REFERENCE.....	10
CHAPTER 2. BACKGROUND INFORMATION AND LITERATURE REVIEW	15
2.1. BACKGROUND INFORMATION ON POC DEVICE DEVELOPMENT IN CKD MONITORING.....	15
2.1.1. <i>Consumable development strategy in POC devices</i>	15
2.1.2. <i>Hardware development strategy in POC device</i>	22
2.1.3. <i>Software development strategy in POC device</i>	27

2.2.	THE REVIEW OF FLUORESCENCE ANALYSING METHOD FOR PORTABLE DEVICE DEVELOPMENT	28
2.2.1.	<i>Fluorescence analysing method for portable biomarker monitoring system – Non-portable device development</i>	29
2.2.2.	<i>Portable fluorescence-detecting device development</i>	30
2.2.3.	<i>Conclusion</i>	36
2.3.	THE REVIEW OF COLORIMETRY MEASURING METHOD FOR PORTABLE DEVICE DEVELOPMENT.....	36
2.3.1.	<i>The portable colorimetry device development</i>	36
2.3.2.	<i>Conclusion</i>	41
2.4.	THE RESEARCH GAP STATEMENT.....	41
	REFERENCE.....	42

CHAPTER 3. ALBUMIN DEVICE – THE OPEN PLATFORM FOR FLUORESCENCE

MEASUREMENT	48	
3.1.	INTRODUCTION.....	48
3.2.	PRINCIPLE OF FLUORESCENCE MONITORING PORTABLE DEVICE DEVELOPMENT.....	49
3.3.	COMPONENT DESIGN, SELECTION, AND OPTIMISATION	50
3.3.1.	<i>Solution cuvette selection – The container of the fluorescent target</i>	50
3.3.2.	<i>Light sources selection, design, and evaluation</i>	50
3.3.3.	<i>Luminescent sensor selection and evaluation</i>	53
3.4.	PLATFORM FABRICATION.....	55
3.4.1.	<i>The fluorescence principal platform</i>	55
3.4.2.	<i>Microcontroller unit, data storage and display</i>	58
3.5.	THE PRE-TEST OF THE PROTOTYPE ON MEASURING ALBUMIN IN THE ARTIFICIAL URINE SAMPLE... 58	
3.5.1.	<i>Idea of confirming the open platform's performance</i>	58
3.5.2.	<i>Evaluation of the flexibility of the open-platform in measuring fluorescence to monitor biomarker in body fluids</i>	59
3.6.	CONCLUSION	61

3.7. SUPPORTING INFORMATION FOR FLUORESCENCE MONITORING DEVICE DEVELOPMENT.....	61
3.7.1. <i>The platform designing information</i>	61
3.7.2. <i>The structure of the AIE probes: TPE-4TA and TC426</i>	63
REFERENCE.....	65

CHAPTER 4. DEVELOPMENT OF THE SAMPLES USED IN THE RE-REFERENCING AND CALIBRATION PROCESS IN THE FLUORESCENCE OPEN PLATFORM 70

4.1. THE RE-PRODUCING PRINCIPLE OF THE FLUORESCENCE OPEN PLATFORM	70
4.2. THE DECISIONS OF THE CALIBRATION AND REFERENCING SAMPLE DEVELOPMENT PROCESSES....	71
4.2.1. <i>Calibration sample</i>	71
4.2.2. <i>Reference sample</i>	73
4.2.3. <i>Conclusion</i>	91
4.3. THE STABILITY OF THE REFERENCE SAMPLES DURING THE EXPERIMENT’S PERIOD.....	91
4.4. CONCLUSION	94
REFERENCE.....	94

CHAPTER 5. CREATININE DEVICE – THE PORTABLE MICROPLATE READER 96

5.1. INTRODUCTION.....	96
5.2. DEVICE DESIGN, WORKING MECHANISM AND POST-PROCESSING ALGORITHM.....	98
5.2.1. <i>Device Design and Fabrication</i>	98
5.2.2. <i>Reagent Kits and Reaction Mechanism</i>	101
5.3. IMAGE PROCESSING ALGORITHM	102
5.3.1. <i>Alignment</i>	102
5.3.2. <i>Calibration</i>	103
5.3.3. <i>Segmentation and Intensity Measurement</i>	103
5.3.4. <i>Measurement</i>	104
5.4. EVALUATION OF THE DEVELOPED PROTOTYPE ON MEASURING CREATININE IN THE ARTIFICIAL URINE SAMPLE IN COMPARED WITH A COMMERCIAL MICROPLATE READER	106

5.4.1. <i>The commercial microplate reader</i>	106
5.4.2. <i>Sample preparation for the test</i>	107
5.4.3. <i>Result and discussion</i>	108
5.4.4. <i>Conclusion</i>	109
5.5. SUPPORTING INFORMATION FOR COLORIMETRY MONITORING DEVICE DEVELOPMENT	109
REFERENCE.....	115
CHAPTER 6. CLINICAL RESULT EVALUATION	119
6.1. PRINCIPLE OF THE CLINICAL EVALUATION.....	119
6.2. ALBUMIN RESULTS IN REAL URINE SAMPLES FROM PATIENTS HAVING KIDNEY-RELATED DISEASES.....	120
6.2.1. <i>Experiment setup</i>	120
6.2.2. <i>Result discussion</i>	120
6.2.3. <i>Conclusion for the fluorescence platform to estimate albumin concentration in the urine sample</i>	124
6.3. CREATININE MEASUREMENT IN REAL URINE SAMPLES FROM PATIENTS HAVING KIDNEY-RELATED DISEASES.....	125
6.3.1. <i>Experiment setup</i>	125
6.3.2. <i>Result discussion</i>	125
6.3.3. <i>Dilution Factor on Creatinine Results</i>	128
6.3.4. <i>Conclusion for the creatinine device to measure creatinine concentration in the urine sample</i>	129
6.4. ALBUMIN-CREATININE RATIO RESULTS OBTAINED FROM THE ALBUMIN AND CREATININE CONCENTRATION MEASUREMENTS	129
6.4.1. <i>Experiment setup</i>	129
6.4.2. <i>Result evaluation</i>	130
6.4.3. <i>Conclusion for clinical evaluation on ACR measurement</i>	132
6.5. SUPPORTING INFORMATION FOR CLINICAL EVALUATION	132

6.5.1. <i>Clinical sample collection</i>	132
6.5.2. <i>Analysis of the fluorescent images</i>	132
6.5.3. <i>Clinical case study analysis</i>	134
REFERENCE.....	134
CHAPTER 7. CONCLUSION, DISCUSSION AND FUTURE DEVELOPMENT	137
7.1. DISCUSSION AND CONCLUSION	137
7.2. CONTRIBUTION TO THE KNOWLEDGE	139
7.3. PLANS FOR THE FUTURE WORK	141
7.3.1. <i>The over-ranged fluorescent intensity from urine samples containing albumin levels above 2000 mg/L</i>	141
7.3.2. <i>The lack of recognising reagent in high concentration albumin measurements</i>	141
7.3.3. <i>The effect of auto-fluorescence from the urine sample itself on the albumin measurement</i>	141
7.3.4. <i>The miss-matching in the creatinine results from the colorimetry device</i>	145
7.3.5. <i>The strategy for measuring ACR value on a single device</i>	145
REFERENCE.....	145

ABSTRACT

The research in this thesis addresses the important question of how to develop a point of care (POC) device that can efficiently and accurately measure urinary albumin and creatinine levels to facilitate the monitoring of chronic kidney disease. It provides a new approach to the integration of fluorescence and colorimetric measurements and presents a comprehensive set of parameters that should be considered in the hardware design and manufacture of an optical POC device. Typically, the development of a POC device requires the harmonization of consumables, hardware, and software. Therefore, although the research focus is on hardware development, the impact on consumables and software are also considered. In this study, strategic choices for those hardware parameters, including decisions about the excitation light source, calibration method, optical filter of the output sensor, and the self-processing module, are presented in a scheme that comprehensively combines all three components. This differs from previous studies that generally focus only on developing some parameters of a single component. This research proves the feasibility of the proposed approach by evaluating the developed devices' performance through clinical validation using real urine samples from patients with kidney-related diseases. The results demonstrate that the developed POC devices have comparable results with clinical measurements. Finally, the research presents the limitations of the current developed POC devices in measuring urine albumin and creatinine to give an indication of the CKD stage for the patients and suggests proposed solutions for future works to further improve the developed devices' performance and expand clinical applications.

This research has provided several contributions to knowledge in optical measurement and hardware design features. For optical measurement features, the research introduces a simple and affordable process to fabricate reference samples, which are made of epoxy resin and cost around AUD 15 cents per sample. These reference samples support the ratiometric method in the calibration and referencing processes, which minimises the error in fluorescence measurement between the expected and simulated values to below 2 % across different measurements over 10 months of urine sample testing. For hardware design features, the research has provided step-by-step instruction for developing a POC device, which performs fluorescence or colorimetry measurement to monitor the albumin and creatinine levels in a urine sample. Also, the developed devices, using the modular structure with the “plug-in and plug-out mechanism”, have proved their ability to examine solution tests for monitoring different biomarkers under various optical conditions, which follow fluorescence and colorimetric measurements. Moreover, the developed devices use the Raspberry Pi, a single computer module, to locally analyse the optical images and provide the albumin and creatinine results in real time, and to enable users to communicate with medical specialists for healthcare discussion or appropriate therapy decision making. The findings of this study can contribute to the development of more cost-effective and accurate POC devices for monitoring kidney-related

diseases, which can improve the diagnosis and management of these diseases in areas less served by clinical laboratories.

This thesis presents the development of two devices for running fluorescence and colorimetry measurements. The ability of both devices to perform the corresponding optical measurements have been confirmed. Their results measuring albumin and creatinine concentrations in artificial urine samples show a linear correlation with a commercial fluorescence spectrometer and a microplate reader, which are currently used in clinical laboratories. In the later stages of development, devices were clinically evaluated with tests for estimating albumin and creatinine concentrations on 88 urine samples from real patients having kidney related diseases. Both devices' testing results have been statistically analysed using paired samples t-test and have shown no significant difference when compared with those provided from SA Pathology. The fluorescence open platform can provide albumin results in real time, and 86 % of the urine samples containing albumin concentration below 300 mg/L were estimated to have CKD status indications in line with the clinical method. Meanwhile, the colorimetry device currently shows a linear correlation in estimating the creatinine level in the urine samples with the clinical method. Moreover, the research has proved that the re-dilution method will potentially improve the quality of creatinine level estimation from the urine samples with strong background colour. Finally, the research utilizes the albumin and creatinine values calculated from both devices to establish the albumin-to-creatinine-ratio (ACR), which is one of the important factors for monitoring CKD in pathology. The calculated ACR values show a linear relationship with the ones from SA Pathology. From the Bland Altman analysis for those ACR values, the difference between the proposed devices and SA Pathology has a mean of 0.631 mg/mmol, showing the potential for these devices to be compared with the clinical method in estimating the ACR values to support CKD monitoring.

ABBREVIATION

AKD – Acute kidney disease

CKD – Chronic kidney disease

WHO – World Health Organization

ICF – Intracellular fluid

GFR – Glomerular filtering rate

ECF – Extracellular fluid

POC – Point of care

HAS – Human serum albumin

ACR – Albumin-creatinine ratio

AIE – Aggregation-induced emission

UV – Ultra violet

LED – Light emitting diode

FMC – Flinders Medical Centre

LOD – Limit of detection

ELISA – Enzyme-linked immunosorbent assay

PSA – Prostate-specific antigen

HRP – Horseradish peroxidase

RGB – Red – Green – Blue

DPA – Pyridine-2,6-dicarboxylic acid

BSA – Bovine serum albumin

AA – Ascorbic acid

CMOS – Complementary metal–oxide–semiconductor

CCD – Charge-coupled device

TAE – Tetraarylethylene

Lox – L-Lactate oxidase

RDT – Rapid-diagnostic-test

TB – Tuberculosis

DPA – Dipicolinic acid

PDMS – Polydimethylsiloxane

HSL – Hue-saturation-luminance analysis

SPR – Surface plasmon resonance

SERS – Surface enhanced Raman spectroscopy

ASSURED – Affordable – Sensitive – Specific – User-friendly – Rapid and robust –
Equipment-free – Deliverable to end-users

PP – Polystyrol/polystyrene

PCB – Printed circuit board

PMT – Photomultiplier tube

MEMS – Micro-electro-mechanical systems

MA – Microalbuminuria

AU – Artificial urine

TPB – Tetraphenylbutadiene

TPE – Tetraphenylethylene

SiO₂ – Silicon Dioxide

TiO₂ – Titanium Dioxide

THF – Tetrahydrofuran

TF – Tint film

Ref – Reference

Pos – Position

96-WM – 96 well microplate

AST – Antimicrobial susceptibility testing

VZV – Varicella zoster virus

CMV – Cytomegalovirus

cTnI – Cardiac Troponin I

FOV – Field of view

PLA – Polylactic acid

OD – Optical density

SALHN – Southern Adelaide Local Health Network

HREC – Human research ethics committee

DECLARATION

I certify that this thesis does not incorporate without acknowledgment any material previously submitted for a degree or diploma in any university; and the research within will not be submitted for any other future degree or diploma without the permission of Flinders University; and that to the best of my knowledge and belief it does not contain any material previously published or written by another person except where due reference is made in the text.

Signed.....Tran Tam Anh Pham.....

Date.....29/05/2023.....

ACKNOWLEDGEMENTS

I am honoured to have the opportunity to express my heartfelt gratitude to everyone who has contributed to the completion of my Ph.D. dissertation.

First and foremost, I am deeply indebted to my primary supervisor, Professor Youhong Tang. I cannot express enough appreciation for the immense support, guidance, and encouragement that you have provided to me since my Master thesis until this final moment of the Ph.D. degree. Thank you for countlessly helping me as a professor, as a friend, and as a family member when I have difficulties in studying, living, and working. I am grateful for your understanding, sympathy, patience, and compassion, and for always making time for discussions. Without your mentorship, I would not have been able to reach this stage of my academic journey.

I would like to express my sincere gratitude to my co-supervisor, Professor Karen J. Reynolds, for her invaluable feedback and advice related to my research work and about being a researcher. Her support and guidance have helped me to improve the quality of my research and to gain a deeper understanding of the research process. I also appreciate the financial support that she provided for my stipend during my Ph.D. study.

I would like to acknowledge the Australia-China Science and Research Fund through the Joint Research Centre for Personal Health Technologies, Department of Industry, Science, Energy and Resources, Australian Government Research Training Program Scholarship for funding this project and supporting me the stipend during my study. I also appreciate Flinders University for providing me with the Tuition fee sponsorship, HDR conferences support, the Industrial Mentoring Network In STEM, and the support for me to access to the necessary resources. Part of my Ph.D. research cooperated with SA Pathology at Flinders Medical Centre, and their clinical support is greatly acknowledged.

I extend my gratitude to Dr. Damian Tohl for supporting me in operating the experiments, data analysis and proofreading my writing thesis draft. I have learned a great deal from his critical thinking, research note-taking, and MATLAB programming. You have saved my days in innumerable times. Thank you very much for your dedicated supports.

I would like to thank Dr. Angus Wallace, Ms. Xinyi Zhang, Mr. Hao Fu and Dr. Thanh Hoang Hai for their invaluable feedback related to my research, and for their support and encouragement throughout my Ph.D. journey. I also would like to express my gratitude to Dr. Joerg Boeselt, Mr. Clarence Chuah, Mr. Yunzhong Wang, Mr. Hu Qi, Mrs. Carolyn Ramsey, and Mrs. Zita Pelling for their technical and administrative support in the course of my research. Also, a special thanks to Associate Professor Yuning Hong and Professor Sheng Xie for their generous donation of HSA specified bio probes for this study.

To Mr. Thang Toan Nguyen, my brother-like friend. Thank you so much for sharing the games, the movies, the exploring trips, the drinks and foods, the physical-build-up challenges, the stories of your life and the time being with me. You are a fantastic friend.

A special thanks to my friends, but not limited, Mrs. Thy Mai Truong, Mrs. Huong Giang Le Vo, Mr. Trung Huy Giap, Ms. Huong Ngoc Thu Do, Mr. Tung Duc Do, Mr. Hai Ky Ho, Dr. Huyen Thi Thuong Nguyen, Mr. Tu Thien Than, Mr. Khang Hoang Nguyen, and Mr. Nguyen Cong Dinh, and those who had been with me during this challenging period, for giving me support, advice, and encouragement throughout this challenging period.

I would like to thank Mr. Anthony John Cramp for professional editing services sought out for the writing included in this thesis.

Last but not least, I would like to deliver my deepest appreciation for the never-ending support from all members of my family back home.

My wife – Thank you for trusting, loving, understanding and patient with me, for being with me when I am in difficult and discouraging times, as well as sharing joy and happiness with me. You have been my motivation to complete this degree, and to improve myself to be a better me. Thank you for being you.

My sister – I really don't know how I can overcome this challenging period without you by my side. Although you still have your own issues and problems, you always appear in the critical times of my life. Your support is invaluable. Thank you for bringing me supplies during those long days and nights in front of the computer. Thank you for always listening to my talks, even most of them are silly and nonsense, and making me laugh when I'm having a hard time. Thank you for reminding me that I have capacity when I feel like I don't. Thank you for being my sister.

My uncle Hung – If it weren't you taking care of my mom at home, I wouldn't have been able to focus on my studies. I cannot remind how many times I can regain my confidence thanks to the experiences I have obtained when living with you in Vietnam. Many of my current skills have been learnt from you, including the calmness and sympathy. Thank you very much for being one of my biggest tutors in my life.

Mum – You are everything for me. Thank you for your constant love and support me for all of my decisions. Thank you for making sure I took breaks and looked after myself. Thank you for always encouraging me and being my biggest tutor. Thank you for everything.

LIST OF FIGURES

Figure 1.1. Water distribution in body's organs and two categories of body fluids. (A) Water distribution varies across different parts of the body, the brain and kidneys contain 80–85 % water while teeth have only 8–10 %. (B) Body fluids consists of Intracellular Fluid (ICF), the fluid inside the cells, and Extracellular Fluid (ECF) being plasma, the fluid component of the blood; and interstitial fluid, the fluid surrounding cells and not comprising blood [12]..... 3

Figure 1.2. The flowchart for monitoring a biomarker in body fluids. When the biomarker (1) in body fluids reacts with the recognising agent(s) (3) following a specific method (2), the reaction will produce an output signal, which may be optical or electrical. By defining the type of output signal (4), we can develop the suitable component to collect that signal (5) and establish the appropriate software to analyse its characteristics (6). Finally, measuring the output signal will help the researcher to monitor the level of the corresponding biomarkers in the biological sample..... 5

Figure 1.3. The general structure of a portable biomarker monitoring device..... 5

Figure 2.1. Traditional schematic of the lateral flow assay [16]. 17

Figure 2.2. The customized microfluidic-based paper strip using AIE probe OPD-TPE-Py-2CN to detect gaseous phosgene; The pictures are taken under the 365 nm UV exposure. A) The schematic illustration of the customized test strip. The paper strip is embedded with the developed AIEgen OPD-TPE-Py-2CN. Without the presence of phosgene, the test strip stays non-fluorescent under the 365 nm UV excitation. With the increase of phosgene's concentration, the fluorescence intensity rises dramatically. B) The variation of fluorescence intensity yielded from the OPD-TPE-Py-2CN loaded test strip when reacting with different phosgene's concentrations [17]..... 18

Figure 2.3. The results of prostate cancer detection using the HRP substrate [ABTS (2,2'-Azinobis [3-ethylbenzothiazoline-6-sulfonic acid]-diammonium salt) to track the presence of prostate-specific antigen (PSA) in serum, A) the negative sample (No PSA) wherein the HRP substrate stays red, and B) the positive result (PSA presence) where the HRP substrate develops a green colour [20]..... 19

Figure 2.4. The response of TPE-4TA to HSA in a urine sample. A) The cuvette contains the mixture of the urine sample and the AIEgen TPE-4TA. There is a critical difference in the mixture's luminescence under the excitation conditions, in that, the solution without UV excitation will stay non-emissive (left cuvette) and turn to fluorescent (right cuvette) under the exposure of 360 nm UV. The fluorescence intensity emitted from the mixture varies proportionally with HSA concentration. B) The fluorescence intensity is proportional to HSA concentration in the range of 0 – 400 ng/mL [9]. 21

Figure 2.5. The schematic for ascorbic acid detection using a colorimetric assay with TMB-

MnO₂ reagent. In the reaction, the serum is injected into the Quartz cuvette, which was located inside the device for measuring. MnO₂ was added to the serum sample, followed by the addition of TMB and HCl to shift the solution's colour from red to blue and yellow, respectively [23]...... 22

Figure 2.6. The hardware components of the optical POC device. (A) The sketched structure for the fluorescence measuring POC device. The light source generates the specific wavelength light to excite the mixture of recognising reagent and biological sample in a controlled ratio. If the target molecule exists in the sample, the mixture will emit fluorescence when exposed to the excitation light. The light isolated environment, i.e., a dark room like section, is a sealed space where the fluorescence transfers from the mixed solution to the imaging sensor. This minimises optical noise from the external environment when taking measurements. The imaging component captures the fluorescent signal. This signal is analysed for fluorescent intensity by the software component. (B) The sketched structure for the colorimetry measuring POC device. The white light source shines on the mixture of recognising reagent and biological sample. If the target molecule exists in the sample, the mixture will develop the responding colour. The colour variation will be captured by the imaging component, then be analysed by the software component. 23

Figure 2.7. The overview of two prototypes using different power supplies for excitation light source: Using 2 AAA battery (A, B, C, D) and using smartphone's battery (E, F, G, H); and the image processing in the built-in software on the smartphone (I). (A) and (B) The front and rear views of the 2-AAA-battery prototype. (C) The sketch of the assembled prototype. (D) General structure for the 2-AAA-battery prototype. (E) and (F) The front and rear views of the smartphone-power-supply prototype. (G) The dimensions and the sketch of the assembled prototype. (H) The general structure of the smartphone's battery supply prototype. (I) The algorithm for the reflection imaging process. (1) The raw fluorescent image is taken by the CMOS camera of the smartphone Samsung Galaxy S2. (2) The raw image is generated as a pixel matrix of 3-channel YUV420 scale. (3, 4, 5) The pixel matrix is converted into grayscale to locate the fluorescent areas of the control and test lines on the RDT strip. (6, 7) The segmentations of the test and control lines are differentiated from the environmental areas. (8) The location of the control line will be checked to estimate whether the measurement is valid. If the test is correct, the test line's colour intensity will be analysed to indicate the positive or negative result [38]. 31

Figure 2.8. (A), (B), (C) The overviews of the solid support attached to the Samsung Galaxy SII and the resulting interface of the analysing app. (D) The structure of the prototype. From the top-left to the bottom-right: The laser diode was powered by 2 AA batteries, with an emitting wavelength at 532 nm. Fluorescent tubes were custom developed to have dimensions of 6 × 2 × 15 mm and were arranged in line with the laser beam so that the laser beam would shine through the test tube (S) first, then the transmission laser beam would excite the control tube (C). The fluorescent emission was captured by the smartphone camera arranged perpendicular to the laser beam. The Tube

Holder was for holding the tubes. Filter, tray and lens were for collecting the fluorescent emission and filtering out the reflected excitation light from the laser source. The laser cooler managed the laser source temperature. The cover was fabricated in filament by 3D printing to secure the positioning of all components, as well as preventing unwanted external light. The batteries used were 2 AA batteries, which could be replaced after usage. The base was the connector between the albumin tester and the smartphone. (E) The resulting images taken from different albumin concentrations: 0, 10, 25, 50, 100, 200 $\mu\text{g}/\text{mL}$. C is the control image and S is the testing sample image. and (F) The resulting screenshot from the app for normal, high, extremely high, and the weekly summary report of the albumin test on the same subject [39]. 33

Figure 2.9. (a) Overview of the test running on the smartphone, the urine test strip and the reference colour chart with 7 greyscale regions and 5 colour regions from blue to red. (b) The correlation between the actual pH value and the pH value measured by the design [48]. 37

Figure 2.10. (A) 100 μL of a urine sample was loaded onto the microfluidic chip ELISA, which was equipped with specific antibodies to detect the presence of biomarker HE4. (B) The smartphone Sony Ericson i790 was used to capture the colour-shifting in the solution. (C) The customized app on the smartphone analysed the picture to generate the red pixel values. Finally, it presented the quantitative HE4 concentration [49]. 37

Figure 2.11. (a) There is a space at the back of the device which can store 6 test strips. Users take out these strips for testing. (b) Users then apply the sweat sample from the forehead or the saliva sample from the tongue onto the paper strip. (c) The strip is then inserted into the prototype for analysis. (d) The app installed on the iPhone analyses the colorimetric measurement and presents the result on the screen. The figure is an example of the sodium pH level result. (e) The overview of the custom strip inserting into the device. The custom strip consists of 3 components: The PDMS diffuser uniformly distributes the flash-light of the phone's camera to the paper strip and the calibration region; the testing paper strip contains Hydrion Spectral pH indicator for sweat testing (ranging from 5.0 to 9.0) or saliva testing (ranging from 1.0 to 14.0), and the known-colour-value plastic piece is used for calibrating the variations from cameras or testing environment's conditions and (f) The cross-section view of the A-B from the left figure [50]. 38

Figure 3.1. Block structure of a general fluorescence monitoring device. Block B1: Test solution – The target of detection. Block B2: The input requirements for the fluorescence monitoring system design. Block B3: The output of the fluorescence monitoring system design. 49

Figure 3.2. (A) The output intensity of three types of LED sources in different testing conditions of beam angles and distances. The LED 1's output has the higher intensity in compared with that of LED 2 and LED 3, respectively. In the distance of 20 mm, the LED 1 also provides a homogenous luminance. Its output starts dropping dramatically from the distance over 30 cm. (B)

The relative output intensities of 3 types of LED sources are tested by using an optical camera to take 42 images of each LED source's operation in 40 minutes. The desired output is the fluorescence light, so the output of the LEDs is observed based on their effect on the reference testing sample, which comprises of albuminuria [400 mg/L] and a fluorescence dye. (C) The illustration of (left) the intensity degradation from a typical LED and (right) the homogeneous intensity compensation of the LED pattern..... 52

Figure 3.3. The sensitive response of the Raspberry Pi Camera v2.0 in terms of the red, green, and blue colours. (From the manufacturer's datasheet). 54

Figure 3.4. (A) Arrangement diagram of the excitation light source, the solution container, and the output imaging sensor. The incident excitation light and the emission fluorescence are in angle of 90 degrees, (B) The sketch of the optical monitoring device following the principle of fluorescence measuring, (C) The dark-room-like environment, (D) The structure of the developed fluorescence measuring platform: (1) Two LED modules; (2) The dark-room-like environment; (3) The Raspberry Pi Camera; (4) The testing solution cuvettes; (5) The Raspberry Pi module; (6) The Raspberry Pi touchscreen; and (7) The 3D printed solid supports and covers, and (E) The optical monitoring device in overview. 57

Figure 3.5. The results obtained by the fluorescence spectroscopy (the blue curves) and the developed open platform (the red curves) from the experiment using (A) TC426 and (B) TPE-4TA..... 60

Figure 3.6. The light source-cuvette holder. The 3D printed component is one base keeping the distance between the light source modules and the chemical cuvettes to be 20 mm. On the cuvettes' sides facing to the camera, there are two rectangular windows with dimensions of 5.5×14 mm, allowing the camera to only capture the fluorescence from the cuvette without collecting the reflecting excitation light from the light sources. These fluorescence windows are placed 18 mm apart from each other to minimize the optical interference. 62

Figure 3.7. (A) Sketches of chemical structures of TPE-4TA and TC426; (B) TC426 is non-emissive without HSA, and will emit a 550 nm fluorescence when binding with HSA under the excitation of 480 nm light; (C) TPE-4TA is non-emissive without HSA, and will emit a 470 nm fluorescence when binding with HSA under the excitation of 360 nm UV [42]. 64

Figure 4.1: The real shapes and colour of six calibration samples used for the commercial fluorescence spectrometer. The sample 4 is TPB, which reacts with the 348-nm UV to generate the 422-nm fluorescence and is chosen to be the standard sample for the developed fluorescence device..... 72

Figure 4.2. The thin quartz cuvette and the setup for measurement. (A) The thin quartz
xvii

cuvette with the light path of 1 mm; (B) The normal setup of the thin cuvette used to perform the fluorescence measurement on powder, an opaque material. The UV beam reaches the surface of the TPE powder in the thin cuvette, then emits fluorescence to every direction. Only the fluorescence coming to the camera placed at an angle of 90 degrees to the central UV beam will be measured and named the target fluorescence output. 74

Figure 4.3: The fluorescence signal from the TPE powder is over the detection range of the camera, causing the saturation in the obtained image. 76

Figure 4.4: The fluorescent results of SiO₂/TPE powder mixture obtained from the fluorescence spectrometer..... 78

Figure 4.5: The fluorescent images of powder mixtures of TiO₂ and TPE in different ratios (sample T1 to T5), and the fluorescent image of the pure TPE powder..... 80

Figure 4.6: The fluorescent intensities of the TiO₂/TPE powder mixtures compared with the pure TPE powder presented as Red-Green-Blue components..... 81

Figure 4.7: The fluorescent images taken in the developed fluorescence prototype of the epoxy resin Kinetix R246 samples containing 2 % and 6 % TPE powder in the thin-cuvette shape and the calibration sample. 82

Figure 4.8: The epoxy resin Kinetix R246 samples containing 2 % and 6 % of TPE powder in the thin-cuvette shape in different light conditions: room light, dark background in low room light, and dark background in the 365 nm UV light. The TPE powder was insoluble in epoxy resin, thus, the powder was unevenly distributed in the epoxy resin samples, causing the non uniform fluorescence at the output..... 83

Figure 4.9: The pure PDMS samples and the PDMS/TPE samples of Momentive RTV615 and NuSil MED-6015 in different optical conditions: The normal room light, the low room light with dark background and the 365-nm UV light with dark background..... 85

Figure 4.10: The fluorescence results of the PDMS/TPE samples, pure PDMS samples and the calibration sample obtained from the fluorescence spectrometer. The pure PDMS samples produced strong fluorescence, thus, the tint film (TF) layers were applied to reduce the fluorescence intensity and to get rid of the reflected UV light. 86

Figure 4.11: The set-up of the fluorescence measurement examining the PDMS/TPE samples with and without the tint film. Without the tint film, there will be potential UV light reflected to the camera at the same time with the fluorescent signal. The tint film is expected to filter out the reflected UV light from the sample cuvette, as well as reduces the visible light passing to the

camera..... 86

Figure 4.12: The fluorescence of the PDMS/TPE samples with the tint film applied to the surface of the cuvette measured in the fluorescence prototype. Both NuSil MED-6015 and Momentive RTV615 mixed with TPE produced fluorescence under the 370-nm UV excitation from the LEDs. Due to the high density of PDMS, the UV light dropped significantly when transferring through the PDMS samples (from left to right). Besides, due to the high viscosity, the TPE powder precipitated downward to the bottom of the PDMS cuvette, causing the high fluorescence at the bottom of the cuvette when compared with the top area. 87

Figure 4.13: The fluorescent signal of the square samples of Kinetix R246 epoxy and Barnes – Epoxycast Clear Casting Resin obtained from the fluorescence spectrometer. Both samples were examined at different wavelengths around the specific UV wavelength of 365 nm. The epoxy Kinetix R246 showed a peak fluorescence closest to the one of the albumin test solutions at 470 nm. 88

Figure 4.14: The fluorescent images of the square samples of Kinetix R246 epoxy and Barnes – Epoxycast Clear Casting Resin with 1 TF layer obtained from the fluorescence prototype. The UV light was absorbed and reduced significantly along the transferring path through the samples, whilst that light was uniform in the calibration sample. 89

Figure 4.15: The setting of the tint film and the thin epoxy sample in the fluorescence measurement in the developed prototype. (A) The thin epoxy was oriented to face the tint film side to the LED. The output had UV reflected from the surface of the tint film, but there was no fluorescence to the camera. (B) The thin epoxy was oriented to face the tint film side to the camera. The output had fluorescence with reduced intensity and no reflected UV..... 90

Figure 4.16: The thin Kinetix R246 sample. (A) The thin Kinetix R246 sample with two layers of tint film in the 3D printed holder. (B) The fluorescence images of the calibration sample, two thin R246 samples and two square R246 samples. 91

Figure 4.17. The fluorescent intensities of the calibration sample and the two referencing samples with error bar during 10 months of urine-test experiments. During the calibration and referencing process of the fluorescence measurement, the referencing samples (Ref1 and Ref2) were placed in different testing positions (Pos1 and Pos2) and the calibration sample was placed in position 2 (Pos2) for taking images at the same time as the tested urine solutions. All samples showed similar decreasing trends of fluorescence response through 10 months of testing. The error bars showed minimal variation of output fluorescence emitted from the individual sample in the measurements of different samples in the same day. 92

Figure 4.18. The variation between the fluorescent intensity and the average value of the corresponding data set of the references in different positions in the fluorescence platform and the

calibration sample during the testing period.	93
Figure 5.1. (A and B) The sketch of a 96-well microplate colorimetry prototype; and (C) a white 96-well microplate image taken by a Raspberry Pi camera in the proposed device (Dark squares are four reference points for image process).	100
Figure 5.2. The Raspberry Pi SONY IMX219 camera RGB sensitivity and the absorption wavelength of the creatinine and glucose.	104
Figure 5.3. The 96-well microplates with the example of creatinine solutions. (A) The sketch of the 96-WM with the standards in wells A(1–8) and the testing solution in other wells; (B) An image of the creatinine solutions taken by the Raspberry Pi camera in the proposed colorimetry device.....	108
Figure 5.4. The unknown testing samples (red dot) are illustrated in the graphs of the standards from (A and B) glucose and (C and D) creatinine commercial test reagents, operated by (A and C) a microplate reader and (B and D) the developed device.....	108
Figure 5.5. Possible progress pathways for the light coming to an optical semi-transparent substance.	110
Figure 5.6. An example of a calibrated test image with red coloured borders indicating the segmentation locations of the 96 wells.....	110
Figure 5.7. The RGB histograms and the detected RGB intensities for well A1 in Figure 5.6.....	111
Figure 5.8. The RGB histograms and the detected RGB intensities for well A6 in Figure 5.6.....	112
Figure 5.9. The flowchart of general steps of the measurement using commercial test reagents in the 96-WM with a microplate reader and the proposed colorimetry device.	112
Figure 5.10. The effect of the exponential fitting curve in calculating the high concentration of creatinine in urine sample. Two data pairs (C1-C2 and C3-C4) have 0.01 unit different in intensities, however, the variations in concentration are 4.0372 and 0.581 units respectively due to the high-range of concentration in the pair C1-C2.....	113
Figure 5.11. The picture of the real colorimetry device: (A) The outer view; and (B) The inner view with the 96 well microplate.....	114
Figure 6.1. (A) The correlation between albumin concentration measured from the open	

platform and the clinical analysis from 88 urine samples of kidney patients. Some representative samples outside the 95% confidence boundary in high albumin range are circled. (B) The saturation of the developed platform when measuring the samples containing the high albumin concentrations over 1600 mg/L, in that, those samples have one or both green and blue components exceeding 255..... 121

Figure 6.2. The saturated Red – Green – Blue components of the fluorescence images from the samples containing high albumin concentrations. 123

Figure 6.3. The correlation between the developed platform and the clinical method in examining 43 urine samples containing albumin concentrations below 300 mg/L. 124

Figure 6.4. Comparison of creatinine concentrations measured by device and obtained from SA Pathology for 88 urine samples. The biggest variation is in sample 49 (the 36th data from the graph), which has a strong intensity in the background colour. Standard deviation is for two replicate samples. 126

Figure 6.5. The effect of the exponential fitting curve in calculating the high concentration of creatinine in urine sample. Two data pairs (C1-C2 and C3-C4) have 0.01 unit difference in intensities, however, the variations in their concentration are 4.0372 and 0.581 units respectively due to the high-range of concentration in the pair C1-C2 in comparison with the lower range of C3-C4. 127

Figure 6.6. The correlation in ACR values between the developed devices and the SA Pathology when examining 43 urine samples containing albumin concentrations below 300 mg/L..... 130

Figure 6.7. The Bland-Altman plot analysis to examine the limits of agreement between the developed devices and the clinical method in determining ACR values for CKD monitoring. The difference in ACR values between the proposed devices and SA Pathology is plotted against the average values in the x-axis. The pink line represents the mean difference in ACR values between two techniques, and the dashed lines are ± 1.96 standard deviation (SD). 131

Figure 6.8. Determining the intensity value that corresponds to the highest frequency of occurrence..... 133

Figure 7.1. The effect of auto-fluorescence on image processing of some highlighted samples. Not only the fluorescence intensity in the blank image affects the albumin calculation, but the colour of the fluorescence also contributes to the variation in albumin results between the developed platform and the clinical measurement..... 144

LIST OF TABLES

Table 2.1. Several reported AIEgens using fluorescence evaluation in health applications.....	16
Table 2.2. Comparison characteristics of LED and laser diode for excitation source of portable device [27, 28].....	24
Table 2.3. Compare the pros and cons of CCD, CMOS cameras and photodiode.....	26
Table 2.4. Portable devices using fluorescence method to detect biomarkers in body fluids.....	34
Table 2.5. Portable devices using colorimetric method to detect biomarkers in body fluids.....	39
Table 3.1. Fluorescent probes excitation and emission peak wavelengths.	65
Table 4.1. Excitation and emission wavelengths of various compounds.	72
Table 4.2: The thin cuvette filled with TPE powder was placed in the spectrometer such that its surface made an angle with the UV excitation beam, then the fluorescence signal was measured on different days.	75
Table 4.3: The ratio of SiO ₂ /TPE and TiO ₂ /TPE in the powder samples. All mixed powders are poured into the thin cuvettes.	77
Table 4.4: The fluorescence images from the developed prototype. This table compares the fluorescent images between the mixture powders of SiO ₂ /TPE and the solution sample containing 400 mg/L albumin concentration.	78
Table 5.1: The prepared concentrations for glucose and creatinine samples, the results obtained from the SpectraMax iD5 microplate reader and the results obtained from the developed colorimetry device.....	115
Table 6.1. The effect of dilution factor on creatinine results with two samples measured for each dilution factor.....	128
Table 6.2. 6 samples are examined in further-dilution strategy.....	129

PUBLICATIONS AND AWARDS RELATED TO THIS THESIS

Publications

Parts of this thesis have been published in the following journal articles:

Pham, A. T. T.; Tohl, D.; Hu, Q.; Li, J.; Reynolds, K.J.; Tang, Y. (2022). *Portable colorimetric device with commercial microplates for quantitative detection of urine biomarkers: design, development, and clinical evaluation*. *Biosensors*, 12, 723, <https://doi.org/10.3390/bios12090723>

Pham, A. T. T.; Tohl, D.; Wallace, A.; Hu, Q.; Li, J.; Reynolds, K.J.; Tang, Y. (2022). *Developing a fluorescent sensing based portable medical open-platform - a case study for albuminuria measurement in chronic kidney disease screening and monitoring*. *Sensing and Bio-Sensing Research*, 100504, <https://doi.org/10.1016/j.sbsr.2022.100504>

Pham, A. T. T.; Wallace, A.; Zhang, X.; Tohl, D.; Fu, H.; Chuah, C.; Reynolds, K.J.; Ramsey, C.; Tang, Y. (2021). *Optical-Based Biosensors and Their Portable Healthcare Devices for Detecting and Monitoring Biomarkers in Body Fluids*. *Journal of Diagnostics*, vol. 11, 1285. <https://doi.org/10.3390/diagnostics11071285>

Pham, A.T.T. & Tang, Y. (2022). Point-of-care in vitro diagnostics devices based on aggregation-induced emission biosensors: current situation and future prospective (Chapter 5). In: *Applications in Biosensing, Bioimaging and Biomedicine, Vol. 1: Aggregation-Induced Emission*. Editors: Ben Zhong Tang and Xinggui Gu, Berlin, Boston: De Gruyter, pp. 83-110. <https://doi.org/10.1515/9783110672220-005>

Pham, A.T.T., Tohl, D., Li, J., Reynolds, K.J. & Tang, Y. (2022). Clinical Evaluation of a Portable Fluorescence Based Medical Device for Chronic Kidney Disease Monitoring, proceedings of the 2022 IEEE EMBS ISC Asia – Pacific conference, 26-28 September, Melbourne, Australia. **(Conference Paper)**.

Award

(2022) – 3rd place for the best post-graduate oral presentation in the 2022 IEEE EMBS ISC Asia – Pacific conference in Melbourne, Australia.

(2022) - 3rd place for the best post-graduate paper in the 2022 IEEE EMBS ISC Asia – Pacific conference in Melbourne, Australia.

Financial acknowledgement

The Tuition Fee Sponsorship for my Doctor of Philosophy degree program at Flinders University has been granted by the Deputy Vice-Chancellor (Research).

My Ph.D. was funded by Australia-China Science and Research Fund through the Joint Research Centre for Personal Health Technologies, Department of Industry, Science, Energy and Resources, Australian Government. (February 2020 – September 2022: AUD \$48,785).

The College of Science and Engineering 2022 HDR Conference Support to present my PhD research at the IEEE EMBS International Student Conference, Asia-Pacific 2022, to be held in Melbourne, Australia (2022: AUD \$500).

CHAPTER 1. INTRODUCTION

Most of this chapter has been published in the following journal paper and book chapter. Additional information has been provided below to satisfy the requirements of the thesis.

The journal article [1]: Pham, A.T.T.; Wallace, A.; Zhang, X.; Tohl, D.; Fu, H.; Chuah, C.; Reynolds, K.J.; Ramsey, C.; Tang, Y. (2021). Optical-Based Biosensors and Their Portable Healthcare Devices for Detecting and Monitoring Biomarkers in Body Fluids. *Diagnostics*, vol. 11, 1285. <https://doi.org/10.3390/diagnostics11071285>

The book chapter [2]: Pham, A.T.T. & Tang, Y. (2022). Point-of-care in vitro diagnostics devices based on aggregation-induced emission biosensors: current situation and future prospective (Chapter 5). In: *Applications in Biosensing, Bioimaging and Biomedicine, Vol. 1: Aggregation-Induced Emission*. Editors: Ben Zhong Tang and Xinggui Gu, Berlin, Boston: De Gruyter, pp. 83-110. <https://doi.org/10.1515/9783110672220-005>

This introductory chapter provides background information on chronic kidney disease (CKD), its burden on modern society, and the need for the development of a portable device to assist patients in monitoring their kidney health in a remote testing setting. Also presented is the proposed principle of developing a point of care (POC) device to detect biomarkers in body fluids to support disease monitoring.

1.1. Chronic kidney disease background

Kidneys are vital organs in the human body. Their three main functions are: to regulate water and balance chemicals in the bloodstream such as potassium, sodium, calcium, and acid content; to filter waste out of the bloodstream through urine; and, to generate significant hormones that contribute to blood pressure control and red blood cell production. When kidney dysfunction occurs, their ability to filter and balance chemicals is compromised, resulting in abnormal accumulations of chemicals and contaminants in the bloodstream or other organs. This causes systemic toxicity and has a significant impact on an individual's health. Thus, monitoring the kidneys' function requires serious attention.

Kidney related health issues are generally classified into two categories: (1) acute kidney disease (AKD) and (2) chronic kidney disease (CKD). AKD, also known as acute kidney failure, refers to the sudden decline in kidney functions caused by illness, medication, or injury. This type of disease typically lasts from 7 to 90 days and many patients can fully recover from AKD [3, 4]. Meanwhile, CKD is characterized by irreversible damage to the kidneys, resulting in a loss of healthy kidney function lasting for over three months. According to World Health Organization (WHO), CKD has long been known as a "silent killer", as medical symptoms only manifest in the later stages of

the disease when patients have already lost up to 90 % of their kidney function, leaving limited options for effective treatments [5]. For those having end-stage CKD, dialysis or kidney transplant are the inevitable treatments to support residual kidney function. The asymptomatic nature of CKD in its early stages has created a global burden of morbidity and mortality in modern society, affecting about 10 % of the population with kidney-related diseases and causing about 1.2 million deaths every year [6, 7]. According to the current trends, CKD is projected to become the 5th leading cause of death globally by 2040 [8].

For those having kidney disease related illnesses, annual costs for medical treatment vary significantly between the mildest and most severe stages of the disease [9]. In a review of the economic burden of CKD on society in 2022, the annual costs for one patient having the mildest hazardous CKD stage ranged from USD 4,626 to USD 16,924, while for a patient at the high end of the disease, costs increased to between USD 14,651 and USD 35,092 [9]. Although there is currently no cure for this deadly disease, the inevitable deterioration of kidney function can be reduced and may even be reversible if patients detect CKD symptoms in the early stages and apply effective treatments with medication, diet, and appropriate changes to their lifestyle. Therefore, monitoring the health of kidneys is essential catch and decrease in their functioning as early as possible.

1.2. Clinical CKD monitoring methods

In general, an effective method for detecting the early stage of diseases is to monitor the amount of specific biomarkers in body fluids [10]. The human body is mainly constructed with water, with the amount differing across age and gender. About 75 % of infant's body mass is water with this amount decreasing in adult males and females to between 50 and 60 %. The figure is around 45 % of an elderly person's body mass [11, 12]. In addition, water distribution varies in different parts of the body, depending on the biological functions of each organ, such as blood, urine, sweat, plasma, and synovial fluid. As such, these are generally known as body fluids [12].

Body fluids are differentiated into two categories: intracellular fluid (ICF) and extracellular fluid (ECF) [12]. ICF includes the fluids inside the cells, which are stable in volume and chemical content, whilst ECF consists of two parts: plasma, the fluid component of the blood; and interstitial fluid, the fluid surrounding cells and not comprising blood. These are strongly dependent of the body's metabolism and are changeable according to the current biological state of the body [12]. In health condition monitoring, scientists usually pay attention to changing values, thus ECF is considered the main target for detection in pathological monitoring. Hence, monitoring the body fluids means monitoring the ECF.

Body fluids, or biofluids, play an indispensable role, being the environment for metabolic activities as well as transporting nutrients around the body, so there is no doubt that they hold a large amount of biological information about the state of human health. Of the 26 common body fluids, the

most popular, due to their ease of collection, storage, and sampling processes, are serum, plasma, urine, saliva, and sweat [13]. In the chemical content of body fluids, biomarkers are the biological analytes contained in those fluids. Biomarkers have been considered to be one of the most important factors in disease monitoring for many years. They can be used to identify the specific diseases or health issues from patients, which helps clinical staff understand their patients' health conditions, as well as to pave the application of effective treatment strategies [5, 10, 14-18].

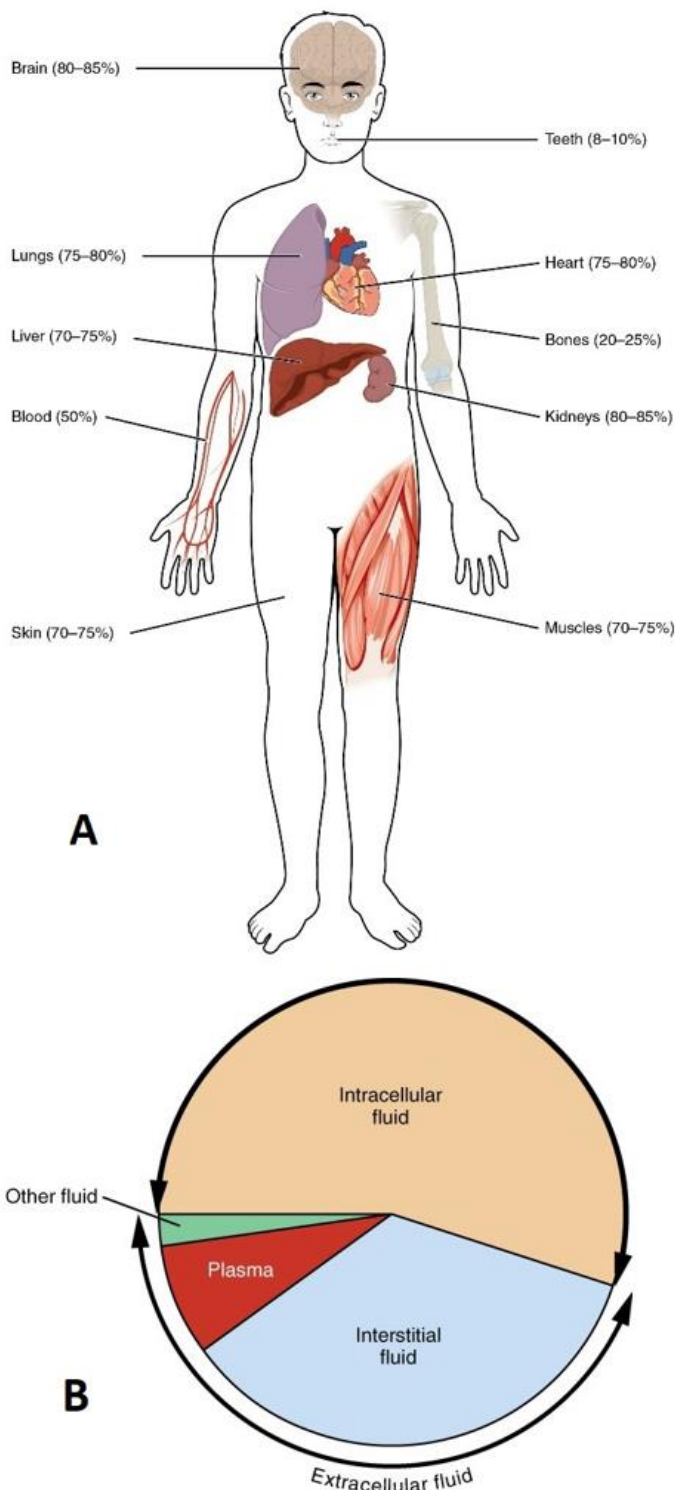


Figure 1.1. Water distribution in body's organs and two categories of body fluids. (A) The

water distributions in different parts of the body, in that, brain and kidneys are constructed by 80-85% of water while teeth have the least proportion of water, only 8-10%. (B) Body fluids are divided into two compartments: The Intracellular Fluid (ICF) includes the fluids inside the cells while the Extracellular Fluid (ECF) consists of two constituents: Plasma – the fluid component of the blood; and Interstitial fluid – the fluid surrounding cells and not comprising blood [12].

In clinical CKD monitoring, two common methods have been used for many decades: estimating overall renal function (glomerular filtration rate (GFR)) by observing the serum creatinine level in blood; and evaluating kidney filtering ability by measuring albuminuria and creatinine level in urine [5, 19, 20]. Both methods require a laboratory to perform the detection tests, leading to disadvantages of the possibility of infection, the ethical responsibility, and the longevity of the biological samples [21]. Therefore, this points to a need for creating on-site alternatives to laboratory testing to improve CKD monitoring activities. The principle of developing portable devices to detect and measure the presence of specific biomarkers in body fluids to give an indication of disease will be discussed in the next section.

1.3. Principle of developing POC devices to detect biomarkers in disease monitoring

Recently, the development of mobile technology has shifted CKD monitoring from traditional laboratory conditions to more user-friendly point-of-care (POC) devices [22]. POC devices help users to perform measurements outside the laboratory, which not only reduces the demand on regular visits to healthcare facilities but also minimises the potential spread of infection amongst a crowd of diseased individuals [23]. Although there are numerous reports on the development of POC systems for monitoring CKD, practical portable devices that can provide required testing accuracy, method compatibility, and resulting reliability, are limited. Therefore, this research focuses on developing a portable device to detect and monitor CKD levels.

The structure of the portable disease tracking device was designed following the biomarker monitoring mechanism, in that, the target biomarker reacts with a selective and specific recognising agent, producing an output signal, either optical or electrical. Then, this output signal will be captured and analysed to observe characteristics such as brightness or intensity, for an optical signal, or the voltage and current, for an electrical signal. The output signal is modelled to be proportional to the concentration of the biomarkers in the testing sample. Therefore, by tracking the output signal, we can compute the quantity of the target analytes. Hence, establishing a portable disease monitoring device is equivalent to developing a portable device that can monitor the identified output signal. For this purpose, a flowchart for detecting and monitoring the biomarkers in body fluids has been drafted

in Figure 1.2.

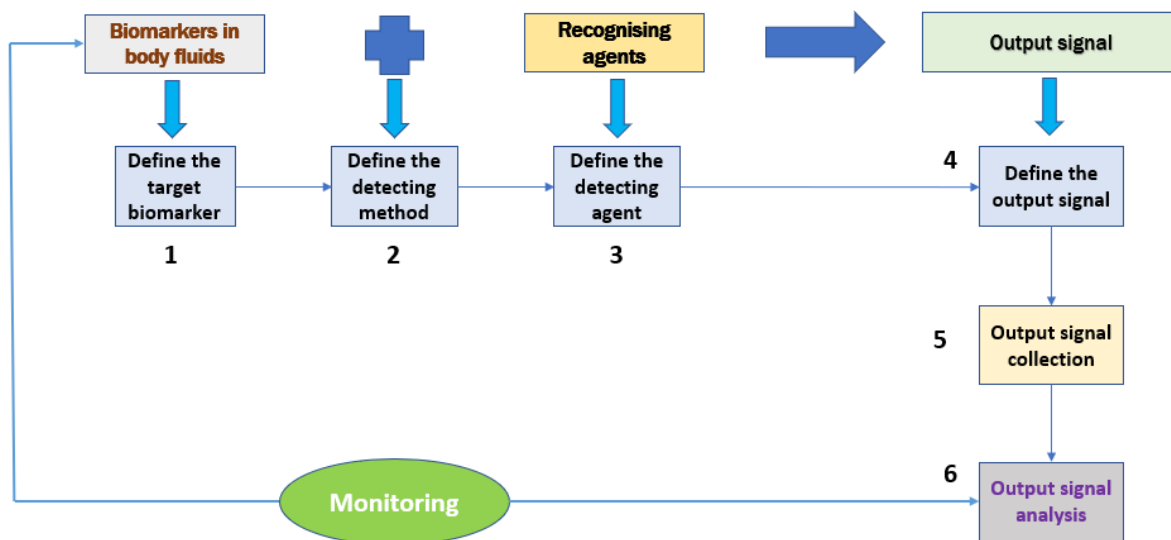


Figure 1.2. The flowchart for monitoring a biomarker in body fluids. When the biomarker (1) in body fluids reacts with the recognising agent(s) (3) following a specific method (2), the reaction will produce an output signal, which may be optical or electrical. By defining the type of output signal (4), we can develop the suitable component to collect that signal (5) and establish the appropriate software to analyse its characteristics (6). Finally, measuring the output signal will help the researcher to monitor the level of the corresponding biomarkers in the biological sample.

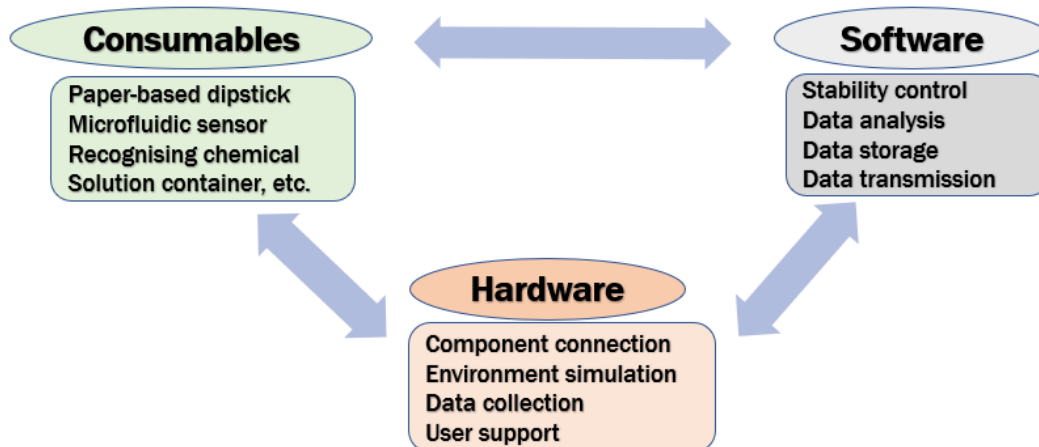


Figure 1.3. The general structure of a portable biomarker monitoring device.

Following the flowchart in Figure 1.2, the structure of the portable biomarker monitoring device can be summarised in three major parts: (1) the consumables; (2) the hardware, being the

electronics and solid supports; and (3) the software. These parts are shown in Figure 1.3. Although the three components are logically separate, each has a reciprocal relationship with others. The harmonious association among these three components is a key determinant of success or failure in medical device development. Thus, when investigating one component for the device development, the other two components require attention from the researcher.

1.4. The methodology and the research question

1.4.1. The methodology

This research focused on designing, developing, and fabricating the hardware of a portable CKD monitoring device. In Figure 1.3, the structure of the device is divided into three separate groups: consumables, hardware, and software. However, in the final device, no one group was more important than the others, and they shared a harmonious relationship such that a decision in one group affected choices made in the other groups. Therefore, although the research focus was on the hardware development, considerations were made for how the hardware development would affect the consumables and software and vice versa. In the flowchart shown in Figure 1.2, decisions 1 to 3 related to the consumables, decisions 4 and 5 related to the hardware and decision 6 related to the software. The first step in the development of this device was to define the suitable parameters for each of the decisions shown in Figure 1.2.

Currently, one of the attractive methods for detecting a biomarker is the electrochemical based analysis, which has been used in developing the POC medical devices for many years [24, 25]. Electrochemical based biosensors have shown several advantages in the measurements, such as good resolution, high sensitivity, quick response, easy operation, excellent repeatability, accuracy, and miniaturization [24]. Those biosensors monitor the specific analytes by converting the biological events to an electronic signal, which can be measured and analysed to present the level of the targeted analytes. However, the signal obtained from those measurements is dependent of many factors, such as the recognition reaction at the delicate electrolyte-electrode interface, the environment factors of temperature and moisture, the dynamic change of pH, flow rate and temperature of the body fluids, the cleanness of the electrode's surface in every measurement, and the signal amplification, which should be designed particularly for the specific measurement. These complex handling processes have limited the application of electrochemical biosensors in commercialized device development [25]. Therefore, there is a need to use another method for the signal detection process.

An efficient method for enhancing signal intensity for measurement is optical evaluation. Amongst POC devices, optical detection has become one of the most widely applied methods for identifying and monitoring biological molecules in body fluids. Optical measuring methods include

(1) colorimetric: colour changing of the final mixture, (2) chemiluminescent: a chemical reaction results in the mixture emitting photons; and (3) fluorescent/phosphorescent: activated molecules are excited by a specific wavelength of light, increasing their energy level such that when they return to their original energy levels, the excess energy is released in the form of photons, which creates fluorescence [22, 23, 26-36]. Their principles are based on the light response produced when the recognising agents react with the specific analytes during the chemical or biochemical reactions. The selection of suitable and effective measuring methods for CKD monitoring will lay a foundation for developing the POC device for this purpose.

As mentioned in the previous section, there are two methods for tracking CKD condition: examining creatinine level in the blood and measuring the concentration of albuminuria and creatinine in urine. Urinalysis is considered a preferred method due to it being non-invasive and simple to collect. For CKD monitoring, a urine sample will be tested to observe the biomarker levels in urine due to the kidneys losing their filtering function. The target biomarkers are albumin and creatinine, and two detecting methods are to assess the level of human serum albumin (HSA) in urine or estimate the albumin-creatinine ratio (ACR). In this research, the fluorescence measurement was employed for HSA estimation, and colorimetry was the preferred method for creatinine evaluation. Hence, the portable CKD monitoring device should be constructed using fluorescence and colorimetry measurements to monitor HSA and creatinine in the urine samples.

From the above discussion, steps 1 and 2 in the procedure (Figure 1.2) have been defined. After defining the target analytes and the testing methods, the next step is to find the suitable sensing chemicals for those detections (Figure 1.2 – step 3). However, defining the recognising reagents for each biomarker, HSA and creatinine, requires further research due to the different methods in monitoring them. As mentioned previously, there are two strategies to monitor CKD by assessing urine sample. The first strategy is to measure only the albumin level in a total urine sample from a patient in one day, in that, the patient will collect all of their urine for one day into a special container, provided by clinical staff. The other method is to estimate the ACR from a random urine sample of the patient in the day. From these two strategies, the first portable device was developed for monitoring only the albumin concentration in urine. The second portable device to detect the creatinine level in urine will be processed later. Following this plan, we can obtain the value for albumin, as well as the value for ACR, from one urine sample collection.

For the portable HSA monitoring device development, the efficient detecting method is fluorescence analysis. An aggregation induced emission (AIE) biosensor was employed for tracking albumin in the urine. An AIE probe is selective and sensitive in detecting albumin amongst other proteins in urine. The chosen recognising reagent was (TPE-4TA), one AIE probe, which has been published in the report of Tu and co-workers (2019) [37]. In principle, TPE-4TA will be mixed with the urine sample and be placed under the stimulation of an ultraviolet (UV) light of 365 nm. If albumin

molecules exist in the urine sample, the mixture will emit a fluorescent light with a peak wavelength varying around 485 nm. TPE-4TA shows a high linear response to varying levels of HSA concentration in urine in the clinical range for CKD tracking [37]. Measuring this fluorescence will potentially allow the calculation of a proper value for the amount of albumin in the urine sample. Hence, the recognising reagent (Figure 1.2 – step 3) for albumin detection employed was TPE-4TA, an AIE probe, and an output signal of 485 nm fluorescence (Figure 1.2 – step 4).

For the portable creatinine monitoring device development, colorimetry evaluation was used following Jaffe's principle, in that, the urine sample was mixed with an alkaline picrate medium [38]. The creatinine presence develops an orange colour with a peak at 520 nm wavelength [38]. The colour intensity will vary proportionally with the change in creatinine concentration in the urine sample. By observing this colour variation, the creatinine amount in the urine sample can be observed. Therefore, steps 3 and 4 in Figure 1.2 for creatinine detection have been determined.

In conclusion, after defining the four factors for the chemical reaction part of the HSA and creatinine monitoring, progress on the development of the portable device can be initiated, and this progress is planned across these six steps:

- **Step 1:** After defining the recognizing reagents for albumin and creatinine in the human urine sample, the selection of the excitation light source is the first component for consideration. The light source is required to provide light with a uniform distribution, stable luminance, and with enough intensity for the measurement. Besides, it should satisfy the device's requirements for portability and effective cost. Herein, the study used a set of light emitting diodes (LEDs) as the light source for the device.
- **Step 2:** The electronic components, such as the LEDs, have a degradation response during usage. Therefore, the study equipped a calibration process into the device to support the measurement evaluation.
- **Step 3:** Two analytes were measured using different methods: fluorescence and colorimetry. These methods have different mechanisms in their produced output signal as well as in how the output signal was collected. Thus, this study decided on a suitable optical sensor to capture the signal yielded from the measurements.
- **Step 4:** To protect the signal collection, an environment-controlled area was created to prevent light from the external environment affecting signal collection. This enhanced the optical parameters for the capturing sensor.
- **Step 5:** The complete device was assessed in a clinical setting. For clinical purposes, the study compared results obtained from the devices with the clinical instruments in the hospital's laboratory. The target organization for clinical evaluation was Flinders Medical Centre. The proposed plan for this evaluation was that the device should be able to monitor the albumin and creatinine values from the non-CKD patients and CKD patients.

The urine check-up method depended on the hospital's testing procedure.

- **Step 6:** The results obtained from all evaluations were summarized to provide a conclusion for the portable CKD monitoring device using albumin and creatinine measurements from the human urine samples. Then, the study discussed the achievements and the drawbacks of the device to suggest a proposed solution for further development.

1.4.2. The research questions

Throughout this report, there is the overall research question that needs to be answered: *“What are those parameters that need to be considered and integrated in the POC hardware design and manufacture for facilitating effective and accurate urine albumin and creatinine monitoring and how to manipulate them?”*

The overall question is divided into several sub-questions:

- What factors limit the feasibility of the portable device in monitoring urine albumin and creatinine in non-relating laboratory condition? How to overcome or mitigate them?
- What features are required in hardware for efficiently collecting the output optical signals in urine albumin and creatinine monitoring; and how to achieve them practically?
- How to maximise the performance of consumables (high sensitivity and selectivity urine albumin and creatinine bio-probes) in terms of sensitivities and accuracy in the hardware design? How can the hardware effectively integrate with the software?
- What are the parameters affecting cost-effective manufacturing and how to manage them?
- What are the environmental parameters and application scenarios for device utilization?

1.5. The thesis outline

The thesis comprises 7 chapters, organized as follows.

The main content of Chapter 1 and Chapter 2 was published in one journal paper [1] in 2021 and one book chapter [2] in 2022. The additional information and structure appearing in this thesis have been modified to satisfy the requirements of this thesis. Chapter 1 introduces the relevant background information about CKD, its burden on modern society, the need for development of a portable device to assist users in monitoring their kidney health function in remote testing settings. Chapter 1 also presents the proposed principle of developing a POC device to detect biomarkers in

body fluids to support disease monitoring.

Chapter 2 introduces the background information for POC device development using fluorescence and colorimetry measurements to monitor biomarkers in body fluids. Then it gives a summary of some existing reports in developing portable devices using fluorescence and colorimetry methods to monitor biomarkers in body fluids to give indications of potential diseases. Research gaps identified from this review are presented along with the research questions.

Content of Chapter 3 was published as a journal paper [39], but the clinical result section from this paper has been moved to Chapter 6 “The clinical result evaluation”. In Chapter 3, the evaluation of hardware selection is presented, followed by the evaluation of the albumin detecting performance by comparing its results with a commercial testing device.

Chapter 4 presents information on the referencing and calibration samples, which significantly contribute to the success of the albumin monitoring platform. The principle for developing the reference and calibration samples is introduced at first, followed by the development process of the reference samples. The chapter concludes with confirmation of the performance of the reference and calibration samples in fluorescence measurements by the developed platform.

Chapter 5 was published in the journal paper [40], but the clinical result section has been moved to Chapter 6 “The clinical result evaluation”. Chapter 5 presents hardware selection and fabrication of the colorimetry device. Its performance on creatinine measurement was evaluated by comparing its results with a commercial colorimetry testing device.

Chapter 6 presents the clinical evaluation progress. The developed devices were used to perform respective tests of urine samples from real kidney disease patients, and the obtained results were compared with clinical results provided by the Flinders Medical Centre.

The thesis concludes with Chapter 7 where the general summary, the contribution to knowledge, and potential future research is discussed.

Reference

1. Pham, A.T.T., Wallace, A., Zhang, X., Tohl, D., Fu, H., Chuah, C., Reynolds, K.J., Ramsey, C., and Tang, Y., *Optical-Based Biosensors and Their Portable Healthcare Devices for Detecting and Monitoring Biomarkers in Body Fluids*. *Diagnostics (Basel)*, 2021. **11**(7). DOI: 10.3390/diagnostics11071285.
2. Pham, A.T.T. and Tang, Y., *Chapter 5 Point-of-care in vitro diagnostics devices based on aggregation-induced emission biosensors: current situation and future prospective*, in *Aggregation-Induced Emission*. 2022. pp. 83-110. DOI: 10.1515/9783110672220-005.

3. Makris, K. and Spanou, L., *Acute Kidney Injury - Definition, Pathophysiology and Clinical Phenotypes*. Clin Biochem Rev., 2016. **37**(2): pp. 85-98.
4. Gameiro, J., Fonseca, J.A., Outerelo, C., and Lopes, J.A., *Acute Kidney Injury: From Diagnosis to Prevention and Treatment Strategies*. J Clin Med, 2020. **9**(6). DOI: 10.3390/jcm9061704.
5. Couser, W.G., Remuzzi, G., Mendis, S., and Tonelli, M., *The contribution of chronic kidney disease to the global burden of major noncommunicable diseases*. Kidney Int, 2011. **80**: pp. 1258-1270. DOI: 10.1038/ki.2011.368.
6. Bikbov, B., et al., *Global, regional, and national burden of chronic kidney disease, 1990–2017: a systematic analysis for the Global Burden of Disease Study 2017*. Lancet, 2020. **395**(10225): pp. 709-733. DOI: 10.1016/s0140-6736(20)30045-3.
7. Xie, Y., Bowe, B., Mokdad, A.H., Xian, H., Yan, Y., Li, T., Maddukuri, G., Tsai, C.Y., Floyd, T., and Al-Aly, Z., *Analysis of the Global Burden of Disease study highlights the global, regional, and national trends of chronic kidney disease epidemiology from 1990 to 2016*. Kidney Int, 2018. **94**(3): pp. 567-581. DOI: 10.1016/j.kint.2018.04.011.
8. Foreman, K.J., et al., *Forecasting life expectancy, years of life lost, and all-cause and cause-specific mortality for 250 causes of death: reference and alternative scenarios for 2016-40 for 195 countries and territories*. Lancet, 2018. **392**(10159): pp. 2052-2090. DOI: 10.1016/S0140-6736(18)31694-5.
9. Mullins, C.D., Pantalone, K.M., Betts, K.A., Song, J., Wu, A., Chen, Y., Kong, S.X., and Singh, R., *CKD Progression and Economic Burden in Individuals With CKD Associated With Type 2 Diabetes*. Kidney Med., 2022. **4**(11). DOI: 10.1016/j.xkme.2022.100532.
10. Su, S.B., Poon, T.C., and Thongboonkerd, V., *Human body fluid*. Biomed Res Int, 2013. **2013**. DOI: 10.1155/2013/918793.
11. Bhave, G. and Neilson, E.G., *Body fluid dynamics: back to the future*. J Am Soc Nephrol, 2011. **22**(12): pp. 2166-2181. DOI: 10.1681/ASN.2011080865.
12. Biga, L.M., Dawson, S., Harwell, A., Hopkins, R., Kaufmann, J., LeMaster, M., Matern, P., Morrison-Graham, K., Quick, D., and Runyeon, J., *Chapter 26 - Fluid, electrolyte, and acid-base balance*, in *Anatomy & Physiology*. 2013, Oregon State University. pp. 2833-2913.
13. De Bock, M., De Seny, D., Meuwis, M.A., Chapelle, J.P., Louis, E., Malaise, M., Merville, M.P., and Fillet, M., *Challenges for biomarker discovery in body fluids using SELDI-TOF-MS*. J. Biomed. Biotechnol, 2010. **2010**. DOI: 10.1155/2010/906082.

14. Ridley, J.W., *Introduction to the Study of Body Fluids*, in *Fundamentals of the Study of Urine and Body Fluids*. 2018, Springer, Cham. pp. 1-7. DOI: doi:10.1007/978-3-319-78417-5_1.
15. Du, J., Gu, Q., Chen, J., Fan, J., and Peng, X., *A novel fluorescent probe for the ratiometric recognition of protein based on intramolecular charge transfer*. *Sens. Actuators B: Chem.*, 2018. **265**: pp. 204-210. DOI: 10.1016/j.snb.2018.02.176.
16. Zhang, X., Yao, B., Hu, Q., Hong, Y., Wallace, A., Reynolds, K., Ramsey, C., Maeder, A., Reed, R., and Tang, Y., *Detection of biomarkers in body fluids using bioprobes based on aggregation-induced emission fluorogens*. *Mater. Chem. Front.*, 2020. **4**: pp. 2548-2570. DOI: 10.1039/D0QM00376J.
17. Abramovitz, M. and Leyland-Jones, B., *A systems approach to clinical oncology: Focus on breast cancer*. *Proteome Sci*, 2006. **4**(5): pp. 1-15. DOI: 10.1186/1477-5956-4-5.
18. Gbinigie, O., Price, C.P., Heneghan, C., Van Den Bruel, A., and Plüddemann, A., *Creatinine point-of-care testing for detection and monitoring of chronic kidney disease: Primary care diagnostic technology update*. *Br. J. Gen. Pract.*, 2015. **65**: pp. 608-609. DOI: 10.3399/bjgp15X687613.
19. Levey, A.S., Becker, C., and Inker, L.A., *Glomerular filtration rate and albuminuria. Systematic Review*. *JAMA.*, 2015. **313**: pp. 837-846. DOI: 10.1001/jama.2015.0602.Glomerular.
20. Vassalotti, J.A., Centor, R., Turner, B.J., Greer, R.C., Choi, M., and Sequist, T.D., *Practical Approach to Detection and Management of Chronic Kidney Disease for the Primary Care Clinician*. *Am. J. Med.*, 2016. **129**(2): pp. 153-162. DOI: 10.1016/j.amjmed.2015.08.025.
21. Mayeux, R., *Biomarkers: Potential Uses and Limitations*. *NeuroRx.*, 2004. **1**: pp. 182-188. DOI: 10.1602/neurorx.1.2.182.
22. Sanjay, S.T., Fu, G., Dou, M., Xu, F., Liu, R., Qi, H., and Li, X., *Biomarker detection for disease diagnosis using cost-effective microfluidic platforms*. *Analyst.*, 2015. **140**: pp. 7062-7081. DOI: 10.1039/c5an00780a.
23. Senf, B., Yeo, W.H., and Kim, J.H., *Recent Advances in Portable Biosensors for Biomarker Detection in Body Fluids*. *Biosensors (Basel)*. 2020. **10**(9): pp. 1-23. DOI: 10.3390/BIOS10090127.
24. Son, M.H., Park, S.W., Sagong, H.Y., and Jung, Y.K., *Recent Advances in Electrochemical and Optical Biosensors for Cancer Biomarker Detection*. *BioChip Journal*, 2022. **17**(1): pp. 44-67. DOI: 10.1007/s13206-022-00089-6.

25. Wu, J., Liu, H., Chen, W., Ma, B., and Ju, H., *Device integration of electrochemical biosensors*. Nat Rev Bioeng., 2023. **1**(5): pp. 346-360. DOI: 10.1038/s44222-023-00032-w.
26. Dincer, C., Bruch, R., Kling, A., Dittrich, S., and Urban, G.A., *Multiplexed Point-of-Care Testing – xPOCT*. Trends Biotechnol., 2017. **35**: pp. 728-742. DOI: 10.1016/j.tibtech.2017.03.013.
27. Gao, Z., Xu, M., Lu, M., Chen, G., and Tang, D., *Urchin-like (gold core)@(platinum shell) nanohybrids: A highly efficient peroxidase-mimetic system for in situ amplified colorimetric immunoassay*. Biosens. Bioelectron., 2015. **70**: pp. 194-201. DOI: 10.1016/j.bios.2015.03.039.
28. John, A.S. and Price, C.P., *Existing and Emerging Technologies for Point-of-Care Testing*. Clin. Biochem. Rev., 2014. **35**(3): pp. 155-167.
29. Li, J., Li, S., and Yang, C.F., *Electrochemical Biosensors for Cancer Biomarker Detection*. Electroanalysis, 2012. **24**: pp. 2213-2229. DOI: 10.1002/elan.201200447.
30. Liu, Y., Deng, C., Tang, L., Qin, A., Hu, R., Sun, J.Z., and Tang, B.Z., *Specific detection of D-glucose by a tetraphenylethene-based fluorescent sensor*. J. Am. Chem. Soc., 2011. **133**(4): pp. 660-663. DOI: 10.1021/ja107086y.
31. Mejía-Salazar, J.R., Cruz, K.R., Vásques, E.M.M., and Novais de Oliveira, O., *Microfluidic point-of-care devices: New trends and future prospects for ehealth diagnostics*. Sensors (Basel). 2020. **20**: pp. 1-19. DOI: 10.3390/s20071951.
32. Nimse, S.B., Sonawane, M.D., Song, K.S., and Kim, T., *Biomarker detection technologies and future directions*. Analyst, 2016. **141**(3): pp. 740-755. DOI: 10.1039/c5an01790d.
33. Tagit, O. and Hildebrandt, N., *Fluorescence Sensing of Circulating Diagnostic Biomarkers Using Molecular Probes and Nanoparticles*. ACS Sensors, 2017. **2**: pp. 31-45. DOI: 10.1021/acssensors.6b00625.
34. Wang, H., Da, L., Yang, L., Chu, S., Yang, F., Yu, S., and Jiang, C., *Colorimetric fluorescent paper strip with smartphone platform for quantitative detection of cadmium ions in real samples*. J. Hazard. Mater., 2020. **392**. DOI: 10.1016/j.jhazmat.2020.122506.
35. Omidfar, K., Ahmadi, A., Syedmoradi, L., Khoshfetrat, S.M., and Larijani, B., *Point-of-care biosensors in medicine: a brief overview of our achievements in this field based on the conducted research in EMRI (endocrinology and metabolism research Institute of Tehran University of medical sciences) over the past fourteen years*. J Diabetes Metab Disord., 2020: pp. 1-5. DOI: 10.1007/s40200-020-00668-0.

36. Tirimacco, R., St. John, A., Astill, K., Weinholt, L., and Merrilees, P., *Point of Care Testing Implementation Guide*. 2019.
37. Tu, Y., et al., *Specific and Quantitative Detection of Albumin in Biological Fluids by Tetrazolate-Functionalized Water-Soluble AIEgens*. ACS Appl. Mater. Interfaces, 2019. **11**(33): pp. 29619-29629. DOI: 10.1021/acsami.9b10359.
38. Toora, B.D. and Rajagopal, G., *Measurement of creatinine by Jaffe's reaction--determination of concentration of sodium hydroxide required for maximum color development in standard, urine and protein free filtrate of serum*. Indian J Exp Biol., 2002. **40**(3): pp. 352-354.
39. Pham, A.T.T., Tohl, D., Wallace, A., Hu, Q., Li, J., Reynolds, K.J., and Tang, Y., *Developing a fluorescent sensing based portable medical open-platform - a case study for albuminuria measurement in chronic kidney disease screening and monitoring*. Sens. Bio-Sens. Res., 2022. **37**. DOI: 10.1016/j.sbsr.2022.100504.
40. Pham, A.T.T., Tohl, D., Hu, Q., Li, J., Reynolds, K.J., and Tang, Y., *Portable Colorimetric Device with Commercial Microplates for Quantitative Detection of Urine Biomarkers: Design, Development, and Clinical Evaluation*. Biosensors (Basel), 2022. **12**(9). DOI: 10.3390/bios12090723.

CHAPTER 2. BACKGROUND INFORMATION AND LITERATURE REVIEW

Most of this chapter has been published in the following journal paper and book chapter. Additional information has been provided below to satisfy the requirements of the thesis.

The journal article [1]: Pham, A.T.T.; Wallace, A.; Zhang, X.; Tohl, D.; Fu, H.; Chuah, C.; Reynolds, K.J.; Ramsey, C.; Tang, Y. (2021). Optical based biosensors and their portable healthcare devices for detecting and monitoring biomarkers in body fluids. *Diagnostics*, vol. 11, 1285. <https://doi.org/10.3390/diagnostics11071285>

The book chapter [2]: Pham, A.T.T. & Tang, Y. (2022). Point-of-care in vitro diagnostics devices based on aggregation-induced emission biosensors: current situation and future prospective (Chapter 5). In: *Applications in Biosensing, Bioimaging and Biomedicine, Vol. 1: Aggregation-Induced Emission*. Editors: Ben Zhong Tang and Xinggui Gu, Berlin, Boston: De Gruyter, pp. 83-110. <https://doi.org/10.1515/9783110672220-005>

According to the research's target of using fluorescence and colorimetry for albumin and creatinine detections, respectively, this chapter focuses on reviewing fluorescence and colorimetry related features and general reports of POC devices using these methods for biomarker detection. Device development is discussed in later sections.

2.1. Background information on POC device development in CKD monitoring

From Figure 1.3 in Chapter 1, the three main parts of a POC device for monitoring biomarkers in body fluids are the consumables, the hardware, and the software. The following subsections review these parts in turn.

2.1.1. Consumable development strategy in POC devices

Consumables include all components relating to the chemical reaction between the analytes of interest with the recognising reagents. They can be, but not limited to, the cuvettes for containing chemicals, paper strips for absorbing the fluid samples, needles for injecting the solution into containers, and the cap/lid for sealing the chemical inside the containers. In this component, the detecting agent is the main factor defining the feasibility of the development of the portable device. It affects the signal intensity resulting from the reaction between the agents and the target analytes. Innumerable reagents and methods have been researched in this field to enhance the optical response of the target analytes.

Aggregation-induced emission (AIE) is the mechanism that can enhance the measurement performance of biological analytes in terms of sensitivity, accuracy, large Stokes shift, and stability of fluorescence evaluation. AIE has been introduced and developed over the last few decades and has drawn attention from researchers in biomarker detections [3-6]. AIE bio-probes have been applied to food safety, drug detection, treatment evaluation, therapy diagnosis, and disease monitoring, and have brought benefits to healthcare research and applications, as shown in Table 2.1. However, although there has been considerable research into AIE biosensors for health applications, further rigorous evaluation is still required before they can be used in POC device development. Hence, researchers have lots of opportunities for developing POC devices with embedded AIE bio-probes. From the above introduction, AIE bio-probes are a significant consideration for the consumables part of a POC device, which plays the role of creating a suitable environment for the chemical or biochemical reactions between the target analytes and the recognising agents. The choice of consumables depends on the type of tests to be undertaken and can be either a microfluidic paper-based test or a liquid-based test.

Table 2.1. Several reported AIEgens using fluorescence evaluation in health applications.

Reference	AIE probes	bio-Medium	Analytes	Method	Achievements
[7]	BSPOTPE	Urine	Albumin	Fluorescence	LOD: 1 nM
[8]	TAE-Re(I)	Urine	Albumin	Fluorescence	LOD: 20 μ M
[9]	TPE-4TA	Urine	Albumin	Fluorescence	LOD: 0.21 nM
[10]	Compound 1	Saliva	Albumin	Fluorescence	Up to 80 mg/L
[11]	DIPIP-Ag+	Saliva	SCN ⁻	Fluorescence	LOD: 7.8 nM
[12]	TPE-Tb	Aqueous sample	DPA	Fluorescence	LOD: 0.187 nM

2.1.1.1. *Paper-based assay protocols*

The microfluidic paper-based strip was first invented by Martin and Synge in 1952, then developed and applied to chemical and biomedical analysis [13, 14]. The paper strip's unique porous structure, created by pressing cellulosic or nitrocellulose fibres together in multiple layers, allows

fluids to be transported from along the paper strip through capillary structures without any requirement for external forces. This transportation property helps the paper strip absorb and interact with the chosen fluids, which is a great advantage in chemical and biomedical analysis. Other advantages are its simple usage, low fabrication cost, high biocompatibility and biodegradation, and the non-requirement for high standard clinical facilities, infrastructure, and well-trained medical staff. This makes paper-based microfluidic platforms one of the best solutions for disease detection and monitoring in developing countries [14]. Nowadays, technology for manufacturing paper-based microfluidic platforms has been improved to be compatible with modern technologies for POC diagnostic application, and most involve immunoassays, which utilise antibodies to track and detect the biomarkers of interest [15]. While having been developed into different forms and applications, the paper-based microfluidic platform still follows the traditional principle of lateral flow, as shown in Figure 2.1 [14].

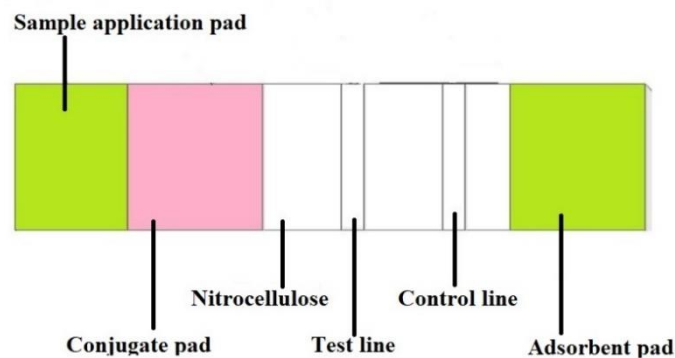


Figure 2.1. Traditional schematic of the lateral flow assay [16].

There are two methods for observing the paper strip result, the sandwich and competitive strategies [15, 16]. The principle of paper strip application in diagnosis involves chemical reactions between the biomarkers in body fluid samples and the specific antibodies or antigens equipped in the cellulose or nitrocellulose membranes of the strip, leading to the fact that most paper strip measurements follow optical detection methods. In the following discussion, the application of paper-based assays with fluorescence and colorimetry in POC device development will be presented.

Nowadays, paper strips are manufactured for commercial usage in clinical facilities with a standard design for common testing, such as monitoring the proteins or glucose in the urine, pH and electrolytes in saliva and sweat samples. This results in a limitation on using commercialized paper strips for detecting biological molecules in the research process as different molecules require specific detection reagents, which may experience a decrease in their sensitivity, quality and stability when assigned to the dry paper test strip. Therefore, researchers have developed microfluidic chips, which follow the capillary principle of the paper's porous structure while allowing the chemical

reaction in a solution state. This new development allows researchers to customize microfluidic paper-based chips to not only satisfy the requirement of their POC devices but also to ensure the performance of the optical measurement.

For biomarker detection by the fluorescence method, an optical excitation source is needed. This stimulates the analyte/antigen or antibody complex to produce fluorescent light. Xie et al. (2017) designed an AIE-based fluorescent test strip of OPD-TPE-Py-2CN to detect gaseous phosgene, an industrial chemical, which can damage the pulmonary alveoli and lead to pulmonary edema, pulmonary emphysema, or death, as shown in Figure 2.2. When combining with phosgene, the AIE probe on the test strip can emit fluorescence and shift the colour from blue to green under the exposure of 365 nm UV light. This research approaches the limit of detection (LOD) of 1.87 ppm, much lower than the minimum allowed level for human health [17]. In 2020, Jiang et al. (2020) developed the filter paper loaded with the AIEgen, i.e., H⁺ DQ2, to monitor the spoilage of seafood by detecting the biogenic amine vapours. The tested strip was excited by a 365 nm UV light, and a 575 nm wavelength emission showed up under the presence of the biogenic amine vapours in the salmon samples. This paper strip was able to detect 10 μM in 50 g of salmon sample [18]. In 2021, Liu and co-workers reported a lateral flow immunoassay strip to detect escherichia coli O157:H7 in food, which causes a dangerous foodborne pathogen to patients [19]. The LOD of this test strip was 105 CFU/mL.

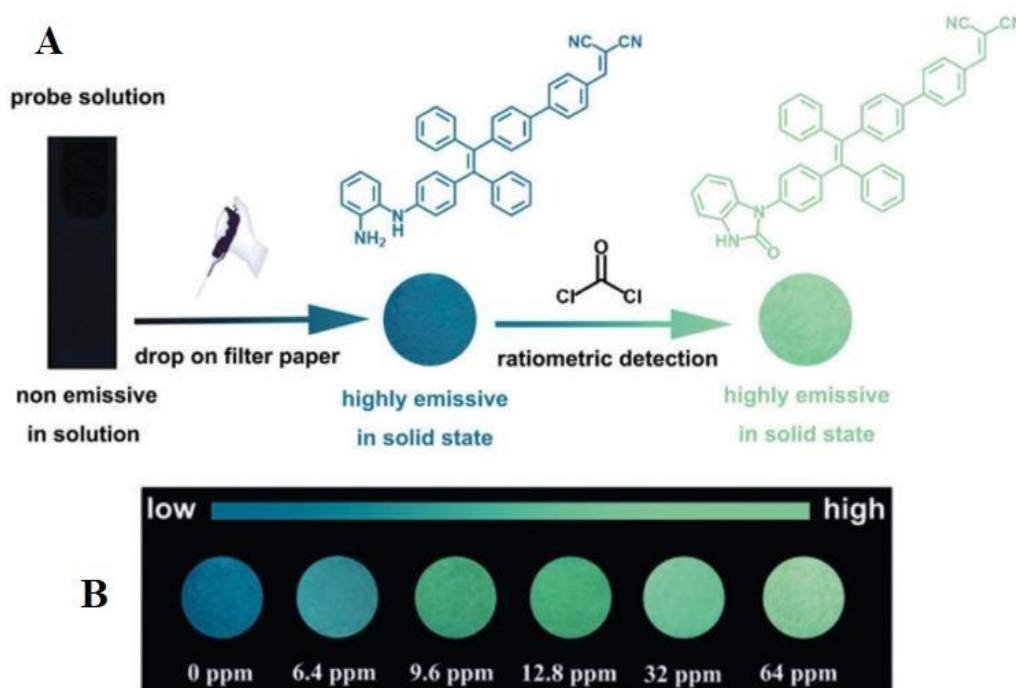


Figure 2.2. The customized microfluidic-based paper strip using AIE probe OPD-TPE-Py-2CN to detect gaseous phosgene; The pictures are taken under the 365 nm UV exposure. A) The schematic illustration of the customized test strip. The paper strip is embedded with the developed

AlEgen OPD-TPE-Py-2CN. Without the presence of phosgene, the test strip stays non-fluorescent under the 365 nm UV excitation. With the increase of phosgene's concentration, the fluorescence intensity rises dramatically. B) The variation of fluorescence intensity yielded from the OPD-TPE-Py-2CN loaded test strip when reacting with different phosgene's concentrations [17].

In colorimetry detection, the paper-based microfluidic platform has also drawn significant attention from researchers in recent years. Colorimetric results can be observed by the naked eye, or analysed by software installed on a programmable device, such as a computer, laptop, or smartphone. This property helps researchers develop a POC testing system to analyse the colour changes from the chemical mixture [13]. For instance, Adel Ahmed and Azzazy (2013) presented a power-free and portable chip, working with liquid chemicals, and using enzyme-linked immunosorbent assay (ELISA) in monitoring prostate-specific antigen (PSA) for prostate cancer detection. Magnetic nanoparticles capture the target analytes in serum. Then this complex flows to the region containing reagents to bind the analytes and the magnetic nanoparticles. This paper-based immunoassay chip performs a sandwich ELISA. When the PSA binds with the horseradish peroxidase (HRP) substrate, a green colour is imaged on the smartphone camera, as shown in Figure 2.3, then analysed by MATLAB software for red-green-blue (RGB) intensity per pixel. The limit of detection was reported to be 3.2 ng/mL [20].

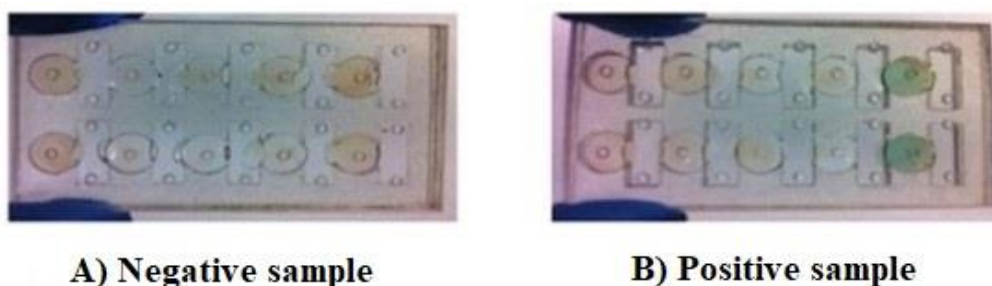


Figure 2.3. The results of prostate cancer detection using the HRP substrate [ABTS (2,2'-Azinobis [3-ethylbenzothiazoline-6-sulfonicacid]-diammonium salt) to track the presence of prostate-specific antigen (PSA) in serum, A) the negative sample (No PSA) wherein the HRP substrate stays red, and B) the positive result (PSA presence) where the HRP substrate develops a green colour [20].

From what has been mentioned above, the paper-based microfluidic platform has critically advanced research into biomarker diagnostics. The specifications of portability, low-cost fabrication, qualitative or semi-quantitative results, simple test procedure, and long shelf-life characterize this dry-testing platform and has supported the improvement of POC systems in recent years. However,

there are some drawbacks with the paper-based platform, such as uncontrolled sample volume consumption, limit of sensitivity due to the restriction on testing volume, strict requirements in choosing suitable antibodies and antigens to detect the biomarkers, the analysing process's dependence on the nature of the sample, equipment for emplacing the antibodies and antigens onto the paper surface and the methods to secure the stability of the antibodies/antigens after being attached to the paper surface [13, 21]. These drawbacks mean that some biomarker detections are preferably processed in solution states of chemical and body fluid samples.

2.1.1.2. Liquid-based detections protocols

Although operating differently from the paper-based microfluidic platform, liquid-based biomarker detections also follow similar principles in that the obtained results come from reactions between the target biomarkers and the detecting agents. Some liquid-based biomarker detections are now presented for fluorescence and colorimetry methods for POC systems. Akraa et al. (2018) used a fluorescence-based AIE probe, BSPOTPE to monitor HSA concentration in urine to indicate the early signs of CKD. A urine sample is mixed with BSPOTPE to produce the testing solution. If HSA is present in the urine sample, the solution emits 480 nm fluorescence under excitation by 340 nm UV, with the fluorescent intensity proportional to the HSA concentration in the sample [22]. Tu et al. (2019) introduced the novel AIE probe TPE-4TA using fluorescence evaluation to monitor albumin in the human urine sample. In the measurement, TPE-4TA was mixed with the urine sample and examined under the excitation of 360 nm UV light. When there has was present, the solution emitted 480 nm fluorescence, with the fluorescent intensity proportional to the HSA concentration in the sample, as shown in Figure 2.4. This AIEgen had a LOD on HSA in urine of 0.21 nM [9]. Recently, Su et al. (2021) presented the novel AIEgens TPE-Tb, which can rapidly detect pyridine-2,6-dicarboxylic acid (DPA), the anthrax spore biomarker, in aqueous solutions. This AIEgen can detect DPA levels as low as 0.187 nM in aqueous samples [12]. Thus, the fluorescence-based AIEgens in solution state show excellent performance in detecting bio-analytes in body fluids.

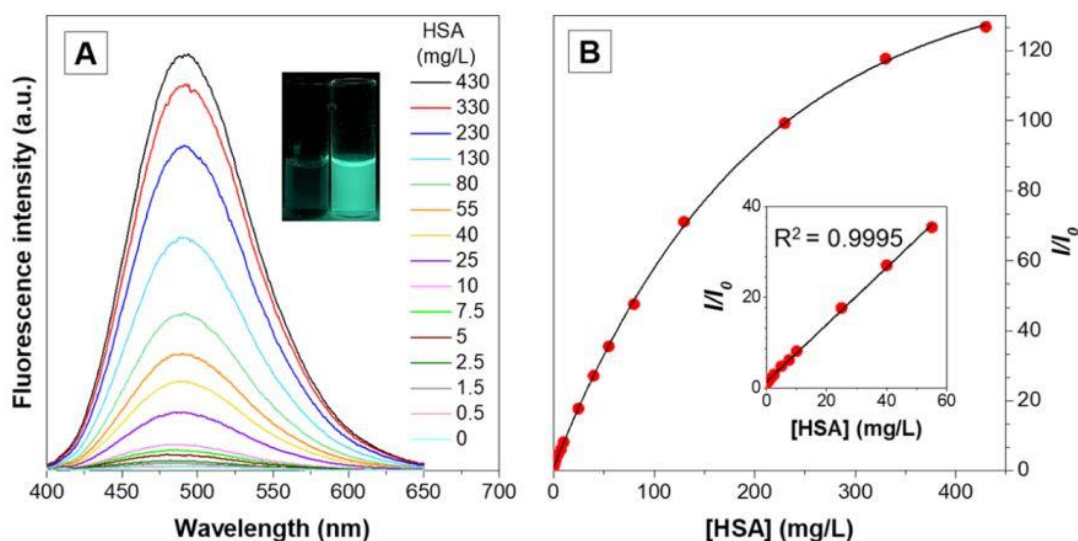


Figure 2.4. The response of TPE-4TA to HSA in a urine sample. A) The cuvette contains the mixture of the urine sample and the AIEgen TPE-4TA. There is a critical difference in the mixture's luminescence under the excitation conditions, in that, the solution without UV excitation will stay non-emissive (left cuvette) and turn to fluorescent (right cuvette) under the exposure of 360 nm UV. The fluorescence intensity emitted from the mixture varies proportionally with HSA concentration. B) The fluorescence intensity is proportional to HSA concentration in the range of 0 – 400 ng/mL [9].

Chen et al. (2014) applied ELISA into colorimetric detection to measure bovine serum albumin (BSA) in serum by developing a microfluidic platform, allowing the reagent of 4:1 VHH/horseradish peroxidase (VHH/HRP) to react with BSA under the support of phosphate-buffered saline. The developed colour images were captured by a smartphone camera and sent to an Arduino microcontroller for analysis of the RGB values in the BSA concentration in the serum sample. The smartphone was used for colour-shifting imaging only, not for signal analysis [21]. Kong et al. (2020) reported a smartphone-based microchip for tracking ascorbic acid (AA) in serum. The serum was injected into a quartz cuvette located inside the measuring device. MnO_2 was added to the serum sample, followed by the addition of TMB and HCl to shift the solution's colour from red to blue and yellow, respectively, as shown in Figure 2.5. The presence of ascorbic acid in the serum enhanced the solution's colour intensity. A smartphone was used to capture colour pictures and customised software installed on said smartphone was used to analyse the HSV values and establish the correlation between the colour intensity and the AA concentration. The limit of detection for AA in serum was $0.4946 \mu M$ [23].

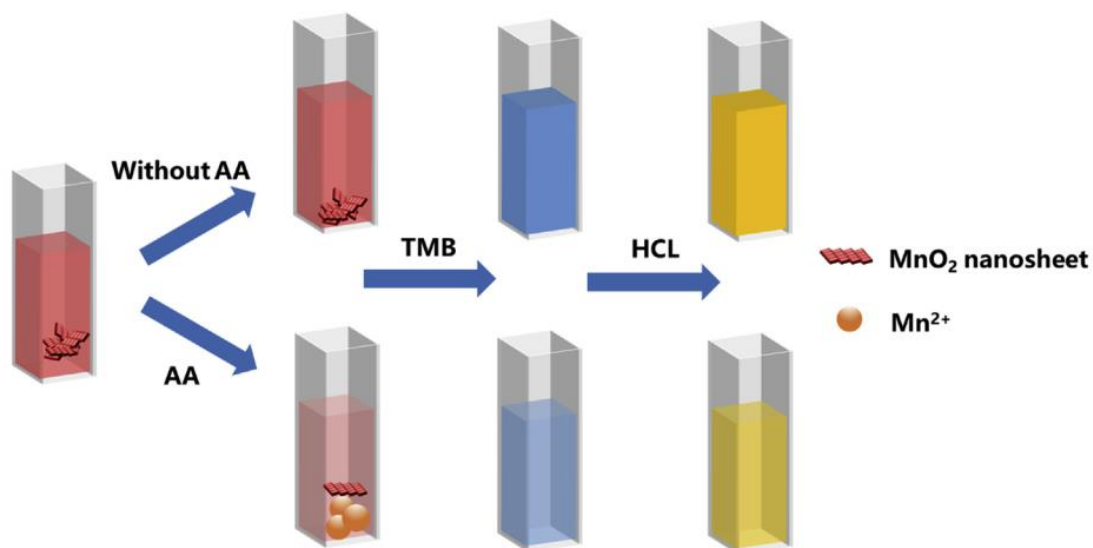


Figure 2.5. The schematic for ascorbic acid detection using a colorimetric assay with TMB-MnO₂ reagent. In the reaction, the serum is injected into the Quartz cuvette, which was located inside the device for measuring. MnO₂ was added to the serum sample, followed by the addition of TMB and HCl to shift the solution's colour from red to blue and yellow, respectively [23].

In conclusion, the consumable is an essential part of the development of a POC device. It affects the choices of the hardware and software design. Both the liquid-based test and the microfluidic paper-based assay have had a long history of development and have obtained numerous achievements in health applications. Considering the use of these two techniques will increase the feasibility of practical POC device development in the future.

2.1.2. Hardware development strategy in POC device

In POC testing systems, consumables are the components supporting the chemical reactions, with hardware parts needed to assist measurement. The hardware part has two sub-components: the electronics and the solid support. The electronics have several functions, including providing the excitation elements for specific tests, capturing the resulting signals, analysing the data, or transferring the data to external instruments. Whilst solid support combines and secures the positioning of all the components; protects the inner electronics and chemical reaction section, and, especially, provides a controlled environment for measurement. The general structure of the hardware consists of three main components: the solution and optical source container, the signal transferring space, and the signal collection section.

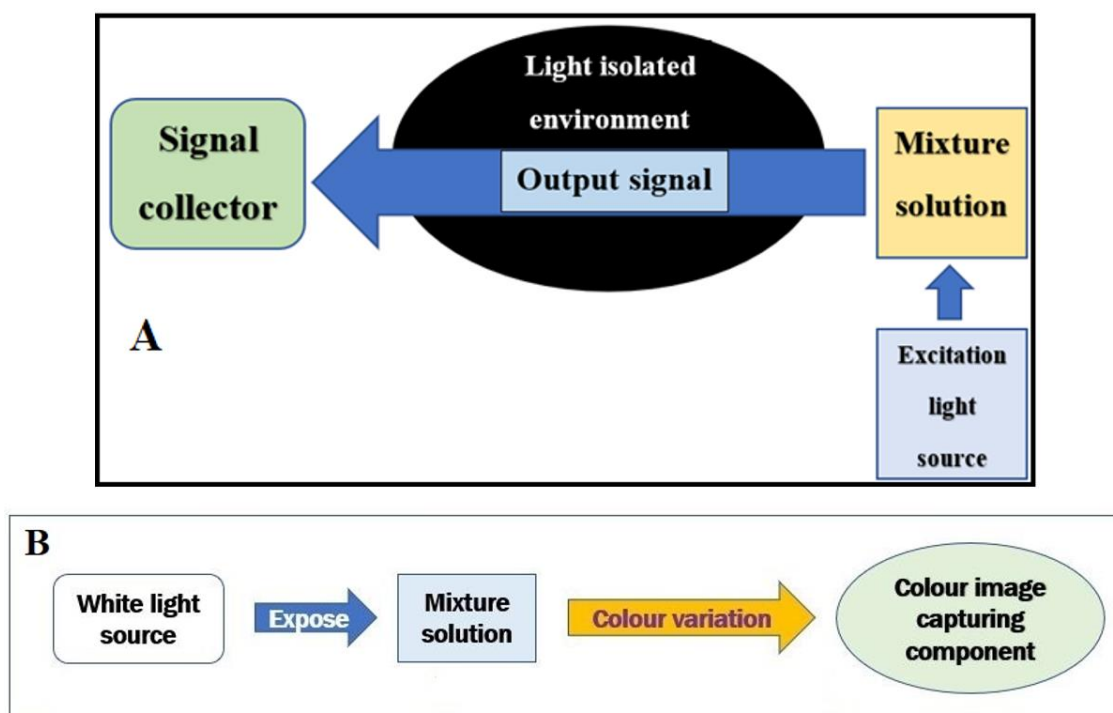


Figure 2.6. The hardware components of the optical POC device. (A) The sketched structure for the fluorescence measuring POC device. The light source generates the specific wavelength light to excite the mixture of recognising reagent and biological sample in a controlled ratio. If the target molecule exists in the sample, the mixture will emit fluorescence when exposed to the excitation light. The light isolated environment, i.e., a dark room like section, is a sealed space where the fluorescence transfers from the mixed solution to the imaging sensor. This minimises optical noise from the external environment when taking measurements. The imaging component captures the fluorescent signal. This signal is analysed for fluorescent intensity by the software component. (B) The sketched structure for the colorimetry measuring POC device. The white light source shines on the mixture of recognising reagent and biological sample. If the target molecule exists in the sample, the mixture will develop the responding colour. The colour variation will be captured by the imaging component, then be analysed by the software component.

From the sketched diagram in Figure 2.6, there are several differences between the fluorescence and colorimetry evaluations in terms of the optical component arrangement. For the colorimetry measurement, the light source, the solution container, and the optical detector are placed in one line. For the fluorescence measurement, the excitation source will be set up perpendicularly to the line of the solution container and the optical sensor.

When developing the hardware components for the optical POC devices, the typical aim is to achieve efficient optical detection. For that purpose, some electronic components will play essential roles in the hardware construction. Not only having high sensitivity and accuracy, but those

components are also required to have an effective cost and reasonable portability.

2.1.2.1. Excitation light source selection

The first component is the luminescence source as it affects the whole system's operation. This component is also the typical difference between fluorescent and colorimetric devices. Fluorescence is a type of photoluminescence, the phenomenon where the molecules have the capability of glowing under certain conditions [24]. Fluorescence involves the electronic absorption of the molecules in a specific medium. In photoluminescence, molecules in a substance absorb photons of unique wavelengths and emit a longer wavelength photon in a critically short time [24, 25]. Hence, fluorescence measuring devices require a light source with a suitable wavelength to stimulate the solution mixture. Meanwhile, the colorimetry detection is based on a changed colour or colour intensity generated by the chemical reactions between the biomolecules of interest and the detecting agents. This results in the light source design in the POC colorimetric device usually being a white light.

In recent POC device developments, LEDs and laser diodes have attracted attention from researchers due to their compact sizes, market distribution, broad working spectrum and low manufacturing cost. Although both have similar characteristics and have been applied into POC device development across many years, the difference in their working principles defines the fields for their applications. Generally, LEDs emit different wavelengths with a considerably narrow peak at a certain wavelength. For example, a 405 nm LED will generate a spectrum between 390 nm and 450 nm with the peak of the intensity at around 405 nm [26]. Meanwhile, a laser diode, which emits coherently and monochromatically, will almost illuminate only at a specific wavelength without bleeding into neighbouring wavelengths. The concentrated light beam of the laser diode leads to a high temperature at the illuminated point, small lighting area and a short lifetime of the diode. A comparison between LED and laser diode in different specifications is shown in Table 2.2, from this the suitable components can be determined to satisfy the fluorescence measurements, and the requirements of the POC platform development.

Table 2.2. Comparison characteristics of LED and laser diode for excitation source of portable device [27, 28].

Light source	Power/light conversion efficiency	Output temper .	Output intensity	Junction area	Eye safety	Popularity	Cost (AUD)	Electronic support
LED	~ 20%	Low	Medium	Scattering	Typically,	High	< 1	Power

				area	eye-safe	(Commercial and research applications)		supplier.
Laser diode	~ 70%	High	Very High	Extremely narrow	Compulsory eye-protector	Medium (Certain application)	~ 10	Power driver.

Although LEDs show a lower output intensity and less precise wavelength emission than a laser diode, they have advantages in lower manufacturing cost, less requirements in supporting electronics, and greater user safety. Moreover, the developed POC device is proposed to operate on solutions, and increased temperature, due to a laser diode, in the chemical medium during the operation is unwanted. In addition, the excitation light source for the device is expected to be exchangeable among different wavelength requirements. Thus, the laser diode with a complicated driver module is considered to be a too bulky component for the design. Therefore, LEDs are preferred for this open POC platform development.

2.1.2.2. *Optical signal sensor selection*

The choice of the optical signal sensor is also a significant factor defining the success of the POC device development. Recent years have witnessed the dramatic revolution of mobile technologies, with the introduction of the smartphone as an essential piece of personal equipment. Being equipped with a highly sensitive complementary metal–oxide–semiconductor (CMOS) camera, many researchers have applied the smartphone’s camera as an optical measuring device, in that, the smartphone was used to take the image of the optical signals. Aside from the CMOS camera, a charge-coupled device (CCD) camera and photodiode are also potential options for measuring the optical values from the luminescence. A brief comparison of these optical sensors is presented in Table 2.3. Similar to the excitation light sources, the decision of optical signal sensor depends on the requirement of the testing system in terms of the signal sensitivity, power consumption, compact size, and affordability issues. Consequently, although some researchers use a CCD camera to have a better resolution in capturing optical images or applying a photodiode to evaluate visual numeric data, the majority of applications use smartphones equipped with a CMOS camera to support portable testing systems, helping to simplify the hardware design, as well as minimizing the device’s cost.

Table 2.3. Compare the pros and cons of CCD, CMOS cameras and photodiode.

Camera	Data type	Resolution	Working Volt (V)	Popularity	Cost	Electronic support
CCD	Analog	High	5 – 12	Medium	High	High. Requires electronic circuits to control the camera, to regulate power supply, to convert the analog-digital signal, etc.
CMOS	Digital	Medium	3.3 – 5	High	Medium	Low. Only power supply circuit required.
Photodiode	Analog	Low	~ 1	Low	Low	Medium. Require a power supply circuit and the signal detecting circuit.

2.1.2.3. *Power supply system, calibration system and others*

Another factor impacting the feasibility of the POC device development is the power supply. Both optical detections require a light source so the power supply should not be overlooked. Opinions vary about using an external power supply (adapter or battery assembly) or drawing energy from integrating the smartphone through an audio output jack or charging input plug. However, harvesting power from a smartphone to supply the luminescence source encounters obstacles: (1) it requires a complicated converter and an amplifier because the obtained current from the audio output jack or the charging input plug on the smartphone is significantly low and (2) the smartphone's USB charging port is specially manufactured with an integrated chip to protect the smartphone from overcharging damage, so the power going through this port is limited. As a result, most developed portable devices use battery or an outlet adapter to supply power for electronic components instead of drawing power from a smartphone's battery. Each solution has advantages and disadvantages in that the battery can efficiently satisfy the portable requirement, but its power will reduce over time, which requires an indicator or a regulator component to manage the power supply from the battery. In contrast, the outer adapter has its regulating component, which can guarantee the stability of the power supply to the device. However, the cons of using an adapter are that it requires the power source and will

affect the portability of the device. Depending on the requirements of the portable device, a suitable power supply will be considered.

As well, most developed devices employ filters in the optical measurement process. In optical measurement, there are lots of confounding factors, such as the effect of external light, light degradation of the luminescent source, reflecting or scattering of light inside the optical evaluating room, or noise from the chemical components themselves, which may add a different light wavelength into the data collection. Using filters helps distinguish these noises from the preferred signal. This also reduces the complexity in designing the analysing component, resulting in a reduction of the device's size and cost.

Simultaneously, to ensure the precision of the testing system, quality control or calibration is an indispensable component for all developed portable devices. There are two opinions about the better method of operating calibration: (1) running periodic calibration and (2) running calibration in every sample test. For the latter method of embedding the calibration step into the device, whenever users perform a single test, two results occur. i.e., one for the new test and one for the calibrated value. Both methods have advantages and disadvantages, and researchers select one according to the requirement for the precision of the test or the design's simplicity. In this, consideration is given to the measurement results' reliability, and the device's portability and cost.

2.1.3. Software development strategy in POC device

The software part will analyse obtained signals to distinguish the change in concentration of the analytes in the sample solution, the power status for the electronics components, or the presence of interference from the external environment.

2.1.3.1. *Data analysis*

The analysed target in fluorescence and colorimetry measurements is the change of the output signal. There are two common methods for analysing the output optical signal: (1) taking images of the optical signal, then analysing the mean values of the pixels in the images, or (2) using a photoelectric semiconductor device to convert the optical signal into an electronic signal.

For the image processing method, RGB analysis is an efficient technique, which measures the red, green and blue values of each pixel in the analysed areas or the whole region of the image. With this method, researchers can observe the change of the luminescent intensity/colour at the pixel level, which improves the sensitivity of the signal analysis. A camera is required to take the image of the output signal. In recent years, many researchers have used smartphones as a powerful assistant to take the images of the output signals. With their high-resolution CMOS camera and a range of settings such as white balance, auto-focus, custom ISO value, as well as their efficient computing processor, high battery capacity and wired or wireless connections, such as Bluetooth,

Wi-Fi, Internet, etc., smartphone-based medical devices have been upgraded to monitor human health conditions and to detect the micro signs of chemical or biological compounds [29]. For the optical-electronic converting method, an electronic component will convert the luminescent signal into the voltage value. According to the principle of the photoelectric semiconductor device, the voltage value will have a relationship with the luminance arriving at the detector. By measuring voltage values, researchers can recalculate the intensity of the output signal. The common optical detector used in this method is the photodiode, which has several advantages in developing the POC device, as shown in Table 2.3.

The signal capture method will dictate the strategy for deciding the software development, in that, devices integrated with a processor, such as smartphones, have the ability to run the analysis software themselves; whilst other capture methods require the data to be transferred to an external computing platform for further analysis. If the output signal has a low detection range, or noise requires multiple steps to process, the optical detecting device will require support from an external device for further processing. An external computing device is also a factor contributing to the feasibility of the POC device development in that it will increase the cost and the compactness of the developed device.

2.1.3.2. Other factors

When processing signals obtained from bio-molecule monitoring tests, researchers usually compare the obtained data against a known standard model to calculate for the concentration value of the molecules in the samples. However, many chemicals, molecules or specimens do not have standard data to refer to, leading to incorrect judgment of the results. There are several solutions for this issue, and the efficient one is using machine learning in data evaluation. Applying machine learning to data processing will help researchers to have a better overview of the bio-molecule measurements, as well as to establish a database as a premise for long-term research in the future.

2.2. The review of fluorescence analysing method for portable device development

Fluorescence and phosphorescence are types of photoluminescence, the phenomenon of molecules glowing under certain conditions [24]. Fluorescence and phosphorescence involve electronic absorption by the molecules in a specific medium. In photoluminescence, molecules in a substance absorb photons of unique wavelengths and emit a longer wavelength photon in a critically short time [25]. The typical difference between fluorescence and phosphorescence is the glowing time, in that fluorescent molecules absorb the excitation photon in 10^{-5} s, internal conversion takes place in 10^{-11} s and the lifetime of the fluorescence after the excitation source vanishes is around 10^{-9} s [30]. In contrast, the phosphorescence process continues for up to several seconds after

excitation [24]. Not all molecules can produce fluorescence, those having fluorescent properties are often called fluorophores [31]. Many researchers have shown that fluorescence is typically proportional to the number of biomolecules attached to fluorophores [25, 32-35]. Following are some highlighted reports using fluorescence evaluation to quantitatively monitor the biomarkers in body fluids.

2.2.1. Fluorescence analysing method for portable biomarker monitoring system – Non-portable device development

There are many reports of fluorescence measurements without discussing related devices. Balwant and Kaur, in 2016, reported a diagnostic method using the fluorescence principle on a test strip to detect sleep disorders in an individual by assessing a saliva sample [36]. In sleep disorders, there are specific biomarkers that can be measured to estimate the disease condition such as arginine, creatine, dihomo-linoleate, tyrosine, beta-endorphin, chromogranin A, linoleate, BDNF, and 3-methyl oxobutyrate [36]. In normal conditions, there is a small amount of these biomarkers in saliva. When these biomarkers are present in amounts exceeding the reference values, the patient is considered to have a sleep disorder. The saliva test strip is prepared with the selective agents for each target biomarker. The test accuracy was reported in the range from 86 % to 91.5 % in a group of 65 patients [36].

In 2017, Gabr and Pigge used an AIEgen to detect HSA in a urine sample [8]. The complex of Re(I) tricarbonyl was prepared from bis (pyridyl)- and bis(quinolyl) tetraarylethylene (TAE) ligands, which are reported to enhance the fluorescent emission of the solution when combining with HSA. The final solution was excited by a 396 nm ultraviolet light, resulting in a light blue fluorescence with a wavelength of 509 nm. This method was claimed to improve the LOD of HSA in the urine sample to 20 μM .

In 2017, Zhang and co-workers (2017) presented an assay using AIE-active fluorophore (TPE-HPro) to detect L-Lactate oxidase (LOx) in aqueous fluid [5]. This assay was excited at a wavelength of 373 nm and yielded a 570 nm green emission. The fluorescent signal lasted around 60 minutes, facilitating the accuracy of the measurement. The limitation of detection was reported to be as low as 5.5 μM [5]. This research identified the potential for applying AIE in tracking the L-Lactate presence in saliva and urine samples.

Meanwhile, Zhang et al. (2020) reviewed the constituents and clinical biomarkers in urine, saliva, and sweat, and the role of currently developed AIE bio-probes that can quantitatively detect disease related biomarkers in these biofluids [37]. The review also highlighted that several applications of AIE bio-probes, such as paper-based strips and POC devices, are currently under development, and offer potential to be simply realized using smartphone data capture and analysis and cloud data storage.

2.2.2. Portable fluorescence-detecting device development

In addition to studies on fluorescence evaluation without the related devices, there are also many reports on the development of POC fluorescence-based devices to monitor biological molecules. Remarkably, many of this reported, not all, the use smartphones as part of the POC device development. Mudanyali et al. (2012) designed a cell phone-based rapid-diagnostic-test (RDT) reader platform, using fluorescent imaging and analysis of commercial lateral flow tests to monitor malaria, HIV, and tuberculosis (TB) [38]. Two Samsung Galaxy S II smartphone-based prototypes were designed: one used 2 AAA batteries to supply power for the LED light source while the other draws energy from the smartphone through the USB port. In the test operation, lateral flow tests were applied to a blood sample before insertion into the prototype. The LEDs were arranged in three rows, providing the excitation wavelength of 565 nm in two ways: two LED arrays were attached under the RDT tray for reflection imaging, and one LED array was located at the top of the RDT tray for transmission imaging. Depending on the test requirement, users can trigger the physical switch on the prototype to choose the most suitable imaging method. The phone's camera captured the raw fluorescent images of the test and control lines on the RDTs. These images were processed by an app on the smartphone with a customized algorithm, as shown in Figure 2.7, to generate the quantified result of the antigen density from the test line colour intensity [38]. In this design, researchers created an isolated area for fluorescent imaging to minimise the effect of the external environment, which secured the stability and repeatability of the measurement. Also, the patient's information and testing results could be stored in the internal memory of the smartphone or uploaded to the internet through wireless communication for further analysis.

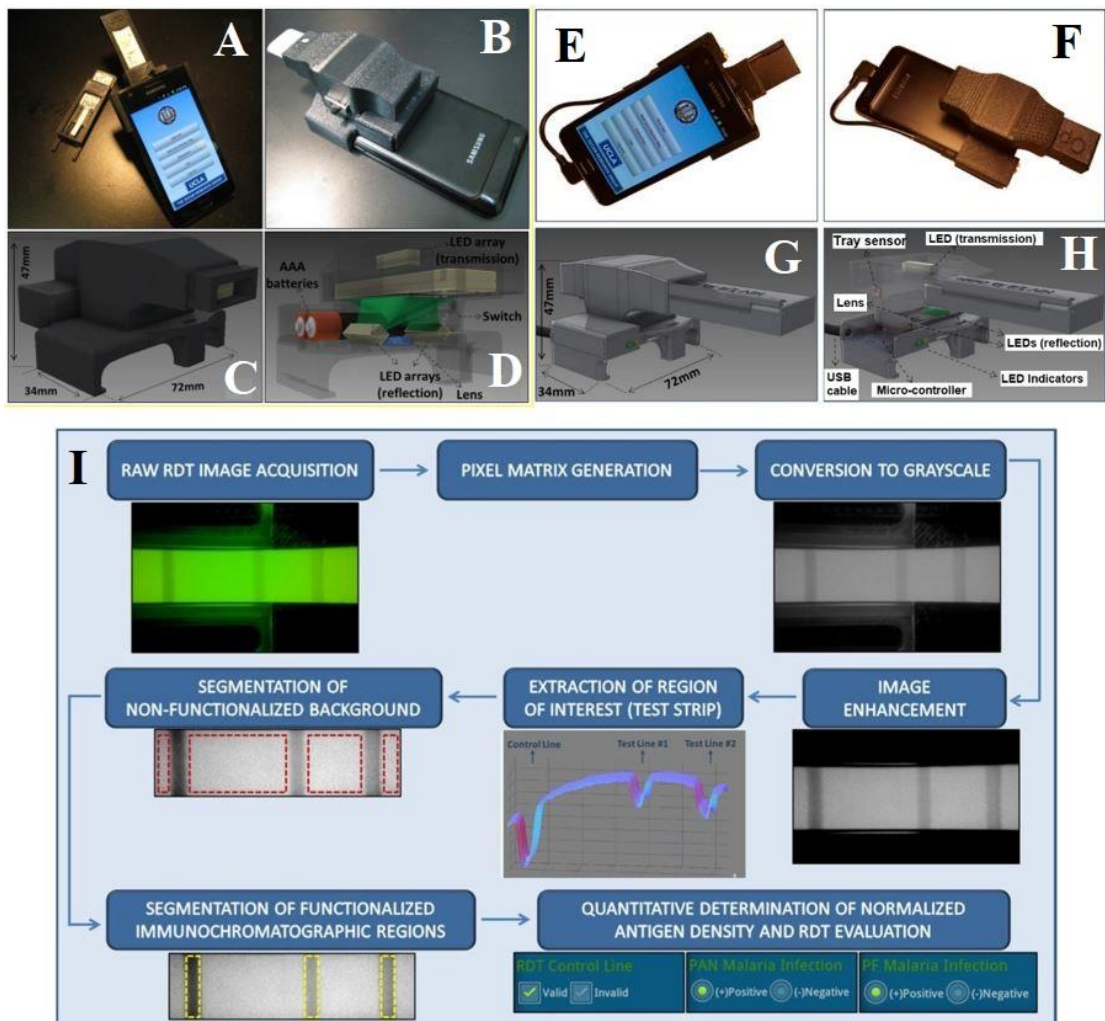


Figure 2.7. The overview of two prototypes using different power supplies for excitation light source: Using 2 AAA battery (A, B, C, D) and using smartphone's battery (E, F, G, H); and the image processing in the built-in software on the smartphone (I). (A) and (B) The front and rear views of the 2-AAA-battery prototype. (C) The sketch of the assembled prototype. (D) General structure for the 2-AAA-battery prototype. (E) and (F) The front and rear views of the smartphone-power-supply prototype. (G) The dimensions and the sketch of the assembled prototype. (H) The general structure of the smartphone's battery supply prototype. (I) The algorithm for the reflection imaging process. (1) The raw fluorescent image is taken by the CMOS camera of the smartphone Samsung Galaxy S2. (2) The raw image is generated as a pixel matrix of 3-channel YUV420 scale. (3, 4, 5) The pixel matrix is converted into grayscale to locate the fluorescent areas of the control and test lines on the RDT strip. (6, 7) The segmentations of the test and control lines are differentiated from the environmental areas. (8) The location of the control line will be checked to estimate whether the measurement is valid. If the test is correct, the test line's colour intensity will be analysed to indicate the positive or negative result [38].

Coskun et al. (2013) developed a Samsung smartphone-based analyser to detect albumin in human urine for CKD indication, as shown in Figure 2.8 [39]. This albumin tester comprised a 148-gram attached support, a two AA battery powered laser diode for light excitation at 532 nm wavelength, two cuvettes sized 6 mm × 2 mm × 15 mm for storing the urine sample and the fluorescent dye, an Android smartphone built-in camera for fluorescent imaging, and an app installed on the same phone for image processing to give the quantitative result. All measurement components were secured in a solid support, which was designed in Inventor software and fabricated by 3D printing. The LOD was claimed to be 5-10 µg/mL, three times lower than the normal range for clinical acceptance (albumin level should be lower than the threshold of 30 µg/mL in human urine) [39, 40]. Two customized cuvettes were used, one for controlling and the other for testing. The control cuvette was wholly filled with a fluorescent dye (albumin blue 580) while the test cuvette was partially filled with the dye, giving space for the urine sample to be added later. A plano-convex lens and a fluorescent interference filter were arranged in the middle of two tubes with the smartphone camera to collect the fluorescent emission and to filter out the scattering excitation light, respectively. After being captured by the CMOS camera of the smartphone, fluorescent images of both tubes were processed to produce the optical values of the test tube (I_{Test}) and the control tube ($I_{Control}$). Then, the app used these values to generate the relative fluorescence unit ($RFU = \frac{I_{Test}}{I_{Control}}$) and calculate the concentration of albumin in the testing sample.

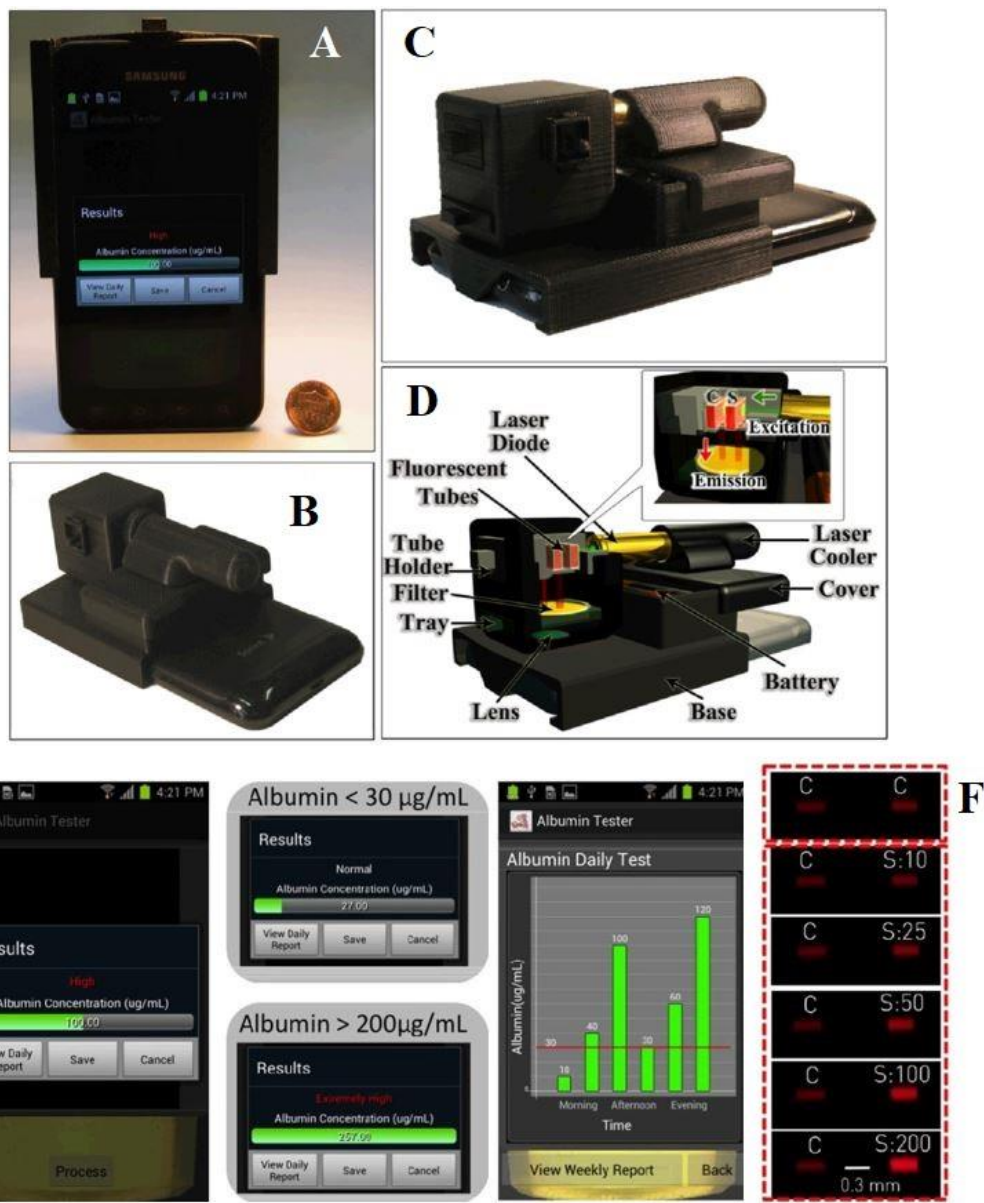


Figure 2.8. (A), (B), (C) The overviews of the solid support attached to the Samsung Galaxy SII and the resulting interface of the analysing app. (D) The structure of the prototype. From the top-left to the bottom-right: The laser diode was powered by 2 AA batteries, with an emitting wavelength at 532 nm. Fluorescent tubes were custom developed to have dimensions of 6 × 2 × 15 mm and were arranged in line with the laser beam so that the laser beam would shine through the test tube (S) first, then the transmission laser beam would excite the control tube (C). The fluorescent emission was captured by the smartphone camera arranged perpendicular to the laser beam. The Tube Holder was for holding the tubes. Filter, tray and lens were for collecting the fluorescent emission and filtering out the reflected excitation light from the laser source. The laser cooler managed the laser source temperature. The cover was fabricated in filament by 3D printing to secure the positioning of all components, as well as preventing unwanted external light. The batteries used were 2 AA batteries, which could be replaced after usage. The base was the connector between the albumin tester and the smartphone. (E) The resulting images taken from different albumin

concentrations: 0, 10, 25, 50, 100, 200 $\mu\text{g/mL}$. C is the control image and S is the testing sample image. and (F) The resulting screenshot from the app for normal, high, extremely high, and the weekly summary report of the albumin test on the same subject [39].

In 2020, Huang and co-workers developed a coffee ring test kit using an AIE bio-probe of TPE-TS@Eu/GMP ICPs to detect dipicolinic acid (DPA), a biomarker for bacillus anthracis (*B. anthracis*) spores, which causes anthrax after germination. A smartphone was used to take fluorescent images of the coffee ring under the excitation of a 405 nm UV lamp. Image processing focussed on analysing the colour of pixels in the blue channel (430–500 nm) and red channel (580–650 nm). On the smartphone, the software Image J analysed the red and blue values, then generated the ratio between the red and blue ($I_{\text{Red}}/I_{\text{Blue}}$). When the DPA level increases, the blue area on the coffee ring will contract, leading to the weakening of the blue signal. Meanwhile, the red area on the coffee ring expands, making the red colour brighter. Following this methodology, evaluating the red/blue ratio will give the quantitative result of DPA level in the biological sample. The detection limit of this coffee ring sensor is claimed to be 27 nM [41].

POC devices using a fluorescence method to detect biomarkers in body fluids are shown in Table 2.4.

Table 2.4. Portable devices using fluorescence method to detect biomarkers in body fluids.

Ref	Target of interest	Consumable	Hardware			Software	Result
			Supporting processor	λ_{Exc} [nm]	λ_{Ems} [nm]		
[42]	NA.	Solution test	Smartphone (Nokia 1020).	465	Depending on the conjugated reagent.	Smartphone (CMOS camera).	Computer (Commercial app). LOD: 80 fluorophores/diffraction-limited spot.
[43]	Chloride in sweat	Solution test.	Smartphone (HTC One M9).	365	441	Smartphone camera.	NA. LOD: 0.8 nM of chloride in sweat.

[38]	Malaria, HIV and tuberculosis (TB) in whole blood.	Commercial paper test strips for each disease.	Smartphone (Samsung Galaxy SII)	565	Depending on the disease detections (NA)	Smartphone (CMOS camera)	Smartphone (Customized app)	Correctly qualitatively detect the infected patients.
[39]	Albumin in urine	Solution test.	Smartphone (Samsung Galaxy SII)	532	NA	Smartphone (CMOS camera).	Smartphone (Customized app)	LOD: 5-10 $\mu\text{g/mL}$
[44]	Chloride, sodium and zinc concentrations in sweat.	Customized test strip.	Smartphone (iPhone 6 Plus).	451	511 nm for chloride. 515 nm for sodium. 519 nm for zinc.	Smartphone camera.	Smartphone (Customized app)	LOD: 28 mM for chloride; 36 mM for sodium; and 3.6 μM for zinc.
[22]	Albumin concentration in urine	Solution test.	Smartphone (iPhone 6s, Samsung Galaxy Note 4, and Galaxy S3).	340	~ 480	Smartphone (CMOS camera).	Smartphone (Customized app)	Quantitatively detect albumin in the urine
[45]	E. coli K12 in urine.	Customized microfluidic chip.	Smartphone (iPhone 6S).	NA.	NA.	Smartphone (CMOS camera).	Smartphone (Customized app).	LOD: 240 CFU/mL for E. coli K12 in urine.
[46]	Human chorionic gonadotropin in urine.	Customized paper test strip.	Smartphone (iPhone 5S).	NA.	NA.	Smartphone (CMOS camera).	Smartphone (Customized app).	LOD: 45 pg/mL for hCG

[41]	Dipicolinic acid from Bacillus anthracis spores	Customized AI-Egen-based paper coffee ring.	Smartphone	405	Blue (430 – 500 nm). Red (580 – 650 nm)	Smartphone (CMOS camera).	Smartphone (Image J).	LOD: 27 nM for DPA.
[47]	Cu ²⁺ in an aqueous sample	Solution test	Raspberry Pi-ARM V11	365	510	Raspberry Pi camera 5MP	Software DAS-6 from IBH to analyse RBG.	LOD: 9 pM of Cu ²⁺ ion.

2.2.3. Conclusion

In summary, most developed devices using the fluorescence method in biomarker detection have a similar mechanism, in that they use light at a specific wavelength to excite the mixed solution. For the chemical reaction support, prominent researchers prefer using a microfluidic paper-based assay to reduce the device's size and to broaden the observable section where the fluorescent intensity or colour changes, which supports the image capturing process. The image processing mainly works on the analysis of RGB values. A critical aspect of portable device design is the solid support component which carries the whole system and secures the positions of every component, as well as providing a suitable environment for running measurements. Finally, alongside the development of digital and computing systems, the POC system is constantly being upgraded to integrate analysis software into portable devices, which reduces the testing time as well as improving the quality of the biomarker measurement.

2.3. The review of colorimetry measuring method for portable device development

2.3.1. The portable colorimetry device development

The colorimetric detection is based on changing the colour or colour intensity generated by the chemical reactions between the biomolecules of interest and the detecting agents. The primary portable device design should consist of three major parts: the chemical reaction carrier, the image capture system, and analysing components. Shen et al. (2012) introduced a smartphone-based device to quantify the chromaticity values from pictures of pH levels on commercial colorimetric

paper test strips [48]. This POC colorimetric analyser used the CMOS camera of HTC and Blackberry smartphones to capture these images. These images were sent to computing devices to run MATLAB for colour intensity analysis. One of the problems in using a smartphone as a colour-photon detector stems from the camera's auto-function settings. To compensate for this, a reference colour chart of 12 known colour intensities with seven greyscale regions and five colour regions ranging from blue to red was used, as shown in Figure 2.9. This reference chart shows the potential to minimise the effects of the smartphone's camera auto-settings and ambient light changes. The LOD of this design was claimed to be 0.5 in pH value [48].

'This image has been removed due to copyright restriction. Available online from [Shen, L., Hagen, J.A., and Papautsky, I., Point-of-care colorimetric detection with a smartphone. *Lab Chip*, 2012. 12(21): pp. 4240-4243. DOI: 10.1039/c2lc40741h.]

Figure 2.9. (a) Overview of the test running on the smartphone, the urine test strip and the reference colour chart with 7 greyscale regions and 5 colour regions from blue to red. (b) The correlation between the actual pH value and the pH value measured by the design [48].

Wang et al. (2011) developed a smartphone-based system running with a customized microchip ELISA to track the presence of HE4 biomarker in urine to indicate ovarian cancer, as shown in Figure 2.10 [49]. When the molecule detector TMB bound with biomarker HE4 in urine, a blue colour developed in the solution, and the 3.2-megapixel camera on the smartphone (Sony Ericson i790) captured this shifting colour in pictures. An app installed on the smartphone analysed these pictures to obtain the RGB pixel values. The red pixel value was chosen to estimate the HE4 concentration in the urine sample. The LOD of this cell phone-based device was claimed to be 19.5 ng/mL [49].

'This image has been removed due to copyright restriction. Available online from [Wang, S., Zhao, X., Khimji, I., Akbas, R., Qiu, W., Edwards, D., Cramer, D.W., Ye, B., and Demirci, U., Integration of cell phone imaging with microchip ELISA to detect ovarian cancer HE4 biomarker in urine at the point-of-care. *Lab Chip*, 2011. 11(20): pp. 3411-3418. DOI: 10.1039/c1lc20479c.]

Figure 2.10. (A) 100 μ L of a urine sample was loaded onto the microfluidic chip ELISA, which was equipped with specific antibodies to detect the presence of biomarker HE4. (B) The smartphone Sony Ericson i790 was used to capture the colour-shifting in the solution. (C) The customized app on the smartphone analysed the picture to generate the red pixel values. Finally, it presented the quantitative HE4 concentration [49].

Oncescu et al. (2013) presented a smartphone-based prototype using colorimetric detection to monitor sweat and saliva pH, as shown in Figure 2.11 [50]. Sweat pH is proportional to sodium concentration, which is used in muscle cramp detection. In contrast, saliva pH is examined to track enamel decalcification, the specific biomarker for monitoring the breakdown of calcium in the teeth. The customized strip comprised three components: a 9 mm×4 mm piece of Hydrion Spectral pH indicator for sweat testing (ranging from 5.0 to 9.0) or saliva testing (ranging from 1.0 to 14.0), a 9 mm×4 mm piece of known colour value, working as the reference for calibration, and a polydimethylsiloxane (PDMS) diffuser for uniformly distributing the camera flash to the sections on the testing paper. All components were covered in a black case fabricated by 3D printing with Vera black material to eliminate the effects from external light sources and to keep a suitable distance between the camera and the test strip. An app for an iPhone was developed to run the colorimetric analysis by examining the hue value from hue-saturation-luminance (HSL) analysis to give the quantitative pH results [50].

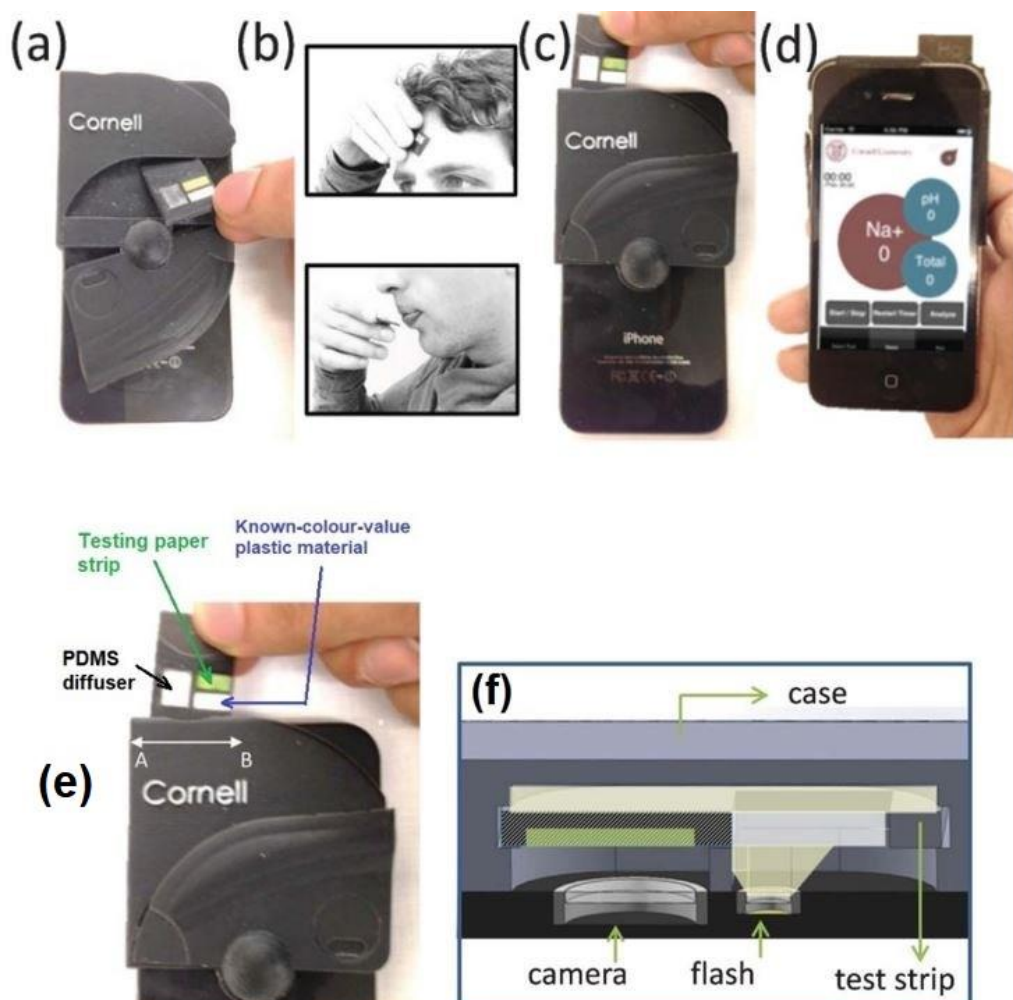


Figure 2.11. (a) A space at the back of the device can store six test strips. Users take out these strips for testing. (b) Users then apply the sweat sample from the forehead or the saliva sample from the tongue onto the paper strip. (c) The strip is then inserted into the prototype for analysis. (d) The app installed on the iPhone analyses the colorimetric measurement and presents the result on

the screen. The figure is an example of the sodium pH level result. (e) Overview of the custom strip being inserted into the device. The custom strip consisted of three components: The PDMS diffuser uniformly distributes the flash-light of the phone's camera to the paper strip and the calibration region; the testing paper strip contains Hydrion Spectral pH indicator for sweat testing (ranging from 5.0 to 9.0) or saliva testing (ranging from 1.0 to 14.0), and the known-colour-value plastic piece is used for calibrating the variations due to the camera or the testing environment's conditions and (f) The cross-section view of the A-B from the left of the figure [50].

Table 2.5. Portable devices using colorimetric method to detect biomarkers in body fluids.

Ref	Biological information	Dry or liquid-based testing	Smartphone or other devices	Light source	Data collecting	Data analysing	Result
[48]	Detect pH level in Urine	Paper test strip	Smartphone (HTC and Blackberry)	White light (5000 K)	Smartphone (CMOS camera)	Computer (MATLAB)	LOD: 0.5 in pH value.
[51]	Monitor Dengue and Chikungunya Viral infections.	Paper test strip.	Customized device.	White light (7500 K)	Raspberry Pi CMOS image sensor module	Computer (MATLAB)	Consistent and accurate in detecting dengue and chikungunya in 30 minutes.
[52]	Detect alpha-fetoprotein and mucin-16 in serum	Customized paper strip.	Smartphone (iPhone 7).	White light (Sunlight).	Smartphone (CMOS camera).	Computer (ImageJ software).	LOD: 1.054 ng/mL for AFP; and 0.413 ng/mL for MUC16.
[21]	Detect bovine	Customized	Smartphone	NA.	Smartphone	Arduino	The system can

	serum albumin in serum.	Customized microfluidic chip.	Smartphone (NA brand).		Smartphone (CMOS camera).	Microcontroller (Custom software).	Immediately present the analysing result of BSA concentration in serum.
[49]	Detect Human epididymis protein 4 biomarker in Urine	Customized microfluidic chip ELISA	Smartphone (Sony Ericson i790)	White light	Smartphone (3.2-megapixel CMOS camera)	Computer (MATLAB).	LOD: 19.5 ng/mL of HE4.
[50]	Detect sodium concentration and enamel decalcification in saliva	Customized paper strip.	Smartphone (iPhone4 and iPhone 4S)	White light (Camera flash)	Smartphone (CMOS camera)	Smartphone (Custom app)	Detect the risk of dehydration and evaluate the impact of dietary changes on the risks of enamel decalcification.
[23]	Detect ascorbic acid in serum.	Liquid test.	Smartphone (Vivo X7).	Custom light source.	Smartphone (CMOS camera).	Smartphone (Custom app).	LOD: 0.4946 μ M for AA in serum.
[53]	Measure nucleic acid	Customized paper strip.	Smartphone.	Smartphone's flashlight	Smartphone (CMOS camera).	Smartphone (Commercial app).	LOD: 0.39 fg/ μ L for RNA in serum.
[53]	Measure urea in urine	Customized paper strip.	Smartphone	NA.	Smartphone (CMOS camera).	Smartphone (Custom app).	LOD: 0.58 mM for urea spiked in human urine sample.

[54]	Measure creatinine in urine	Customized paper strip.	Smartphone	NA.	Smartphone (CMOS camera).	Smartphone (Customized app).	The first time DNBA method was used in paper-based sensors for the determination of creatinine.
------	-----------------------------	-------------------------	------------	-----	---------------------------	------------------------------	---

2.3.2. Conclusion

In summary, as shown in Table 2.5, most developed devices using the colorimetric method in biomarker detection have a similar mechanism, in that the primary light source uses white light, which can be achieved by using the flashlight from the camera through an equipped diffuser. Another critical point in colorimetry evaluation is that this method is preferred to be analysed by an image processing method, due to its output signal's characteristic: the change of colour and its intensity. This is an essential parameter affecting the development of the related POC device.

2.4. The research gap statement

Although there have been many claims of POC devices for CKD monitoring using optical measurements with an emphasis on bio-probe development:

(1) There is lack of solid evidence that the associated hardware is well designed and integrated with consumables and software for practical usage like blood glucose monitors used at home.

(2) The scientific approach and pathway for designing the hardware of POC devices has not been well developed and illustrated to achieve suitable sensitivity, which has been claimed as the advantage of the reported bio-probe.

(3) Development of a multiple biomarker monitoring strategy within a single device has not been demonstrated in the literature, which provides another opportunity here for study.

Therefore, this Ph.D. research tries to fill these above-mentioned gaps to achieve hardware with modular design that can integrate well with consumables and software for effective and accurate monitoring of albumin and creatinine in urine and can be further explored as a platform for multi-biomarker monitoring.

Reference

1. Pham, A.T.T., Wallace, A., Zhang, X., Tohl, D., Fu, H., Chuah, C., Reynolds, K.J., Ramsey, C., and Tang, Y., Optical-Based Biosensors and Their Portable Healthcare Devices for Detecting and Monitoring Biomarkers in Body Fluids. *Diagnostics (Basel)*, 2021. 11(7). DOI: 10.3390/diagnostics11071285.
2. Pham, A.T.T. and Tang, Y., Chapter 5 Point-of-care in vitro diagnostics devices based on aggregation-induced emission biosensors: current situation and future prospective, in *Aggregation-Induced Emission*. 2022. pp. 83-110. DOI: 10.1515/9783110672220-005.
3. Halder, S., Samanta, S., and Das, G., Exploring the potential of a urea derivative: An AIE-luminogen and its interaction with human serum albumin in aqueous medium. *Analyst*, 2019. 144(8): pp. 2696-2703. DOI: 10.1039/c9an00102f.
4. Luo, J., et al., Aggregation-induced emission of 1-methyl-1,2,3,4,5-pentaphenylsilole. *Chem. Commun.*, 2001. 18: pp. 1740-1741. DOI: 10.1039/b105159h.
5. Zhang, Z., Kwok, R.T.K., Yu, Y., Tang, B.Z., and Ng, K.M., Sensitive and Specific Detection of L-Lactate Using an AIE-Active Fluorophore. *ACS Appl Mater Interfaces*, 2017. 9(44): pp. 38153-38158. DOI: 10.1021/acsami.7b10178.
6. Zhu, C., Kwok, R.T.K., Lam, J.W.Y., and Tang, B.Z., Aggregation-Induced Emission: A Trailblazing Journey to the Field of Biomedicine. *ACS Appl Bio Mater.*, 2018. 1(6): pp. 1768-1786. DOI: 10.1021/acsabm.8b00600.
7. Hong, Y., Feng, C., Yu, Y., Liu, J., Wing, J., Lam, Y., Luo, K.Q., and Tang, B.Z., Quantitation, Visualization, and Monitoring of Conformational Transitions of Human Serum Albumin by a Tetraphenylethene Derivative with Aggregation-Induced Emission Characteristics. *Anal Chem.*, 2010. 82(16): pp. 7035-7043. DOI: 10.1021/ac1018028.
8. Gabr, M.T. and Pigge, F.C., Rhenium tricarbonyl complexes of AIE active tetraarylethylene ligands: Tuning luminescence properties and HSA-specific binding. *Dalton Trans.*, 2017. 46(43): pp. 15040-15047. DOI: 10.1039/c7dt03380j.
9. Tu, Y., et al., Specific and Quantitative Detection of Albumin in Biological Fluids by Tetrazolate-Functionalized Water-Soluble AIEgens. *ACS Appl. Mater. Interfaces*, 2019. 11(33): pp. 29619-29629. DOI: 10.1021/acsami.9b10359.
10. Dey, N., Maji, B., and Bhattacharya, S., Motion-Induced Changes in Emission as an Effective Strategy for the Ratiometric Probing of Human Serum Albumin and Trypsin in Biological Fluids.

Chem Asian J., 2018. 13(6): pp. 664-671. DOI: 10.1002/asia.201701795.

11. Bu, F., Zhao, B., Kan, W., Wang, L., Song, B., Wang, J., Zhang, Z., Deng, Q., and Yin, G., A phenanthro[9,10-d]imidazole-based AIE active fluorescence probe for sequential detection of Ag⁺_AgNPs and SCN⁻ in water and saliva samples and its application in living cells. *Spectrochim Acta A Mol Biomol Spectrosc.*, 2019. 223: pp. 1386-1425. DOI: <https://doi.org/10.1016/j.saa.2019.117333>.
12. Su, P., Liang, L., Wang, T., Zhou, P., Cao, J., Liu, W.S., and Tang, Y., AIE-based Tb³⁺ complex self-assembled nanoprobe for ratiometric fluorescence detection of anthrax spore biomarker in water solution and actual spore samples. *Chem. Eng. J.*, 2021. 413. DOI: 10.1016/j.cej.2020.127408.
13. Sanjay, S.T., Fu, G., Dou, M., Xu, F., Liu, R., Qi, H., and Li, X., Biomarker detection for disease diagnosis using cost-effective microfluidic platforms. *Analyst.*, 2015. 140: pp. 7062-7081. DOI: 10.1039/c5an00780a.
14. Shah, P., Zhu, X., and Li, C.Z., Development of paper-based analytical kit for point-of-care testing. *Expert Rev Mol Diagn.*, 2013. 13(1): pp. 83-91. DOI: 10.1586/erm.12.130.
15. Hristov, D.R., Rodriguez-Quijada, C., Gomez-Marquez, J., and Hamad-Schifferli, K., Designing paper-based immunoassays for biomedical applications. *Sensors (Basel)*. 2019. 19(3). DOI: 10.3390/s19030554.
16. Sajid, M., Kawde, A.N., and Daud, M., Designs, formats and applications of lateral flow assay: A literature review. *J. Saudi Chem. Soc.*, 2015. 19: pp. 689-705. DOI: 10.1016/j.jscs.2014.09.001.
17. Xie, H., Wu, Y., Zeng, F., Chen, J., and Wu, S., An AIE-based fluorescent test strip for the portable detection of gaseous phosgene. *Chem Commun (Camb)*. 2017. 53(70): pp. 9813-9816. DOI: 10.1039/c7cc05313d.
18. Jiang, Y., Zhong, Z., Ou, W., Shi, H., and Alam, P., Semi-quantitative evaluation of seafood spoilage using filter-paper strips loaded with an aggregation-induced emission luminogen. *Food Chem.*, 2020. 327: pp. 127056. DOI: 10.1016/j.foodchem.2020.127056.
19. Liu, C., Fang, S., Tian, Y., Wu, Y., Wu, M., Wang, Z., Xu, D., Hou, D., and Liu, Q., An Aggregation-Induced Emission Material Labeling Antigen-Based Lateral Flow Immunoassay Strip for Rapid Detection of Escherichia coli O157 : H7. *SLAS Technol.*, 2021. 26(4): pp. 377-383. DOI: 10.1177/2472630320981935.
20. Adel Ahmed, H. and Azzazy, H.M.E., Power-free chip enzyme immunoassay for detection of

- prostate specific antigen (PSA) in serum. *Biosens Bioelectron.*, 2013. 49: pp. 478-484. DOI: 10.1016/j.bios.2013.05.058.
21. Chen, A., Wang, R., Bever, C.R.S., Xing, S., Hammock, B.D., and Pan, T., Smartphone-interfaced lab-on-a-chip devices for field-deployable enzyme-linked immunosorbent assay. *Biomicrofluidics.*, 2014. 8(6): pp. 1-11. DOI: 10.1063/1.4901348.
 22. Akraa, S., Pham Tran Tam, A., Shen, H., Tang, Y., Tang, B.Z., Li, J., and Walker, S., A smartphone-based point-of-care quantitative urinalysis device for chronic kidney disease patients. *J. Netw. Comput. Appl.*, 2018. 115: pp. 59-69. DOI: 10.1016/j.jnca.2018.04.012.
 23. Kong, L., Gan, Y., Liang, T., Zhong, L., Pan, Y., Kirsanov, D., Legin, A., Wan, H., and Wang, P., A novel smartphone-based CD-spectrometer for high sensitive and cost-effective colorimetric detection of ascorbic acid. *Anal Chim Acta.*, 2020. 1093: pp. 150-159. DOI: 10.1016/j.aca.2019.09.071.
 24. Pohl, H. What is the difference between fluorescence, phosphorescence and luminescence? 2019. Available online: <https://www.enzolifesciences.com/science-center/technotes/2019/december/what-is-the-difference-between-fluorescence-phosphorescence-and-luminescence?/> (Accessed on 09-08-2020).
 25. Taraska, J.W. and Zagotta, W.N., Fluorescence applications in molecular neurobiology. *Neuron*, 2010. 66(2): pp. 170-189. DOI: 10.1016/j.neuron.2010.02.002.
 26. Gillespie, J.B., Maclean, M., Given, M.J., Wilson, M.P., Judd, M.D., Timoshkin, I.V., and MacGregor, S.J., Efficacy of Pulsed 405-nm Light-Emitting Diodes for Antimicrobial Photodynamic Inactivation: Effects of Intensity, Frequency, and Duty Cycle. *Photomed Laser Surg.*, 2017. 35(3): pp. 150-156. DOI: 10.1089/pho.2016.4179.
 27. Jamaludin, J., et al., Analysis on the Performance of Led and Laser Diode with Charge Coupled Device (Ccd) Linear Sensor Measuring Diameter of Object. *J. Teknol. (Sci. Eng.)*, 2015. 77(17). DOI: 10.11113/jt.v77.6418.
 28. Toora, B.D. and Rajagopal, G., Measurement of creatinine by Jaffe's reaction--determination of concentration of sodium hydroxide required for maximum color development in standard, urine and protein free filtrate of serum. *Indian J Exp Biol.*, 2002. 40(3): pp. 352-354.
 29. Agu, E., Pedersen, P., Strong, D., Tulu, B., He, Q., Wang, L., and Li, Y. The smartphone as a medical device: Assessing enablers, benefits and challenges. In *Proceedings of The IEEE International Conference on Sensing, Communications and Networking (SECON)*. 2013. New Orleans, LA, USA: IEEE. DOI: 10.1109/SAHCN.2013.6644964.

30. Mahović Poljaček, S., Tomašegović, T., Leskovšek, M., and Stanković Elesini, U., Effect of SiO₂ and TiO₂ Nanoparticles on the Performance of UV Visible Fluorescent Coatings. *Coatings*, 2021. 11(8). DOI: 10.3390/coatings11080928.
31. Yasuda, R., 3 - Principle and Application of Fluorescence Lifetime Imaging for Neuroscience: Monitoring Biochemical Signaling in Single Synapses Using Fluorescence Lifetime Imaging, in *Nanophotonics*, Editors: Alfano, R.R. and Shi, L.B.T. 2019, Elsevier. pp. 53-64. DOI: <https://doi.org/10.1016/B978-0-323-48067-3.00003-2>.
32. Tagit, O. and Hildebrandt, N., Fluorescence Sensing of Circulating Diagnostic Biomarkers Using Molecular Probes and Nanoparticles. *ACS Sensors*, 2017. 2: pp. 31-45. DOI: 10.1021/acssensors.6b00625.
33. Nimse, S.B., Sonawane, M.D., Song, K.S., and Kim, T., Biomarker detection technologies and future directions. *Analyst*, 2016. 141(3): pp. 740-755. DOI: 10.1039/c5an01790d.
34. Gibbs, J., Vessels, M., and Rothenberg, M., Selecting the Detection System - Colorimetric, Fluorescent, Luminescent Methods for ELISA Assays, in *ELISA Technical Bulletin - No 5*, Corning Life Sciences. 2017, Corning Incorporated: Corning: NY, USA. pp. 1-14.
35. Zhong, W., Nanomaterials in fluorescence-based biosensing. *Anal Bioanal Chem.*, 2009. 394(1): pp. 47-59. DOI: 10.1007/s00216-009-2643-x.
36. Bauwant, R. and Kaur, J., Methods and systems for diagnosing sleep disorders, 2016. U.S., Patent: 15/510,812. 04.01.2018.
37. Zhang, X., Yao, B., Hu, Q., Hong, Y., Wallace, A., Reynolds, K., Ramsey, C., Maeder, A., Reed, R., and Tang, Y., Detection of biomarkers in body fluids using bioprobes based on aggregation-induced emission fluorogens. *Mater. Chem. Front.*, 2020. 4: pp. 2548-2570. DOI: 10.1039/D0QM00376J.
38. Mudanyali, O., Dimitrov, S., Sikora, U., Padmanabhan, S., Navruz, I., and Ozcan, A., Integrated rapid-diagnostic-test reader platform on a cellphone. *Lab Chip*, 2012. 12(15): pp. 2678-2686. DOI: 10.1039/c2lc40235a.
39. Coskun, A.F., Nagia, R., Sadeghia, K., Phillips, S., and Ozcan, A., Albumin testing in urine using a smart-phone. *Lab Chip*, 2013. 13(21): pp. 4231-4238. DOI: 10.1039/c3lc50785h.
40. Jones, S.L., Close, C.F., Mattock, M.B., Jarrett, R.J., Keen, H., and Viberti, G.C., Plasma lipid and coagulation factor concentrations in insulin dependent diabetics with microalbuminuria. *BMJ.*, 1989. 298(6672): pp. 487-490. DOI: 10.1136/bmj.298.6672.487.

41. Huang, C., Ma, R., Luo, Y., Shi, G., Deng, J., and Zhou, T., Stimulus Response of TPE-TS@Eu/GMP ICPs: Toward Colorimetric Sensing of an Anthrax Biomarker with Double Ratiometric Fluorescence and Its Coffee Ring Test Kit for Point-of-Use Application. *Anal Chem.*, 2020. 92(19): pp. 12934-12942. DOI: 10.1021/acs.analchem.0c01570.
42. Wei, Q., Acuna, G., Kim, S., Vietz, C., Tseng, D., Chae, J., Shir, D., Luo, W., Tinnefeld, P., and Ozcan, A., Plasmonics enhanced smartphone fluorescence microscopy. *Sci Rep.*, 2017. 7(1): pp. 1-10. DOI: 10.1038/s41598-017-02395-8.
43. Zhang, C., Kim, J.P., Creer, M., Yang, J., and Liu, Z., A smartphone-based chloridometer for point-of-care diagnostics of cystic fibrosis. *Biosens Bioelectron.*, 2017. 97: pp. 164-168. DOI: 10.1016/j.bios.2017.05.048.
44. Sekine, Y., et al., A fluorometric skin-interfaced microfluidic device and smartphone imaging module for: In situ quantitative analysis of sweat chemistry. *Lab Chip.*, 2018. 18(15): pp. 2178-2186. DOI: 10.1039/c8lc00530c.
45. Alves, I.P. and Reis, N.M., Microfluidic smartphone quantitation of *Escherichia coli* in synthetic urine. *Biosens Bioelectron.*, 2019. 145: pp. 111624. DOI: 10.1016/j.bios.2019.111624.
46. Paterson, A.S., Raja, B., Mandadi, V., Townsend, B., Lee, M., Buell, A., Vu, B., Brgoch, J., and Willson, R.C., A low-cost smartphone-based platform for highly sensitive point-of-care testing with persistent luminescent phosphors. *Lab Chip.*, 2017. 17(6): pp. 1051-1059. DOI: 10.1039/c6lc01167e.
47. Kathiravan, A., Khamrang, T., Dhenadhayalan, N., Lin, K.-C., Ramasubramanian, K., Jaccob, M., and Velusamy, M., Internet of Things-Enabled Aggregation-Induced Emission Probe for Cu²⁺ Ions: Comprehensive Investigations and Three-Dimensional Printed Portable Device Design. *ACS Omega*, 2020. 5(50): pp. 32761-32768. DOI: 10.1021/acsomega.0c05262.
48. Shen, L., Hagen, J.A., and Papautsky, I., Point-of-care colorimetric detection with a smartphone. *Lab Chip*, 2012. 12(21): pp. 4240-4243. DOI: 10.1039/c2lc40741h.
49. Wang, S., Zhao, X., Khimji, I., Akbas, R., Qiu, W., Edwards, D., Cramer, D.W., Ye, B., and Demirci, U., Integration of cell phone imaging with microchip ELISA to detect ovarian cancer HE4 biomarker in urine at the point-of-care. *Lab Chip*, 2011. 11(20): pp. 3411-3418. DOI: 10.1039/c1lc20479c.
50. Oncescu, V., O'Dell, D., and Erickson, D., Smartphone based health accessory for colorimetric detection of biomarkers in sweat and saliva. *Lab Chip*, 2013. 13(16): pp. 3232-3238. DOI: 10.1039/c3lc50431j.

51. Wang, R., Ongagna-Yhombi, S.Y., Lu, Z., Centeno-Tablante, E., Colt, S., Cao, X., Ren, Y., Cárdenas, W.B., Mehta, S., and Erickson, D., Rapid Diagnostic Platform for Colorimetric Differential Detection of Dengue and Chikungunya Viral Infections. *Anal Chem.*, 2019. 91(8): pp. 5415-5423. DOI: 10.1021/acs.analchem.9b00704.
52. Aydindogan, E., Ceylan, A.E., and Timur, S., Paper-based colorimetric spot test utilizing smartphone sensing for detection of biomarkers. *Talanta*, 2020. 208. DOI: 10.1016/j.talanta.2019.120446.
53. Wang, L.X., Fu, J.J., Zhou, Y., Chen, G., Fang, C., Lu, Z.S., and Yu, L., On-chip RT-LAMP and colorimetric detection of the prostate cancer 3 biomarker with an integrated thermal and imaging box. *Talanta*, 2020. 208. DOI: 10.1016/j.talanta.2019.120407.
54. Choi, C.K., Shaban, S.M., Moon, B.S., Pyun, D.G., and Kim, D.H., Smartphone-assisted point-of-care colorimetric biosensor for the detection of urea via pH-mediated AgNPs growth. *Anal Chim Acta*, 2021. 1170: pp. 338630. DOI: 10.1016/j.aca.2021.338630.
55. Lewińska, I., Speichert, M., Granica, M., and Tymecki, Ł., Colorimetric point-of-care paper-based sensors for urinary creatinine with smartphone readout. *Sens. Actuators B: Chem.*, 2021. 340. DOI: 10.1016/j.snb.2021.129915.

CHAPTER 3. ALBUMIN DEVICE – THE OPEN PLATFORM FOR FLUORESCENCE MEASUREMENT

This chapter has been published in the following journal paper, but the clinical result section has been moved to chapter 6 – The clinical result evaluation. The minor points have been modified to suit the harmonic structure of the thesis.

The journal article [1]: Pham, A.T.T.; Tohl, D.; Wallace, A.; Hu, Q.; Li, J.; Reynolds, K.J.; Tang, Y. (2022). Developing a fluorescent sensing based portable medical open-platform - a case study for albuminuria measurement in chronic kidney disease screening and monitoring. *Sensing and Bio-Sensing Research*, 100504, <https://doi.org/10.1016/j.sbsr.2022.100504>

3.1. Introduction

Fluorescence monitoring is a powerful technique in optical based measurement used to detect and evaluate the presence of one or multiple chemical(s) in substances. Although fluorescence monitoring is not as sensitive as electrochemical assays, chemiluminescence detection, surface plasmon resonance (SPR), surface enhanced Raman spectroscopy (SERS) or gel electrophoresis, these techniques require complicated sample preparation, skilfully trained operators, are costly and bulky, and dependent on laboratory equipment [2-6].

Fluorescence monitoring has shown the potential for applications in point-of-care (POC) medical device development due to the small sample volume requirement, the controlled emission time, the high sensitivity, and selectivity, as well as the ability to detect a wide range of biomarkers. In recent years, POC techniques have demonstrated many benefits to users, such as the ability to run tests on-site, immediacy of results facilitating timely clinical decision-making and follow up, significant cost savings, reduced requirement for regular clinic visits, simple sample collection, easier sample storage and transportation conditions, and minimising the potential spread of infection among populations of diseased individuals [7]. There have been numerous reports and research in developing POC medical devices using fluorescence detecting techniques to monitor chemicals or biomarkers in bio-samples. However, these devices encounter some problems, namely, device packaging, lack of adaptability to different situations and limitations in particular conditions of measurement, leading to the fact that most developed POC devices do not progress past laboratory conditions or research applications [8-14]. These devices show potential in detecting specific chemicals. However, during the literature review, these devices face certain challenges, such as packaging, adaptability to different situations, and limitations in specific measurement conditions. As a result, many of the POC devices that have been developed do not advance beyond laboratory conditions or research applications [7, 15]. Consequently, this is an area of active research and

development.

In this study, we establish an open platform to work as a POC fluorescence monitoring device. The open platform can provide suitable optical excitation for the different fluorescence processes, a flexible optical signal detector, either wired or wireless connection for transferring and storing data, as well as a single computer module to locally analyse the fluorescent signal.

3.2. Principle of fluorescence monitoring portable device development

Fluorescence is one type of phenomena of photoluminescence, where molecules are capable of glowing under suitable excitation conditions. For fluorescence, molecules in a specific medium absorb higher energy photons with shorter wavelengths, then emit lower energy photons with longer wavelengths in a critically short time [16]. Not all molecules can satisfy the fluorescence requirements; the specific molecules which have these fluorescence properties are called fluorophores [17]. To achieve a certain fluorescence state, the fluorophores must receive the unique wavelength excitation illumination. Thus, the two most critical parameters requiring attention when investigating fluorescence are the excitation and emission wavelengths. Figure 3.1 shows a system which can provide a light source with a suitable excitation wavelength (λ_{EXC}) for fluorescence, while also equipping a sensor capable of detecting and measuring the emitted fluorescence signal (λ_{EMS}) (Figure 3.1(B3)), the system can be considered as a monitoring platform for the fluorescence signal from the solution (Figure 3.1(B1) and 3.1(B2)). Therefore, the excitation light source and the fluorescent signal sensor are the most essential components in platform development and require detailed investigation.

According to World Health Organization (WHO), a POC medical device should follow the ASSURED criteria, which are affordable (A), sensitive (S), specific (S), user-friendly (U), rapid and robust (R), equipment-free (E) and deliverable to end-users (D). So, the developed platform for fluorescence monitoring should satisfy the requirements of the POC device criteria, as well as the required parameters of the fluorescence measuring system.

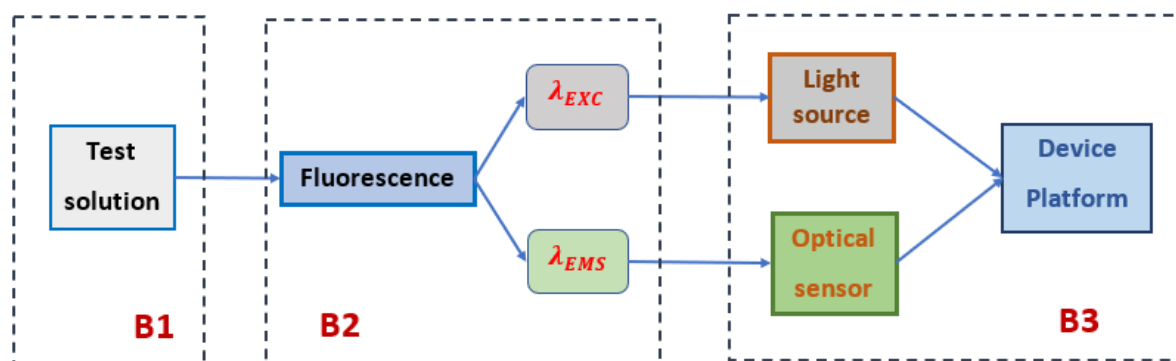


Figure 3.1. Block structure of a general fluorescence monitoring device. Block B1: Test

solution – The target of detection. Block B2: The input requirements for the fluorescence monitoring system design. Block B3: The output of the fluorescence monitoring system design.

3.3. Component design, selection, and optimisation

3.3.1. Solution cuvette selection – The container of the fluorescent target

The proposed platform is developed to examine the fluorescence emitted from a solution, and the desired container will be a commercially available square cuvette type. There are numerous types of cuvettes in the market which vary according to price, dimensions, shape, and hardness as well as optical properties and chemical properties. The decision of the cuvette type depends on the type of chemicals used to provide fluorescence, the optical spectrum, and the affordability of the prototype design. Priority will be given to chemicals that are less hazardous and safe for the end-users.

Commonly, the excitation wavelengths for most solution-based fluorescence measurement ranges from UVA (315 - 400 nm) to the visible spectrum (400 - 700 nm) [16, 18-21]. There are three general types of cuvettes with efficient performance in optical testing with the UVA and the visible spectrums: the quartz cuvette, the glass cuvette, and the plastic cuvette (especially the polystyrol/polystyrene cuvette). Plastic cuvette has the working spectrum of 340-900 nm, normally is a disposal and is not fragile. Glass cuvette has the working spectrum of 400-2500 nm but not suitable for UV range. It is reusable but is fragile. Quartz cuvette has an excellent work spectrum of 190-2500 nm and can be reused, but it is quite expensive and fragile. The chosen cuvette for this study will be the polystyrol/polystyrene (PP) cuvette, which can satisfy the optical requirements of the measurement, as well as being affordable and possessing the common properties for the portable device design. This type of cuvette is affordable at about 0.5 Australian dollar each, and is readily available in the market, which is suitable for disposal use in a POC device. Therefore, the container of the fluorescent solution has been defined for illumination by the excitation light and is also considered as the source for the fluorescence emission.

3.3.2. Light sources selection, design, and evaluation

3.3.2.1. Light source selection

In recent POC device developments, the optical source for the portable device development in this research will be a set of LEDs. Different light LED sources have various luminous areas, in that, the farther from the central axis, the less intensity the light source will emit. The values to be considered are the beam angle and the distance, which establish the luminous area of the light source [22, 23]. The luminous area of the light source should cover the solution in the testing cuvette,

whose dimensions are 10×10×35 mm. Thus, when choosing the LEDs for the light source of the device, those LEDs should be examined for the illumination responses in different angles and distances. An example of the test for three LED sources with varying output intensities is presented here, which will be used in the case study.

As shown in Figure 3.2(A) the luminous areas of the LED 1 and LED 2 (through hole modules with different output intensities) can satisfy the requirement of the luminous section (40 degrees of output beam angle and 35-40 mm of luminous distance). In comparison, LED 3 (surface mount module) shows a critically low intensity. Thus, the LED 1 and LED 2 are the preferred components for selection. However, although the luminous area is undoubtedly a crucial criterion to consider when selecting LEDs for a specific application, it is not the only determinant of their suitability. In fact, the stability of LEDs is an equally significant factor that contributes to the overall choice of LEDs.

3.3.2.2. Light source evaluation

The LED's output power tends to decrease under the effect of temperature and time of usage [24, 25]. This variation will affect the output luminescence, which may lead to an inaccurate optical measurement. The research should ensure this decline will not impact on the measurement or prepare a method of compensating for the effect to maintain the accuracy of the measurement. The three LED sources above were tested to observe the stability of each LED over time and the results are shown in Figure 3.2(B). The target of detection is the fluorescence of the solution under the UV excitation. Thus, in this test, three LED sources were placed to excite the controlled testing solution (400 mg/L of albumin in artificial urine mixed with the fluorescent dye) and the intensity of the fluorescence was measured (Figure 3.2(B)).

From Figure 3.2(B), although LED 1 shows a high intensity, its output varies significantly over 40 minutes of operating. In contrast, LED 3 (surface mount module) has considerable stability, however, its intensity shows a critically low level when compared with the other LED sources. LED 2 not only shows a medium intensity for the fluorescence excitation, but also stays stable in output illumination during the whole testing period. Consequently, LED 2 is the preferred component for the excitation light source in the case study. These processes of testing will be applied for other LED light sources for alternate conditions for the fluorescence measurements.

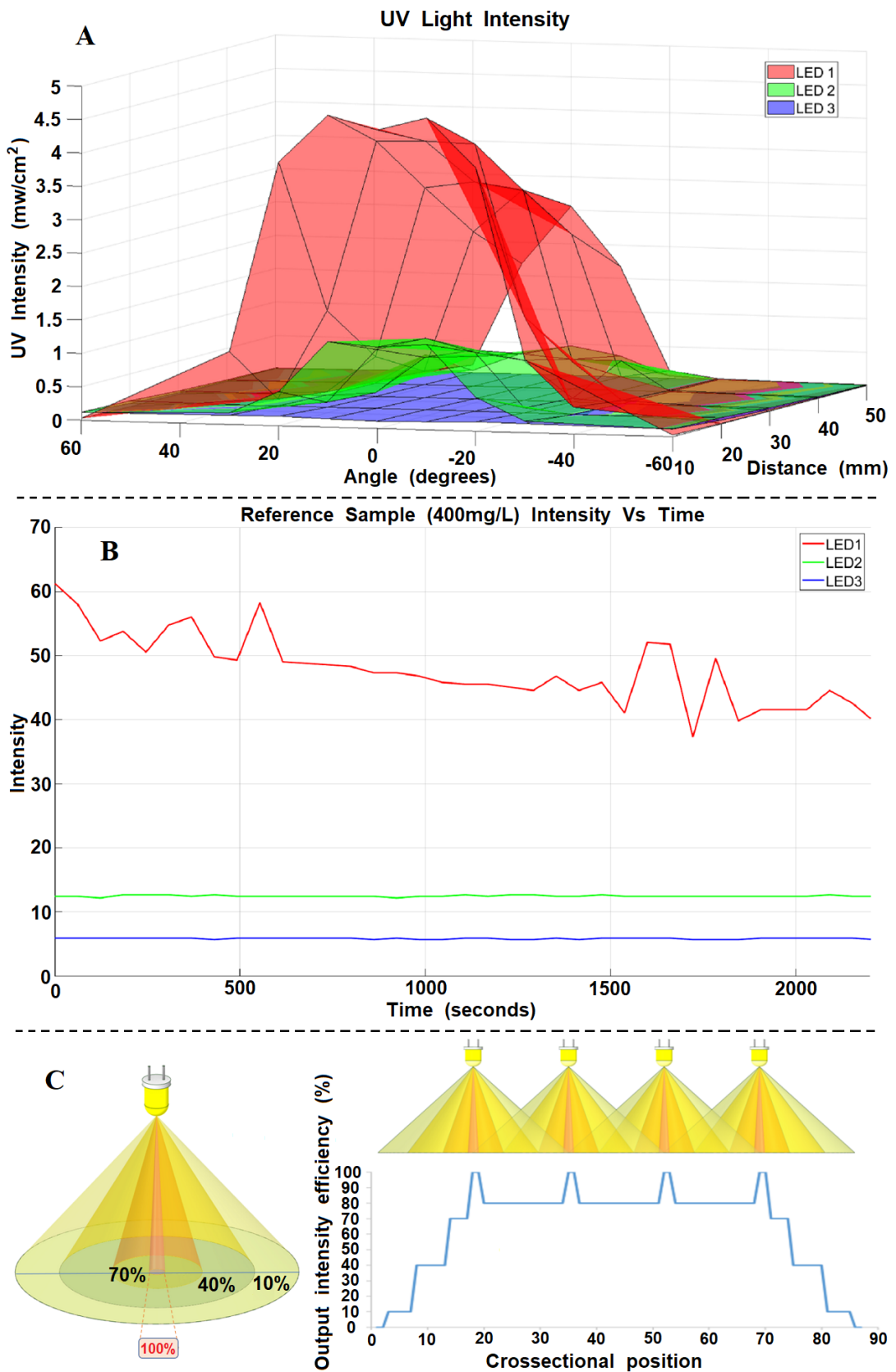


Figure 3.2. (A) The output intensity of three types of LED sources in different testing conditions of beam angles and distances. The LED 1's output has the higher intensity in compared with that of LED 2 and LED 3, respectively. In the distance of 20 mm, the LED 1 also provides a homogenous luminance. Its output starts dropping dramatically from the distance over 30 cm. (B)

The relative output intensities of 3 types of LED sources are tested by using an optical camera to take 42 images of each LED source's operation in 40 minutes. The desired output is the fluorescence light, so the output of the LEDs is observed based on their effect on the reference testing sample, which comprises of albuminuria [400 mg/L] and a fluorescence dye. (C) The illustration of (left) the intensity degradation from a typical LED and (right) the homogeneous intensity compensation of the LED pattern.

After choosing the LED, the uniformity of light distribution should be considered. Generally, through hole LEDs have a narrow light beam, whereby the output intensity is strongest at the central axis and decreases when further from the central axis, as shown in Figure 3.2(C). Using a single LED cannot satisfy the uniform luminescence at the required luminous section. Researchers have come to an idea arranging LEDs in the patterns, expecting the scattering light from different LEDs will resonate to compensate the light degradation [26-28]. Then, a set of LEDs will be arranged in a grid pattern to generate the homogeneous luminous area, as shown in Figure 3.2(C).

A typical commercial LED has the output beam angle of about 30-60 degrees. The distance between the LED source and the cuvette is 20 mm, the proposed LED source will comprise of four LEDs, arranged in a line along the cuvette's vertical axis. With this pattern, the excitation LED source will guarantee to generate a uniform light distribution to the cuvette placed at 20 mm away. Moreover, this compact LED pattern can be imported into a simple printed circuit board (PCB) module, which can be plugged in and out of the device for replacing with various LEDs with the assigned wavelength. Therefore, providing a flexible excitation light source for the POC device.

3.3.3. Luminescent sensor selection and evaluation

3.3.3.1. Selection of luminescent sensor

As technology has improved with time, researchers have applied many high-performance imaging devices into POC device designs, such as complementary CMOS camera, CCD camera, photodiode, optoelectronics, optical fibres, micro-optics, photomultiplier tube (PMT) or optical micro-electro-mechanical systems (MEMS) [24, 29, 30]. One of the most common devices used as optical imaging sensor is smartphone. Equipped with a powerful processor, which can run multiple tasks, from acquiring optical images, transferring wireless data, measuring temperature, or performing complex calculations and analysis, smartphones have appeared in many reports for optical monitoring platform development [31-35]. However, applying smartphones in the POC medical devices requires the consideration from the researcher on some criteria, such as the limited interference with the optical sensor settings, async between the applications and the operating systems and the increased cost for rapid technology development [36, 37]. Alternatively, Raspberry

Pi Camera has been widely used as a fluorescence sensor. It not only can take 8-megapixel images, but also has an affordable market price (about 25 AUD), is light weight and has a compact size (32×32 mm for PCB module). The Raspberry Pi camera is controlled by an open script, which allows users to freely modify the settings of the imaging sensor to suit the requirements of the optical measurement. Furthermore, the Pi camera also satisfies the optical requirement of the fluorescence measurement, in that, its sensitivity spreads along the whole visible spectrum, which covers most of the fluorescence spectrum emitted from the solution chemicals. In this study, Raspberry Pi camera v2.0 has been selected as the fluorescence sensor for the platform.

3.3.3.2. Mechanism of fitting the camera sensitivity with fluorescence in different wavelengths

The Raspberry Pi camera can capture the whole visible spectrum with an output of three discrete values representing the RGB colour system at each pixel. The sensitivity of the camera in the three RGB channels varies at different wavelengths, as shown in Figure 3.3. It can be seen that the Raspberry Pi camera is most sensitive to the RGB colours at the wavelengths of 600 nm, 520 nm and 460 nm, respectively. As only a single intensity value of the emitted fluorescence light is required, this can be estimated based on the sensitivity of the camera at the emission wavelength. The weighted average of the three RGB components is as follows:

$$y = aR + bG + cB \quad (3.1)$$

where R, G and B are the red, green, and blue intensity values in the image and a, b and c are the coefficients corresponding to the sensitivity of the camera at each wavelength.

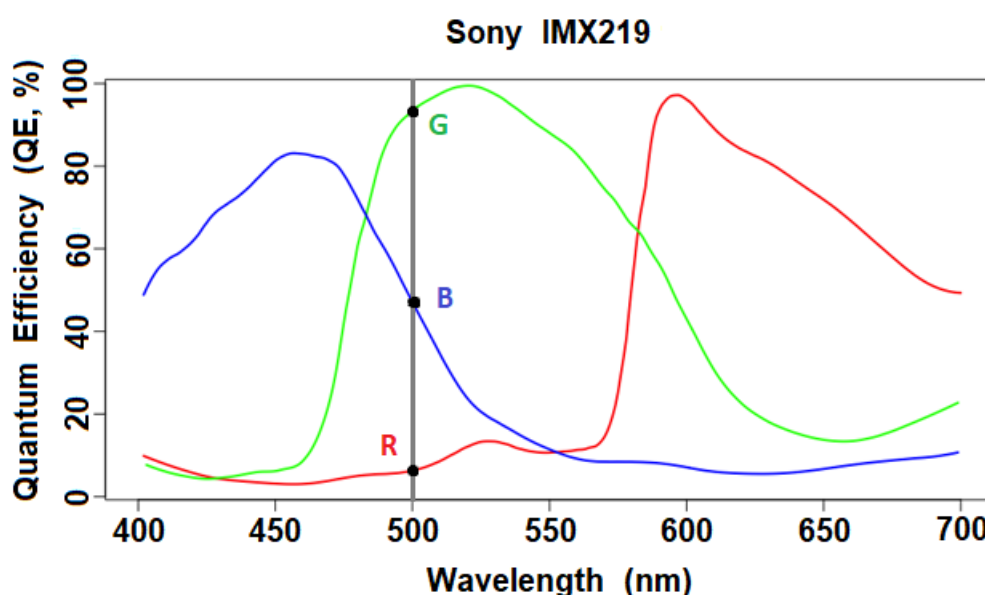


Figure 3.3. The sensitive response of the Raspberry Pi Camera v2.0 in terms of the red,

green, and blue colours. (From the manufacturer's datasheet).

For example, in Figure 3.3, the grey line shows the camera sensitivity at a fluorescence emission wavelength of 500 nm. The sensitivity in the camera's response to the red, green, and blue channels is 5%, 95% and 45%, respectively, this gives values for the a, b and c coefficients as follows:

$$a = \frac{5}{(5+95+45)} = 0.03 \quad (3.2)$$

$$b = \frac{95}{(5+95+45)} = 0.66 \quad (3.3)$$

$$c = \frac{45}{(5+95+45)} = 0.31 \quad (3.4)$$

Substituting these values into Equation (3.1) gives the intensity of fluorescence at the wavelength of 500 nm. Adjusting the a, b and c coefficients based on the sensitivity of the camera's response at different wavelengths allows the weighted average to be tuned to the specific wavelength of the emitted fluorescence signal.

3.4. Platform fabrication

The developed fluorescence measuring device has three functional blocks: (1) The fluorescence principal platform, (2) the microcontroller unit, and (3) data storage and display. All components are supported by the 3D printed solid hardware for the positioning, the measuring environment, the optical hazard, and electronic component protections for users.

3.4.1. The fluorescence principal platform

This is the most important block for the developed open platform, the device will use a set of 4 LEDs for the excitation light source and the Raspberry Pi Camera v2.0 for the output signal detector. From the principle of the typical fluorescence measuring system, the excitation light source, the solution container and the optical image sensor are arranged so that the excitation light from the LED source to the solution cuvette will be in 90 degrees with the fluorescence emitted from the solution toward the camera, reducing the optical noise, as shown in Figure 3.4(A) [8, 34]. This arrangement prevents the imaging sensor from accidentally capturing the interference of the transmitting light from the LED source. The proposed device is presented in Figure 3.4(B), the distance between the LED module and the solution cuvette is 20 mm, which ensures that the cuvette can receive the homogenous excitation light distribution. Furthermore, the Raspberry Pi camera is placed at 50 mm away from the solution cuvette, which not only keeps the cuvette in the focal length

of the camera to guarantee the quality of the taken images, but also minimises the dimensions of the whole device to satisfy the portable requirements of the POC device.

The proposed device is built with double cuvettes and double LED modules, as shown in Figure 3.4(B). The two LED modules have the same design and components to generate similar excitation light for both cuvettes. They are built as plug-and-play components to provide the flexibility of exchanging LED modules to suit different excitation wavelength requirements. Meanwhile, the two cuvette positions will contain different components, in that, position 1 holds the testing solution cuvette, and the position 2 holds a reference component. This reference component is the blank sample, prepared when working with the real urine samples to measure the auto-fluorescence in the urine (Refer to the supporting information for clinical evaluation in chapter 6). Both cuvettes are designed to stay in the middle of the camera field of view and will be captured simultaneously in the images, which then will be analysed to determine the fluorescence intensity.

The fluorescence principal platform with all components is built in a dark-room-like environment, as shown in Figure 3.4(C). This section is a component fabricated by 3D printing with the dimensions of 49×65×51 mm. The component is made from polylactic acid, which is the least expensive material for 3D printing and quite common in the market for medical application. In addition, this component is made in one printed piece and covered in black coating. The black surfaces are ideal to stop any reflections of the fluorescent light within the environment and the one-piece design stops any external light from the outside environment interfering with the measurement. Therefore, the Raspberry Pi camera will only capture the direct fluorescence emitted from the solution. All of these design criteria aim to maximize the quality of the fluorescence signal collection, improving the accuracy and precision of the result. Some of the detail information regarding platform design and fabrication, please refer to the later supporting section of this chapter.

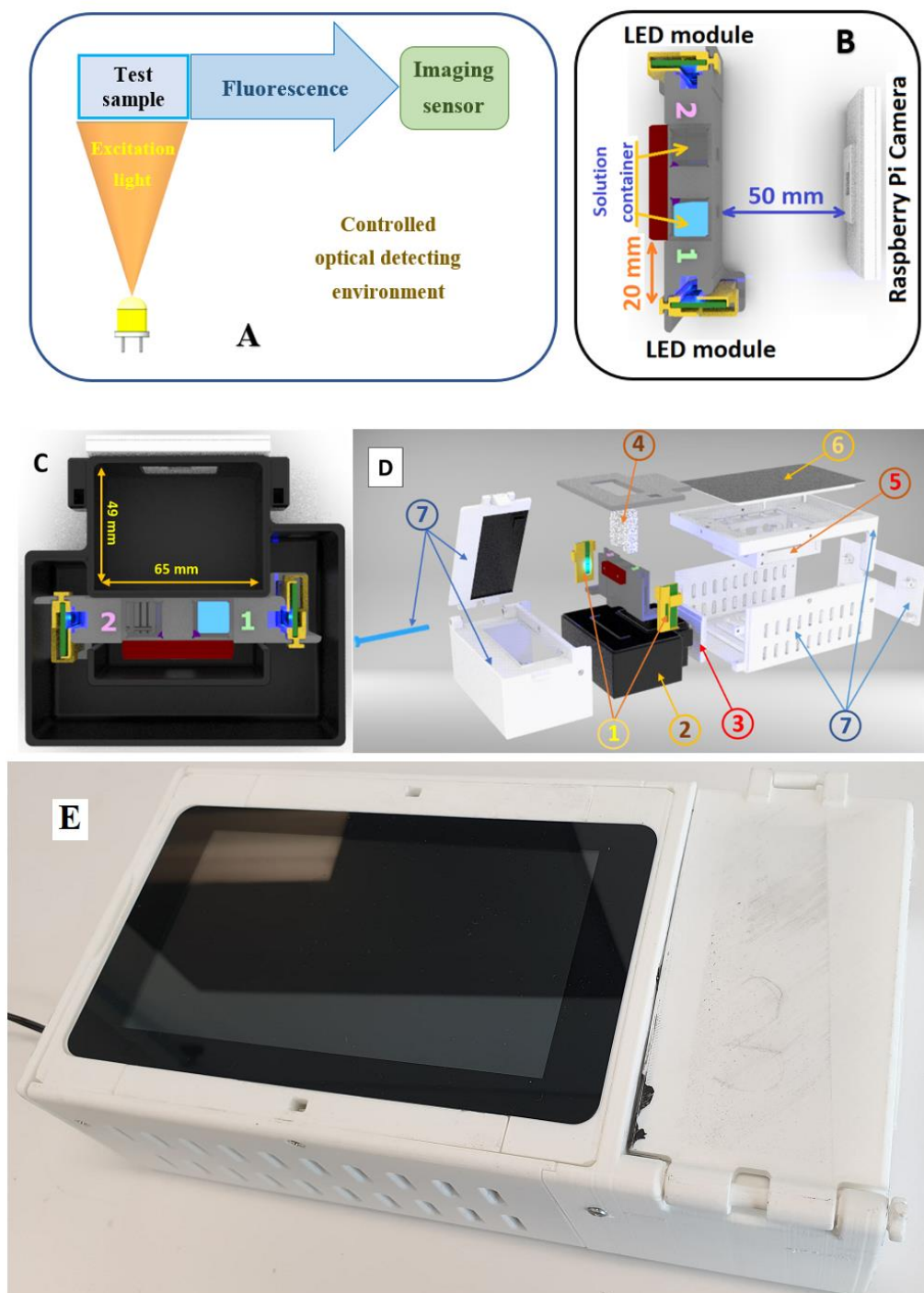


Figure 3.4. (A) Arrangement diagram of the excitation light source, the solution container, and the output imaging sensor. The incident excitation light and the emission fluorescence are in angle of 90 degrees, (B) The sketch of the optical monitoring device following the principle of fluorescence measuring, (C) The dark-room-like environment, (D) The structure of the developed fluorescence measuring platform: (1) Two LED modules; (2) The dark-room-like environment; (3) The Raspberry Pi Camera; (4) The testing solution cuvettes; (5) The Raspberry Pi module; (6) The Raspberry Pi touchscreen; and (7) The 3D printed solid supports and covers, and (E) The optical monitoring device in overview.

3.4.2. Microcontroller unit, data storage and display

The main electronic controller of the platform is the Raspberry Pi module. This single computer module is embedded inside the device to supply and manage power of the LED modules, the Pi camera, and the Raspberry Pi 7-inch touchscreen. This Pi module can be powered by the external 5 V adapter through the micro-USB type B port, or by the 3.7 V 2500 mAh lithium polymer battery module, depending on the working conditions of the testing area. In addition, this Pi module is built with the 64-bit Quad Core CPU, making the device able to run the image analysis without requiring an external computer. The users interact with the device through a 7-inch touchscreen, which guides them through the measurement process, as well as presenting the results. Moreover, the on-board Bluetooth 4.1 Wi-fi, the MicroSD card support, 4 USB ports and 10/100 LAN port provide many options for users to store the results, transfer results to an external computer or upload results to an online digital cloud. This allows users to communicate and consult with their healthcare specialists and discuss the appropriate therapy for their kidney's health conditions. Being integrated with numerous specifications brings the developed device closer to the end-users in rural areas or developing countries, where conditions are inconvenient for visiting a hospital or clinic regularly.

3.5. The pre-test of the prototype on measuring Albumin in the artificial urine sample

3.5.1. Idea of confirming the open platform's performance

A fluorescence monitoring open platform has been built, which is flexible to detect and evaluate the fluorescent signal in different optical conditions, such as various wavelengths of excitation and emission light. In this section, the developed platform has been used to examine the fluorescence signal of a particular biomarker in biofluid samples. The chosen biomarker is human serum albumin (HSA) in a urine sample. Urine albumin is a biomarker which can be used in detection and monitoring of chronic kidney disease (CKD). Clinically, there is minimal albumin excreted in urine (<30 mg/day) in a healthy person. Albumin can be secreted into the urine through the dysfunction of the kidney filtration barrier [38]. The current definition of microalbuminuria (MA) is an amount of urinary albumin greater than 30 to 300 mg/24 hours. Macroalbuminuria, on the other hand, is classified as greater than 300 mg/24 hours. Persistent albuminuria is an indication for kidney disease. If albuminuria is present, aggressive measures should ensue with the ultimate goal of slowing the progression of CKD and decreasing the risk of cardiovascular complications [39].

In the fluorescence method to detect albumin in urine, researchers use a specific recognising reagent, which reacts with albumin and emits the fluorescence signal for detection under a certain excitation condition. One effective technique to enhance the fluorescence measurement is using Aggressive Induced Emission (AIE) bio-probes, which provides a high sensitivity, accuracy, large

Stokes shift, and excellent stability of fluorescence evaluations [40]. Thanks to those highlighted features, AIE bio-probe development brings a lot of benefits to healthcare research in recent years, especially, in portable diagnosis device development [41]. In this project, two reported fluorescent probes, TPE-4TA and TC426 [42], are used as the recognising reagents to detect HSA in the urine samples. These two chemicals have been chosen for their selectivity, sensitivity, and accuracy in measuring HSA in urine samples with the limit of detections of TPE-4TA and TC426 to be 14.2 µg/L and 253 µg/L, respectively [42]. The reason for using these two reagents is because of their different working conditions, in that, TPE-4TA requires the excitation of 365 nm wavelength to emit the fluorescence of 470 nm; meanwhile TC426 needs the excitation of 480 nm to trigger the emission of 550 nm fluorescence, please refer to the supporting information at the end of this chapter. By using the developed open platform to evaluate the presence of HSA in urine samples using different reagents, it will be shown that the device satisfies the design requirements as an open platform.

3.5.2. Evaluation of the flexibility of the open-platform in measuring fluorescence to monitor biomarker in body fluids

In this stage, the device will perform the albuminuria measurements using the above two fluorescent probes. The biological samples used in the experiments are artificial urine (AU). All chemicals used for making AU are purchased from Sigma-Aldrich, Australia. Microalbuminuria, the albumin presenting in urine, is commonly diagnosed by elevated protein concentration (30-300 mg/L) in the urine [38]. Thus, in this experiment, we will evaluate the artificial urine samples spiking with HSA to create the samples of HSA/AU in the range of 0 - 400 mg/L (0, 25, 50, 100, 200 and 400 mg/L, respectively) with the expectation that the device can detect the change of albumin concentration in the clinical testing range.

Two set of HSA/AU samples with the above concentrations will be prepared simultaneously. The concentrations of the fluorescent probes are prepared to be TPE-4TA [10 mg/L] and TC426 [4.65 mg/L]. TPE-4TA is mixed in the sample set 1, and TC426 is mixed in the sample set 2. Both mixing sample sets are tested with a fluorescence spectroscopy (Cary Eclipse, Australia) and then tested by the developed device. To provide the suitable wavelength for each fluorescent probe, two pairs of LED modules were prepared: the 365 nm ultraviolet (UV) LED module and the 480 nm blue LED module. Due to the plug-and-play LED module design, the LED modules can be easily replaced to provide the different excitation wavelengths when starting the tests with the specific fluorescent probes. In the developed device, the Raspberry Pi camera will take images of the fluorescent samples and the software integrated in the Raspberry Pi module will analyse these images. The relative results between the fluorescence intensity and the real concentration of HSA/AU will be displayed on the touchscreen of the device. The results from the device will be compared with the ones obtained from the fluorescence spectroscopy to observe the performance of the developed device.

After the incubation time of 30 minutes for mixtures of TPE-4TA and 10 minutes for the TC426, the sets of samples are tested in the fluorescence spectroscopy. The excitation wavelengths and the emission scanning spectrums are set to be 365 nm and 400-600 nm for TPE-4TA, and 480 nm and 500-700 nm for TC426, respectively. Then, the sets of samples are placed into the open platform to measure the fluorescence intensity. The 365 nm UV LED module is used in the platform when testing the TPE-4TA mixtures, and the 470 nm blue LED module is used to test the TC426 mixtures. After obtaining the results from the device and the fluorescence spectroscopy, they are compared to examine the response of the developed device, as shown in Figure 3.5(A) and Figure 3.5 (B).

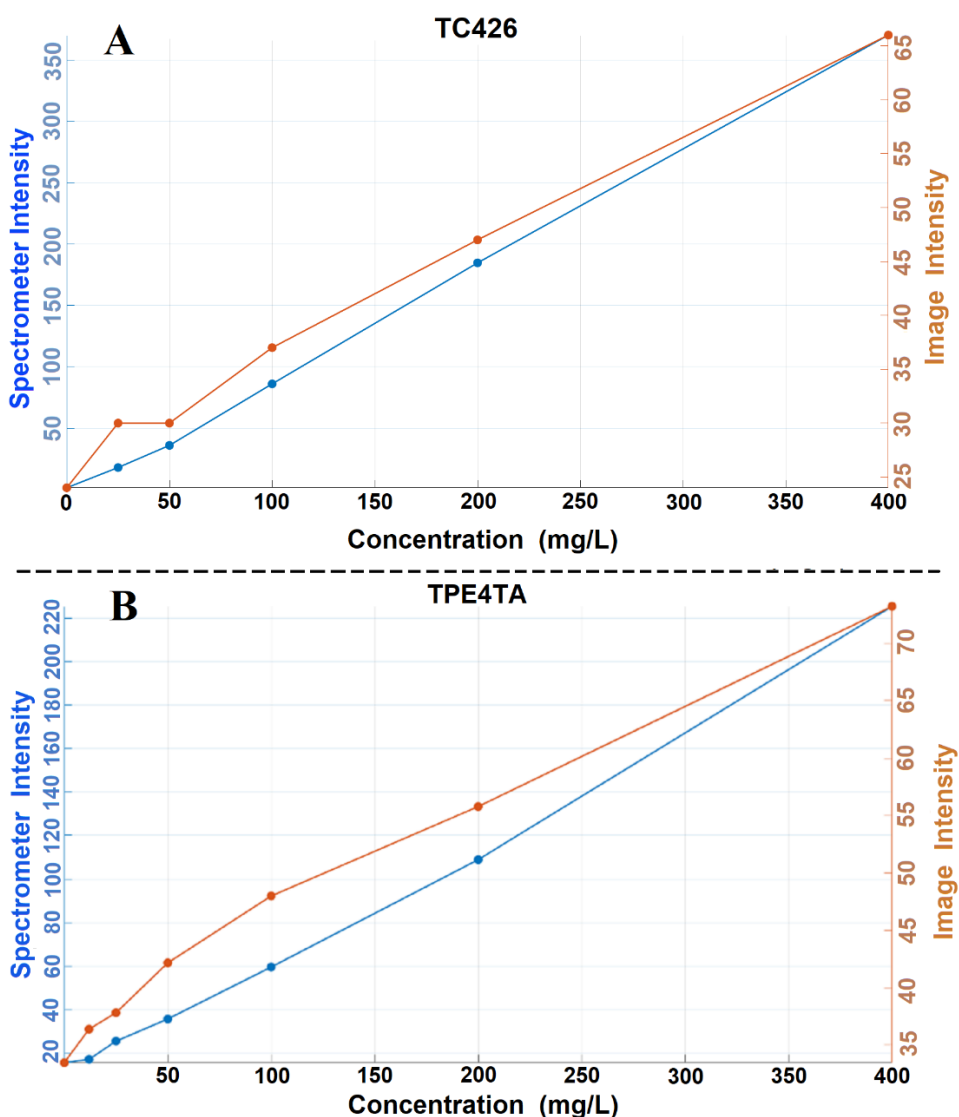


Figure 3.5. The results obtained by the fluorescence spectroscopy (the blue curves) and the

developed open platform (the red curves) from the experiment using (A) TC426 and (B) TPE-4TA.

3.6. Conclusion

From the comparison, the device shows a consistent response with the commercial fluorescence spectroscopy in measuring fluorescence to monitor the HSA level in the urine samples. This result confirms the flexible criteria of the platform in that it provides the consistent responses in measuring one type of biomarkers in artificial urine samples under different conditions for the optical measurements. Furthermore, the developed platform can detect the variations of HSA level down to 25 mg/L, lower than the clinical detection threshold of CKD (30 mg/L), providing an opportunity for early detection of CKD. In the next progress, the open-platform will be evaluated through a clinical process, which will be described in Chapter 6.

3.7. Supporting information for Fluorescence Monitoring Device Development

3.7.1. The platform designing information

The light sources of the device are two LED modules, which contain four 5 mm through-hole LEDs each. The four LEDs are aligned in a vertical line with a distance between adjacent LEDs of 1 mm. The expected output angle of the light beam is over 60 degrees. The luminance boundary of the LED light aims to cover the field between 20 and 30 mm from the LEDs head, which will be the position of the chemical container. In addition, the platform is designed so that the LED modules can be simply swapped with a different LED module when a different excitation wavelength is required. Depending on the measurements, users can purchase different light source modules and replace them by themselves, which helps them to save their resources of time and effort from contacting technical staffs.

The cuvette used in the device is the SARSTEDT polystyrene cuvette with four clear sides and dimensions of 45×45×12 mm. When the cuvette is filled with the mixture of the urine sample containing albumin and the recognising chemical, and placed under a suitable excitation light, there will be fluorescence emitted in every direction from the cuvette. The target of detection is the fluorescence rays emitted in the direction of 90 degrees from the excitation beam, as shown in Figure 3.4(B). In the device, two cuvettes are used: one to hold the test sample and one to hold a reference sample to provide a referencing value among different measurements. This configuration permits the image acquisition of both samples concurrently. The windows to each cuvette are separated by 18 mm, as shown in Figure. 3.6.

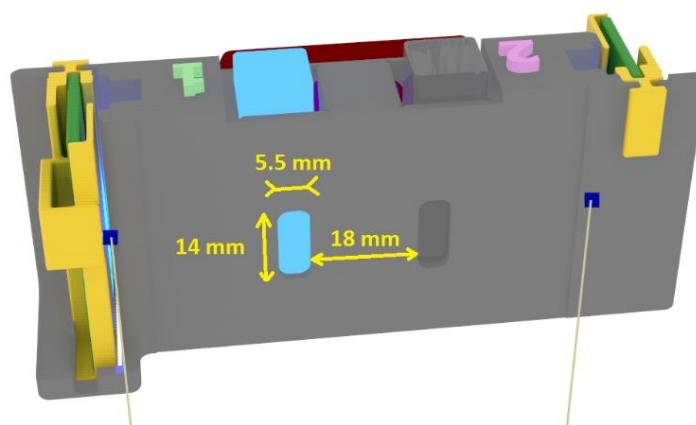


Figure 3.6. The light source-cuvette holder. The 3D printed component is one base keeping the distance between the light source modules and the chemical cuvettes to be 20 mm. On the cuvettes' sides facing to the camera, there are two rectangular windows with dimensions of 5.5×14 mm, allowing the camera to only capture the fluorescence from the cuvette without collecting the reflecting excitation light from the light sources. These fluorescence windows are placed 18 mm apart from each other to minimize the optical interference.

The Raspberry Pi Camera v2.0 is used as a fluorescent image sensor to capture the emitted fluorescence from the chemical cuvette. The Pi camera is placed at 50 mm away from the solution cuvette with a 90-degree angle to the excitation light to prevent noise from the LED source, as shown in Figure 3.4(C). Two important processes for the fluorescent measurement are the activation by the excitation wavelength and the image capture, these processes play an essential role in achieving an accurate and reliable result. Both processes are quite sensitive to the optical interference, such as environmental light or light leakage from other electrical components. Therefore, these processes and their relative components are held in a dark room like environment. The 3D printed component is fabricated for this purpose, as shown in Figure 3.4(C) and 3.4(D). To improve the quality of the optical measurement, this dark room like component is painted in black to achieve the homogenous fluorescence transmission from the chemical cuvettes to the Raspberry Pi camera.

The main controller of the device is the Raspberry Pi model 3B+. It is powered by the external 5V adapter through the micro-USB type B port, or by the 3.7V - 2500 mAh lithium polymer battery module, which helps to improve the portability of the device. The Raspberry Pi module can manage the power supply for all other electronic components in the device, such as the LED source, the Raspberry Pi camera, and the 7-inch touchscreen. This Raspberry Pi module is attached under the Raspberry Pi 7-inch touchscreen, which provides the interface for inputting the relevant data for the measurements; the user's information; presenting the guide for users to operate the device; and extracting the analysed results of the measurements and transferring the captured images from the devices to the external storages. The positions of these components are secured by the 3D printed

supporters.

The 3D printed supporters create the structural frame for the device. The structural frame comprises of four parts: (1) The dark-room protector; (2) The main body cover; (3) The Raspberry Pi module and touchscreen protector; and (4) The communication-port lid, as shown in Figure 3.4(D). The dark-room protector surrounds the dark-room component. It has a top lid to access the solution section in the dark-room component, as shown in Figure 3.4(D). There is a safety switch on the LED board, which only allows the light sources and the device to operate when the top-lid is entirely closed. This function protects the users from being exposing the UV light sources, as well as preventing the device from taking measurements while there may be interference from other environmental light sources. The main body cover is perforated with a grid of rectangular holes to aid in heat dissipation during the operation while ensuring connectivity and protecting the electronics inside. The Raspberry Pi module and touchscreen protector keeps the touchscreen and the Raspberry Pi module connected, protecting the electronic wirings, as well as supporting the screen to prevent damage. The communication-port lid is a rectangular piece equipped at the end of the device, providing accesses to power supply, USB and Ethernet ports, allowing users to use an external hard drive to store the collected data and captured images, or transfer the data through a network cable. The structural frame has four main functions: (1) Secure the positions of all optical components to meet the requirements for the optical measurements; (2) Protect the optical measurement from interfering from the external environment; (3) Protect the internal components from external impacts; and (4) Protect the users from optical hazards in the case a UV light source is required to provide the excitation wavelength.

3.7.2. The structure of the AIE probes: TPE-4TA and TC426

In this report, two AIE bio-probes, TPE-4TA and TC426, are used as the recognising reagents to detect HSA in urine samples.

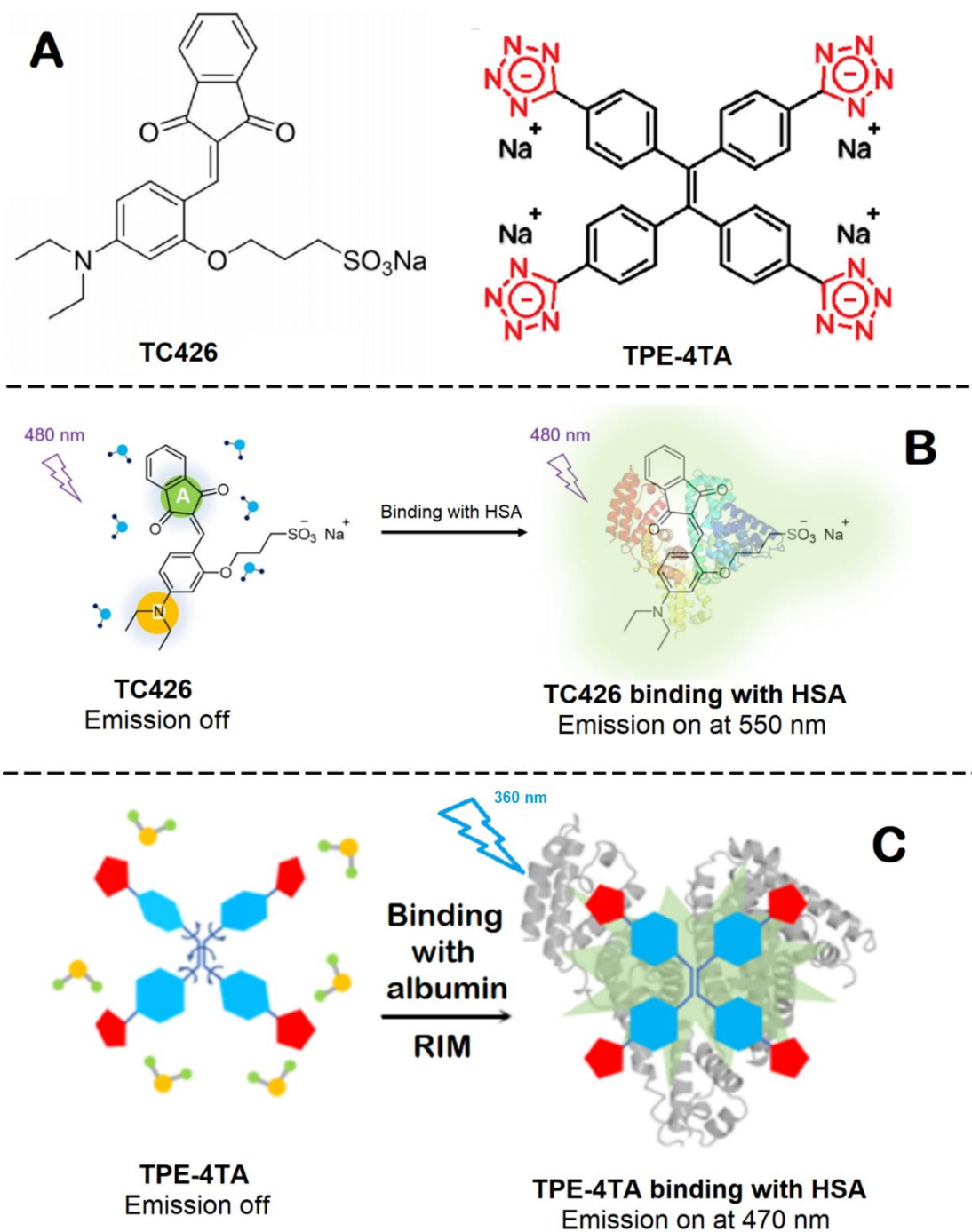


Figure 3.7. (A) Sketches of chemical structures of TPE-4TA and TC426; (B) TC426 is non-emissive without HSA, and will emit a 550 nm fluorescence when binding with HSA under the excitation of 480 nm light; (C) TPE-4TA is non-emissive without HSA, and will emit a 470 nm fluorescence when binding with HSA under the excitation of 360 nm UV [42].

These two AIE probes have different features of excitation requirement and emission wavelength, shown in Table 3.1:

Table 3.1. Fluorescent probes excitation and emission peak wavelengths.

Probe	TPE-4TA	TC426
Excitation (nm)	365	480
Fluorescence emission (nm)	450 - 500	550

Reference

1. Pham, A.T.T., Tohl, D., Wallace, A., Hu, Q., Li, J., Reynolds, K.J., and Tang, Y., *Developing a fluorescent sensing based portable medical open-platform - a case study for albuminuria measurement in chronic kidney disease screening and monitoring*. Sens. Bio-Sens. Res., 2022. **37**. DOI: 10.1016/j.sbsr.2022.100504.
2. Barati, A., Shamsipur, M., and Abdollahi, H., *Hemoglobin detection using carbon dots as a fluorescence probe*. Biosens Bioelectron., 2015. **71**: pp. 470-475. DOI: 10.1016/j.bios.2015.04.073.
3. Han, G.C., Su, X., Hou, J., Ferranco, A., Feng, X.Z., Zeng, R., Chen, Z., and Kraatz, H.B., *Disposable electrochemical sensors for hemoglobin detection based on ferrocenoyl cysteine conjugates modified electrode*. Sens. Actuators B: Chem., 2019. **282**: pp. 130-136. DOI: 10.1016/j.snb.2018.11.042.
4. Liu, Y., Wang, Y., Jiang, K., Sun, S., Qian, S., Wu, Q., and Lin, H., *A persistent luminescence-based label-free probe for the ultrasensitive detection of hemoglobin in human serum*. Talanta, 2020. **206**. DOI: 10.1016/j.talanta.2019.120206.
5. Mozammal Hossain, M.D., Moon, J.M., Gurudatt, N.G., Park, D.S., Choi, C.S., and Shim, Y.B., *Separation detection of hemoglobin and glycated hemoglobin fractions in blood using the electrochemical microfluidic channel with a conductive polymer composite sensor*. Biosens Bioelectron, 2019. **142**. DOI: 10.1016/j.bios.2019.111515.
6. Yang, Q., Li, J., Wang, X., Xiong, H., and Chen, L., *Ternary Emission of a Blue-, Green-, and Red-Based Molecular Imprinting Fluorescence Sensor for the Multiplexed and Visual Detection of Bovine Hemoglobin*. Anal Chem., 2019. **91**(10): pp. 6561-6568. DOI: 10.1021/acs.analchem.9b00082.

7. Senf, B., Yeo, W.H., and Kim, J.H., *Recent Advances in Portable Biosensors for Biomarker Detection in Body Fluids*. Biosensors (Basel). 2020. **10**(9): pp. 1-23. DOI: 10.3390/BIOS10090127.
8. Akraa, S., Pham Tran Tam, A., Shen, H., Tang, Y., Tang, B.Z., Li, J., and Walker, S., *A smartphone-based point-of-care quantitative urinalysis device for chronic kidney disease patients*. J. Netw. Comput. Appl., 2018. **115**: pp. 59-69. DOI: 10.1016/j.jnca.2018.04.012.
9. Alves, I.P. and Reis, N.M., *Microfluidic smartphone quantitation of Escherichia coli in synthetic urine*. Biosens Bioelectron., 2019. **145**: pp. 111624. DOI: 10.1016/j.bios.2019.111624.
10. Coskun, A.F., Nagia, R., Sadeghia, K., Phillips, S., and Ozcan, A., *Albumin testing in urine using a smart-phone*. Lab Chip, 2013. **13**(21): pp. 4231-4238. DOI: 10.1039/c3lc50785h.
11. Huang, C., Ma, R., Luo, Y., Shi, G., Deng, J., and Zhou, T., *Stimulus Response of TPE-TS@Eu/GMP ICPs: Toward Colorimetric Sensing of an Anthrax Biomarker with Double Ratiometric Fluorescence and Its Coffee Ring Test Kit for Point-of-Use Application*. Anal Chem., 2020. **92**(19): pp. 12934-12942. DOI: 10.1021/acs.analchem.0c01570.
12. Paterson, A.S., Raja, B., Mandadi, V., Townsend, B., Lee, M., Buell, A., Vu, B., Brgoch, J., and Willson, R.C., *A low-cost smartphone-based platform for highly sensitive point-of-care testing with persistent luminescent phosphors*. Lab Chip., 2017. **17**(6): pp. 1051-1059. DOI: 10.1039/c6lc01167e.
13. Wei, Q., Acuna, G., Kim, S., Vietz, C., Tseng, D., Chae, J., Shir, D., Luo, W., Tinnefeld, P., and Ozcan, A., *Plasmonics enhanced smartphone fluorescence microscopy*. Sci Rep., 2017. **7**(1): pp. 1-10. DOI: 10.1038/s41598-017-02395-8.
14. Zhang, C., Kim, J.P., Creer, M., Yang, J., and Liu, Z., *A smartphone-based chloridometer for point-of-care diagnostics of cystic fibrosis*. Biosens Bioelectron., 2017. **97**: pp. 164-168. DOI: 10.1016/j.bios.2017.05.048.
15. Omidfar, K., Ahmadi, A., Syedmoradi, L., Khoshfetrat, S.M., and Larijani, B., *Point-of-care biosensors in medicine: a brief overview of our achievements in this field based on the conducted research in EMRI (endocrinology and metabolism research Institute of Tehran University of medical sciences) over the past fourteen years*. J Diabetes Metab Disord., 2020: pp. 1-5. DOI: 10.1007/s40200-020-00668-0.
16. Taraska, J.W. and Zagotta, W.N., *Fluorescence applications in molecular neurobiology*. Neuron, 2010. **66**(2): pp. 170-189. DOI: 10.1016/j.neuron.2010.02.002.

17. Yasuda, R., *3 - Principle and Application of Fluorescence Lifetime Imaging for Neuroscience: Monitoring Biochemical Signaling in Single Synapses Using Fluorescence Lifetime Imaging*, in *Nanophotonics*, Editors: Alfano, R.R. and Shi, L.B.T. 2019, Elsevier. pp. 53-64. DOI: <https://doi.org/10.1016/B978-0-323-48067-3.00003-2>.
18. Gibbs, J., Vessels, M., and Rothenberg, M., *Selecting the Detection System - Colorimetric, Fluorescent, Luminescent Methods for ELISA Assays*, in *ELISA Technical Bulletin - No 5, Corning Life Sciences*. 2017, Corning Incorporated: Corning: NY, USA. pp. 1-14.
19. Nimse, S.B., Sonawane, M.D., Song, K.S., and Kim, T., *Biomarker detection technologies and future directions*. *Analyst*, 2016. **141**(3): pp. 740-755. DOI: 10.1039/c5an01790d.
20. Tagit, O. and Hildebrandt, N., *Fluorescence Sensing of Circulating Diagnostic Biomarkers Using Molecular Probes and Nanoparticles*. *ACS Sensors*, 2017. **2**: pp. 31-45. DOI: 10.1021/acssensors.6b00625.
21. Zhong, W., *Nanomaterials in fluorescence-based biosensing*. *Anal Bioanal Chem.*, 2009. **394**(1): pp. 47-59. DOI: 10.1007/s00216-009-2643-x.
22. Wang, K., Luo, X., Liu, X., Zhou, B., Gan, Z., and Liu, S., *Optical analysis of an 80-W light-emitting-diode street lamp*. *Opt Eng.*, 2008. **47**(1). DOI: <https://doi.org/10.1117/1.2835010>.
23. Dong, J., van Driel, W., and Zhang, G., *Automatic diagnosis and control of distributed solid state lighting systems*. *Opt Express*, 2011. **19**(7): pp. 5772-5784. DOI: 10.1364/OE.19.005772.
24. Jamaludin, J., et al., *Analysis on the Performance of Led and Laser Diode with Charge Coupled Device (Ccd) Linear Sensor Measuring Diameter of Object*. *J. Teknol. (Sci. Eng.)*, 2015. **77**(17). DOI: 10.11113/jt.v77.6418.
25. Liang, B., Wang, Z., Qian, C., Ren, Y., Sun, B., Yang, D., Jing, Z., and Fan, J., *Investigation of Step-Stress Accelerated Degradation Test Strategy for Ultraviolet Light Emitting Diodes*. *Materials (Basel)*, 2019. **12**(19). DOI: 10.3390/ma12193119.
26. Giang, D.T., Pham, T.S., Ngo, Q.M., Nguyen, V.T., Tien, T.Q., and Duong, P.H., *An Alternative Approach for High Uniformity Distribution of Indoor Lighting LED*. *IEEE Photonics Journal*, 2020. **12**(2): pp. 1-10. DOI: 10.1109/jphot.2020.2979609.
27. Vu, H., Kieu, N.M., Gam, D.T., Shin, S., Tien, T.Q., and Vu, N.H., *Design and Evaluation of Uniform LED Illumination Based on Double Linear Fresnel Lenses*. *Appl. Sci.*, 2020. **10**(9). DOI: 10.3390/app10093257.

28. Wu, R., Zheng, Z., Li, H., and Liu, X., *Optimization design of irradiance array for LED uniform rectangular illumination*. Appl Opt., 2012. **51**(13): pp. 2257-2263. DOI: 10.1364/AO.51.002257.
29. Kuswandi, B., Nuriman, Huskens, J., and Verboom, W., *Optical sensing systems for microfluidic devices: a review*. Anal Chim Acta, 2007. **601**(2): pp. 141-155. DOI: 10.1016/j.aca.2007.08.046.
30. Zhu, H., Isikman, S.O., Mudanyali, O., Greenbaum, A., and Ozcan, A., *Optical imaging techniques for point-of-care diagnostics*. Lab Chip, 2013. **13**(1): pp. 51-67. DOI: 10.1039/c2lc40864c.
31. Banik, S., Mahato, K.K., Antonini, A., and Mazumder, N., *Development and characterization of portable smartphone-based imaging device*. 2020. **83**(11): pp. 1336-1344. DOI: <https://doi.org/10.1002/jemt.23525>.
32. Banik, S., Melanthota, S.K., Arbaaz, Vaz, J.M., Kadambalithaya, V.M., Hussain, I., Dutta, S., and Mazumder, N., *Recent trends in smartphone-based detection for biomedical applications: a review*. Anal Bioanal Chem, 2021. **413**(9): pp. 2389-2406. DOI: 10.1007/s00216-021-03184-z.
33. Hunt, B., Ruiz, A., and Pogue, B., *Smartphone-based imaging systems for medical applications: a critical review*. J Biomed Opt, 2021. **26**(4). DOI: 10.1117/1.JBO.26.4.040902.
34. Pham, A.T.T., Wallace, A., Zhang, X., Tohl, D., Fu, H., Chuah, C., Reynolds, K.J., Ramsey, C., and Tang, Y., *Optical-Based Biosensors and Their Portable Healthcare Devices for Detecting and Monitoring Biomarkers in Body Fluids*. Diagnostics (Basel), 2021. **11**(7). DOI: 10.3390/diagnostics11071285.
35. Sun, A.C. and Hall, D.A., *Point-of-Care Smartphone-based Electrochemical Biosensing*. 2019. **31**(1): pp. 2-16. DOI: <https://doi.org/10.1002/elan.201800474>.
36. Gill, P.S., Kamath, A., and Gill, T.S., *Distraction: an assessment of smartphone usage in health care work settings*. Risk Manag Healthc Policy, 2012. **5**: pp. 105-114. DOI: 10.2147/RMHP.S34813.
37. Roda, A., Michelini, E., Zangheri, M., Di Fusco, M., Calabria, D., and Simoni, P., *Smartphone-based biosensors: A critical review and perspectives*. TrAC - Trends Anal. Chem., 2016. **79**: pp. 317-325. DOI: 10.1016/j.trac.2015.10.019.
38. Hong, Y., Feng, C., Yu, Y., Liu, J., Wing, J., Lam, Y., Luo, K.Q., and Tang, B.Z., *Quantitation , Visualization , and Monitoring of Conformational Transitions of Human Serum Albumin by*

- a Tetraphenylethene Derivative with Aggregation-Induced Emission Characteristics*. Anal Chem., 2010. **82**(16): pp. 7035-7043. DOI: 10.1021/ac1018028.
39. Johnson, D.W., et al., *Chronic kidney disease and measurement of albuminuria or proteinuria: a position statement*. Med J Aust, 2012. **197**(4): pp. 224-225. DOI: 10.5694/mja11.11468.
40. Naghibi, S., Chen, T., Jamshidi Ghahfarokhi, A., and Tang, Y., *AI-Egen-enhanced protein imaging: Probe design and sensing mechanisms*. Aggregate, 2021. **2**(3). DOI: 10.1002/agt2.41.
41. Jiao, Z., Guo, Z., Huang, X., Yang, J., Huang, J., Liu, Y., Liu, G., Zhang, P., Song, C., and Tang, B.Z., *3D-Printed, Portable, Fluorescent-Sensing Platform for Smartphone-Capable Detection of Organophosphorus Residue Using Reaction-Based Aggregation Induced Emission Luminogens*. ACS Sensors, 2021. **6**(8): pp. 2845-2850. DOI: 10.1021/acssensors.1c01178.
42. Hu, Q., Yao, B., Owyong, T.C., Prashanth, S., Wang, C., Zhang, X., Wong, W.W.H., Tang, Y., and Hong, Y., *Detection of Urinary Albumin Using a "Turn-on" Fluorescent Probe with Aggregation-Induced Emission Characteristics*. Chem Asian J., 2021. **16**(10): pp. 1245-1252. DOI: 10.1002/asia.202100180.

CHAPTER 4. DEVELOPMENT OF THE SAMPLES USED IN THE RE-REFERENCING AND CALIBRATION PROCESS IN THE FLUORESCENCE OPEN PLATFORM

The process of re-referencing and calibration has been published in the following journal paper, but the development of the samples used for that process have not yet been published. The paper contributed to the development of the reference samples, the proper selection of the calibration sample, and testing the performance of the reference samples in the fluorescence measurement. This chapter introduces the process of developing the reference and calibration samples to support a referencing procedure in the fluorescence open platform to produce measurements that are comparable over time and between devices. The chapter will conclude with confirmation of the stable performance of the reference and calibration samples, which significantly contributes to the reproducibility of the measurements in the developed platform.

The journal article [1]: Tohl, D., Teferra, M.N., Wallace, A., **Pham, A.T.T.**, and Tang, Y. (2022), Re-Referencing and Calibration for Robust Ratiometric Light Intensity Measurement. IEEE Trans. Instrum. Meas., DOI: 10.1109/tim.2022.3194929

4.1. The re-producing principle of the fluorescence open platform

The accuracy and repeatability of measurements in devices that perform fluorescence measurements, as well as in devices measuring optical intensity in general, are influenced by factors such as variations in electronic components, light source arrangement, and camera manufacturing. These factors can cause errors in output results for different measurements within a single device and across different devices [2]. To overcome this issue, the ratiometric measurement was employed, in that, the fluorescence intensity obtained from the testing sample was compared with a standard, known constant fluorescent value [1].

According to the fluorescence measurement principle, the obtained fluorescent signal yielded from the samples is dependent on the type and intensity of the UV light source, as well as the camera's performance at the time of the measurement. If there is variation in the UV intensity or the camera's response to the fluorescent signal, that variation will have a related effect on both the test sample and the standard. By knowing that the standard is constant, the researcher can calculate the ratio between the generated fluorescence of the test sample and the output value of the standard, then apply the ratio onto the fluorescent value of the testing sample to calculate the real concentration of the biomarker in that sample [1, 2]. The application of referencing and calibration processes in this fluorescence device development was expected to minimize the variation in fluorescent outputs of the testing samples in different measurements within the single device, as well

as among the reproduced devices. In fact, this method has been applied to the commercial measuring devices for many decades, where it is known as a calibration process.

During this research, a calibration and referencing method was developed and reported through the paper “Re-referencing and calibration for robust ratiometric light intensity measurement” by Dr. Damian Tohl and colleagues 2022 [1]. In that report, the methodology showed that the error between the expected and simulated value remained below 2 % [1]. This is a significant outcome for the current fluorescence device development. The sections that follow describe the process of defining the standards for the calibration and referencing samples. The standard samples are usually made with a specific material, whose values are constant throughout long-time usage. In this project, we chose standard samples that can suitably work with the fluorescence measurement for monitoring albumin in the urine sample.

4.2. The decisions of the calibration and referencing sample development processes

4.2.1. Calibration sample

In the scope of the fluorescence device development in this thesis, the optical values of excitation and emission wavelengths were chosen according to the TPE-4TA, an AIE bio-probe used to detect albumin concentration in urine samples. The excitation wavelength of 370 nm was chosen to work with the recognising chemical to detect albumin in the urine samples, and the testing mixture yielded a fluorescent signal of around 470 nm, as introduced in the optical working conditions for TPE-4TA in Chapter 3.

For the standard sample selection, the chosen sample was supposed to satisfy three criteria: (1) Having close absorption and emission wavelengths with the solution measurement; (2) Having stable response to UV excitation in the measurement range; and (3) Having no or less dependence on the laboratory operation. For the first criteria, the standard was required to have similar responses to the excitation light source as compared with the testing solution, in that, the standard sample should be able to react to the 370-nm UV excitation light source and to generate a fluorescence signal close to the 470-nm wavelength emitted from the testing solution. Among the commercial standard samples used in laboratories, the calibration samples for fluorescence spectrometer were popular with superior accuracy, reliability, and repeatability, which could satisfy requirements (2) and (3). Having the excitation and emission wavelengths of 348 nm and 422 nm, respectively, the tetraphenyl butadiene (TPB) compound was the preferred object for the standard sample, as shown in Table 4.1.

Table 4.1. Excitation and emission wavelengths of various compounds.

Sample Number	Compound	Excitation Wavelength [nm]	Emission Wavelength [nm]
1	Anthracene	360	402
	Napthalene	290	330
2	Ovalene	342	482
3	P – Terphenyl	295	338
4	Tetraphenyl butadiene	348	422
5	Compound 610	440	475
6	Rhodamine	562	573

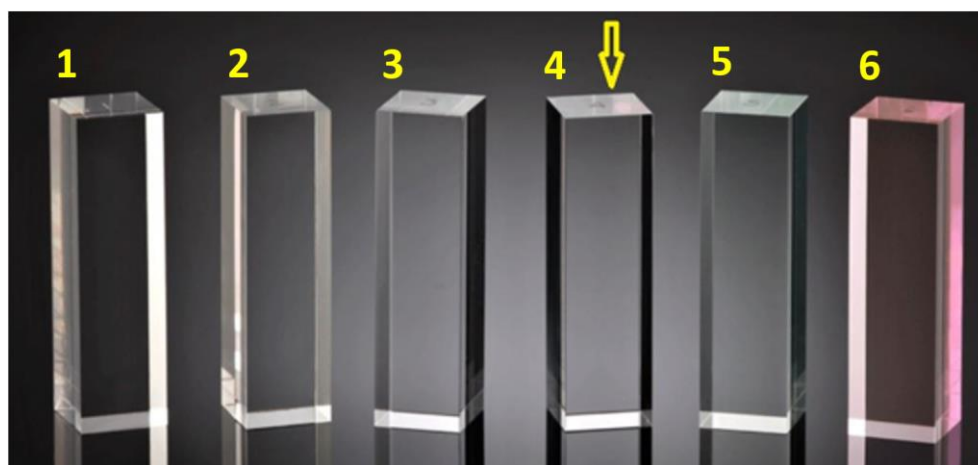


Figure 4.1: The real shapes and colour of six calibration samples used for a commercial fluorescence spectrometer. Sample 4 is TPB, which reacts to 348-nm UV to generate 422-nm fluorescence and was chosen to be the standard sample for the developed fluorescence device.

According to the principle of ratiometric measurement above, the user was required to measure the fluorescent signal from both the testing solution and the calibration sample in every measurement. This resulted in the need that one calibration sample should be provided for every developed fluorescence device. However, with the significantly high cost of approximately 200 AUD/piece, providing one calibration sample along with the fluorescence measuring device was not

suitable for the requirement of POC device development. There existed a need to find another solution for the calibrating process, in that, a low-cost material was selected to create the sub-calibration sample, which was called a “reference sample”. Having low-cost in material and fabrication, the reference sample was suitable for providing the fluorescence device the ability to run the calibration process in every single test without worrying about the variation of the optical measurements.

4.2.2. Reference sample

The principle of replacing the calibration sample with a reference sample was that if the reference sample could provide a stable and repeatable result in fluorescence measurement, a fixed ratio could be calculated between the calibration and the referencing values. So, the reference sample would play the sub-calibration role for the measuring devices. Then, instead of performing the ratiometric measurement between the fluorescence of the testing solution and the calibration sample, the fluorescence of the testing solution was matched with the one from the reference sample. This helped to cancel any effects from variations in the hardware used in the fluorescence measurement. From the explanation, the reference sample was not required to have a close emission wavelength with the solution measurement, but needed stable and repeatable results when reacting to the excitation light. For the required output signal, the reference samples were expected to provide output fluorescent intensity close to that of the real urine samples, which contained an albumin concentration of 400 mg/L. This level was chosen due to the clinical range of the albuminuria levels of CKD patients (30 – 300 mg/L). In addition, the reference sample must be low cost to be equipped with every single fluorescence device. Hence, there were several requirements that the reference sample should satisfy:

- (1) Providing a stable fluorescent response over time under the excitation condition of the device.
- (2) Providing fluorescence intensity close to the one resulting from a urine sample containing 400 mg/L albuminuria level.
- (3) Having no or less dependence on laboratory operation.
- (4) Being affordable.

From those requirements, several options were examined:

- (1) Using commercially available tetraphenylethylene (TPE) powder as the reference sample
- (2) Using another powder as the environment to mix with the TPE powder

(3) Using a compound as the environment to disperse the TPE powder

(4) Using the compound to work as a fluorescent agent

The fluorescence tests were performed for each option to examine their suitability to be the reference sample.

4.2.2.1. *Using TPE powder as the reference sample*

Tetraphenylethylene (TPE) is one of the commercially available materials following the AIE mechanism. TPE has a simple molecular structure but shows a splendid AIE effect, supporting the fluorescence measurements in much research [3-6]. In the current research, the recognising chemical (TPE-4TA) used for detecting albumin in urine was a derivative of TPE, thus, they have similar response to the 370 nm UV excitation and provided fluorescence at around 450 nm wavelength. In the solid state, TPE molecules have a strong photoluminescent reaction under the excitation of UV light [3]. Thus, TPE in powder form had been chosen as the first subject for the reference sample development.

The powder test required a different container because it was opaque, unlike the solution which is transparent. For the powder test, due to the opaque property, the UV light can only reach and react with the molecules on the outer surface. This means we only need a thin layer of TPE powder to react with the UV beam and then to produce the fluorescence for the measurement. Hence, a thin quartz cuvette was employed as the container for the powder tests in this research. The cuvette had dimensions of 45×12.5×3.5 mm, as shown in Figure 4.2(A). Under excitation, the UV beam reached the surface of the TPE powder in the thin cuvette, then reflected to the surround environment of the measurement, as shown in Figure 4.2(B). Simultaneously, the TPE powder at the top layers of the sample emitted fluorescence in every direction. Only the fluorescence, named the target fluorescence output, in the direction of the camera placed at an angle of 90 degrees to the central UV beam was measured and analysed, as shown in Figure 4.2(B).

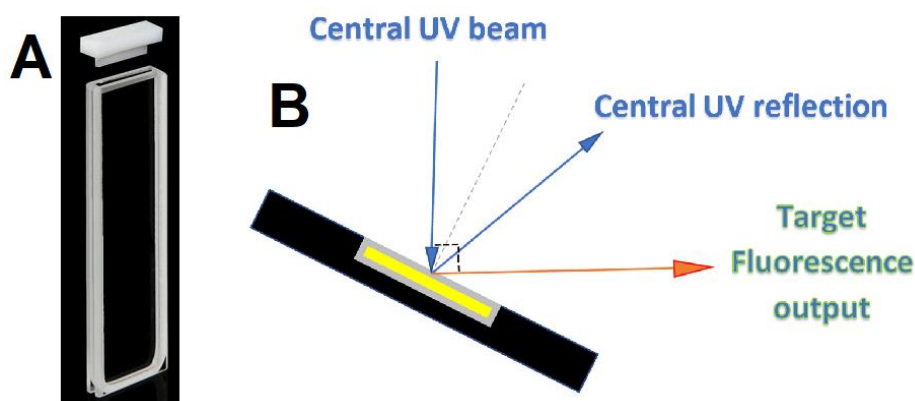


Figure 4.2. The thin quartz cuvette and the setup for measurement. (A) The thin quartz

cuvette with the light path of 1 mm; (B) The normal setup of the thin cuvette used to perform the fluorescence measurement on powder, an opaque material. The UV beam reached the surface of the TPE powder in the thin cuvette, then emitted fluorescence to every direction. Only the fluorescence coming to the camera placed at an angle of 90 degrees to the central UV beam was measured and named the target fluorescence output.

From the principle of fluorescence measurement device setup, the optical camera captured the fluorescence beam at an angle of 90-degrees to the excitation central UV light beam. This captured output was named the target fluorescence output in Figure 4.2. The cuvette should be placed such that the UV reflected from the surface of the cuvette, or the powder molecules, did not interfere with the output fluorescent beam. As shown in Figure 4.2, the θ value should be between 0 and 45 degrees to guarantee the above requirement.

A test of different angles between the cuvette and UV light beam was undertaken in the fluorescence spectrometer to define the suitable angle for the device development. The TPE powder was poured into the cuvette and shielded with the white cuvette cap, as shown in Figure 4.2(A). Then, the cuvette filled with TPE powder was placed inside the spectrometer in different angles to the UV beam: 15, 20, 25 and 30 degrees. After securing the cuvette position with the specific angle, a 365 nm UV excitation light was incident on the cuvette surface, and the fluorescent output was recorded. The results are presented in Table 4.2. It could be stated that the larger the angle was, the higher the fluorescence signal; and the powder's fluorescence was stable over time. Thus, the angle between the cuvette surface and the UV beam was chosen to be 30 degrees to achieve the high fluorescence intensity. However, when put into the developed fluorescence device for the measurement, the thin cuvette with the pure TPE powder yielded output fluorescence over the detecting range of the camera, causing saturation in fluorescence measuring, as shown in Figure 4.3. The saturation not only occurred at the angle of 30 degree, but at all other angles. Hence, the pure TPE powder was not suitable as the reference sample for the current research. Another option needed to be considered to develop the reference sample.

Table 4.2: The thin cuvette filled with TPE powder was placed in the spectrometer such that its surface made an angle with the UV excitation beam, then the fluorescence signal was measured on different days.

The angle between the cuvette surface	Fluorescence result of the spectrometer [a.u.]		
	17/07/2020	26/08/2020	15/09/2020

and the UV beam			
15	231.414	233.217	215.742
20	298.476	292.526	285.231
25	362.129	363.339	345.926
30	423.098	416.640	409.017



Figure 4.3: The fluorescence signal from the TPE powder was over the detection range of the camera, causing the saturation in the obtained image.

4.2.2.2. Using another powder as the environment to mix with the TPE powder

Due to the strong fluorescence property exceeding the detectable range of the camera, the pure TPE powder could not be used as the reference sample. One solution tried was to use another powder as a substrate to be mixed with the TPE powder for the purpose of reducing the output fluorescence intensity of the measurement. The substrate powder was required to having minimal interaction with the UV light to produce fluorescence. This requirement guaranteed there would be minimal interference in the fluorescence measurement of TPE powder. Two powders were tested: Silicon Dioxide (SiO_2) and Titanium Dioxide (TiO_2). Both were fine powders and absorbed UV. Thus, the expectation was that the fluorescence intensity would reduce after diluting the concentration of TPE powder in the testing cuvette.

SiO_2 and TiO_2 were mixed separately with TPE powder into different containers. This was done by first dissolving the TPE powder in the solvent tetrahydrofuran (THF), then the SiO_2 or TiO_2 was added to the solvent solution in certain ratios. The mixture was then dried by the Rotavapor (Buchi, German) to remove the water from the solution. The final product was a fine-powder mixture of TPE and $\text{SiO}_2/\text{TiO}_2$, the ratios of which are presented in Table 4.3. The responses of these fine-

powder mixtures were then examined under the 370-nm UV excitation light.

Table 4.3: The ratio of SiO₂/TPE and TiO₂/TPE in the powder samples. All mixed powders were poured into the thin cuvettes.

Sample	S1	S2	S3	S4	S5
SiO ₂ : TPE	100 : 0	99 : 1	98 : 2	96 : 4	90 : 10
Notice	Pure SiO ₂				

Sample	T1	T2	T3	T4	T5
TiO ₂ : TPE	100 : 0	70 : 30	60 : 40	20 : 80	10 : 90
Notice	Pure TiO ₂				

All thin cuvettes filled with powder were placed such that the cuvette surface receiving UV excitation faced the receiver, as shown in Figure 4.2. Both sample sets were examined with the fluorescence spectrometer to evaluate their response to the 370 nm UV excitation.

In the SiO₂ mixture, all samples showed significantly high optical intensity under the 370 nm UV excitation in the fluorescence spectrometer and in the developed prototype. From the spectrometer scanning, when using the same settings with the solution test condition, all powder samples yielded intensities outside the detectable range of the sensor. To observe the output of the powder samples, the measurement settings had been changed to scale down the output intensity until they stayed in the detectable range. The results are presented in Figure 4.4, which shows that the more TPE added into the SiO₂ powder, the lower the output optical intensity. From Figure 4.4, the sample S1, with 0 % of TPE powder, showed the highest optical intensity, whilst the samples S4 and S5 containing 4 % and 10 % of TPE powder, respectively, produced the lowest optical intensities. Besides, the difference between the outputs of S4 and S5 was insignificant. Therefore, there was no need to further dilute the TPE powder with SiO₂. Further supporting evidence was observed from the fluorescent images taken from the Raspberry Pi camera, in that, the pure SiO₂ powder gave the highest fluorescent intensity, which slightly decreased as TPE concentration increased in the powder mixtures, as shown in Table 4.4. Due to the similar output intensity, S4 and S5 were represented in the same picture in Table 4.4. This result raised the concern whether the output from the mixture powder of SiO₂/TPE was reflected UV or the fluorescence from SiO₂. To examine this issue, the sample S3 had been used in the developed prototype. In detail, a UV filter

was inserted in front of the camera before taking an image of the optical output signal. The result showed that there existed a strong fluorescence signal from the SiO₂/TPE powder mixture besides the reflected UV, as shown in Table 4.4. Meanwhile, the solution sample of 400 mg/L of albumin did not show significant UV reflection. This gave the evidence that SiO₂ powder not only reflected a significant amount of UV light into the optical sensor, but it also produced a strong fluorescent signal, which caused the saturation in the detection of the spectrometer sensor and the Raspberry Pi camera. Thus, the SiO₂ was concluded to be not suitable for the reference sample development.

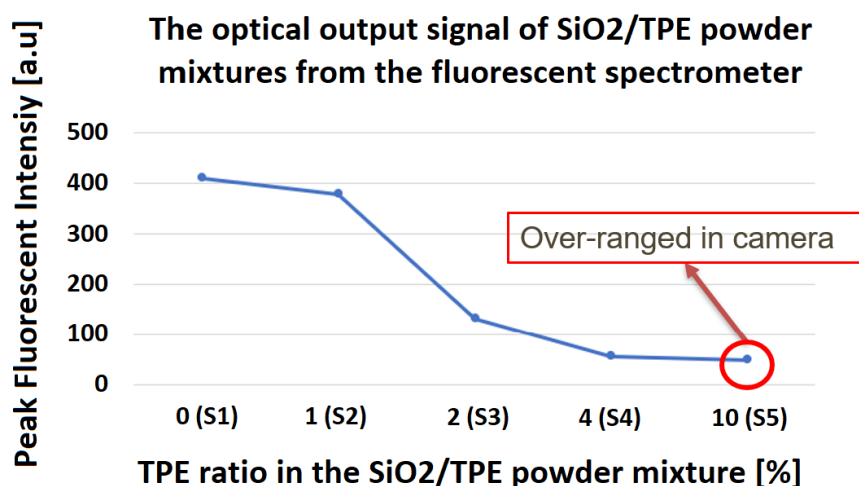


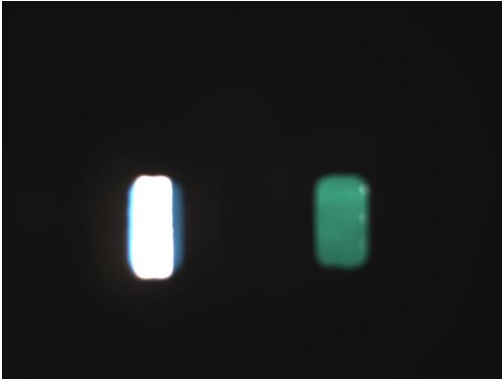









Figure 4.4: The fluorescent results of SiO₂/TPE powder mixture obtained from the fluorescence spectrometer.

Table 4.4: The fluorescence images from the developed prototype. This table compares the fluorescent images between the mixture powders of SiO₂/TPE and the solution sample containing 400 mg/L albumin concentration.

	SiO ₂ /TPE powder	Sample with 400 mg/L albumin	SiO ₂ /TPE powder	Sample with 400 mg/L albumin
S1			S2	
S3			S4 & S5	
For UV filter examination	Without UV filter	With UV filter		
S3				

The second option in this section was to use the TiO₂ to dilute the TPE powder. In contrast to SiO₂, TiO₂ not only absorbed the incoming UV light, but it also did not produce fluorescence.

Mixing powders of TiO_2 and TPE was prepared following the procedure of making the mixture of SiO_2 /TPE powder. For TiO_2 , the mixing ratio is shown in Table 4.3. The measurement results of the TiO_2 /TPE powder mixtures are shown in Figure 4.5. It was clear that TiO_2 powder worked efficiently in reducing fluorescence in the mixed TPE powder samples. The sample T1 was considered to absorb most of the incoming 370-nm UV light and did not produce a fluorescent signal. When TPE powder was added into the mixture, the more TPE present, the higher the fluorescent signal. However, the fluorescence variation was unremarkable. With just a small amount of TiO_2 in the powder (10% of the TPE mixture), fluorescence barely showed up in the output signal of the sample T5. This signal was much lower than the signals from the pure TPE powder and the calibration sample, as shown in Figure 4.5 and Figure 4.6. Thus, TiO_2 powder was also not suitable for the reference sample development. This required other methods to be considered.

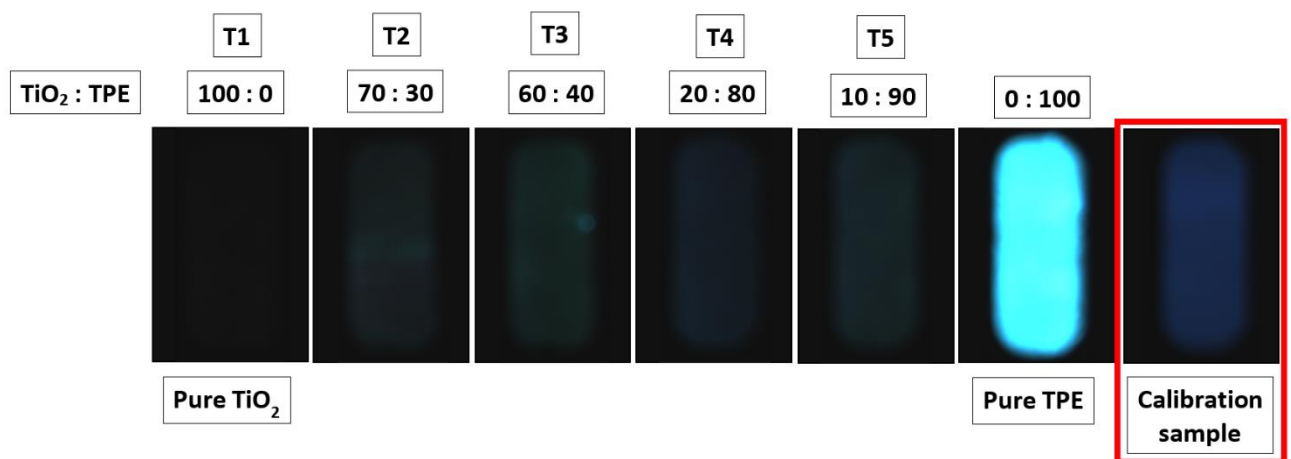


Figure 4.5: The fluorescent images of powder mixtures of TiO_2 and TPE in different ratios (sample T1 to T5), and the fluorescent image of the pure TPE powder.

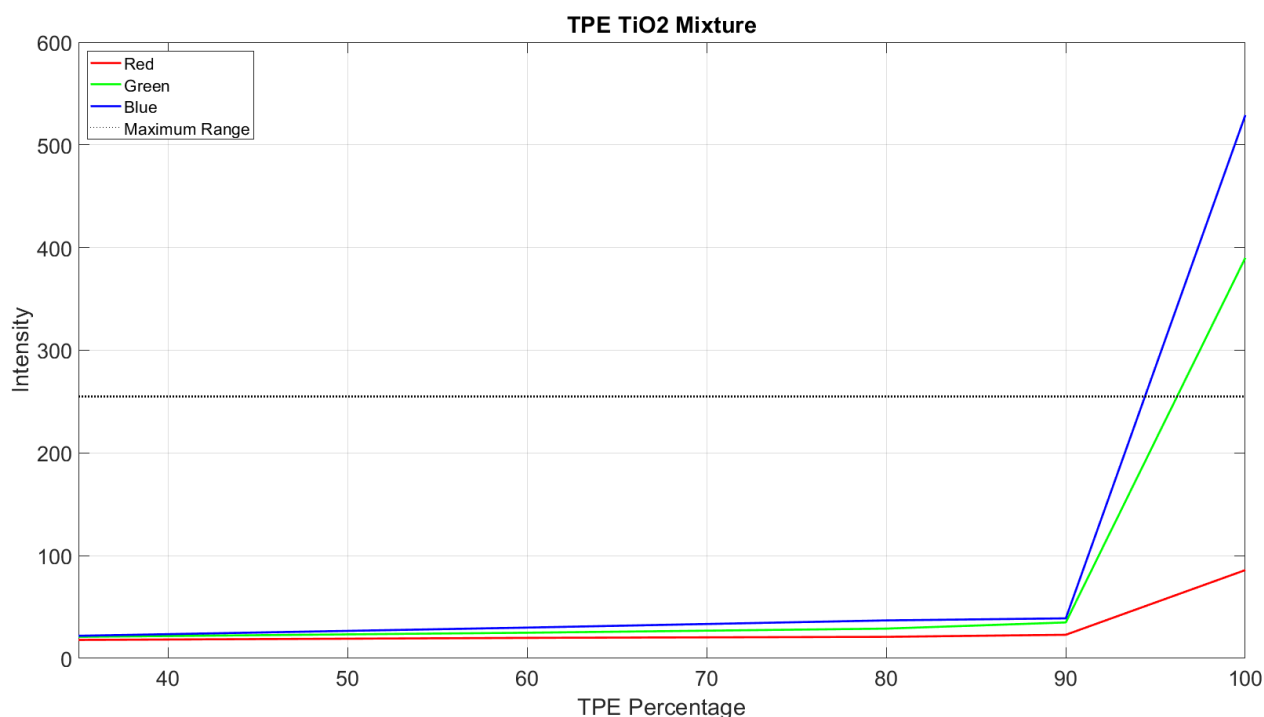


Figure 4.6: The fluorescent intensities of the TiO₂/TPE powder mixtures compared with the pure TPE powder presented as Red-Green-Blue components.

4.2.2.3. *Using a compound as the environment to disperse the TPE powder*

After using other powder to dilute the concentration of TPE in the sample, and obtaining unsuitable results, the idea of using a transparent/semi-transparent material to work as a frame to disperse the TPE powder was raised. This method was expected to hold TPE particles in the solid sample to achieve a suitable fluorescence intensity. There were two materials examined in this section: epoxy resin and polydimethylsiloxane (PDMS).

Epoxy resin

Epoxy resin is a member of the aromatic groups, which have strong absorption in the UV range at about 300 nm [7]. With this high absorption, epoxy resin was expected to reduce the fluorescence intensity of the TPE powder down to the detecting range of the camera. Epoxy Kinetix R246 was examined for the reference sample development. The epoxy Kinetix R246 comprised of two parts: part A – laminating epoxy monomer and part B – hardener. The epoxy sample was prepared following the procedure of the manufacturer. Firstly, the Kinetix R246 epoxy was prepared by mixing its part A and part B in the ratio of 4:1 and was divided into two containers. Then the fine powder of TPE was poured and well-stirred into the two containers while the epoxy was still in the liquid state to make ratios of 2 % and 6 % of TPE. After mixing the powder and the epoxy well, the containers were placed into vacuum chambers to remove bubbles. Finally, the epoxy in the two

containers was slowly poured into moulds in the shape of a thin-cuvette and left at room temperature overnight to cure. The cured epoxy/TPE samples were placed in the developed fluorescence prototype to examine their response under the 370-nm UV excitation.

From the results, the epoxy/TPE samples produced a significantly higher fluorescent intensity than the calibration. These outputs saturated the camera detection, as shown in Figure 4.7. The TPE powder was insoluble in the epoxy samples, thus, the powder was unevenly distributed in the epoxy resin samples, causing a non-uniform fluorescence at the output. This issue had been clearly observed in the fluorescent images under the 365 nm UV light, as shown in Figure 4.8. Therefore, the epoxy resin mixing with TPE powder was unsuitable for the reference sample development. Therefore, other methods were required to create the reference samples.

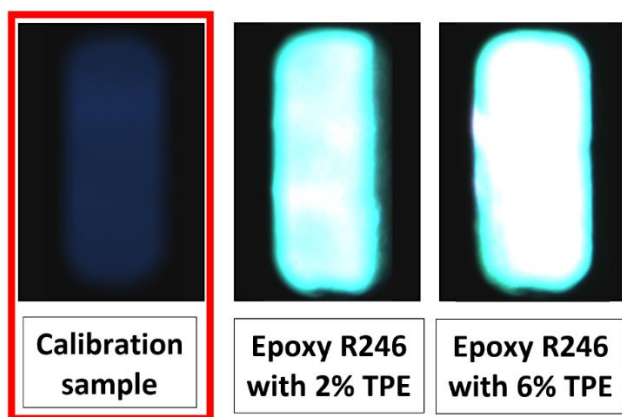


Figure 4.7: The fluorescent images taken in the developed fluorescence prototype of the epoxy resin Kinetix R246 samples containing 2 % and 6 % TPE powder in the thin-cuvette shape and the calibration sample.

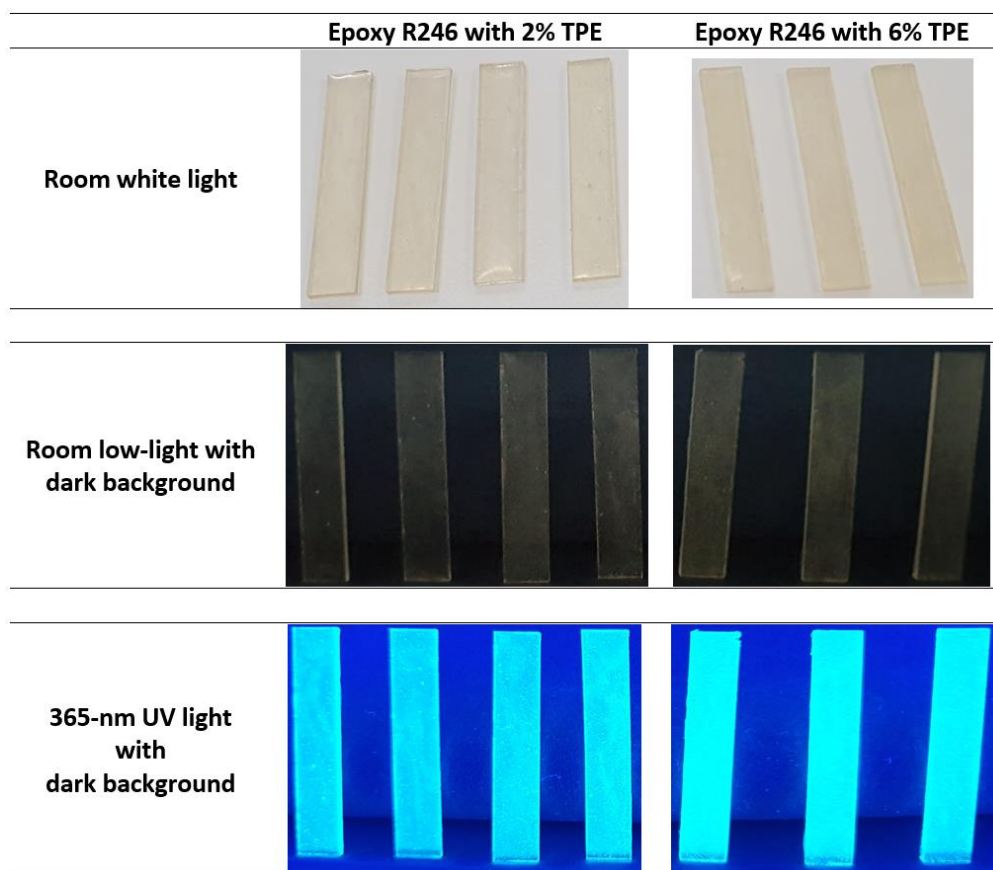


Figure 4.8: The epoxy resin Kinetix R246 samples containing 2 % and 6 % of TPE powder in the thin-cuvette shape in different light conditions: room light, dark background in low room light, and dark background in the 365 nm UV light. The TPE powder was insoluble in epoxy resin, thus, the powder was unevenly distributed in the epoxy resin samples, causing the non uniform fluorescence at the output.

Polydimethylsiloxane (PDMS)

For the purpose of creating a frame to mix TPE powder, PDMS has several properties similar with epoxy resin, such as UV absorption and not dissolving TPE. It also does not emit fluorescence under the 370 nm UV excitation. Thus, PDMS can be mixed with fluorescent pigments to yield fluorescence under UV exposure without UV noise due to the PDMS background. It has potential to control fluorescence intensity and specific excitation wavelengths. There were two types of PDMS used in testing:

- Momentive RTV615.
- NuSil MED-6015.

After the high fluorescence emission from the epoxy samples containing 2 % and 6 % TPE powder, the ratios of TPE powder in the PDMS samples were reduced to 1 % for Momentive RTV615

and 2 % for Nusil MED-6015. One issue that needed to be considered during the PDMS sample preparation was the viscosity of PDMS being much higher than epoxy resin, causing a challenge when pouring the PDMS into the thin cuvette shape with 1-mm light path. Thus, the 10×10×45 mm PP cuvette was used as the container for PDMS samples. Four PP cuvettes (four clear sides) were employed: two cuvettes were filled with the clear Momentive RTV615 and Nusil MED-6015, the other two were filled with the mixture of TPE powder and the two PDMS types. The four cuvettes were degassed in the vacuum chamber for three hours, incubated in the oven at 65 °C for four hours, and left in the oven to cure for three days. Then the PDMS cuvettes were placed in the spectrometer to measure fluorescence response. From the results, both pure PDMS samples did not show considerable fluorescence emission. This confirmed that PDMS could absorb UV light and did not cause additional fluorescence in the output signal, as shown in Figure 4.9 and Figure 4.10. However, when TPE was mixed into the PDMS samples, the mixtures produced significantly high fluorescence, double the fluorescent output of the calibration sample, as shown in Figure 4.10. This led to the result that PDMS was unsuitable for application as the reference sample development.

To deal with these issue, the idea of using an optical filter was raised to cut down the fluorescent intensity of the samples without affecting the UV excitation on the samples, thanks to the semi-transparent property of PDMS material. In detail, a thin tint film (TF) was applied to the surface of the cuvettes facing the camera, as shown in Figure 4.11. The tint film used could filter out 99 % of UV light, as well as cut 35 % of the passing visible light. The PDMS samples mixed with TPE were measured with the application of one TF layer and two TF layers, in turn. The results of the PDMS/TPE samples with tint film application are presented in Figure 4.12. From the graph, the mixture of NuSil MED-6015 yielded a higher optical output than that of Momentive RTV615. After applying the TF layer, the results reversed. This showed that there was a potential of UV reflection from the mixture sample to the camera. By applying the tint film, the measurement could get rid of the interference of UV reflection from the testing cuvette to the camera. For the fluorescent intensity, the outputs from the samples with one TF layer produced a similarity in level with the calibration sample. Thus, the measurement from the fluorescence spectrometer showed that this setting had the potential to be used in the reference sample development.

However, when measuring those samples in the fluorescence prototype, the fluorescent images of the samples illustrated another issue. Due to the high density of PDMS, the UV light dropped significantly when transferring through the PDMS samples from left to right, as shown in Figure 4.12. Besides, due to the high viscosity, the TPE powder precipitated downward to the bottom of the PDMS cuvette, causing high fluorescence at the bottom of the cuvette when compared with the top area, as shown in Figure 4.12. These properties of PDMS caused the non-uniform distribution of TPE powder in the cuvette, leading to the uncontrolled fluorescence in the output signal. Therefore, the option of PDMS mixed with TPE powder was inapplicable for the reference sample development.

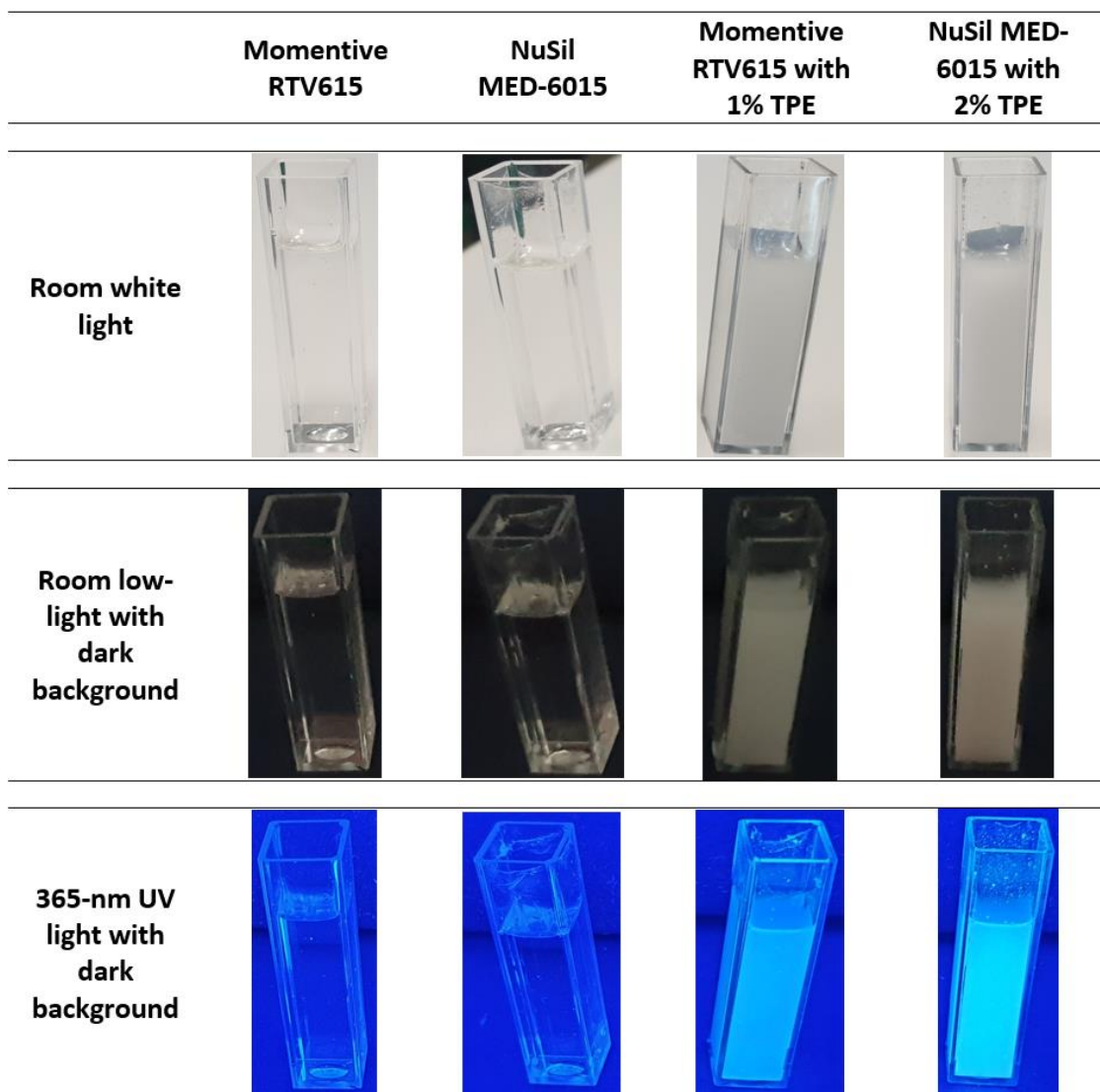


Figure 4.9: The pure PDMS samples and the PDMS/TPE samples of Momentive RTV615 and NuSil MED-6015 in different optical conditions: The normal room light, the low room light with dark background and the 365-nm UV light with dark background.

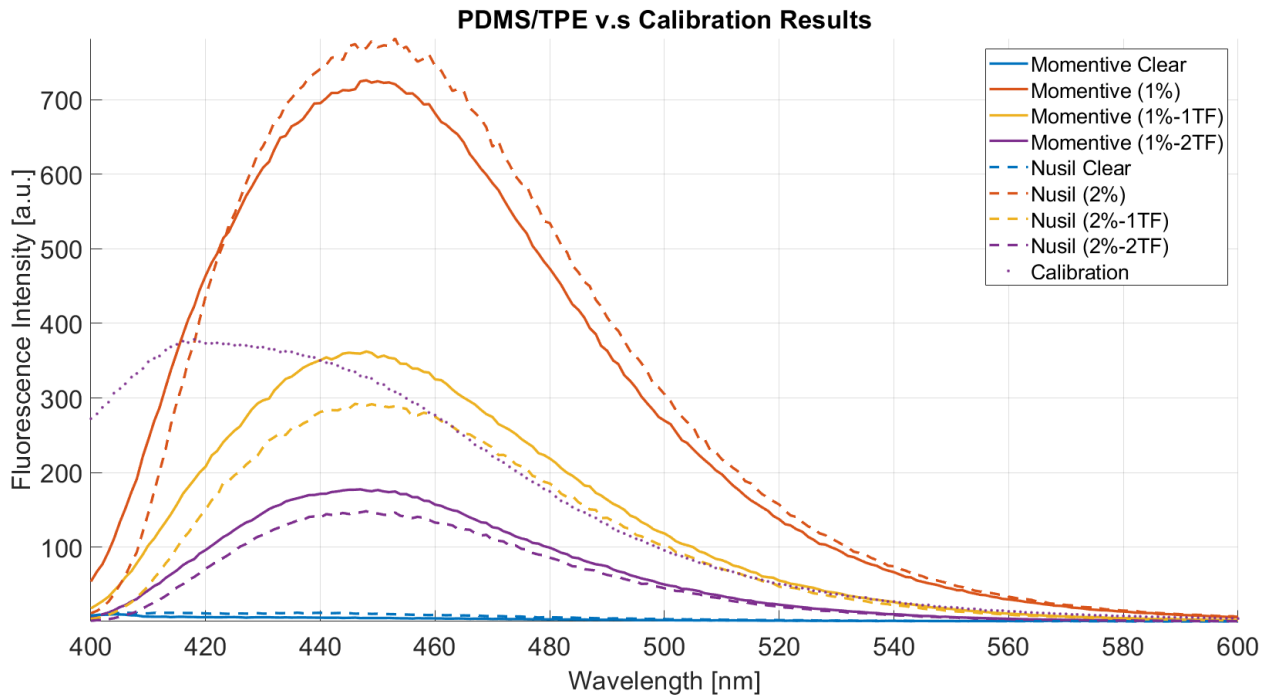


Figure 4.10: The fluorescence results of the PDMS/TPE samples, pure PDMS samples and the calibration sample obtained from the fluorescence spectrometer. The pure PDMS samples produced strong fluorescence, thus, the tint film (TF) layers were applied to reduce the fluorescence intensity and to get rid of the reflected UV light.

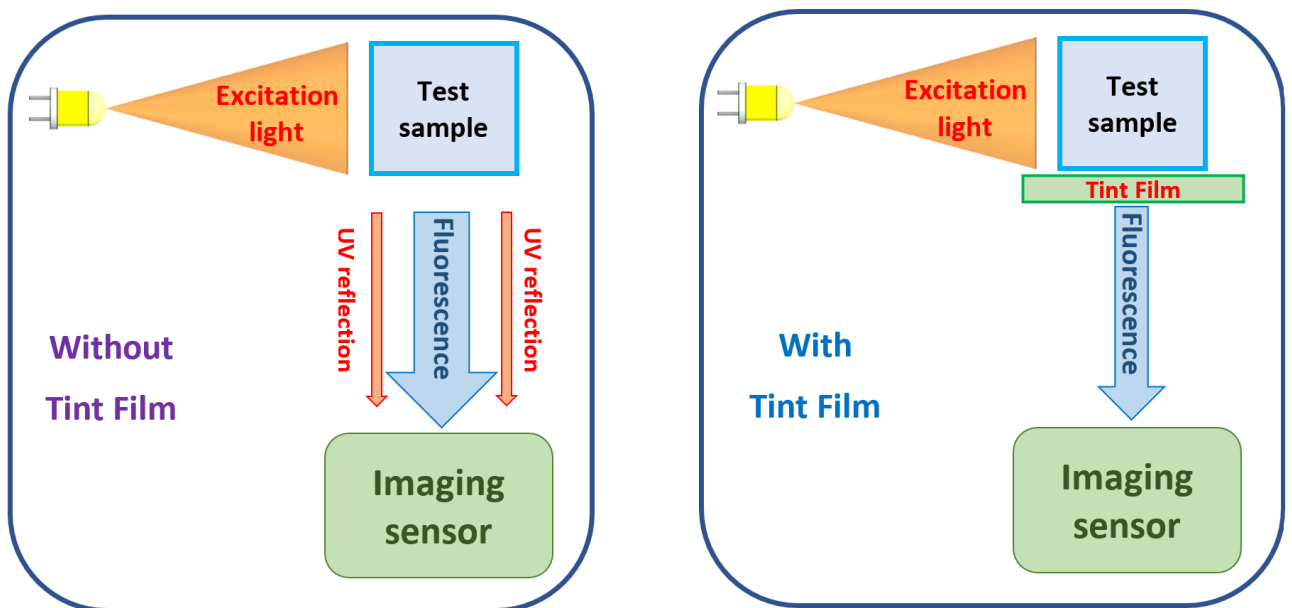


Figure 4.11: The set-up of the fluorescence measurement examining the PDMS/TPE samples with and without the tint film. Without the tint film, there would be potential UV light reflected

to the camera at the same time with the fluorescent signal. The tint film was expected to filter out the reflected UV light from the sample cuvette, as well as to reduce the visible light passing to the camera.

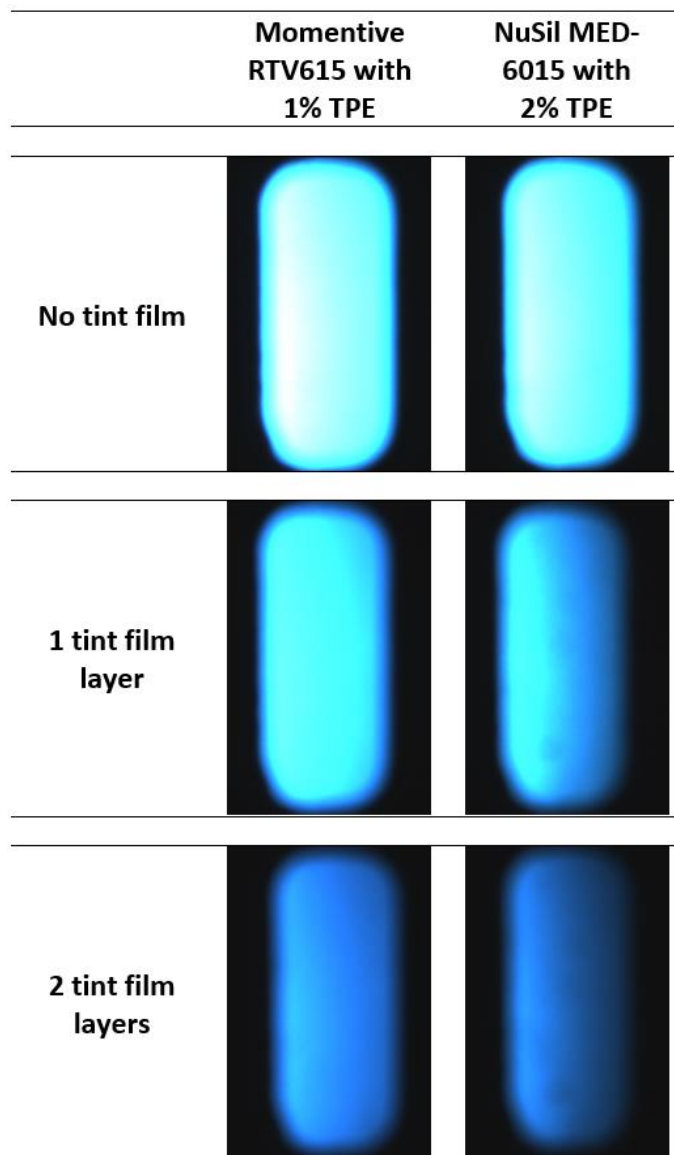


Figure 4.12: The fluorescence of the PDMS/TPE samples with the tint film applied to the surface of the cuvette measured in the fluorescence prototype. Both NuSil MED-6015 and Momentive RTV615 mixed with TPE produced fluorescence under the 370-nm UV excitation from the LEDs. Due to the high density of PDMS, the UV light dropped significantly when transferring through the PDMS samples (from left to right). Besides, due to the high viscosity, the TPE powder precipitated downward to the bottom of the PDMS cuvette, causing the high fluorescence at the bottom of the cuvette when compared with the top area.

4.2.2.4. Using the compound to work as a fluorescent agent

After measuring the fluorescence from the epoxy resin sample, it was found the epoxy itself produced fluorescence under the 370 nm UV light, and that the fluorescent signal was in the blue range of the visible spectrum. Thus, if a sample was made from the pure epoxy resin, its solid sample would have a uniform fluorescence emission under the UV excitation. The epoxy's fluorescence response was evaluated to estimate its potential to be used for the reference sample development. Two types of epoxy resin were examined:

- The Kinetix R246.
- The Barnes – Epoxycast Clear Casting Resin – Starter Kit.

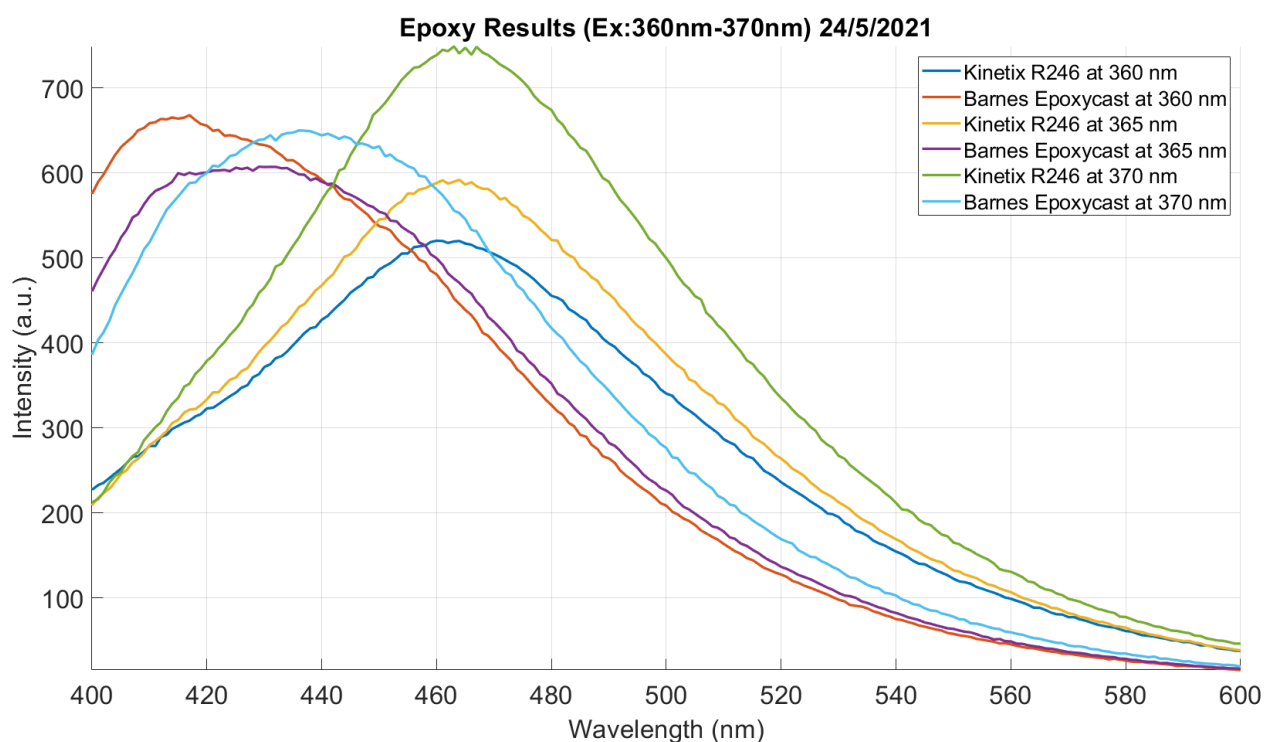


Figure 4.13: The fluorescent signal of the square samples of Kinetix R246 epoxy and Barnes – Epoxycast Clear Casting Resin obtained from the fluorescence spectrometer. Both samples were examined at different wavelengths around the specific UV wavelength of 365 nm. The epoxy Kinetix R246 showed a peak fluorescence closest to the one of the albumin test solutions at 470 nm.

Firstly, both epoxy samples were prepared in the square PP cuvettes following the procedure of the manufacturers. Due to the high fluorescent emission, both epoxy cuvettes were applied with one layer of tint film to prevent reflected UV being directed to the camera and to cut their fluorescence

intensities down to the range of the calibration sample and the albumin testing solution. Both cuvettes were then examined in the fluorescence spectrometer at three different UV wavelengths to confirm their responses when compared with the testing albumin solution. The graph in Figure 4.13 shows that the Barnes Epoxycast sample gave fluorescence peaks at lower wavelengths (418 nm, 430 nm and 438 nm) under three UV excitation wavelengths (360 nm, 365 nm and 370 nm) respectively, which were lower than the peak fluorescence wavelength of the albumin testing solution. The Kinetix R246 yielded a fluorescence peak at a similar wavelength with the albumin testing solution. Thus, the epoxy Kinetix R246 was the potential material for the reference sample development. However, the square epoxy samples encountered the similar issue with the square PDMS samples, in that, the high density of the sample caused the UV light to drop significantly along the transferring path through the samples, as shown in Figure 4.14. This led to the result of non-uniform fluorescence in the output collection. Thus, the square shape was not an ideal option to create the reference sample.

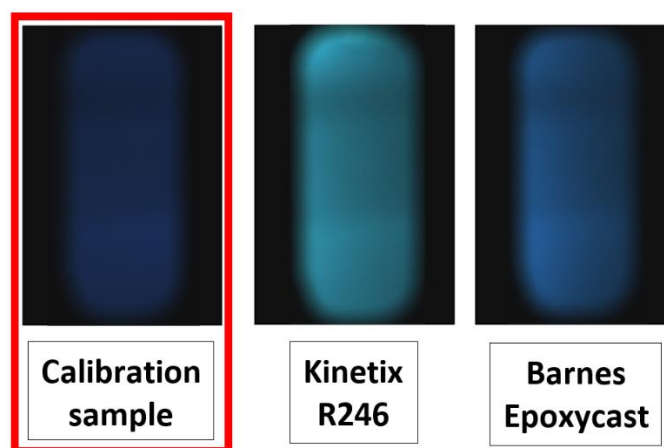


Figure 4.14: The fluorescent images of the square samples of Kinetix R246 epoxy and Barnes – Epoxycast Clear Casting Resin with 1 TF layer obtained from the fluorescence prototype. The UV light was absorbed and reduced significantly along the transferring path through the samples, whilst that light was uniform in the calibration sample.

In the second test, the epoxy Kinetix R246 was chosen to make the solid sample in the thin-cuvette shape. This thin epoxy sample was supported by the tint film layer to remove the reflected UV from the LED source, as well as to decrease the fluorescence intensity to level similar with the calibration sample and the albumin testing solution. In this measurement, due to the semi-transparent property of epoxy, the thin sample was placed such that the surface with the tint film faced the camera while the other side faced the UV LED source, as shown in Figure 4.15. With this setting, the epoxy not only could react with UV excitation to yield fluorescence for the camera detection, but it also filtered out the UV reflection from the measurement. The thin cuvette was supported with a 3D printed holder, which held the thin sample such that the angle between the thin

sample and the UV beam was about 45 degrees to achieve the optimal fluorescence intensity at the camera, as shown in Figure 4.16. From the fluorescent images, the calibration sample and the two thin Kinetix R246 samples gave uniform fluorescence in the horizontal direction under the 370 nm UV excitation of the LED light source, which was optimal in compared with the two square R246 samples. The cause of this non-uniform fluorescence in the vertical direction came from the LED source, in that, the LED source used 4 UV-LEDs arranged in a vertical line, and emitting UV to the calibration and reference samples in horizontal direction. This non-uniform fluorescence distribution could be optimized by using the UV-LEDs with wider beam angle, which could be improved in the future development. Therefore, the thin Kinetix R246 sample was chosen for the reference sample development.

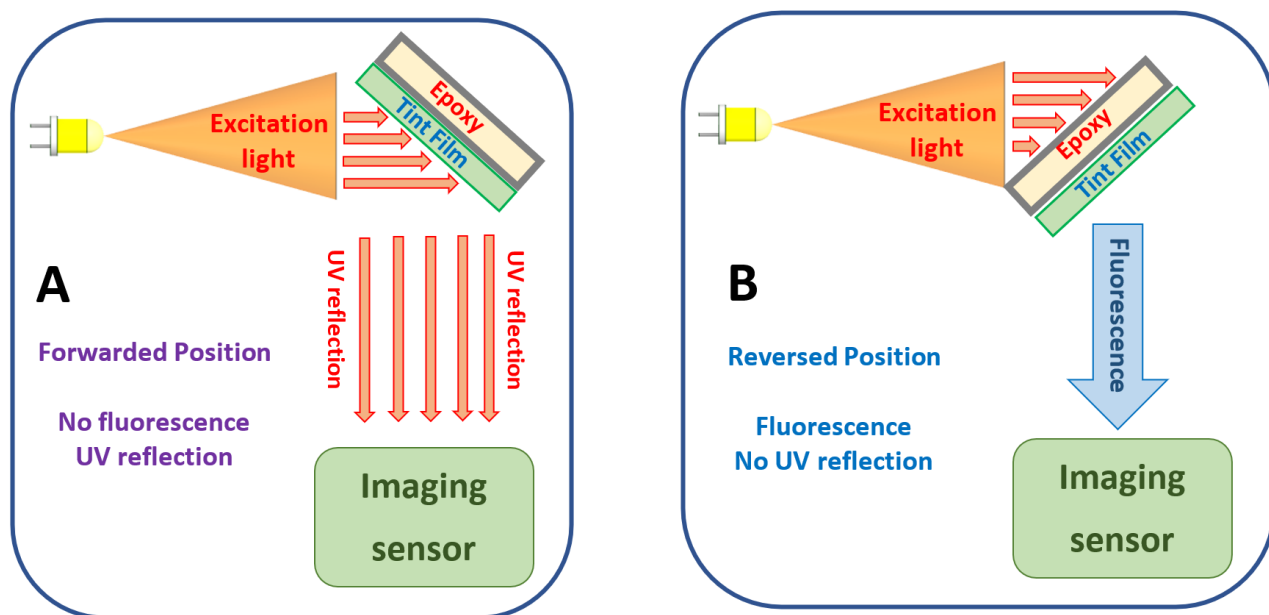


Figure 4.15: The setting of the tint film and the thin epoxy sample in the fluorescence measurement in the developed prototype. (A) The thin epoxy was oriented to face the tint film side to the LED. The output had UV reflected from the surface of the tint film, but there was no fluorescence to the camera. (B) The thin epoxy was oriented to face the tint film side to the camera. The output had fluorescence with reduced intensity and no reflected UV.

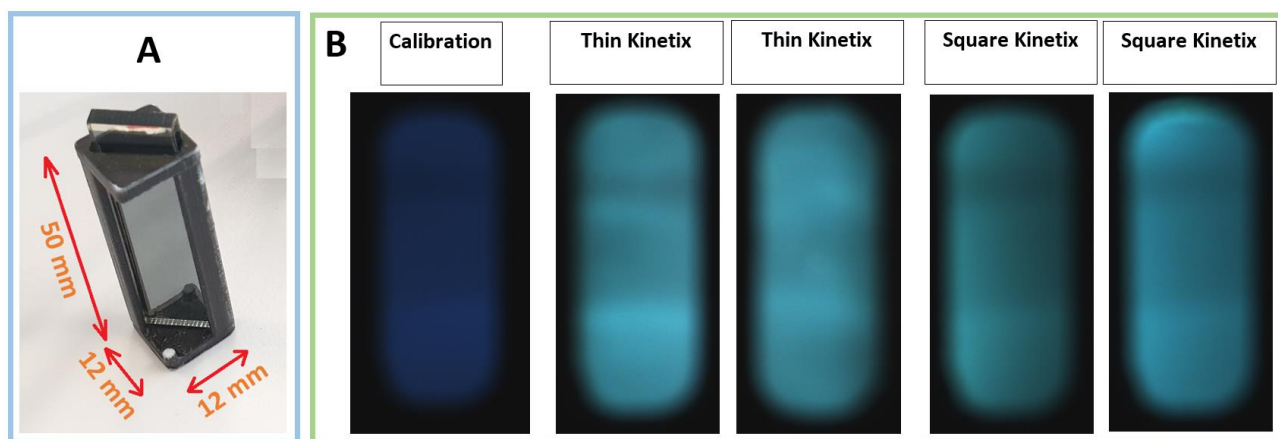


Figure 4.16: The thin Kinetix R246 sample. (A) The thin Kinetix R246 sample with two layers of tint film in the 3D printed holder. (B) The fluorescence images of the calibration sample, two thin R246 samples and two square R246 samples.

4.2.3. Conclusion

The above discussion described the selection of the calibration and reference samples. In detail, the calibration was the tetraphenyl butadiene (TPB) compound in a square-cuvette shape. Due to the issue of uncontrollable optical distribution, all powder compounds mentioned above will not be used in the reference sample development. The reference sample was the pure Kinetix R246 epoxy resin in a thin-cuvette shape. According to the reference and calibration processes of the developed fluorescence platform, we fabricated two reference samples with the same procedure. It was expected that these two references would provide similar responses to UV excitation. The two references and the calibration sample were tested in the fluorescence open platform to observe their response to the UV excitation and to examine their fluorescence stability over a time period.

4.3. The stability of the reference samples during the experiment's period

To examine the performance of the two references and the calibration sample, their fluorescence response was measured in the developed platform following the calibration and referencing processes. The process of calibration and referencing was referred to in the report "Re-referencing and calibration for robust ratiometric light intensity measurement" by Tohl and colleagues published in 2022 [1]. In the measurements, the calibration and referencing samples were placed into two testing positions (pos1 and pos2) in the fluorescence platform and fluorescent images taken to establish the relationship between two UV LED light sources (The detail of the calibration and referencing process is referred to in the supporting information of Chapter 6 and in the paper [1]). This process was executed across 88 measurements from November 2021 to September 2022,

resulting in a set of fluorescent intensities for the calibration and two referencing samples. By observing this set of intensities, plotted in Figure 4.17, we have a better view on the stability of the developed referencing samples over 10 months of usage.

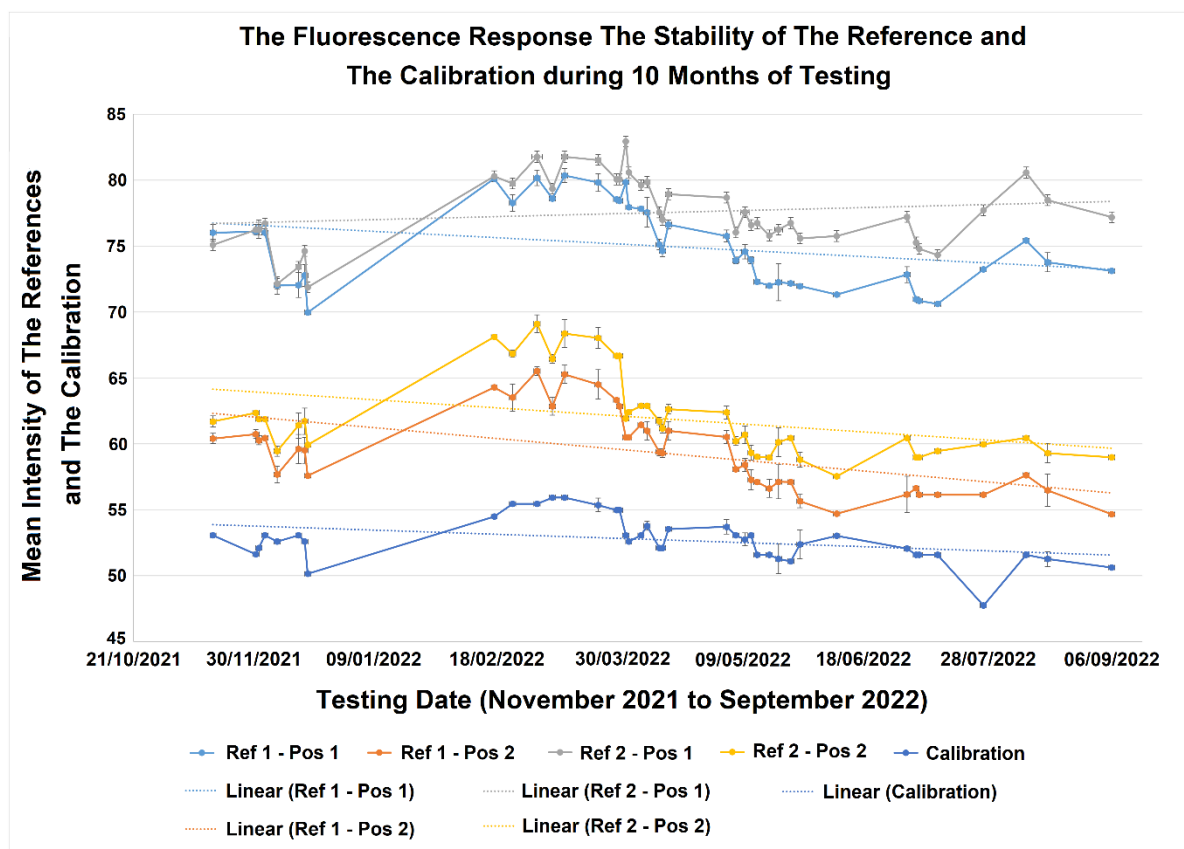


Figure 4.17. The fluorescent intensities of the calibration sample and the two referencing samples with error bar during 10 months of urine-test experiments. During the calibration and referencing process of the fluorescence measurement, the referencing samples (Ref1 and Ref2) were placed in different testing positions (Pos1 and Pos2) and the calibration sample was placed in position 2 (Pos2) for taking images at the same time as the tested urine solutions. All samples showed similar decreasing trends of fluorescence response through 10 months of testing. The error bars showed minimal variation of output fluorescence emitted from the individual sample in the measurements of different samples in the same day.

Due to the experiment conditions, 88 measurements had been processed in the fluorescence platform across 41 days from the 16th of November 2021 to the 6th of September 2022. In one measurement, calibration and referencing samples had been placed in two positions in the platform, then the fluorescent images under the UV excitation were captured using the same LED light sources for the whole experiment. One fluorescent image comprised of two fluorescent sections, which could be reference 1, reference 2 or the calibration. These fluorescent intensities of the references and the

calibration were observed in Figure 4.17. One point of data represented the mean fluorescent intensity of the corresponding references or the calibration in different measurements in the same day. The error bar of each data point confirmed the minimal variation in fluorescent response of the references and the calibration among the measurements within one testing day. In general, the fitting trends of the five datasets indicated a decrease in LED performance after 10 months of testing. According to the requirements of the reference samples, they were not required to produce similar fluorescent values when compared with the calibration one, but they should provide similar fluorescence response under the same UV excitation with the calibration. In Figure 4.17, the references and calibration sample in two positions emitted fluorescence with different intensities, and it was unclear about the relative response among these standards. Thus, we investigated another method to observe their relationship in the fluorescence response. In detail, we examined how far the fluorescent intensity varied from the average value of the data set of the individual standard. Those variations are illustrated in Figure 4.18. From Figure 4.18, two reference samples provided generally similar trends to the calibration sample. Thus, we could achieve a stable ratio between the references and the calibration to support the ratiometric method in the calibration and referencing processes.

As a result, the two reference samples satisfied requirements for the reference sample development in terms of stable fluorescence response. Moreover, the references were made of pure Kinetix R246 epoxy resin, which was common in the Australia market with an affordable price of about 15 cents per reference sample. Therefore, the developed references were eligible to be used as the standard for the fluorescence measurement in the proposed platform.

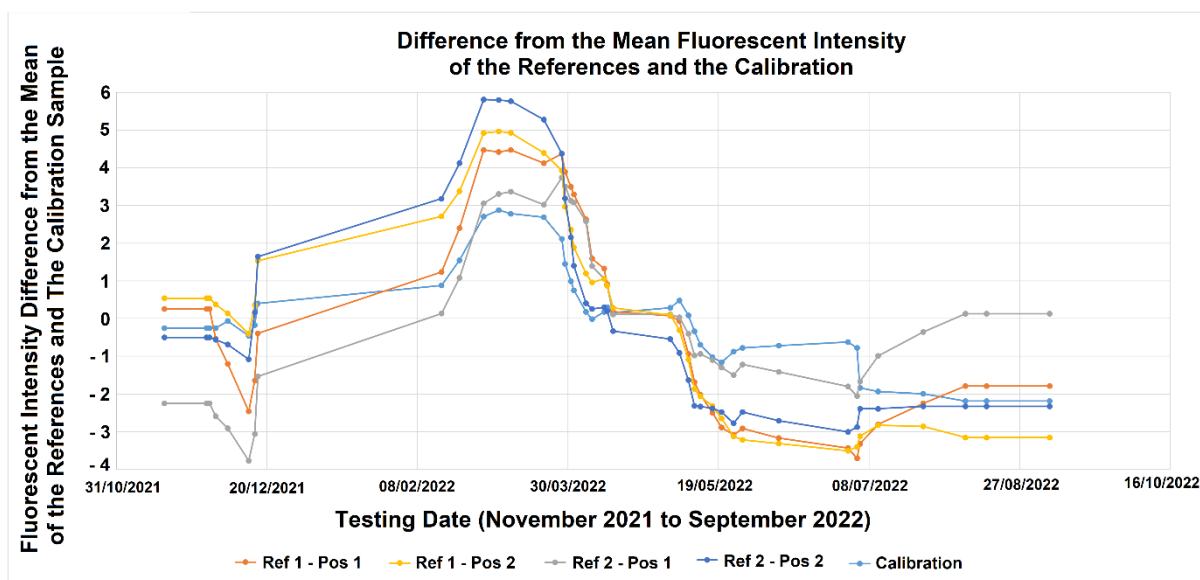


Figure 4.18. The variation between the fluorescent intensity and the average value of the corresponding data set of the references in different positions in the fluorescence platform and the

calibration sample during the testing period.

4.4. Conclusion

This chapter introduced the principle of calibration and reference procedures, the decision of the calibration sample, and the development process of reference samples, which contributed to ensuring the repeatability of fluorescence measurements in one developed platform or between different cloned platforms. Across 88 fluorescence measurements over 10 months, two reference samples confirmed the stability in fluorescence response under excitation of a 370 nm UV LED light sources in the developed platform. Furthermore, they also showed a stable relationship in terms of fluorescence intensity with the tetraphenyl butadiene (TPB) calibrator standard from a commercial spectrophotometer. In addition, with the simple fabrication and affordable price of 15 cents per sample, the development of this reference sample would greatly contribute to the development of a fluorescence POC device for monitoring the concentration of biomarkers in body fluids.

Reference

1. Tohl, D., Teferra, M.N., Wallace, A., Pham, A.T.T., and Tang, Y., *Re-Referencing and Calibration for Robust Ratiometric Light Intensity Measurement*. IEEE Trans. Instrum. Meas., 2022. **71**: pp. 1-8. DOI: 10.1109/tim.2022.3194929.
2. Tohl, D., Pham, A.T.T., Li, J., and Tang, Y., *Point-of-care image-based quantitative urinalysis with commercial reagent strips: design and clinical evaluation*. Biosens Bioelectron, 2023 (Submitted).
3. Hu, Q., Yao, B., Owyong, T.C., Prashanth, S., Wang, C., Zhang, X., Wong, W.W.H., Tang, Y., and Hong, Y., *Detection of Urinary Albumin Using a "Turn-on" Fluorescent Probe with Aggregation-Induced Emission Characteristics*. Chem Asian J., 2021. **16**(10): pp. 1245-1252. DOI: 10.1002/asia.202100180.
4. Liu, Y., Deng, C., Tang, L., Qin, A., Hu, R., Sun, J.Z., and Tang, B.Z., *Specific detection of D-glucose by a tetraphenylethene-based fluorescent sensor*. J. Am. Chem. Soc., 2011. **133**(4): pp. 660-663. DOI: 10.1021/ja107086y.
5. Zhao, Z., Lam, J.W.Y., and Tang, B.Z., *Tetraphenylethene: a versatile AIE building block for the construction of efficient luminescent materials for organic light-emitting diodes*. J. Mater. Chem., 2012. **22**(45): pp. 23726-23740. DOI: 10.1039/c2jm31949g.
6. La, D.D., Bhosale, S.V., Jones, L.A., and Bhosale, S.V., *Tetraphenylethylene-Based AIE-*

Active Probes for Sensing Applications. ACS Appl Mater Interfaces, 2018. **10**(15): pp. 12189-12216. DOI: 10.1021/acsami.7b12320.

7. Nikafshar, S., Zabihi, O., Ahmadi, M., Mirmohseni, A., Taseidifar, M., and Naebe, M., *The effects of UV light on the chemical and mechanical properties of a transparent epoxy-diamine system in the presence of an organic UV absorber*. Materials, 2017. **10**: pp. 1-18. DOI: 10.3390/ma10020180.

CHAPTER 5. CREATININE DEVICE – THE PORTABLE MICROPLATE READER

This chapter has been published in the following journal paper, but the clinical result section has been moved to chapter 6 – The clinical result evaluation. The minor points have been modified to suit the harmonic structure of the thesis.

The journal article: Pham, A. T. T.; Tohl, D.; Hu, Q.; Li, J.; Reynolds, K.J.; Tang, Y. (2022). Portable colorimetric device with commercial microplates for quantitative detection of urine biomarkers: design, development, and clinical evaluation. *Biosensors*, 12, 723, <https://doi.org/10.3390/bios12090723>

5.1. Introduction

Colorimetric examination is a common analytical method for measuring chemicals in both research and clinical fields. The principle of this method is to observe the colour changes of a mixture solution of the specific analyte and the recognising agent due to their chemical or biochemical reactions [1-5]. The operator can read the semi-quantitative result of the chemical presence by observing the colour changes of the mixture with a standard colour chart by naked eyes [1, 3, 4, 6, 7]. Thanks to the rapid results, friendly operation, and simple storage, the colorimetric detection method has been used widely in society, such as the haemoglobin blood test, glucose test strip, and urine test strip, or commercial test kits for solution-based tests. Of these tools, commercial test kits are being used for research and in clinical laboratories due to their high sensitivity, various analyte tests, and especially, quantitative results. The effective accessory supporting commercial test kits is the microplate, which can be described as a pattern of microwells, equipped on a flat platform. The microplate supports the measurements of multiple samples at the same time, saving time and effort for the users. There are several types of microplates with various numbers of wells, i.e., 6, 24, 48, 96, or 384 wells, and different colours, i.e., black, white, or clear [8, 9]. Currently, the 96-well microplate (96-WM) is the plate most used in research and clinical facilities as it provides more options for the number of tests and has standard dimensions for use with commercial testing instruments [10, 11]. Although they can support multiple tests simultaneously, 96-WM reading requires specific equipment to examine multiple wells in the plate, which is usually cumbersome and non-portable, and this causes the operators to remain in a laboratory environment [12-14]. In recent years, many research and development for bringing the microplate reader to the remote testing conditions have been reported. In 2016, Feng et al. developed a portable 3D-printed device using a smartphone to perform the antimicrobial susceptibility testing (AST) on a 96-well microplate, targeting the gram-negative bacteria, *Klebsiella pneumoniae* with the measurement accuracy being over 95% [11]. In the same year, Fu et al. introduced another smartphone-based device, using

commercial chemicals to measure various biomarkers spiked in blood and urine samples [12]. Their device showed good results in the limit of detection of 17.54 U/L for alanine aminotransferase, 15.56 U/L for alkaline phosphatase, 0.00135 mmol/L (1.35 μ M) for creatinine spiked in urine samples, and other biomarkers. Other researchers also reported smartphone-related devices developed using microplate with clinical-approved testing kits to detect particular biomarkers of infectious diseases, such as varicella zoster virus IgG (VZV) for detecting chicken pox (varicella) and shingles (herpes zoster), cytomegalovirus IgG (CMV) for detecting herpes viruses, or the protein CFP-10 for detecting tuberculosis [13, 15], female reproductive steroid hormone profiles [14], or the progesterone concentration in the whole blood sample [16]. Although these devices reported high sensitivity and stability, most are only used in research applications. In these devices, a smartphone is commonly used as the optical sensor, but the rapid development of mobile technology and the varied dimensions of smartphones face the compatibility challenge, and the internal processing of the optical cameras affect the measurement accuracy, as well as potentially raising the concerns of user confidentiality and cross contamination hazards [5].

Another parameter for consideration when developing a chemical analysis device is the target analyte. As mentioned above, portable colorimetry devices can detect various chemical or biomolecules in solutions, which can be used as biomarkers, such as the presence of albumin in urine indicating kidney disease, a reduced citrate level in urine suggesting prostate cancer, the level of cardiac Troponin I (cTnI) in blood helping the diagnosis of acute myocardial infarction, or the absence of glutathione in saliva indicating the potential of head-neck cancer [5, 17-20]. The detection target will influence the design choices, such as the sensitivity of the detecting sensor, the background light intensity, and the recognising reagent type. In this research, urine has been chosen as the target biofluid due to its clinical importance in healthcare and the non-invasive method of collection. The chosen biomarkers are creatinine and glucose, which are two of the common biomarkers tested in human urine examination. In normal conditions, creatinine in urine varies from 2.5 to 17 mmol/L (28.28 to 192.304 mg/dL), while glucose is not present in urine [21]. The presence of glucose molecules in urine is a sign of biological dysfunction, whilst a high concentration of creatinine may be an indication of diabetes, muscle damage, or kidney disorder [22, 23]. In clinical urine tests, creatinine and glucose in urine samples can be first observed by using dip sticks. However, the dip-stick method only provides initial screening; therefore, medical staff often measure them on automated analysers using colorimetric or enzymatic assays with high accuracy and reliability. If the measurements from these methods can be equipped into a compact portable device, it will provide potential for use in rural and remote areas.

In this report, we have developed a portable colorimetry device to facilitate a 96-WM with a commercial test reagent. The targets of detection biomarkers in this research are glucose and creatinine, two common biomarkers present in human urine. The device was tested with two commercial test reagents, and its performance compared firstly with results from a clinical microplate

reader, and secondly, using urine samples from renal patients and comparing the results with clinical results provided by a local pathology laboratory.

5.2. Device Design, Working Mechanism and Post-Processing Algorithm

5.2.1. Device Design and Fabrication

Following the principle of a colorimetric reader, the device is comprised of four main components: a camera, a microplate, a white light source with detachable LEDs, and a controlled optical environment for the colorimetric measurement. During design and fabrication, there were several features to be considered to support device performance, such as a uniform background luminance for the measurement, a suitable luminance source to improve the quality of the optical measurement, an optical sensor to capture the visible colour change of the chemical, a modifiable structure to support the requirements of different measurements, and dimension and weight to support the device's portability.

The device was designed and developed to have the flexibility to work with multiple testing chemicals and optical wavelength requirements. The device hardware provides a controllable optical environment for the measurement. A detachable LED light source provides the flexibility to change LEDs for different chemical test requirements, where certain testing chemicals show a higher sensitivity with a certain optical wavelength. Moreover, 3D printing technology was used to achieve lightweight, affordable, and simple fabrication. A low-cost Raspberry Pi camera (Raspberry Pi Australia) with wide visible light spectrum sensitivity was used to capture the colour changes of the chemical mixtures. Image processing was applied for device calibration and colour change detection to increase the accuracy and robustness of the measurements. The device has the capacity to test multiple biomarkers with minimal operation. The device also has the potential to be extended for testing with other technologies, such as paper test strips, which have been employed in portable medical device development for many years [24, 25]. The detailed design of the device is explored below.

5.2.1.1. *The Camera and Microplate*

There are different types of 96-WM, specifically transparent and opaque plates. The transparent microplate is a common choice for the bottom-reading measurement performed in spectrometer, which is often operated in laboratory-condition spaces, whilst opaque microplates, white or black, are used for top-reading measurements. In this device, the colour solution is observed from the top and the colour development is captured by a digital camera; thus, a white opaque 96-WM was employed for the device. The 96-WM has dimensions of 127.76 × 85.48 × 14.22 mm, as shown in Figure 5.1A, which defines the minimum size for the device development.

In this study, a low-cost but high-performance digital Raspberry Pi camera v2.0 was used to capture images of the microplate. This camera's electronic board not only has a compact dimension of 32 × 32 mm with an affordable retail price of AUD 25.00, but it also shows adequate sensitivity for optical signals in the visible spectrum. The field of view (FOV) of the camera is an essential feature [18] for designing the device. The focal length of the Raspberry Pi camera requires the object to be placed further than 50 mm to guarantee the quality of the taken images. In addition, to support the image processing in the later stage, four black reference points were equipped around the microplate, as shown in Figure 5.1.A and C. Therefore, the height of the camera is optimally set at 112 mm for its FOV to cover both the microplate and the reference points, as shown in Figure 5.1.B and C. By placing the camera along the central axis of the microplate, the captured images are symmetric to minimise the optical distortion, or aberration effect, of the circular wells from the centre of the plate to the outer edges.

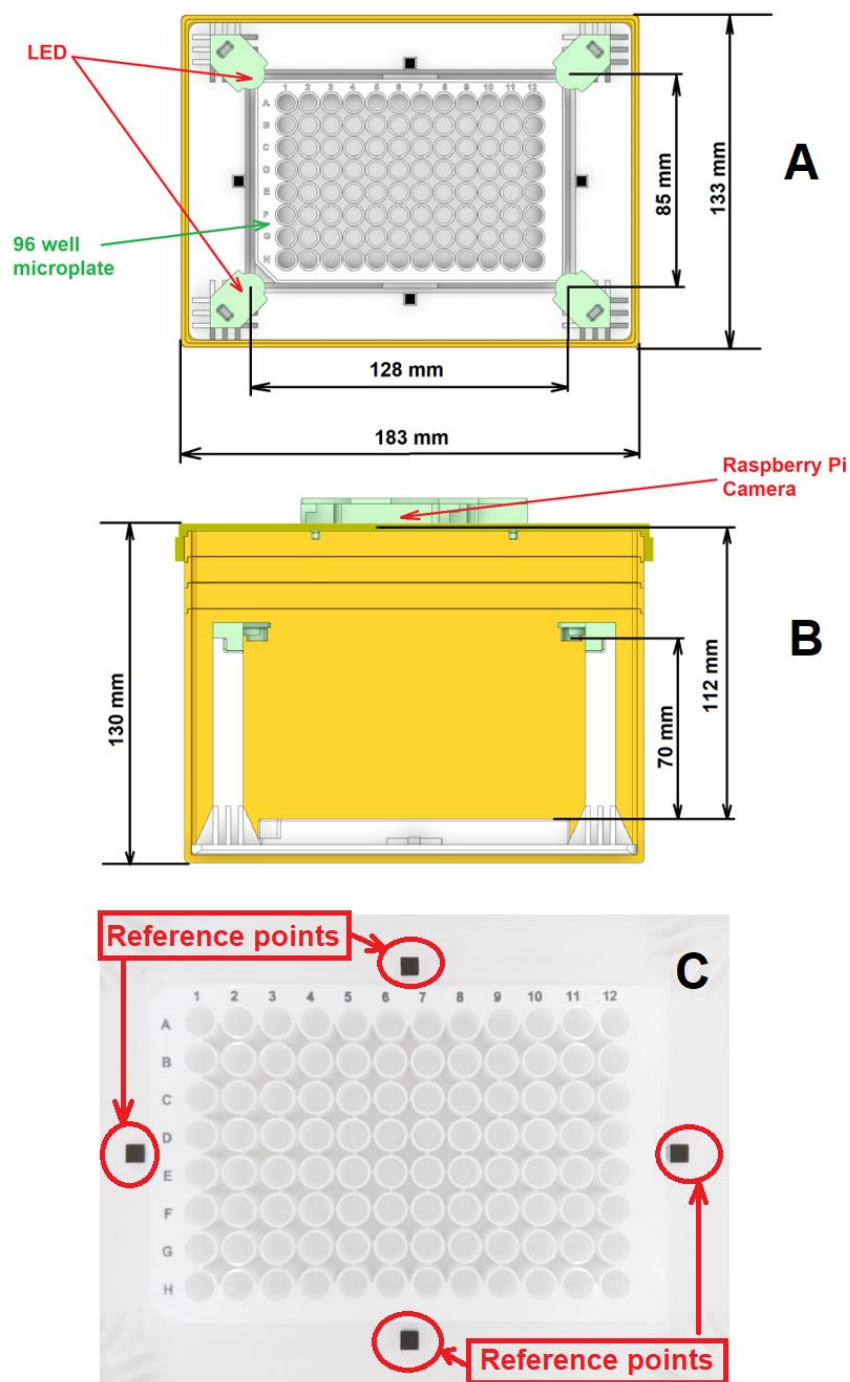


Figure 5.1. (A and B) The sketch of a 96-well microplate colorimetry prototype; and (C) a white 96-well microplate image taken by a Raspberry Pi camera in the proposed device (Dark squares are four reference points for image process).

5.2.1.2. The White Light Sources

An essential component for colorimetry measurement is the light source because it provides the optical input to the testing solution. When the white light illuminates the semi-transparent

substance, one portion of the light will be absorbed by the substance, another portion will be reflected from the substance, and the rest of the light will transmit through the substance, called the transferred light, as shown in Figure 5.5 in the supporting section. From the colorimetry principle, the concentration of chemicals affects the absorption property of the substance. By using a selective recognising reagent for a targeted chemical, the measurement aims to specifically capture the presence of the targeted chemical among the complex mixture of other chemicals. Researchers can detect the presence of the targeted chemical in the solution by estimating how much the light intensity varies after transmitting through or reflecting from the colour medium [26]. In this device, a white light source is employed since it can provide a full visible spectrum for the colorimetry measurement. In addition, the light source satisfies other design requirements, i.e., it can provide even illumination over the microplate's surface to minimise the interference noise from shadows on the microplate, minimising the footprint of the light source to minimise the dimensions of the prototype and adding the flexibility to change light sources for various types of colorimetry measurement that may be used in the future. In this device, four cool white LEDs with a 120-degree beam angle were placed at the corners of the microplate. The white LEDs, purchased online from CH_Town Electronics, have a colour temperature of 4000–4500 K with 500–600 lumen output for the maximum 5W output power. The LEDs are orientated so that the beam direction is perpendicular to the plate, and the distance from the LED to the plate's surface is 70 mm. These LEDs can be powered by a 9 V battery or the Raspberry Pi module, increasing the portability of the device. Moreover, the LEDs are detachable for easy replacement with different light sources to support other colorimetric measurements.

5.2.1.3. Main Hardware Body

To minimise interference from ambient environmental light, all optical components, including a 96-WM, a light source, and a camera, are enclosed within a box. The box is fabricated from polylactic acid (PLA) material using 3D-printing technology, which is affordable and common on the market. All inner components are fixed in position to prevent shaking and blurring of colour images. There are four black squares at each side of the testing plate, to be used as reference points to support the image processing, as shown in Figure 5.1.C.

5.2.2. Reagent Kits and Reaction Mechanism

The commercial test reagent of glucose and creatinine (Thermo Fisher Scientific, Australia) are used. Both reagents are designed to give quantitative results for glucose and creatinine concentrations in urine samples. Each test provides a set of standards, which can be used to generate a standard fitting curve, showing the relationship between colour intensity and concentration. MATLAB (Version R2021b) was used to perform the image processing to identify the colour intensities of the testing samples, the standard fitting curve and to determine the concentrations of the biomarker in the testing solution.

5.2.2.1. Creatinine Test Reagent and Sensing Mechanism

The creatinine test reagent follows the Jaffe reaction, a specific technique of colorimetry for monitoring creatinine in biofluids. In the Jaffe method, when creatinine reacts with picric acid in an alkaline environment, it develops a red colour [27]. The red intensity varies proportionally depending on the creatinine concentration in the solution. From the set of 7 standards with concentration increasing from 0 to 1.77 mmol/L (20 mg/dL), the operator can produce the standard fitting curve for creatinine. When testing urine samples, the operator will dilute the samples with distilled water to lower the concentration of creatinine to fit in the range of detection. After being mixed with the testing reagent and incubating at the room temperature for 30 min, if creatinine is present in the sample, the mixture will turn to a red colour, which will be matched to the fitting curve to calculate the creatinine concentration. In clinical measurement, the abnormal creatinine concentration in urine samples may be much higher than the detection range; thus, further dilution and re-testing are recommended to achieve a reliable result. The further detail of the commercial creatinine test kit is introduced later.

5.2.2.2. Glucose Test Reagent and Sensing Mechanism

The glucose test reagent uses colorimetric substrate, horseradish peroxidase (HRP) and glucose oxidase as the recognising reagents. When combined with any glucose in the urine sample, the mixture turns from colourless to a pink solution, and the strength of the pink colour level corresponds to the concentration of glucose in the urine sample. A beta-D-glucose standard is prepared to give the standard fitting curve with the detection range of 0 to 32 mg/dL of glucose. When testing, the urine sample is diluted with a glucose buffer to a certain level, then mixed with the other dye reagents, i.e., the glucose substrate, the horseradish peroxidase (HRP) and the glucose oxidase. After being mixed with the urine sample and left for incubation at room temperature for 30 min, if glucose is present in the solution, the mixture will turn a pink colour, which will be captured and analysed to give the concentration of glucose in the urine sample. Similarly with the creatinine test kit, if the glucose in the urine samples is over the detection range, further dilution and re-testing are recommended to obtain a reliable and accurate measurement of glucose concentration. The further detail of the commercial glucose test kit is introduced later.

5.3. Image Processing Algorithm

5.3.1. Alignment

To reduce the complexity of image alignment and segmentation, the device includes four reference points, shown in Figure 5.1.C. The points are used to align the test and calibration images, and they are also used as a reference to define the segmentation locations of the test and reference colour blocks in 96-WM. The details on detecting the location of the four reference points and performing alignment can be found here [28].

5.3.2. Calibration

A single test image contains both the test and reference colour blocks in a 96-WM. To measure the correct concentration of a biomarker, it is important that the illumination across the whole image is homogeneous. In practice, this is not possible as the illumination at different points across the image can be affected by variations among the four light sources and light source intensity over time, variations in camera sensitivity within an image regarding the flat fielding effect and colour sensitivity, and variations between devices. To make the biomarker concentration measurement invariant to these changes, a calibration process has been developed that uses an image of a white block to correct the test image, as reported previously [28].

5.3.3. Segmentation and Intensity Measurement

Following the image alignment process, the position of the 96 wells within an image will not change significantly. Therefore, the segmentation locations for each well are defined relative to the four reference points. These segmentation locations are indicated in Figure 5.6 (in the supporting section) by red borders. To obtain three single RGB intensity values from each well, intensity values that correspond to the highest frequency of occurrence in the respective RGB histograms are found using the method described in [18, 29]. The intensity is calculated in this way to ensure that it is robust to different noise sources that may affect the image, such as sensor noise and artefacts such as reflections, glare, bubbles, and parts of the well that do not include the solution. The Raspberry Pi camera can capture the whole visible spectrum, but to obtain a single intensity value, the three RGB intensity values can be combined in a weighted average based on the camera sensitivity at absorbance wavelengths [18, 29]. The absorbance wavelength has been used in previous analytical devices because it is constant and has the largest dynamic range for measurement with respect to the concentration of the analyte [30-32]. The peak absorbance wavelength for creatinine is 490 nm, and the peak absorbance wavelength for glucose is 560 nm (Refer to the manual documents of commercial test kit of glucose and creatinine). The sensitivity of the Raspberry Pi camera in the three RGB channels, from the Sony IMX219 datasheet and [33], is shown in Figure 5.2, along with the absorption wavelengths. The weighted average of the three RGB components is as follows:

$$y = aI_R + bI_G + cI_B \quad (4.1)$$

where I_R , I_G , and I_B are the red, green, and blue intensity values in the image and a , b , and c are the coefficients corresponding to the sensitivity of the camera at the peak absorbance wavelength. The a , b , and c coefficients are found using the RGB sensitivities, namely, R_S , G_S , and B_S , respectively, as follows:

$$a = \frac{R_S}{R_S + G_S + B_S} \quad (4.2)$$

$$b = \frac{G_S}{R_S + G_S + B_S} \quad (4.3)$$

$$c = \frac{B_S}{R_S + G_S + B_S} \quad (4.4)$$

The camera sensitivity values for creatinine and glucose are $R_S = 0.07$, $G_S = 0.82$, and $B_S = 0.66$ and $R_S = 0.13$, $G_S = 0.83$, and $B_S = 0.11$, respectively, as shown in Figure 5.2.

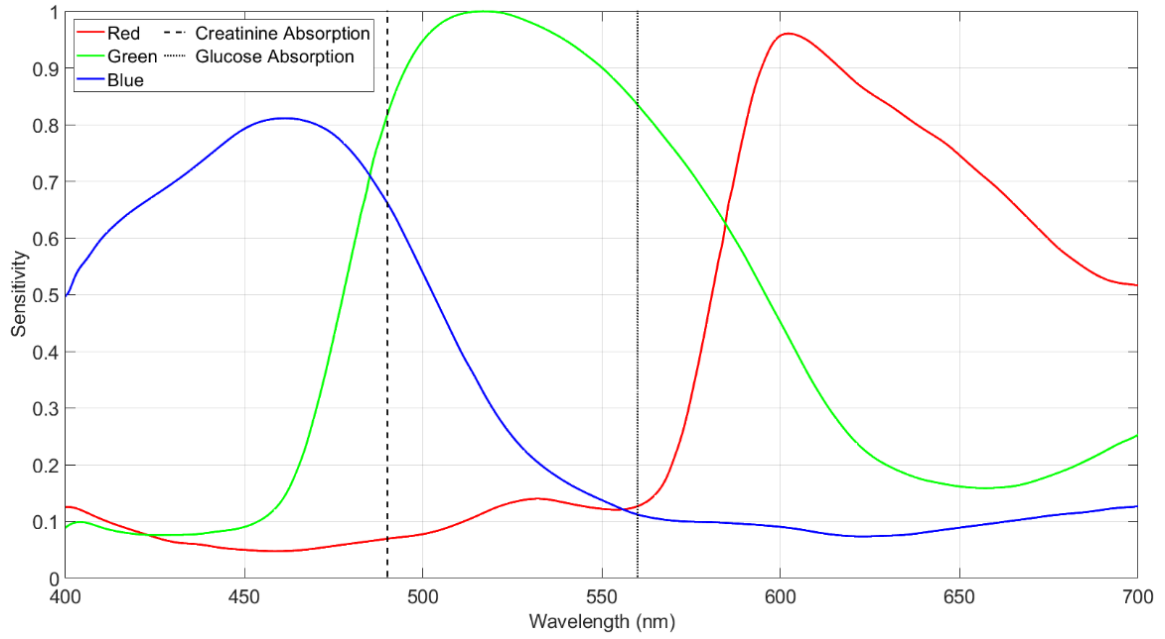


Figure 5.2. The Raspberry Pi SONY IMX219 camera RGB sensitivity and the absorption wavelength of the creatinine and glucose.

5.3.4. Measurement

The absorption of the solution is measured using optical density (OD), which is a logarithmic intensity ratio of the light reaching the solution to the light transmitted through the solution as follows [34]:

$$OD = -\log_{10} \frac{I_o}{I_t} \quad (4.5)$$

where I_o and I_t are the intensities of the incident and transmitted lights, respectively.

The transmitted light is the intensity at the absorption wavelength found in Equation (4.5) and

the incident light is estimated based on the intensity values of the empty wells. As the intensity of the wells can change slightly from the centre to the edges of the plate, the mean of the empty well intensity in the 5×5 neighbourhood of the current well is used to estimate the incident light intensity. To estimate the local incident light intensity, first, a histogram of the intensities of all 96 wells is constructed as follows:

$$H_y(y_k) = n_{y_k} \quad (4.6)$$

where $k = 0, 1, \dots, L - 1$ and n_{y_k} represents the number of times that the intensity level y_k appears across the 96 wells. Considering the wells containing the solution will have varying intensity values and empty wells will have similar values, the intensity of the empty wells will be the value that appears most frequently in the histogram. The most frequent empty well intensity value can be determined using a maximum operator as follows:

$$w = n: (H_y(n) = \operatorname{argmax}(H_y)) \quad (4.7)$$

To find the mean value of the intensity of the empty wells adjacent to the current well, let S_y be the set of all well intensities in the 5×5 neighbourhood. The set of empty wells, S_w , is then determined as those with an intensity greater than or equal to 95% of the most frequent empty well value, w , as follows:

$$S_w = \{S_y(p): S_y(p) \geq 0.95w\} \quad (4.8)$$

where $p = 1, 2, \dots, P$ and P is the cardinal number of S_y .

The mean intensity of the local empty wells is found as follows:

$$w_L = \frac{\sum_{q=1}^Q S_y(q)}{Q} \quad (4.9)$$

where $q = 1, 2, \dots, Q$ and Q is the cardinal number of S_w .

The OD is calculated using the mean of the empty well intensity in the 5×5 neighbourhood to estimate the incident light input as follows:

$$OD = -\log_{10} \frac{w_L}{y} \quad (4.10)$$

To determine the actual concentration from an OD value, the line of best fit is found using

the standard concentration samples. The known concentration values have a logarithmic relationship to the OD values; therefore, the log value of the concentration is used when determining the line of best fit. The diluted concentration value is found as follows:

$$C_d = e^{(xOD+z)} \quad (4.11)$$

where x and z are the linear coefficients from the line of best fit.

The actual concentration value is then determined by multiplying the diluted concentration value with the dilution factor, d_f , as follows:

$$C = C_d d_f \quad (4.12)$$

To reduce the complexity of image alignment and segmentation, the device includes four reference points, shown in Figure 5.1.C. The points are used to align the test and calibration images, and they are also used as a reference to define the segmentation locations of the test and reference colour.

5.4. Evaluation of the developed prototype on measuring Creatinine in the artificial urine sample in compared with a commercial microplate reader

5.4.1. The commercial microplate reader

The performance of the prototype device was evaluated by comparing results obtained by the device using commercial test reagents to detect biomarkers in the biofluid samples with results from a commercial microplate reader. A microplate reader is a common instrument used in clinical and research laboratories. It can provide specific wavelength luminescence for different colorimetry measurement. In addition, with the high-sensitive photocell, the reader can examine the colour of the single well on the microplate. By testing the colour wells in an enclosed dark-space with precise illumination and detection, the reader gives an accurate colour value for the individual well. The microplate reader for this evaluation is the multi-mode microplate reader, SpectraMax iD5. When working with the glucose and creatinine commercial kits, the SpectraMax iD5 is required to use the bottom-read luminescence method, thus using the transparent microplate as opposed to the white opaque microplate used in the prototype device. The general steps of obtaining a measurement using the commercial test kits in the 96-WM with the microplate reader and the proposed colorimetry device are described in the flowchart shown in Figure 5.9.

5.4.2. Sample preparation for the test

When preparing the solutions for the microplate test, the standards are often placed in the wells across the top row of the plate, and the test solutions are prepared in the other wells, as shown in Figure 5.3A. For the measurement with a microplate reader, all chemicals were poured into a transparent plate to support the bottom-reading process. Then, all chemicals were transferred to a white opaque microplate for measurement in the device, as shown in Figure 5.3.B. Finally, the white plate with chemicals was put in the device for image capture prior to colour analysis. An image of the test in the developed device is shown in Figure 5.3B. The results of testing samples obtained from the colorimetry device and the microplate reader were compared with the expectation that the calculated results from the device and the microplate reader will be close to the real concentration of the biomarkers in the prepared samples.

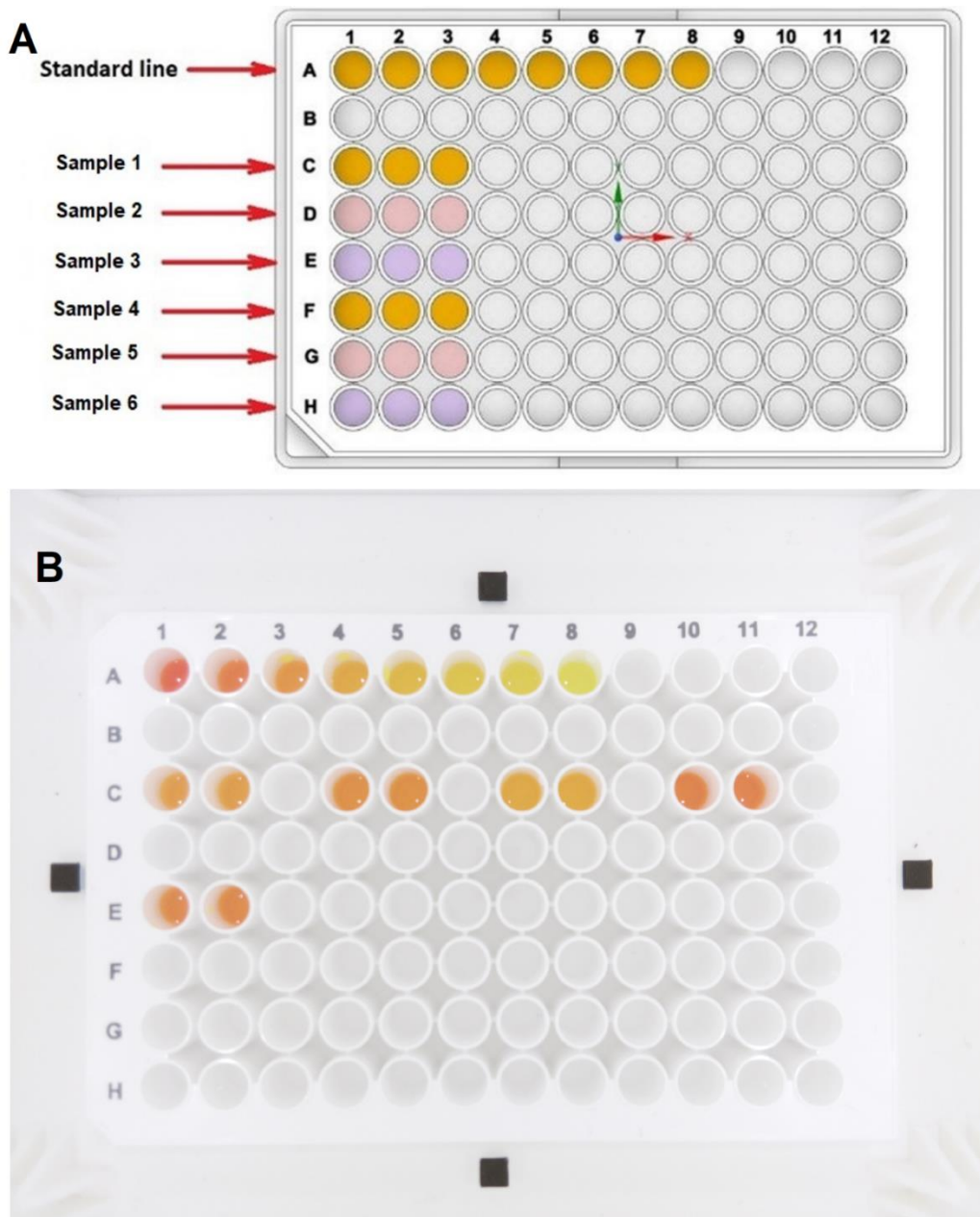


Figure 5.3. The 96-well microplates with the example of creatinine solutions. (A) The sketch of the 96-WM with the standards in wells A(1–8) and the testing solution in other wells; (B) An image of the creatinine solutions taken by the Raspberry Pi camera in the proposed colorimetry device.

5.4.3. Result and discussion

For the comparison of the device with the commercial reader, standard samples were compared. As shown in Figure 5.4, the device and the commercial reader produce a similar fit for the standard samples. The log of the known concentration values was used with the device for a linear fit. In this comparison, one of the standard samples was used as an unknown concentration; the 4 mg/dL glucose sample and the 0.221 mmol/L (2.5 mg/dL) creatinine sample and the concentration of these samples was determined using the linear fits from Figure 5.4. Table 5.1 (in the supporting section) shows that the device produced a more accurate concentration value for the unknown samples for both the glucose and creatinine measurements. When testing the samples with the known concentrations for glucose and creatinine, the developed device can detect and indicate the biomarkers concentrations, within 10% of the gold standard [16], as shown in Table 5.1 (in the supporting section). These results have confirmed the ability of the device to perform as a reader for the measurement of glucose and creatinine using commercial test kits and the 96-WM.

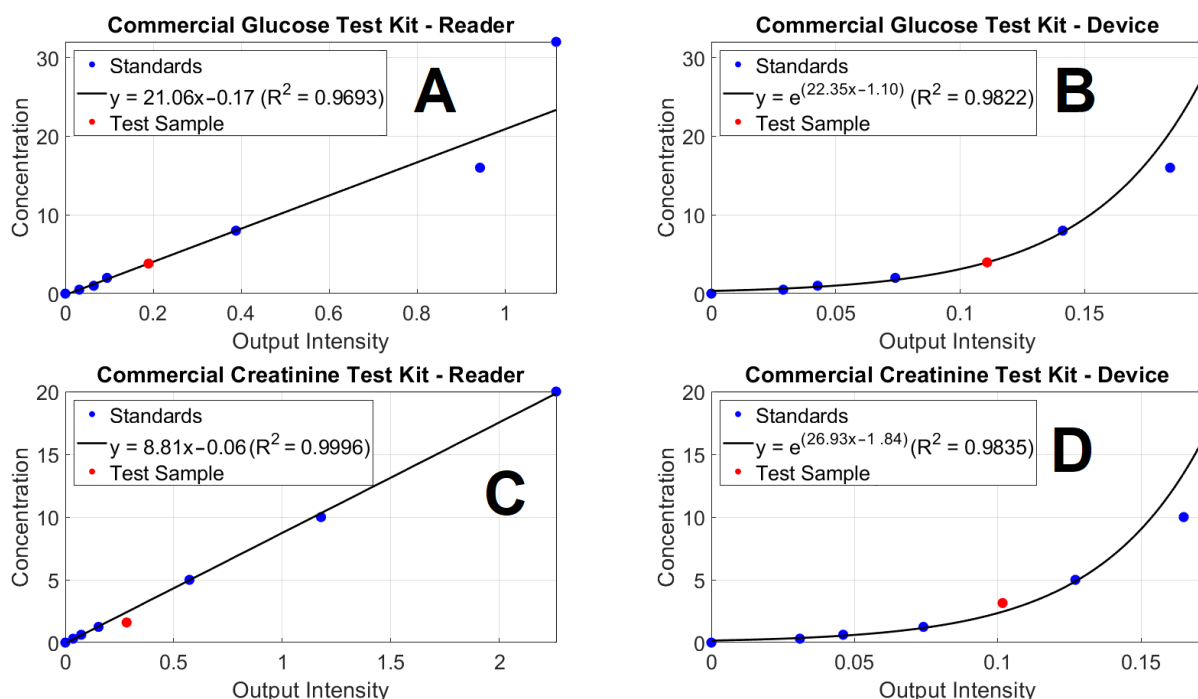


Figure 5.4. The unknown testing samples (red dot) are illustrated in the graphs of the standards from (A and B) glucose and (C and D) creatinine commercial test reagents, operated by

(A and C) a microplate reader and (B and D) the developed device.

5.4.4. Conclusion

From the results, the developed colorimetry measuring prototype can achieve the linear response in compared with a commercial microplate reader in examining glucose and creatinine levels in the testing solution by using the commercial test kits. When running the reference test, the developed prototype can detect the concentrations of glucose and creatine in an “unknown” standard sample, which is consistent to the results obtained from the commercial reader. In the next progress, the colorimetry prototype will be evaluated through a clinical process, which will be described in chapter 6.

5.5. Supporting information for Colorimetry Monitoring Device Development

The details of the commercial test kits are described in detail in the manual documents of the commercial test kits of urine glucose and creatinine, which can be obtained from Thermo Fisher Scientific, Australia websites:

For the Invitrogen™ Creatinine Urinary Detection Kit (EIACUN):
<<https://www.thermofisher.com/order/catalog/product/EIACUN>>

For the Invitrogen™ Glucose Colorimetric Detection Kit (EIAGLUC):
<<https://www.thermofisher.com/order/catalog/product/EIAGLUC>>

In the colorimetry monitoring device in this research, the optical transferring substance was a mixture of the urine sample and the recognising chemical; the incoming light was the white light produced from four white LEDs equipped inside the device. The Raspberry Pi camera was set-up at the same side with the LEDs to the solution, thus the detected optical signal was the reflecting light from the solution after being illuminated by the white light, as shown in Figure 5.5.

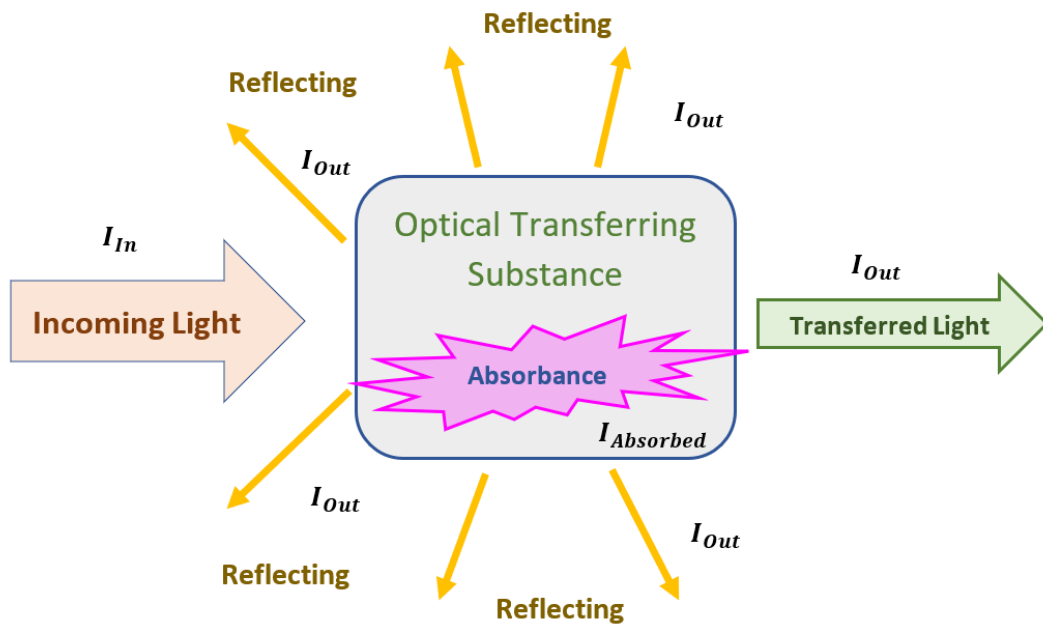


Figure 5.5. Possible progress pathways for the light coming to an optical semi-transparent substance. The target signal of the developed colorimetry monitoring device in the research is the reflecting light.

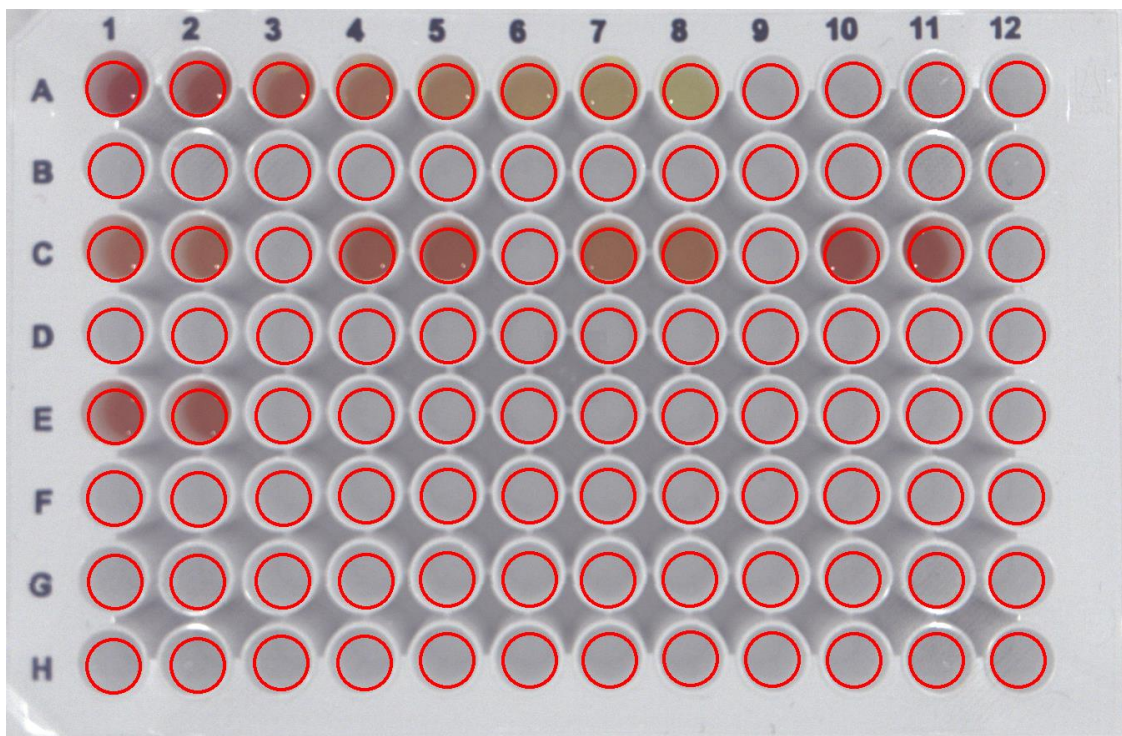


Figure 5.6. An example of a calibrated test image with red coloured borders indicating the segmentation locations of the 96 wells.

The segmentation locations for the 96 wells in the test plate are shown in Figure 5.6. The RGB intensity detection process is robust to different noise sources which may affect the image, such as sensor noise and artefacts like reflections, glare, bubbles and parts of the well which do not include the solution. Figure 5.7 shows the RGB histograms and the detected RGB intensities for well A1 in Figure 5.6, the sides of the well in the segmentation region correspond to the upper tail in the histogram, which does not affect the detection of the RGB intensities. For comparison, Figure 5.8 shows the RGB histograms and the detected RGB intensities for well A6 in Figure 5.6, the upper tail in the histogram is reduced because there is less of the well background included in the segmentation region. Therefore, the size of the segmentation region was defined to include a larger area of the solution, as the intensity measurement is unaffected by the sides of the well included in the segmentation region.

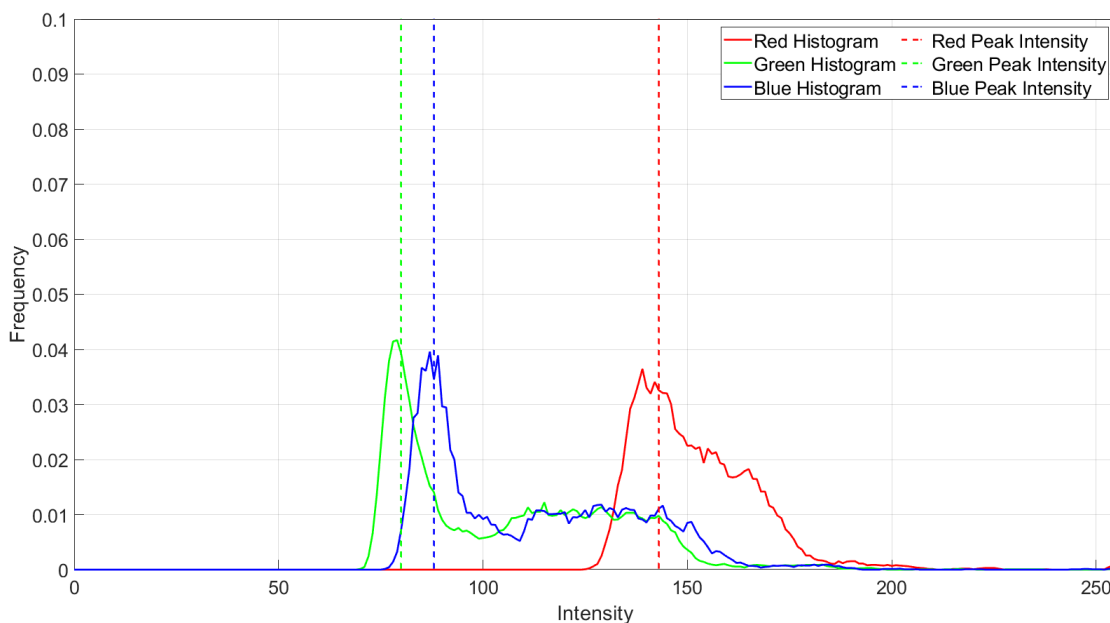


Figure 5.7. The RGB histograms and the detected RGB intensities for well A1 in Figure 5.6.

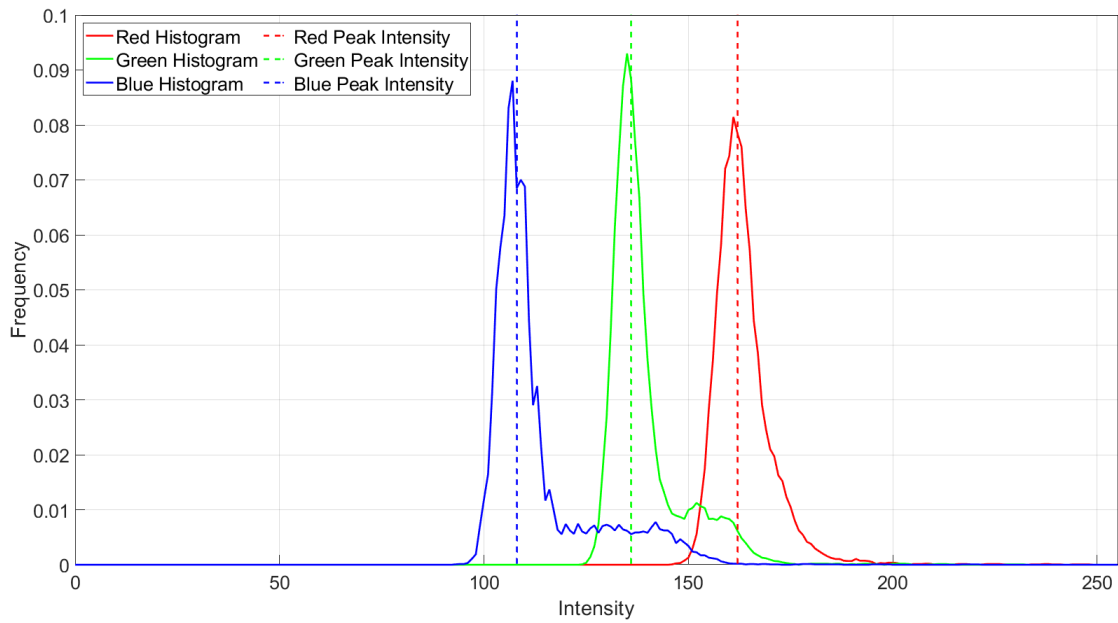


Figure 5.8. The RGB histograms and the detected RGB intensities for well A6 in Figure 5.6.

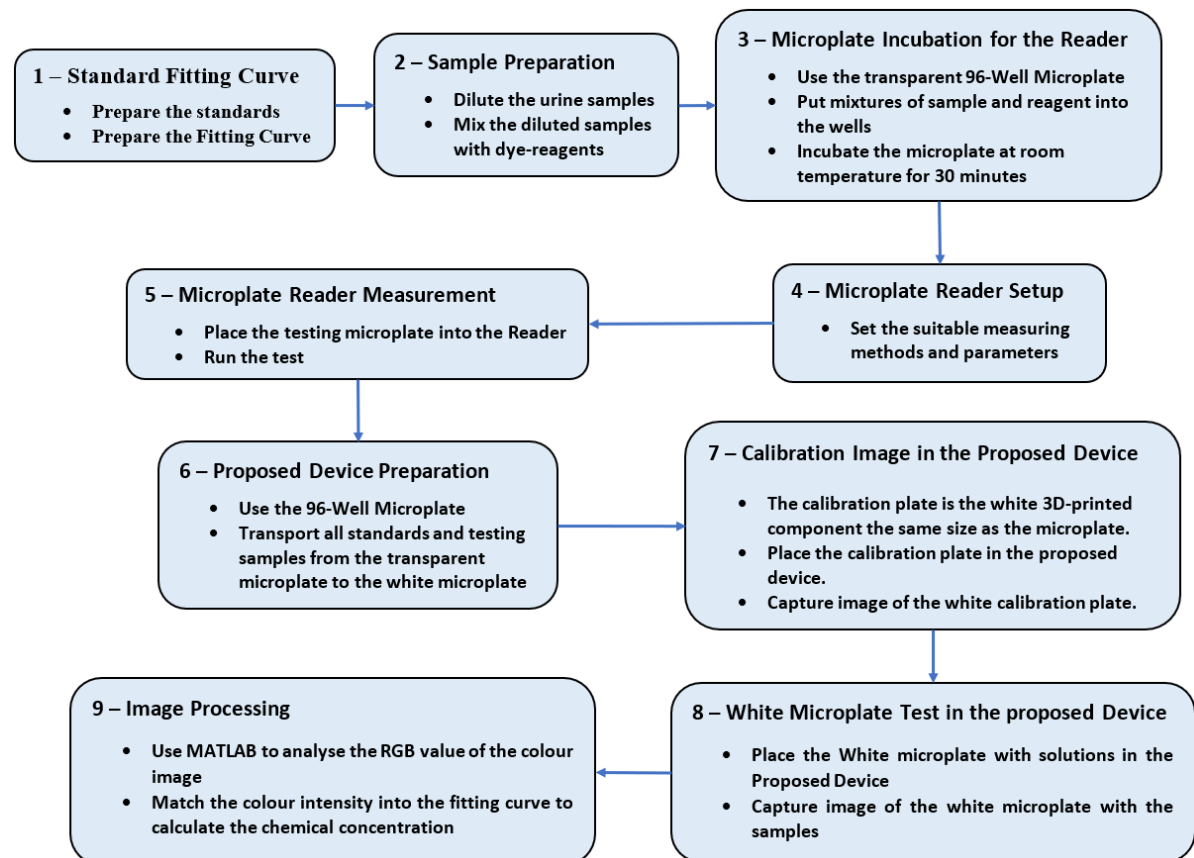


Figure 5.9. The flowchart of general steps of the measurement using commercial test reagents in the 96-WM with a microplate reader and the proposed colorimetry device.

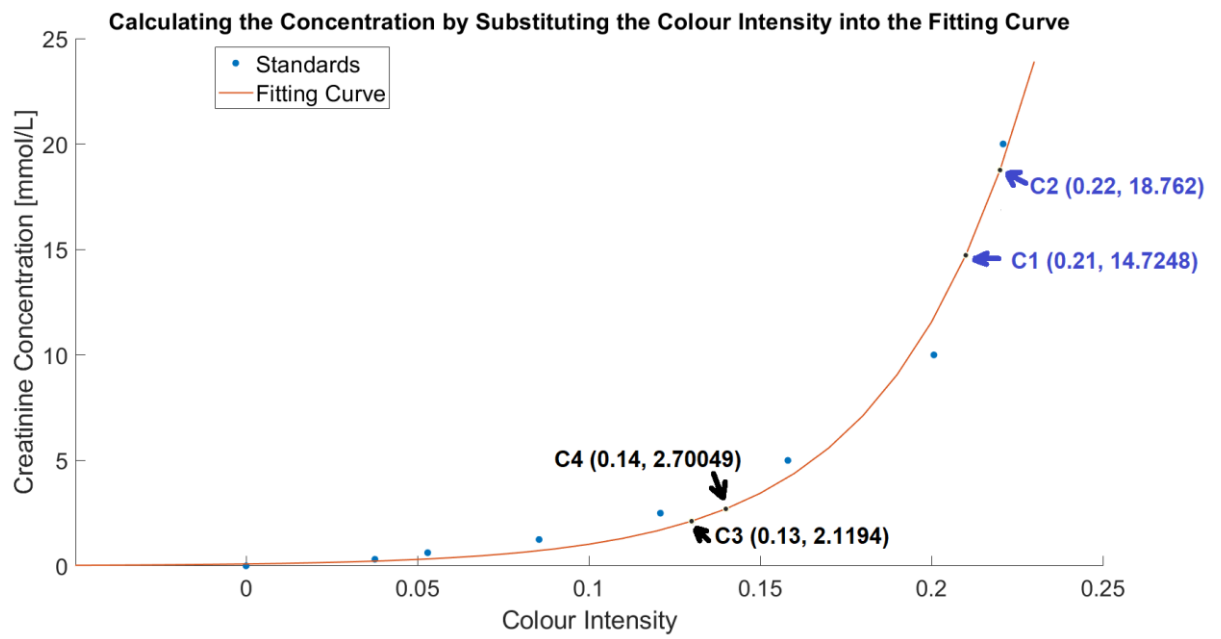


Figure 5.10. The effect of the exponential fitting curve in calculating the high concentration of creatinine in urine sample. Two data pairs (C1-C2 and C3-C4) have 0.01 unit different in intensities, however, the variations in concentration are 4.0372 and 0.581 units respectively due to the high-range of concentration in the pair C1-C2.

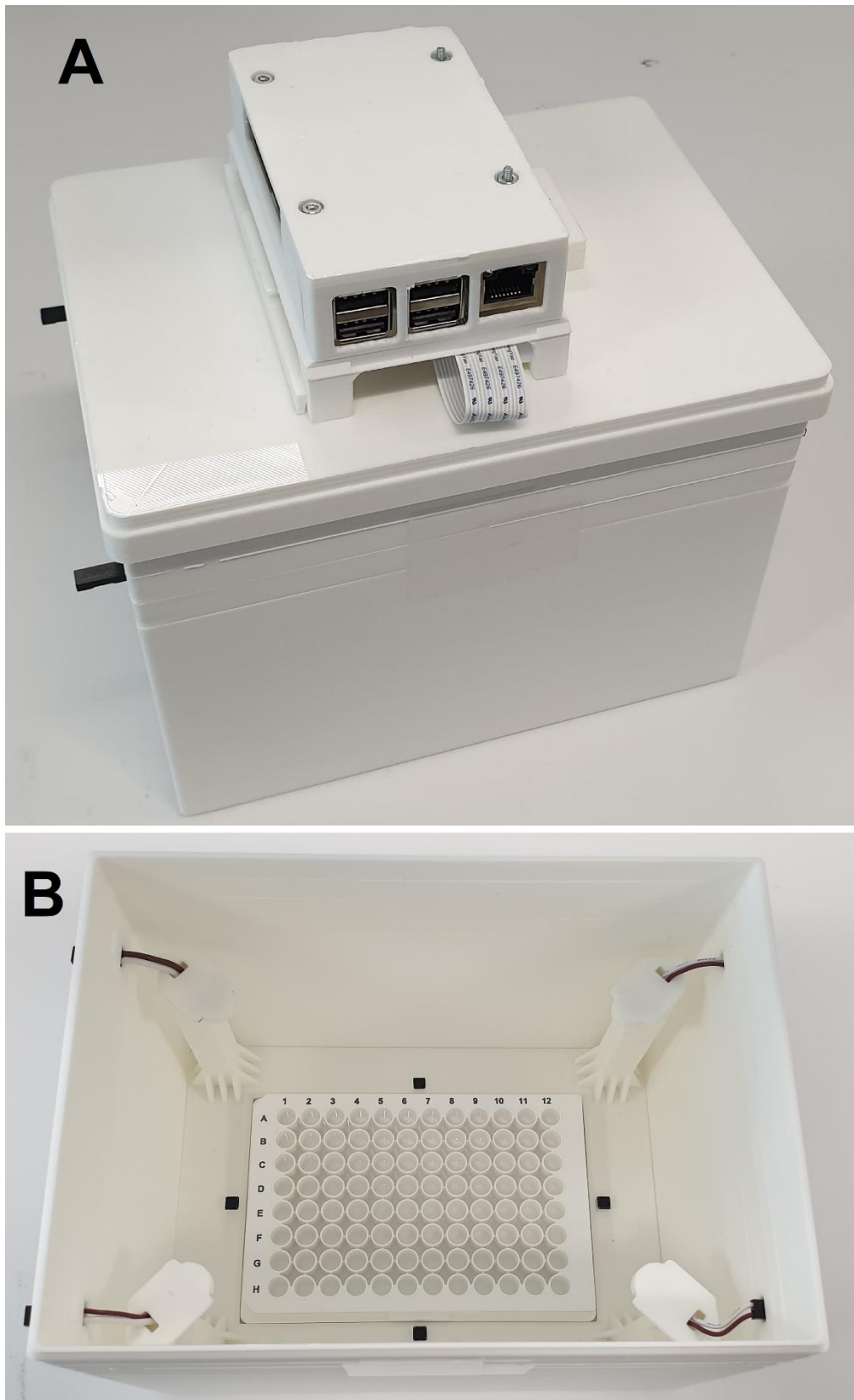


Figure 5.11. The picture of the real colorimetry device: (A) The outer view; and (B) The inner view with the 96 well microplate.

Table 5.1: The prepared concentrations for glucose and creatinine samples, the results obtained from the SpectraMax iD5 microplate reader and the results obtained from the developed colorimetry device.

Biomarker	Prepared concentration	Result from the microplate reader	Result from the colorimetry device
Glucose (mg/dL)	4.00	3.82	3.97
Creatinine (mg/dL)	2.50	2.42	2.46

Reference

1. Sanjay, S.T., Fu, G., Dou, M., Xu, F., Liu, R., Qi, H., and Li, X., *Biomarker detection for disease diagnosis using cost-effective microfluidic platforms*. *Analyst.*, 2015. **140**: pp. 7062-7081. DOI: 10.1039/c5an00780a.
2. Gao, Z., Xu, M., Lu, M., Chen, G., and Tang, D., *Urchin-like (gold core)@(platinum shell) nanohybrids: A highly efficient peroxidase-mimetic system for in situ amplified colorimetric immunoassay*. *Biosens. Bioelectron.*, 2015. **70**: pp. 194-201. DOI: 10.1016/j.bios.2015.03.039.
3. Vilela, D., González, C.M., and Escarpa, A., *Sensing colorimetric approaches based on gold and silver nanoparticles aggregation: Chemical creativity behind the assay. A review*. *Anal Chim Acta.*, 2012. **751**: pp. 24-43. DOI: 10.1016/j.aca.2012.08.043.
4. Gibbs, J., Vessels, M., and Rothenberg, M., *Selecting the Detection System - Colorimetric, Fluorescent, Luminescent Methods for ELISA Assays*, in *ELISA Technical Bulletin - No 5, Corning Life Sciences*. 2017, Corning Incorporated: Corning: NY, USA. pp. 1-14.
5. Pham, A.T.T., Wallace, A., Zhang, X., Tohl, D., Fu, H., Chuah, C., Reynolds, K.J., Ramsey, C., and Tang, Y., *Optical-Based Biosensors and Their Portable Healthcare Devices for Detecting and Monitoring Biomarkers in Body Fluids*. *Diagnostics (Basel)*, 2021. **11**(7). DOI: 10.3390/diagnostics11071285.
6. Cho, Y.-T., Su, H., Wu, W.-J., Wu, D.-C., Hou, M.-F., Kuo, C.-H., and Shiea, J., *Chapter Six - Biomarker Characterization by MALDI-TOF/MS*, in *Advances in Clinical Chemistry*, Editor: Makowski, G.S. 2015, Elsevier. pp. 209-254. DOI: <https://doi.org/10.1016/bs.acc.2015.01.001>.

7. Wu, L. and Qu, X., *Cancer biomarker detection: Recent achievements and challenges*. Chem Soc Rev., 2015. **44**(10): pp. 2963-2997. DOI: 10.1039/c4cs00370e.
8. Bergua, J.F., Alvarez-Diduk, R., Idili, A., Parolo, C., Maymo, M., Hu, L., and Merkoci, A., *Low-Cost, User-Friendly, All-Integrated Smartphone-Based Microplate Reader for Optical-Based Biological and Chemical Analyses*. Anal Chem, 2022. **94**(2): pp. 1271-1285. DOI: 10.1021/acs.analchem.1c04491.
9. Yang, Y., et al., *A laser-engraved wearable sensor for sensitive detection of uric acid and tyrosine in sweat*. Nat Biotechnol, 2020. **38**(2): pp. 217-224. DOI: 10.1038/s41587-019-0321-x.
10. Ringuet, S., Sassano, L., and Johnson, Z.I., *A suite of microplate reader-based colorimetric methods to quantify ammonium, nitrate, orthophosphate and silicate concentrations for aquatic nutrient monitoring*. J Environ Monit, 2011. **13**(2): pp. 370-376. DOI: 10.1039/c0em00290a.
11. Feng, S., Tseng, D., Di Carlo, D., Garner, O.B., and Ozcan, A., *High-throughput and automated diagnosis of antimicrobial resistance using a cost-effective cellphone-based micro-plate reader*. Sci Rep, 2016. **6**. DOI: 10.1038/srep39203.
12. Fu, Q., Wu, Z., Li, X., Yao, C., Yu, S., Xiao, W., and Tang, Y., *Novel versatile smart phone based Microplate readers for on-site diagnoses*. Biosens Bioelectron, 2016. **81**: pp. 524-531. DOI: 10.1016/j.bios.2016.03.049.
13. Wang, L.J., Naude, N., Demissie, M., Crivaro, A., Kamoun, M., Wang, P., and Li, L., *Analytical validation of an ultra low-cost mobile phone microplate reader for infectious disease testing*. Clin Chim Acta, 2018. **482**: pp. 21-26. DOI: 10.1016/j.cca.2018.03.013.
14. Ogirala, T., Eapen, A., Salvante, K.G., Rapaport, T., Nepomnaschy, P.A., and Parameswaran, A.M., *Smartphone-based colorimetric ELISA implementation for determination of women's reproductive steroid hormone profiles*. Med Biol Eng Comput, 2017. **55**(10): pp. 1735-1741. DOI: 10.1007/s11517-016-1605-7.
15. Shabut, A.M., Hoque Tania, M., Lwin, K.T., Evans, B.A., Yusof, N.A., Abu-Hassan, K.J., and Hossain, M.A., *An intelligent mobile-enabled expert system for tuberculosis disease diagnosis in real time*. Expert Syst. Appl., 2018. **114**: pp. 65-77. DOI: 10.1016/j.eswa.2018.07.014.
16. Zhdanov, A., Keefe, J., Franco-Waite, L., Konnaiyan, K.R., and Pyayt, A., *Mobile phone based ELISA (MELISA)*. Biosens Bioelectron, 2018. **103**: pp. 138-142. DOI:

10.1016/j.bios.2017.12.033.

17. Zhang, X., Yao, B., Hu, Q., Hong, Y., Wallace, A., Reynolds, K., Ramsey, C., Maeder, A., Reed, R., and Tang, Y., *Detection of biomarkers in body fluids using bioprobes based on aggregation-induced emission fluorogens*. Mater. Chem. Front., 2020. **4**: pp. 2548-2570. DOI: 10.1039/D0QM00376J.
18. Pham, A.T.T., Tohl, D., Wallace, A., Hu, Q., Li, J., Reynolds, K.J., and Tang, Y., *Developing a fluorescent sensing based portable medical open-platform - a case study for albuminuria measurement in chronic kidney disease screening and monitoring*. Sens. Bio-Sens. Res., 2022. **37**. DOI: 10.1016/j.sbsr.2022.100504.
19. Traverso, N., Ricciarelli, R., Nitti, M., Marengo, B., Furfaro, A.L., Pronzato, M.A., Marinari, U.M., and Domenicotti, C., *Role of glutathione in cancer progression and chemoresistance*. Oxid Med Cell Longev., 2013. **2013**. DOI: 10.1155/2013/972913.
20. Derindag, G., Akgul, H.M., Kiziltunc, A., Ozkan, H.I., Kiziltunc Ozmen, H., and Akgul, N., *Evaluation of saliva glutathione, glutathione peroxidase, and malondialdehyde levels in head-neck radiotherapy patients*. Turk J Med Sci, 2021. **51**(2): pp. 644-649. DOI: 10.3906/sag-2006-84.
21. Lewińska, I., Speichert, M., Granica, M., and Tymecki, Ł., *Colorimetric point-of-care paper-based sensors for urinary creatinine with smartphone readout*. Sens. Actuators B: Chem., 2021. **340**. DOI: 10.1016/j.snb.2021.129915.
22. Liu, Y., Deng, C., Tang, L., Qin, A., Hu, R., Sun, J.Z., and Tang, B.Z., *Specific detection of D-glucose by a tetraphenylethene-based fluorescent sensor*. J. Am. Chem. Soc., 2011. **133**(4): pp. 660-663. DOI: 10.1021/ja107086y.
23. Chen, T., Xie, N., Viglianti, L., Zhou, Y., Tan, H., Tang, B.Z., and Tang, Y., *Quantitative urinalysis using aggregation-induced emission bioprobes for monitoring chronic kidney disease*. Faraday Discuss., 2017. **196**: pp. 351-362. DOI: 10.1039/C6FD00153J.
24. Kim, S.C., Jalal, U.M., Im, S.B., Ko, S., and Shim, J.S., *A smartphone-based optical platform for colorimetric analysis of microfluidic device*. Sens. Actuators B: Chem., 2017. **239**: pp. 52-59. DOI: 10.1016/j.snb.2016.07.159.
25. Charbaji, A., Heidari-Bafroui, H., Rahmani, N., Anagnostopoulos, C., and Faghri, M. *A 3D Printed Lightbox for Enhancing Nitrate Detection in the Field Using Microfluidic Paper-Based Devices*. In Proceedings of *Innovations in Microfluidics & SCA 2022*. 2022. Boston, USA.
26. Choudhury, A.K.R., *Colour measurement instruments*, in *Principles of Colour and*

- Appearance Measurement*. 2014. pp. 221-269. DOI: 10.1533/9780857099242.221.
27. Delanghe, J.R. and Speeckaert, M.M., *Creatinine determination according to Jaffe-what does it stand for?* NDT Plus, 2011. **4**(2): pp. 83-86. DOI: 10.1093/ndtplus/sfq211.
 28. Tohl, D., Pham, A.T.T., Li, J., and Tang, Y., *Point-of-care image-based quantitative urinalysis with commercial reagent strips: design and clinical evaluation*. Biosens Bioelectron, 2023 (Submitted).
 29. Tohl, D., Teferra, M.N., Wallace, A., Pham, A.T.T., and Tang, Y., *Re-Referencing and Calibration for Robust Ratiometric Light Intensity Measurement*. IEEE Trans. Instrum. Meas., 2022. **71**: pp. 1-8. DOI: 10.1109/tim.2022.3194929.
 30. Kim, J.-H., Lee, Y.-J., Ahn, Y.-J., Kim, M., and Lee, G.-J., *In Situ Detection of Hydrogen Sulfide in 3D-Cultured, Live Prostate Cancer Cells Using a Paper-Integrated Analytical Device*. Chemosensors, 2022. **10**(1). DOI: 10.3390/chemosensors10010027.
 31. Charbaji, A., Heidari-Bafroui, H., Anagnostopoulos, C., and Faghri, M., *A New Paper-Based Microfluidic Device for Improved Detection of Nitrate in Water*. Sensors (Basel), 2020. **21**(1). DOI: 10.3390/s21010102.
 32. Ferreira, F., Mesquita, R.B.R., and Rangel, A., *Novel microfluidic paper-based analytical devices (muPADs) for the determination of nitrate and nitrite in human saliva*. Talanta, 2020. **219**: pp. 121183. DOI: 10.1016/j.talanta.2020.121183.
 33. Pagnutti, M., Ryan, R.E., Cazenavette, G., Gold, M., Harlan, R., Leggett, E., and Pagnutti, J., *Laying the foundation to use Raspberry Pi 3 V2 camera module imagery for scientific and engineering purposes*. J. Electron. Imaging, 2017. **26**(1). DOI: 10.1117/1.Jei.26.1.013014.
 34. Zhang, J.X.J. and Hoshino, K., *Chapter 5 Optical transducers: Optical molecular sensing and spectroscopy*, in *Molecular Sensors and Nanodevices*. 2019. pp. 231-309. DOI: 10.1016/b978-0-12-814862-4.00005-3.

CHAPTER 6. CLINICAL RESULT EVALUATION

This chapter contains evaluations of the clinical results from the two journal publications listed below. This chapter also updates the results of all urine samples that have been collected and tested since those papers were published. Thus, the chapter has been updated to suit the harmonious structure of the thesis.

The journal article: Pham, A.T.T.; Tohl, D.; Wallace, A.; Hu, Q.; Li, J.; Reynolds, K.J.; Tang, Y. (2022). Developing a fluorescent sensing based portable medical open-platform - a case study for albuminuria measurement in chronic kidney disease screening and monitoring. Sensing and Bio-Sensing Research, 100504, <https://doi.org/10.1016/j.sbsr.2022.100504>

The journal article: Pham, A. T. T.; Tohl, D.; Hu, Q.; Li, J.; Reynolds, K.J.; Tang, Y. (2022). Portable colorimetric device with commercial microplates for quantitative detection of urine biomarkers: design, development, and clinical evaluation. Biosensors, 12, 723, <https://doi.org/10.3390/bios12090723>

6.1. Principle of the clinical evaluation

From the purpose of the research to develop portable devices to support CKD monitoring in less laboratory-dependent conditions, two devices were fabricated: an open platform for running a fluorescence measurement to detect albumin level and a colorimetry device using the colorimetry method to determine the concentration of creatinine in urine samples. Albumin and creatinine were chosen for the detection due to their contribution to the albumin-creatinine ratio (ACR), which is one of the golden keys in CKD monitoring in clinics [1, 2]. Previous chapters have confirmed the performance of both prototypes for fluorescence and colorimetry measurements in comparison with a commercial fluorescence spectrometer and microplate reader, respectively.

This chapter reports on the evaluation of the prototypes by comparing their performances on testing the urine samples of kidney disease patients with clinical measurements. All urine samples were collected from kidney related-disease patients being treated at the Flinders Medical Centre (FMC), South Australia under ethics approval from Southern Adelaide Local Health Network (SALHN) Human Research Ethics Committee with HREC reference number HREC/20/SAC/27 and SSA reference number LNR/20/SAC/21. The targets of detection were the concentrations of albumin and creatinine, and the calculated ACR values. According to the clinical procedure, the urine samples are expected to be tested as soon as possible after collection to guarantee the quality of the measurements [3, 4]. If the samples are tested in 24 hours, they should be kept at a cool temperature of 2–8 degrees Celsius or be kept frozen for longer waiting times before the desired

tests. However, due to the limited access to the hospital during the COVID pandemic, the urine samples were transported to another laboratory for testing with the proposed devices. Thus, there is a gap of a minimum one day to a maximum five days for the test results between the clinical and the researcher's laboratories. This should be taken into consideration when comparing the results. The desired outcome from the evaluation was that the prototypes were able to achieve results close those from clinical methods and would give the proposed CKD status close to the clinical indication.

6.2. Albumin results in real urine samples from patients having kidney-related diseases

6.2.1. Experiment setup

Due to the sampling conditions, only 88 urine samples were tested for albumin concentration from the set of patients' urine samples. The fluorescent probe TPE-4TA was used to quantitatively obtain albumin values in 88 patient urine samples. The results from the device were compared with the clinical results from SA Pathology, South Australia. For detailed information regarding sample collection, please refer to Section 6.5 "The supporting information". After collecting the patients' urine samples, the samples were diluted with DI water and divided into two cuvettes: one for blank measurement and the other for testing. The TPE-4TA [10 mg/L] was mixed well with the diluted urine samples in the testing cuvette, then both cuvettes were left to incubate for 30 minutes. The cuvettes were placed in the platform for the image capture and analysis. For the process on fluorescent images, please refer to Section 6.5 "The supporting information".

6.2.2. Result discussion

As shown in Figure 6.1(A), the developed platform shows a linear regression with the clinical evaluations through the set of patients' urine samples with the value R^2 of 78.74 %, where the fitting line of the data ($y = 0.99563x + 12.34$) is close to the identity line between the results obtained from the fluorescence platform and the clinical method. From Figure 6.1(A), the data shows more scattering along the increase of albumin concentration in the urine samples. When plotting the boundaries of 95 % confidence, most of the outliers gather at the high range of albumin concentrations over 2000 mg/L. From the numeric values of the albumin results in Figure 6.1(B), the albumin concentrations keep increasing from around 1700 mg/L up to about 6600 mg/L in the clinical reports but showing a fluctuation between 2000 mg/L and 4000 mg/L in the device's analysis. This indicates a significant mismatch between the device's results and the clinical measurements at the high ranges of albumin concentration. There are several potential factors causing this issue, and one of those can be considered as a system limitation, in that, the fluorescent signal of the high-albumin-level samples has exceeded the detection range of the Raspberry Pi camera, causing saturation in the optical images during the measurement. In detail, when digging into the red, green, and blue

intensities of the testing images, some samples with high albumin levels resulted in saturation in one or both of the green and blue values. For instance, in Figure 6.1(A), some specific samples have been circled and marked, such as S15, S17, S29, S31, S59, S65, S67, S75, S83 and S89. For these samples, their fluorescence images contain one or both green and blue components reaching the maximum optical value of 255, as shown in Figure 6.2. Also, another factor that could create the mismatch in the results is that the recognising reagent concentration was not high enough to bind with the albumin protein in the urine sample. The lack of recognising reagent concentration leads to the fact that the fluorescence emitted from the testing solution does not represent the whole albumin amount in the solution. This causes the estimated albumin level in those samples to be much lower than the ones from SA Pathology.

From those explanations, the evaluation of the developed device's performance on estimating albumin results on those samples will possibly be inaccurate. Therefore, the data set should be divided into smaller groups to have a clearer view on the comparison between the developed platform and the clinical measurement. In this step, the data set has been divided into 6 smaller groups of albumin concentrations: 0 – 30 mg/L; 30 – 300 mg/L; 300 – 1000 mg/L; 1000 – 2000 mg/L; 2000 – 3000 mg/L and over 3000 mg/L. When grouping and comparing the results, the group-matching ratio between the developed platform and the clinical method reaches 68.2 % (60 in 88 samples). Although that leaves 31.8 % (28 in 88 samples) of the results mismatched, this mostly happens with samples containing albumin levels above 1000 mg/L. The fluorescence platform has shown a linear relationship in the resulting urine albumin concentrations with clinical evaluation of those samples containing albumin level below 1000 mg/L.

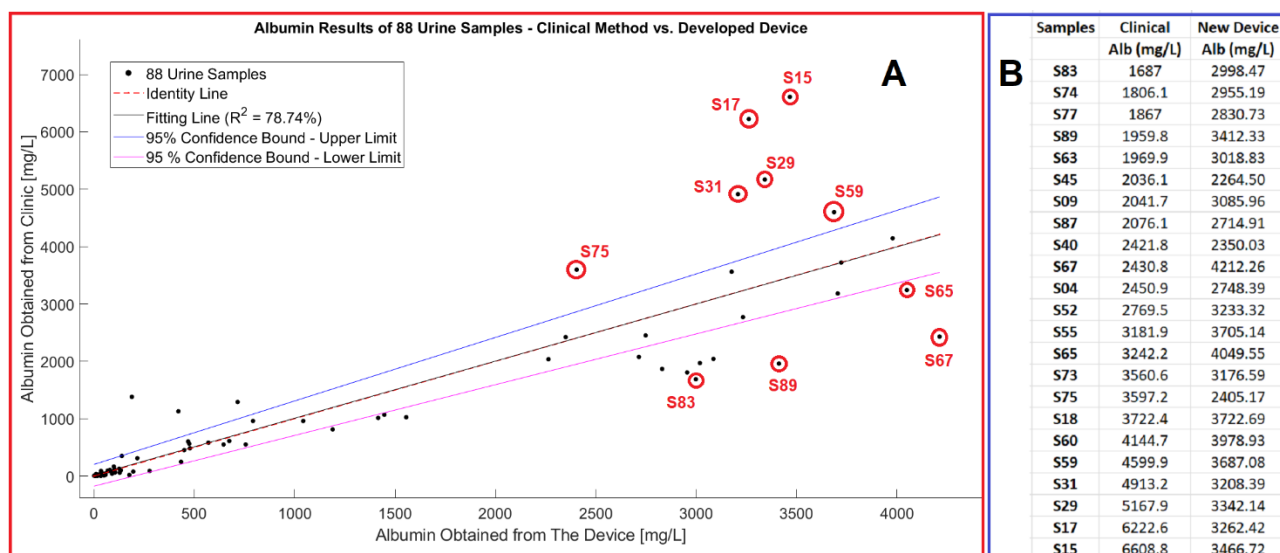


Figure 6.1. (A) The correlation between albumin concentration measured from the open platform and the clinical analysis from 88 urine samples of kidney patients. Some representative samples outside the 95% confidence boundary in high albumin range are circled. (B) The saturation of the developed platform when measuring the samples containing the high albumin concentrations

over 1600 mg/L, in that, those samples have one or both green and blue components exceeding 255.

A potential solution to deal with the samples causing a saturated fluorescent signal is to adjust the exposure time of the Raspberry Pi camera. This action will bring the captured intensity down to the detectable range of the camera. However, the extremely high albumin concentrations in those samples are out of the desired detecting range for monitoring CKD. Therefore, those samples will be excluded from the data analysis in this research. For further examination, 43 urine samples containing albumin level below 300 mg/L have been analysed. This 43-sample set was divided into two smaller groups of CKD Trace (0 – 30 mg/L) and CKD Indication (30 – 300 mg/L). In this comparison, the fluorescence platform categorised 37 of 43 samples into the similar groups in line with the clinical evaluation, achieving 86 % accuracy in identifying the CKD status of patients.

The results of the 43-sample set are illustrated in the scatterplot in Figure 6.3. As shown in the Figure 6.3, the fitting line ($y = 0.9918x + 5.619$) of the 43-sample set is parallel to the identity line, presenting the linear correlation between the platform and the clinical measurement. The results between the device and the clinical method are statistically analysed using the paired samples t-test that gives $t = -1.229$ with 42 degrees of freedom and $p = 0.226 > 0.05$ at the significant level. This indicates there is no significant difference between the albumin concentrations measured by the developed device and those from the clinical method. On average, the albumin concentration measured by the clinical method was 5.256 mg/L higher (95% Confidence Interval: 0.00, 10.53) than the concentrations estimated by the fluorescence device. Although there appear several variations between the fluorescence values of the platform and the clinical method, the statistical analysis has shown that the platform's performance has achieved a linear correlation with the clinical measurements. This has clarified the potential of the developed platform to work as a CKD monitoring tool to support users in out of laboratory-dependent conditions, such as home use and rural areas.

Sample	Test_R_raw	Test_G_raw	Test_B_raw
s077	63	255	142
s074	65	255	136
s083	67	255	141
s063	72	255	161
s004	75	255	152
s045	75	255	174
s009	76	255	155
s087	78	255	167
s102	78	255	171
s089	79	255	163
s073	85	255	198
s052	87	255	193
s055	91	255	255
s029	92	255	255
s040	93	255	255
s015	97	255	255
s031	97	255	255
s067	97	255	255
s075	98	255	255
s065	99	255	255
s018	100	255	255
s060	103	255	255
s059	106	255	255
s017	109	255	255

Figure 6.2. The saturated Red – Green – Blue components of the fluorescence images from the samples containing high albumin concentrations.

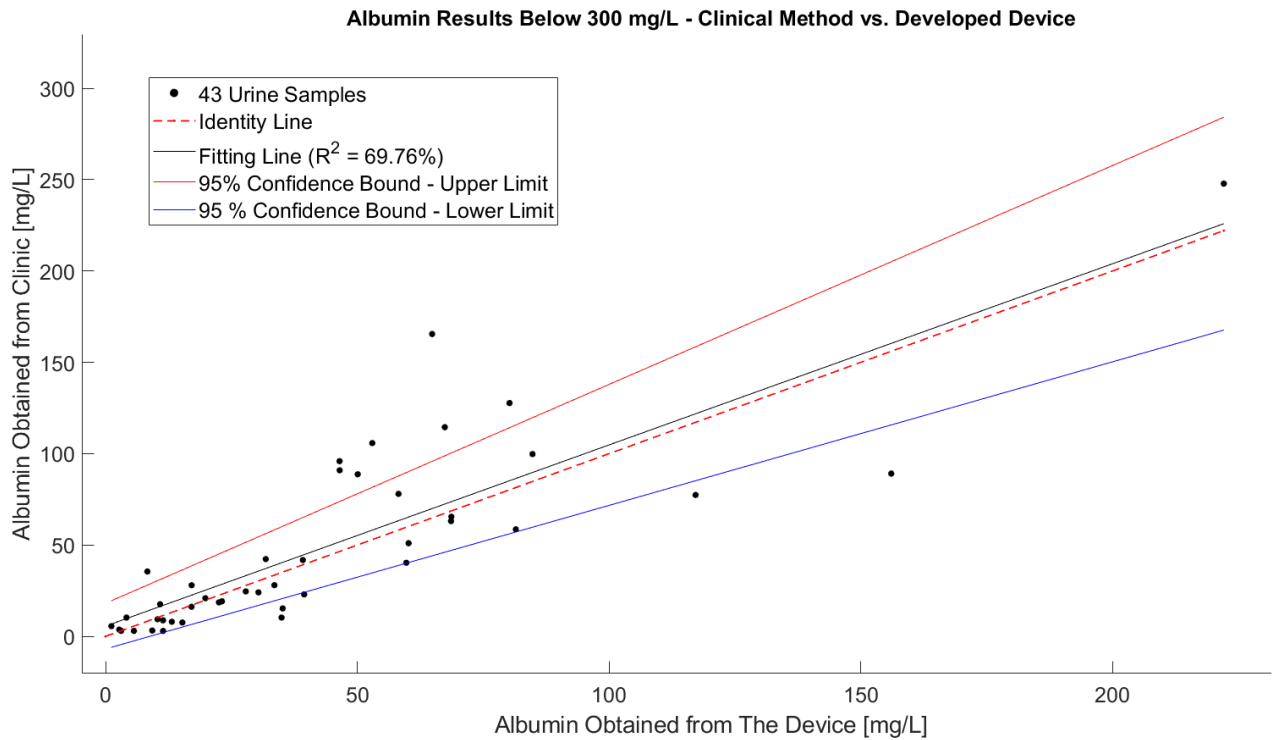


Figure 6.3. The correlation between the developed platform and the clinical method in examining 43 urine samples containing albumin concentrations below 300 mg/L.

6.2.3. Conclusion for the fluorescence platform to estimate albumin concentration in the urine sample

Using simple instruction and operation, the platform allows users to evaluate their kidney's function by running the test at home or in rural areas and discussing the results with clinical staff by sending the results online. This also reduces the need for regular hospital visits and the workload for both patients and clinical facilities. This is especially beneficial in during an infectious disease pandemic such as COVID-19 [5, 6].

The device can, in real-time, produce results that match clinical methods about 86 % of the time, indicating the CKD status of patients and satisfying the rapid and robust requirement of the POC device development. In addition, by using common electronics component, commercial consumables, and popular 3D printing technology for fabrication, the device has met the requirements of POC device development, such as affordability, portability, user friendly, and deliverable to end users. Moreover, the platform can be easily modified to suit the requirements of fluorescence measurement for different chemicals, biomarkers, or molecules, providing beneficial support for daily monitoring of various markers based on the fluorescence principle.

6.3. Creatinine measurement in real urine samples from patients having kidney-related diseases

6.3.1. Experiment setup

In the clinical evaluation stage, the performance of the device was evaluated with urine samples collected from patients at Flinders Medical Centre, South Australia, Australia. Following ethics approval, 88 urine samples from renal patients were analysed. The urine samples were tested using the device and compared with clinical values provided by SA Pathology. When using the proposed colorimetry device, the samples were prepared following the standard procedure from the commercial test reagent manual. The prepared testing solution was then placed in a 96 WM and left at room temperature for a 30 min incubation. Then, the 96 WM filled with colour testing solutions was placed in the device for imaging and analysis.

6.3.2. Result discussion

The results obtained from the device and from SA Pathology are shown in Figure 6.4. The results indicate a very consistent response between the values from the device when compared with the clinical values throughout the set of 88 urine samples from kidney-related disease patients. The results were statistically analysed using the paired samples t-test that gave $t = 1.2905$ with 87 degrees of freedom and $p = 0.2003 > 0.05$ at the significant level. This indicates there was no significant difference between the creatinine concentrations measured by the proposed device and those provided by SA Pathology. On average, the creatinine concentration measured by the proposed device was 0.566 mmol/L higher (95% Confidence Interval: 0.00, 1.13) than the concentrations provided by SA Pathology.

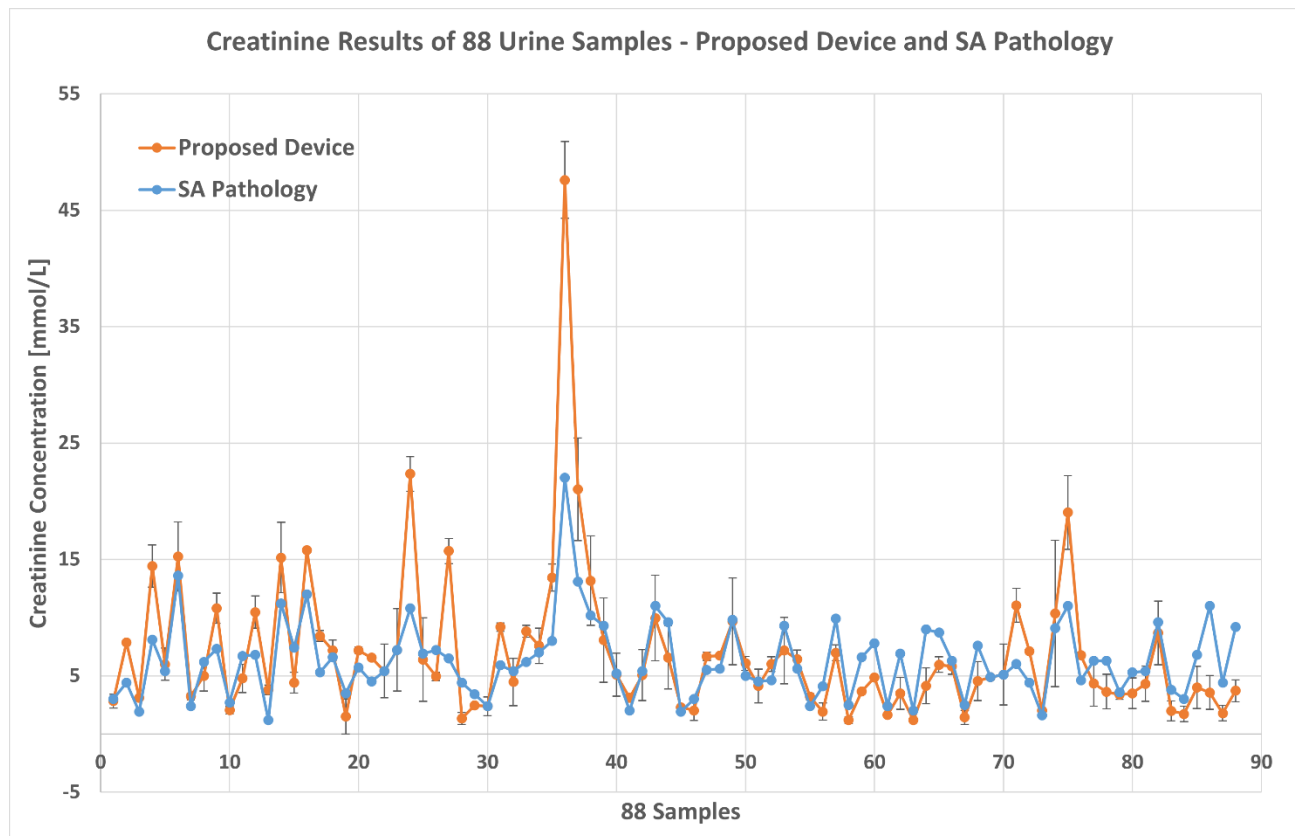


Figure 6.4. Comparison of creatinine concentrations measured by device and obtained from SA Pathology for 88 urine samples. The biggest variation is in sample 49 (the 36th data from the graph), which has a strong intensity in the background colour. Standard deviation is for two replicate samples.

From the information provided for the creatinine commercial kit (refer to the supporting information section 5.5 of chapter 5), the sensitivity value based on the mean optical density plus two standard deviations for a zero-concentration standard assayed 20 times is 0.0017 mmol/L. For comparison, a zero-concentration standard was assayed 17 times in the proposed device and returned a sensitivity value of 0.22 mmol/L. This value is higher than that specified by the commercial kit, but still acceptable given that the clinical creatinine values had a range of 1.2 mmol/L to 22 mmol/L.

There were a few samples for which the device indicated a higher value than the clinical value. One reason for the variation can be deduced from the operating procedure of the commercial test reagent. The creatinine test reagent provides the standards, which can be used to generate a fitting curve in a certain range of detection. The urine test samples are diluted to a certain level, which can be up to 100 times according to the test manual, before being mixed with the testing chemicals. From the colorimetry measuring principle, the purpose of diluting the urine sample is to bring the creatinine concentration of the sample into the detection range of the fitting curve. However,

for the device, the fitting curve of the creatinine test kit is an exponential curve, as shown in Figure 4.4 in the section on supporting information for colorimetry monitoring. If a creatinine concentration is in the high range of the fitting curve, a small variation in intensity can result in a large difference in the calculated concentrations. For example, as shown in Figure 6.5, the two pairs of C1-C2 and C3-C4 have a minor difference in intensity (0.01 unit), but the variation in the concentrations depends on the region of the fitting curve. For C3-C4, the variation in concentration is only 0.58 units, but for C1-C2, the variation is 4.04 units. The difference between these two pairs of examples is because the pair C1-C2 is located in the high range of detection, whilst the pair C3-C4 is located in the medium range of detection. This can explain some of the variations between the device and the clinical values. The potential solution for this is provided in the protocol of the commercial test reagent. If the urine samples contain a significantly high concentration of creatinine, the 10-time dilution used to obtain these results will not be enough and these samples require further dilution.

Another possible reason for the variation could come from the background colour of the urine samples. Colorimetry is a measuring method working on monitoring the change or the development of the colour from the testing solutions. In this research, the testing solutions were urine samples, which are comprised of multiple compounds and chemicals with complicated structures. If the urine sample has a very strong colour background, such as dark yellow or orange, it may add interference to the colour evaluation. To deal with this issue, further dilution of the urine sample can be a possible solution, as high dilution can reduce the background colour of the sample.

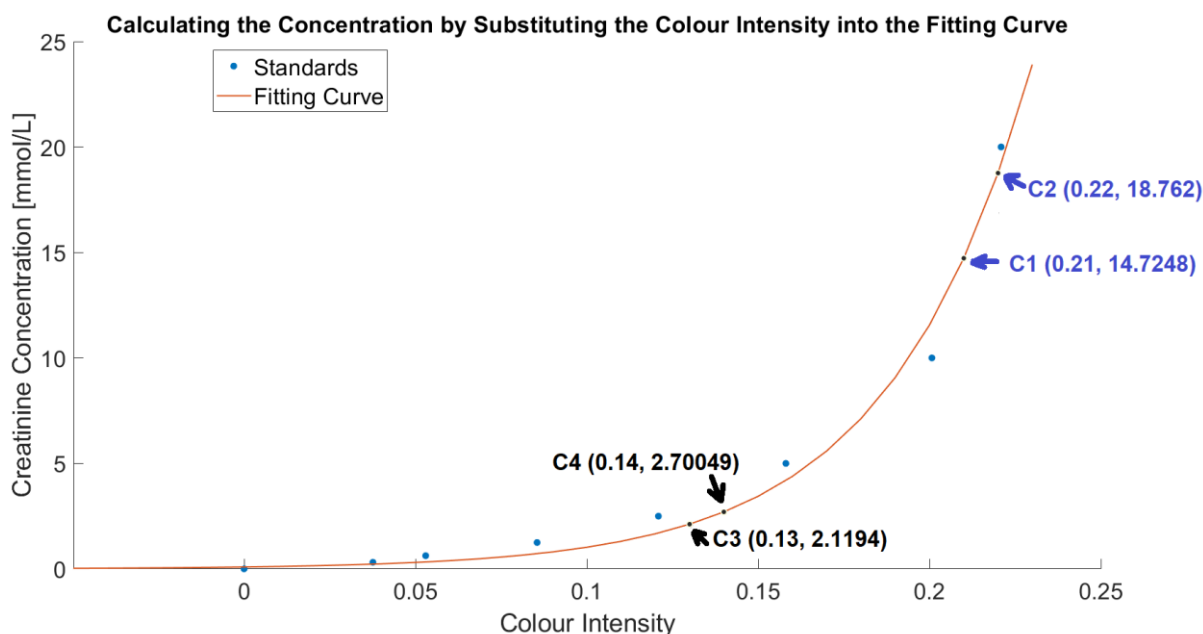


Figure 6.5. The effect of the exponential fitting curve in calculating the high concentration of creatinine in urine sample. Two data pairs (C1-C2 and C3-C4) have 0.01 unit difference in intensities, however, the variations in their concentration are 4.0372 and 0.581 units respectively due to the

high-range of concentration in the pair C1-C2 in comparison with the lower range of C3-C4.

6.3.3. Dilution Factor on Creatinine Results

To examine the effect of the dilution factor on the creatinine result, a urine sample (Sample 49) was diluted by multiple factors with distilled water, i.e., 10, 50, 100, 150, and 200 times. Two diluted samples with the same dilution factor were then tested with the device. Table 6.1 shows the original dilution factor of 10 times had a higher standard deviation (SD) when compared to the samples with stronger dilution factors of 50, 100, and 150. However, if the sample was diluted too much (with a dilution factor of 200), then it may fall below the lower limit of detection and the standard deviation will increase. To further evaluate this strategy, a group of six samples were processed to examine the impact of dilution-factor, as shown in Table 6.2. Each sample was diluted with distilled water with two samples for each level of 10, 50, 100, 150 and 200 times. In these cases, those samples having dilution ranges from 50 to 150 times provided fewer errors in creatinine calculation when compared with the other dilution values of 10 and 200 times. This confirmed that proper dilution can minimize the error in creatinine results between the proposed device and the clinical measurement. Therefore, increasing the dilution to a proper level can improve the accuracy of the concentration measurement for higher concentration samples. From the results of this research, the 50–150 fold dilutions are the ideal factors for urine samples of patients having kidney-related diseases.

Table 6.1. The effect of dilution factor on creatinine results with two samples measured for each dilution factor.

Dilution Factor	1st Sample	2nd Sample	Average	SD of Two Samples' Results
10	2.83	5.31	4.07	1.75
50	6.00	6.30	6.15	0.21
100	7.14	7.41	7.28	0.19
150	7.28	7.64	7.46	0.25
200	5.28	6.68	6.68	0.99

Table 6.2. 6 samples are examined in further-dilution strategy.

Sample	Dilution [Times]					Clinical Cre [mmol/L]	Optimal Error range [%]
	10	50	100	150	200		
1	3.50	5.52	5.96	5.22	4.77	5.3	1.53 – 12.41
2	4.31	3.95	4.83	5.47	4.92	5.4	1.36 – 26.88
3	8.68	12.10	10.73	9.86	8.20	9.6	2.69 – 26.01
4	4.00	6.39	6.59	6.94	5.89	6.8	2 – 6.04
5	1.78	3.84	5.54	8.35	4.97	3.47	12.84 – 24.81
6	3.71	8.66	9.49	7.17	5.05	9.2	3.2 – 22.08

6.3.4. Conclusion for the creatinine device to measure creatinine concentration in the urine sample

From the evaluation and the results, the device showed good performance when compared to the clinical values. Having simple instruction, affordable fabrication, and compact size, the device has the potential for use as a portable colorimetry reader for commercial test reagents with a microplate for rural and remote areas.

6.4. Albumin-Creatinine Ratio results obtained from the albumin and creatinine concentration measurements

6.4.1. Experiment setup

In the clinical evaluation for CKD monitoring, ACR is one of the golden keys to assess the status of CKD for patients [1, 2, 7]. In clinical settings, the ACR range for a healthy person is below 2.5 mg/mmol. The warning range for microalbuminuria is where ACR stays between 2.5 and 35 mg/mmol [1, 8]. Thus, the focus ranges of ACR in this research was below 35 mg/mmol. From the previous evaluation sections for albumin and creatinine measurements, the concentrations of those

two biomarkers were obtained and were used to calculate ACR values using the ACR formula [2]:

$$ACR [mg/mmol] = \frac{\text{Albumin concentration [mg/L]}}{\text{Creatinine concentration [mmol/L]}}$$

6.4.2. Result evaluation

The ACR is a result combining the albumin and creatinine concentrations. If one of these parameters is incorrect, the ACR result will possibly be inaccurate. From the result discussion in section 6.2, the fluorescence open platform encountered saturation in optical measurement for samples containing significantly high albumin levels. Only 43 urine samples with albumin concentration below 300 mg/L were processed to obtain the albumin estimation. Correspondingly, that threshold 300 mg/L of albumin level also results in a normal threshold of ACR values in clinical CKD monitoring, which is below 35 mg/mmol. Thus, this ACR evaluation will focus on these highlighted 43 samples. The ACR results of the 43-sample set between the developed devices and SA Pathology is illustrated in Figure 6.6. The results were statistically analysed using the paired samples t-test giving $t = 0.67$ with 42 degrees of freedom and $p = 0.5065 > 0.05$ at the significant level. This indicates there is no significant difference between the ACR values calculated by the proposed devices and those provided by SA Pathology. On average, the ACR values measured by the proposed device were 0.63 mg/mmol higher (95 % Confidence Interval: 0.00, 1.26) than the ACR values provided by SA Pathology.

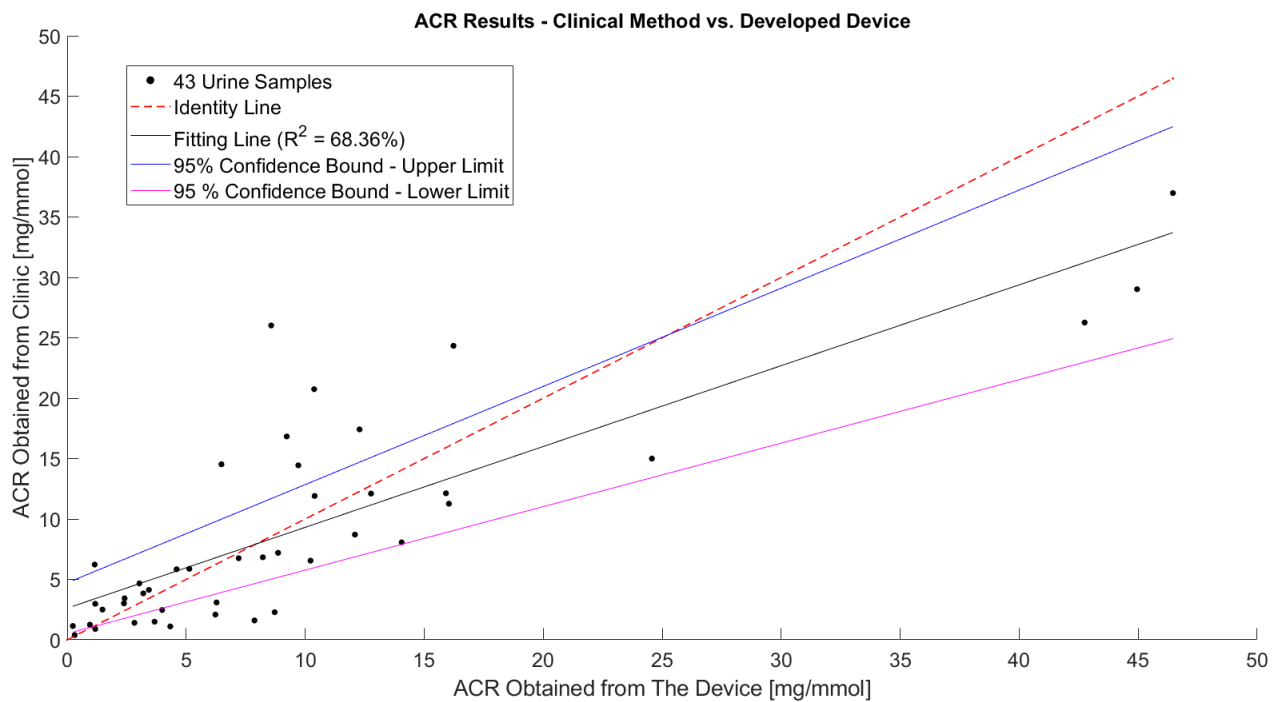


Figure 6.6. The correlation in ACR values between the developed devices and SA Pathology

when examining 43 urine samples containing albumin concentrations below 300 mg/L.

Although having a linear performance when compared with clinical measurement, the developed devices still show some noticeable variations in ACR results. Thus, the limits of agreement between the developed devices and the clinical method will be examined to evaluate the differences in performances between these two measuring methods. The ACR results from both techniques are visualized in the Bland Altman plot in Figure 6.7 [9]. The graph illustrates an agreement in ACR estimation between two techniques in the range of low values, where the mean of difference (mean = 0.6310 mg/mmol) is close to zero and most data gather around this mean value [9]. However, there exist outliers at some points, which cause 95 % of the difference in ACR results between the developed devices and the clinical measurement to vary from -11.5041 mg/mmol to 12.7662 mg/mmol. The data has a normal distribution around the mean, indicating that there are some random relative errors but the devices are free from any systematic errors. In fact, ACR values are calculated from albumin and creatinine concentrations, which have already had some variations during the measurements as introduced in previous studies. As the ACR value is the ratio of albumin to creatinine, any errors in either of those values is compounded in the ACR value, leading to the highlighted outliers lying far from the mean value, as shown in Figure 6.7. The potential solution for enhancing the limits of agreement is to filter out the outliers, which requires further research in the future work.

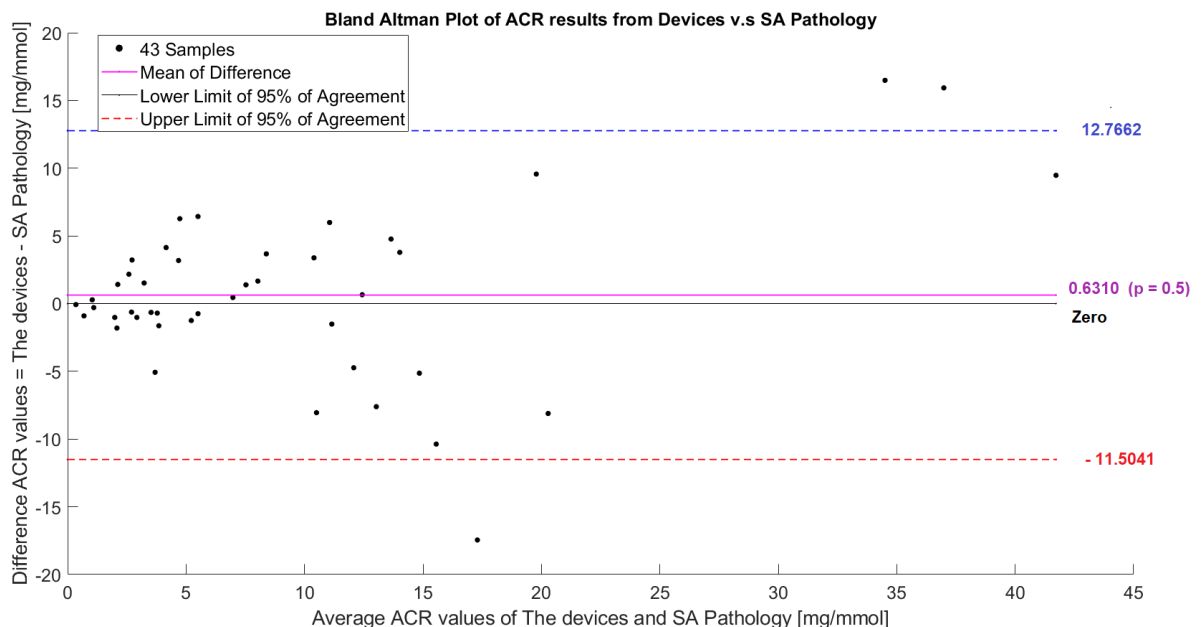


Figure 6.7. The Bland-Altman plot analysis to examine the limits of agreement between the developed devices and the clinical method in determining ACR values for CKD monitoring. The difference in ACR values between the proposed devices and SA Pathology is plotted against the

average values in the x-axis. The pink line represents the mean difference in ACR values between two techniques, and the dashed lines are ± 1.96 standard deviation (SD).

6.4.3. Conclusion for clinical evaluation on ACR measurement

From the above evaluation and discussion, although the developed devices have not achieved high agreement in the individual measurement of ACR values, they have confirmed their performance in comparison with the clinical method via the linear relationship in the ACR measurements. This has shown that the devices have the potential to support the CKD monitoring activities without the need for laboratory conditions thanks to their simple instruction, compact size, and affordable fabrication.

6.5. Supporting information for clinical evaluation

6.5.1. Clinical sample collection

The targets of the evaluation were 88 urine samples from patients having kidney relating diseases, such as CKD or membranous nephropathy. The samples from each patient were collected by clinical staff in Flinders Medical Centre (FMC), South Australia, Australia. In this clinical evaluation, the albumin and creatinine levels in the urine samples were measured by the developed devices and the results compared with the clinical results from SA Pathology. After being collected, the individual urine sample were divided into two sealed containers, one was sent to SA Pathology in less than one hour for clinical processing, the other was stored at 2–8 degrees Celsius before being transported to the Advanced Material Laboratory at Tonsley campus, Flinders University, where testing with the developed platforms was conducted. Due to limited access to the hospital during the COVID 19 pandemic, there was a gap of 1 to 5 days between the sample measurements conducted by SA Pathology and those due to the developed devices.

6.5.2. Analysis of the fluorescent images

The luminance of the fluorescent images is found by determining the intensity that corresponds to the highest frequency of occurrence in the image histogram. The luminance is calculated in this way to ensure that it is robust to different noise sources that may affect the image, such as sensor noise and artefacts like bubbles in the solution or marks on the cuvette. To obtain the luminance, first let X be the fluorescent image in RGB colour space where $X = \{R, G, B\}$, each RGB colour layer has an intensity range of $[0, L - 1]$ and for an 8-bit image $L = 256$.

Let H_R be the histogram of the red colour layer, R , of the RGB image.

$$H_R(R_k) = \frac{n_k}{n} \quad (\text{S6.1})$$

where $k = 0, 1, \dots, L - 1$ and n_k represents the number of times that the intensity level R_k appears in the image R and n is the total number of pixels in the image.

An alpha-trimmed mean filter [10] is used to remove any outliers and smooth the histogram H_R to produce the output, H_{RS} . The intensity value with the highest frequency of occurrence is represented by the largest peak in the histogram. To determine this intensity, first the maximum value in the smoothed histogram is found using a maximum operator as follows:

$$M = \operatorname{argmax}\{H_{RS}\}. \quad (\text{S6.2})$$

The intensity value that corresponds to the highest frequency of occurrence is then determined as follows:

$$I_R = q: (H_{RS}(q) = M). \quad (\text{S6.3})$$

Figure 6.8 shows the histogram calculated from a fluorescent image input with the alpha-trimmed mean filter output and the intensity value that corresponds to the highest frequency of occurrence in the smoothed histogram.

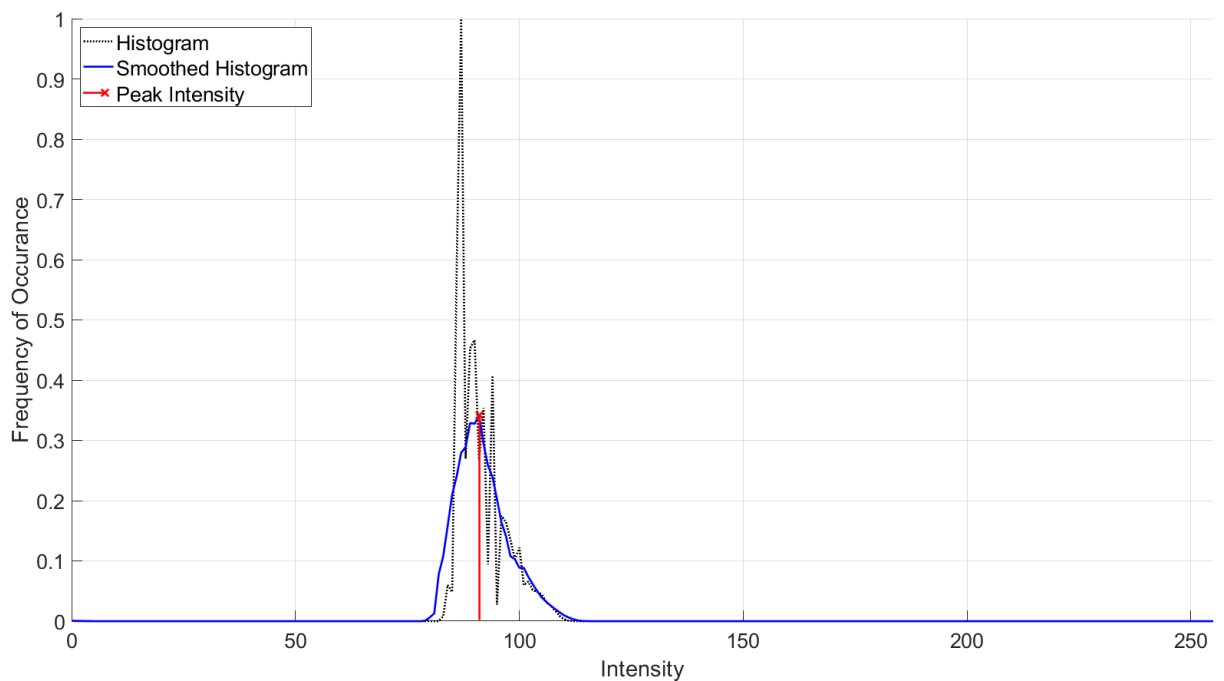


Figure 6.8. Determining the intensity value that corresponds to the highest frequency of occurrence.

This process is repeated for the green and blue colour layers to give the red, green, and blue intensity values, I_R , I_G and I_B , respectively, which represent the intensity with the highest frequency of occurrence for each colour layer. The three intensity values are then combined in a standard linear equation as follows [11]:

$$I = aI_R + bI_G + cI_B, \quad (\text{S6.4})$$

where a , b and c are coefficients used to control the ratio of each colour intensity in the sum. The three coefficients can then be determined based on the Raspberry Pi camera sensitivity shown in Figure 3.3 (presented in Chapter 3) at the wavelengths for the two fluorescent chemicals. The emission wavelength for TC426 is 550 nm, the Raspberry Pi camera sensitivity at 550 nm is 12 %, 90 %, and 14 % for the red, green, and blue channels, respectively. That results in the coefficient vales of $a = 0.11$, $b = 0.78$, and $c = 0.12$ and an intensity at 550 nm as follows:

$$I_{550} = 0.11I_R + 0.78I_G + 0.12I_B. \quad (\text{S6.5})$$

The emission wavelength for TPE4TA is 480 nm, the Raspberry Pi camera sensitivity at 485 nm is 7 %, 72 %, and 71 % for the red, green, and blue channels, respectively. That results in the coefficient vales of $a = 0.05$, $b = 0.48$, and $c = 0.47$ and an intensity at 485 nm as follows:

$$I_{485} = 0.05I_R + 0.48I_G + 0.47I_B. \quad (\text{S6.6})$$

Calculating the intensities from the three colour layers in this way allows the flexibility to alter the linear combination of the three intensity values appropriate to the emission wavelength of the fluorescence.

6.5.3. Clinical case study analysis

Human urine has an auto-fluorescence property that varies over time and from person-to-person [12, 13], this auto-fluorescence phenomenon adds a component of noise to the fluorescent measurement in the device. To measure the value of auto-fluorescence, a blank sample containing only the urine was used in the reference cuvette position and the urine sample with the chemical reagent was used in the test cuvette position. The auto-fluorescence value was then subtracted from the test sample fluorescence value to give then resulting intensity values used in Figure 6.1.

Reference

1. Vassalotti, J.A., Centor, R., Turner, B.J., Greer, R.C., Choi, M., and Sequist, T.D., *Practical Approach to Detection and Management of Chronic Kidney Disease for the Primary Care Clinician*. Am. J. Med., 2016. **129**(2): pp. 153-162. DOI: 10.1016/j.amjmed.2015.08.025.

2. Bikbov, B., et al., *Global, regional, and national burden of chronic kidney disease, 1990–2017: a systematic analysis for the Global Burden of Disease Study 2017*. Lancet, 2020. **395**(10225): pp. 709-733. DOI: 10.1016/s0140-6736(20)30045-3.
3. Albert, R., Stephen, J.S., Sheila, M.W., Douglas, B.A., Miguel, A., Donald, A.D., Max, R., and Barbara, A.S., *Urinalysis and Collection, Transportation, and Preservation of Urine Specimens; Approved Guideline—Second Edition*, in *NCCLS document GP16-A2*. 2009, National Committee for Clinical Laboratory, Standards: USA.
4. Tripathi, A., Sathua, K., Pachauri, V., and Flora, S.J.S., *Collection, storage, and transportation of samples for offsite analysis*, in *Handbook on Biological Warfare Preparedness*. 2020. pp. 133-149. DOI: 10.1016/b978-0-12-812026-2.00007-4.
5. De Kock, J.H., Latham, H.A., Leslie, S.J., Grindle, M., Munoz, S.A., Ellis, L., Polson, R., and O'Malley, C.M., *A rapid review of the impact of COVID-19 on the mental health of healthcare workers: implications for supporting psychological well-being*. BMC Public Health, 2021. **21**(1). DOI: 10.1186/s12889-020-10070-3.
6. Quigley, A.L., Stone, H., Nguyen, P.Y., Chughtai, A.A., and MacIntyre, C.R., *Estimating the burden of COVID-19 on the Australian healthcare workers and health system during the first six months of the pandemic*. Int J Nurs Stud, 2021. **114**. DOI: 10.1016/j.ijnurstu.2020.103811.
7. *Chronic Kidney Disease. Diagnosis and Treatment*, Editors. Yang, J. and He, W. 2020, Singapore: Springer Singapore.
8. Johnson, D.W., et al., *Chronic kidney disease and measurement of albuminuria or proteinuria: a position statement*. Med J Aust, 2012. **197**(4): pp. 224-225. DOI: 10.5694/mja11.11468.
9. Hoffman, J.I.E., *Linear Regression*, in *Biostatistics for Medical and Biomedical Practitioners*. 2015. pp. 451-500. DOI: 10.1016/b978-0-12-802387-7.00027-5.
10. Bednar, J. and Watt, T., *Alpha-trimmed means and their relationship to median filters*. IEEE Trans. Acoust., Speech Signal Process., 1984. **32**(1): pp. 145-153. DOI: 10.1109/TASSP.1984.1164279.
11. Gonzalez, R.C. and Woods, R.E., *Digital image processing*. Image Processing. 2008, New Jersey: Prentice Hall.
12. Steenbeke, M., De Bruyne, S., Van Aken, E., Glorieux, G., Van Biesen, W., Himpe, J., De Meester, G., Speeckaert, M., and Delanghe, J., *UV Fluorescence-Based Determination of Urinary Advanced Glycation End Products in Patients with Chronic Kidney Disease*.

Diagnostics (Basel), 2020. **10**(1). DOI: 10.3390/diagnostics10010034.

13. Zvarik, M., Martinicky, D., Hunakova, L., Lajdova, I., and Sikurova, L., *Fluorescence characteristics of human urine from normal individuals and ovarian cancer patients*. Neoplasma, 2013. **60**(5): pp. 533-537. DOI: 10.4149/neo_2013_069.

CHAPTER 7. CONCLUSION, DISCUSSION AND FUTURE DEVELOPMENT

7.1. Discussion and conclusion

Chronic kidney disease monitoring is still a highlighted matter in the modern society. Although many reports have been published with an emphasis on bio-probe development for optical based POC devices to monitor CKD, the scientific approach and pathway for designing the hardware of POC devices has not been well developed and illustrated to achieve suitable sensitivity, which has been claimed as the advantage of the reported bio-probe. In addition, the ability to monitor multiple biomarkers within a single device has not been demonstrated in previous reports. In this research, the aim of the thesis has been to design, optimise and fabricate the hardware of a portable medical device to support CKD monitoring. Two portable devices have been designed, developed, and their performance when monitoring albumin and creatinine concentrations in human urine samples has been shown. This research addresses several limitations from previous studies, which includes the lack of a detailed description of the scientific approach and pathway for designing and developing a POC device using the optical methods to achieve the suitable sensitivity in monitoring biomarker level in body fluid samples, the lack of solid evidence that the associated hardware is well designed and integrated with consumables and software for practical use, the evidence of developing the POC device for monitoring multiple biomarkers within a single device, and the evaluation of the reported devices through a clinical trial [1-20].

During the design and development of the device, the parameters which need to be considered and integrated in the POC hardware design and manufacture for facilitating effective and accurate urine albumin and creatinine monitoring have been fully investigated. These parameters include the stability and the uniformity of the excitation light source, the sensitivity of the optical output sensor, the integrated self-calibration process of device, reflected light from the excitation light source to the sensor, the communication between the user and the clinical staff to support the testing result evaluation, the simplicity of the measurement operation, which can be guided through a display component employed in the device, and the cost of the hardware fabrication. Previously, most reports have focused on describing a specific design, and not presenting a systematic design process, thus, those reports did not show the development process for a general POC optical device [2-4, 6, 10-13, 16, 17]. Unlike previous studies, which describe only one or a few parameters, a detailed presentation of the whole design and development processes has been shown to provide a clear view for future developers when choosing suitable components for POC device development. Moreover, the design flowchart presented in this thesis will help future developers identify which parameters are ready for the development, and which ones have been overlooked or require further investigation before making the desired POC device. This design process has been validated by the

two proposed devices which use different biomarker monitoring methods, but have both achieved linear correlations with the clinical measurements when measuring the target biomarker concentrations in 88 urine samples from patients with kidney related diseases.

This thesis has also validated the open platform design principle for multi-biomarker monitoring. By using a modular structure with the “plug-in and plug-out mechanism,” the devices are flexible and their electronic components can be easily modified to suit the requirements of different excitation light sources, various optical sensitivity, and background colour, which are all dependent on the target biomarker. While previous studies presented POC devices which focused on monitoring a specific biomarker [2, 4-6, 8, 10-12, 14, 17-20], or biomarkers with similar requirements in the optical measurement [1, 3, 7, 9, 13, 15, 16], the proposed fluorescence platform has performed the albumin-concentration measurements under different optical requirements by using the two AIE recognising probes of TPE-4TA and TC426. The TPE-4TA probe requires UV excitation light of 370 nm to produce fluorescence at around 470 nm, whilst the TC426 probe requires visible excitation light of 480 nm to produce fluorescence at 550 nm. Results based on the measurements of albumin concentrations in urine samples using the different recognising reagents of TPE-4TA and TC426 with a single device, after providing the simple hardware modification of the light sources, show that the proposed design overcomes the limitations of measuring biomarkers that require different optical conditions of previous studies [2, 4-6, 8, 10-12, 14, 17-20].

Moreover, from the literature review, although some previous reports presented the development of POC devices with a calibration process to calculate the level of the target biomarkers/chemicals, most studies lack the solid evidence of a method to provide repeatable of output signal measurements within a single device or between multiple devices [1-3, 5-9, 14, 16-20]. To address this limitation, this thesis explores the process for selecting a calibration sample and the process of developing the reference sample, which contributed to method for providing repeatable fluorescence measurements. These measurements were collected over the course of 10 months and the results confirmed the stability of the reference samples under the UV excitation light source of 370 nm. Furthermore, the reference samples also showed a stable relationship with respect to the fluorescence intensity of the tetraphenyl butadiene (TPB) calibration sample measured in a commercial spectrophotometer. In addition, with simple fabrication and an affordable price of 15 cents per sample, the development of this reference sample greatly contributes to the development of the fluorescence POC device for monitoring the concentration of biomarkers in body fluids.

Real urine samples from patients with kidney disease related illnesses were used to confirm the practical applications of the proposed devices and their results have shown a good correlation with those results obtained from SA Pathology. Based on the results from these 88 urine samples, although there is some variation between the proposed devices and clinical method, the developed fluorescence open platform showed about an 86% match to the clinical values when indicating the

CKD status of patients whose urine samples contain an albumin concentration below 300 mg/L, whilst the colorimetry device has shown consistency in estimating the creatinine level in those urine samples. These results have shown that the proposed devices can provide a point-of-care alternative to clinical instruments for monitoring CKD. Thus, when compared with previous studies from the literature review, which mostly operated with artificial samples or samples spiked with known concentrations of the target biomarkers/chemicals [1, 2, 5-10, 14, 17, 19, 20], the research in this thesis has furthered the development on optical testing devices to improve their performance in practical applications by testing with real urine samples obtained from 88 CKD patients.

By using common electronic components, commercial consumables and popular 3D printing technology for fabrication, the proposed devices have met the requirements of POC device development, that is, affordability, portability, user friendly and deliverable to end users. Moreover, these two platforms can be easily modified to suit the requirements of fluorescence and colorimetry measurements for different chemicals, biomarkers, or molecules, providing a beneficial support for daily monitoring of various markers based on these two methods of optical measurement. By combining all these criteria, the research has confirmed the potential of the developed devices to support users to evaluate their kidney's function by running the test at home or in rural areas and discussing results with the clinical staff by sending those results online. This also reduces the need for regular hospital visits and the workload for both patients and clinical facilities, especially in the pandemic of spreading diseases, such as COVID-19 [21, 22].

7.2. Contribution to the knowledge

This research has achieved the contributions in two features of the POC device development for biomarker monitoring:

(1) For optical measurement features

- Applying the referencing and calibration processes to minimize the errors in different measurements within the single device or among the reproduced devices. This principle has been reported by Dr. Tohl, myself and other colleagues in the journal publication of "Re-referencing and calibration for robust ratiometric light intensity measurement" in 2022 [23]. In that report, two reference samples were employed to account for variations between the two LED light sources of the device. By using the ratiometric method to define a relationship between the reference samples and the calibration sample, which has a reliable and stable fluorescent response, the fluorescence platform achieved an error below 2% between the expected and simulated measurements under variable LED light conditions [23].
- Designing and evaluating the fabrication of the reference samples, made from the pure Kinetix R246 epoxy resin in thin-cuvette shape. This epoxy resin is a common material on the market, with an affordable fabrication cost of about 0.15 AUD per reference sample. In

addition, the reference sample showed a linear relationship in fluorescence response when compared with the calibration standard from the commercial fluorescence spectrometer under the 370-nm UV excitation for over 10 months of testing.

(2) For hardware designing features

- This research has provided step-by-step instructions for developing portable devices, which perform the fluorescence and colorimetry measurements to monitor albumin and creatinine levels in a urine sample. This type of device requires a harmonious association between three components - the consumables, the hardware, and the software. This harmonious association is a key determinant of success or failure in portable medical device development.
- This research has shown the parameters which need to be considered and integrated in POC hardware design and manufacture to facilitate effective and accurate urine albumin and creatinine monitoring. These are the stability and the uniformity of the excitation light source, the sensitivity of the optical output sensor, the integrated self-calibration process of device, the reflection properties of the excitation light to the sensor, the communication between the user and clinical staff to support evaluation of the test results, the simplicity of device operation, which can be guided through on a display component employed in the device, and the cost of the hardware fabrication.
- Both developed devices have shown the ability to measure different solutions under the fluorescence and colorimetric principles for monitoring different biomarkers under various optical conditions. By using the modular structure with the “plug-in and plug-out mechanism,” the devices are flexible and can be simply modified to suit the requirements of different excitation light sources, various optical sensitivity and background colour, which are dependent on the target biomarkers.
- Both devices use 3D printing and common electronic components for fabrication, thus, they enable the accessibility of manufacturing in a developing country.
- Both devices use the raspberry pi, a single computer module, to locally analyse the optical images and provide the albumin and creatinine results in real time. In addition, the raspberry pi module is integrated with wire and wireless connection options to support users to communicate with clinical staff. This allows users to send their test results to the healthcare specialists for discussion of the appropriate therapy and enables the data to be held in storage for further analysis or used for the machine learning in the future. These features support users to perform the measurements to monitor their kidney's function at their own sites in a convenient time, reducing the need for regular hospital visits, the workload for both patients and clinical facilities and benefit users in rural areas.

7.3. Plans for the future work

In regards future work, several potential directions are listed below.

7.3.1. The over-ranged fluorescent intensity from urine samples containing albumin levels above 2000 mg/L

As discussed in the result evaluation section, the fluorescence open platform faces the issue of optical saturation of images from the raspberry pi camera when measuring the urine samples with an albumin level above 2000 mg/L. One potential solution for this is to adaptively adjust the camera exposure time to shift the over-range fluorescent intensity values below the saturation point of the camera. However, one consideration should be made for the relationship between the camera exposure time and the measured intensity values so the is that the low exposure time will provide the lower fluorescent intensities from the calibration and referencing samples. If so, other referencing and calibration samples should be considered to achieve the suitable fluorescent intensities for the calibration and referencing processes.

7.3.2. The lack of recognising reagent in high concentration albumin measurements

Another potential factor causing the variation in albumin measurement between the proposed platform and SA Pathology is the lack of recognising reagent in the testing solution. From the principle of the fluorescence measurement, the target of detection is the intensity of the fluorescence emitted from the testing solution under the 370-nm UV excitation. This fluorescent intensity is defined by the chemical bonding between the albumin protein molecules with the AIE molecules in the recognising reagent. If the albumin concentration is too high, it may be that the current [10 mg/L] AIE solution does not provide enough AIE molecules to bind with all of the albumin molecules, leading to a saturation point of fluorescence intensity in the proposed platform. The potential solution to deal with this issue is to increase the concentration of the AIE probe used to mix with the urine samples. The suitable concentrations of the AIE probe should be carefully considered, depending on the ranges of the albumin concentrations in the urine sample, to provide a reasonable fluorescent signal for image processing.

7.3.3. The effect of auto-fluorescence from the urine sample itself on the albumin measurement

During the fluorescence monitoring device development, the calibration and referencing processes has been applied to minimise the effect of the auto-fluorescence from the urine samples. However, a variation in albumin results between the estimated albumin of the developed fluorescence platform and the clinical measurement is still observed, as shown in Figure 6.1 and 6.3 of chapter 6. One of the potential factors causing this variation may be from the auto fluorescence

of the urine sample itself. To examine this issue, further investigation has been applied on the fluorescent images from 43 urine samples with an albumin concentration below 300 mg/L, shown in Figure 6.3. A calculation for the error in albumin between the two methods has been produced following the formula of $Error = \left| \frac{Device\ Result - Clinical\ Result}{Clinical\ Result} \right|$. When dividing these 43 samples into 5 ranges of error level: 0 – 20 %, 20 – 40 %, 40 – 60 %, 60 – 80 %, and over 80%, the potential cause of the variation can be considered in Figure 7.1. This figure shows the fluorescent image of both the blank and test samples of some highlighted data in the set of 43 samples in ascending order of the error. From the Figure 7.1, the blank images consist of the diluted urine samples excited by the 370 nm UV light and the test images consist of the diluted urine samples mixed with the TPE-4TA chemical excited by the 370 nm UV light. Currently, the intensity of the blank sample is subtracted from the intensity of the test sample before it is used to calculate the albumin concentration in the urine sample. From this process, the difference in fluorescent intensity between the blank and the test samples will be the essential factor affecting the albumin level results. For the results from the developed platform, in error range from 0 to 40%, the test image of sample S100 has a higher optical signal than the sample S48 does, but the calculated albumin levels are very similar of 80.228 mg/L and 81.475 mg/L, respectively. This is because of the variation of the fluorescence in their blank samples, in that, the blank sample of S100 also has a higher optical intensity than S48. This effect is also seen in sample S12, whilst the fluorescence intensity of the test sample of S12 is not far from that of S100, the remarkable difference between the fluorescence of the blank and test images gives the high albumin value of 222.077 mg/L for S12, which is about triple that of S100. However, these results vary from the clinical ones, in that, the clinical albumin concentrations are 247.8 mg/L, 127.7 mg/L and 58.6 mg/L for samples S12, S100 and S48, respectively. It appears that the lower the fluorescent intensity in the blank sample, the smaller the error is between the developed platform measurement and the clinical measurement.

Moreover, for results in error range of 40% to 80%, not only the does the fluorescent intensity of the blank sample affect the albumin calculation, but the colour of the fluorescence also contributes to the error of the results. In sample S02, S33 and S07 of the range 40% to 80%, while their test samples emit primarily green fluorescence, their blank samples show a range of colour from green to blue, which is different from the primarily green fluorescence of the blank samples S12, S100 and S48 in the previous error ranges. The larger the colour difference between the blank and the test sample, the higher error value in albumin measurement between the developed platform and the clinical value (S02 has a 41.2% error, S33 has a 51.4% error and S07 has a 75.1% error). In addition, the a blue fluorescence colour in the blank samples is more pronounced for urine samples with low albumin concentrations, as shown in Figure 7.1 for sample S47 (239.4% error) and S41 (280.7% error) in the error range over 80%. Urine is a complex body fluid, as described in section 6.5, containing various components which can emit fluorescence under the UV light of 370 nm. These components can emit fluorescence with red, green or blue colours, depending on the types and

amount of chemicals, protein, bacteria or blood in the urine sample. The auto-fluorescence is currently uncontrollable in this research, contributing to the variation of the albumin calculation between the developed platform and the clinical measurement. Therefore, minimizing the effect of autofluorescence of urine samples can help increase the accuracy of the proposed device, and there exists the requirement for further research to reduce this effect on the albumin calculation.

















$Error = \left \frac{Device - Clinic}{Clinic} \right $	0 – 20 %		21 – 40 %		41 – 60 %		61 – 80 %		81 – 100 %	
	Sample	S12	S100	S48	S02	S33	S07	S47	S41	
Clinical value	247.8	127.7	58.6	114.5	77.4	89.1	10.3	15.3		
Device value	222.077	80.228	81.475	67.373	117.174	156.032	34.956	35.183		
Blank										
Test										

Figure 7.1. The effect of auto-fluorescence on image processing of some highlighted samples. Not only the fluorescence intensity in the blank image affects the albumin calculation, but the colour of the fluorescence also contributes to the variation in albumin results between the developed platform and the clinical measurement.

7.3.4. The miss-matching in the creatinine results from the colorimetry device

As presented in chapter 5, the dilution factor plays an essential role in estimating the creatinine concentration from the urine samples. From the discussion of the dilution factor, the dilution ranges of 50 – 150 times are ideal to minimize the error of the creatinine measurement. However, the results presented in this thesis used a dilution factor of 10 times for the creatinine measurement. Despite this, the results from the developed device show a linear regression in creatinine concentrations when compared with the SA Pathology results. Thus, the strategy of applying the further dilution factors on the real urine samples will likely result in a higher accuracy for the creatinine results of the developed device.

7.3.5. The strategy for measuring ACR value on a single device

After designing and fabricating two devices to perform the fluorescence and colorimetry measurements, there exists the option to combine both devices into one platform, which can perform the measurements with both optical examining techniques. This combination will improve the feasibility of the POC device in monitoring CKD for patients in the less-laboratory conditions where the users only need to purchase and operate one device to obtain the ACR values. However, the background requirements for these two optical techniques are quite different in the excitation light source, the light paths, the testing solution containers, as well as the background colour for the measurements. Therefore, this will require some development to make this opinion practical.

Reference

1. Mudanyali, O., Dimitrov, S., Sikora, U., Padmanabhan, S., Navruz, I., and Ozcan, A., Integrated rapid-diagnostic-test reader platform on a cellphone. *Lab Chip*, 2012. 12(15): pp. 2678-2686. DOI: 10.1039/c2lc40235a.
2. Coskun, A.F., Nagia, R., Sadeghia, K., Phillips, S., and Ozcan, A., Albumin testing in urine using a smart-phone. *Lab Chip*, 2013. 13(21): pp. 4231-4238. DOI: 10.1039/c3lc50785h.
3. Wei, Q., Acuna, G., Kim, S., Vietz, C., Tseng, D., Chae, J., Shir, D., Luo, W., Tinnefeld, P., and Ozcan, A., Plasmonics enhanced smartphone fluorescence microscopy. *Sci Rep.*, 2017. 7(1): pp. 1-10. DOI: 10.1038/s41598-017-02395-8.
4. Zhang, C., Kim, J.P., Creer, M., Yang, J., and Liu, Z., A smartphone-based chloridometer for point-of-care diagnostics of cystic fibrosis. *Biosens Bioelectron.*, 2017. 97: pp. 164-168. DOI: 10.1016/j.bios.2017.05.048.
5. Paterson, A.S., Raja, B., Mandadi, V., Townsend, B., Lee, M., Buell, A., Vu, B., Brgoch, J., and Willson, R.C., A low-cost smartphone-based platform for highly sensitive point-of-care

- testing with persistent luminescent phosphors. *Lab Chip.*, 2017. 17(6): pp. 1051-1059. DOI: 10.1039/c6lc01167e.
6. Akraa, S., Pham Tran Tam, A., Shen, H., Tang, Y., Tang, B.Z., Li, J., and Walker, S., A smartphone-based point-of-care quantitative urinalysis device for chronic kidney disease patients. *J. Netw. Comput. Appl.*, 2018. 115: pp. 59-69. DOI: 10.1016/j.jnca.2018.04.012.
 7. Sekine, Y., et al., A fluorometric skin-interfaced microfluidic device and smartphone imaging module for: In situ quantitative analysis of sweat chemistry. *Lab Chip.*, 2018. 18(15): pp. 2178-2186. DOI: 10.1039/c8lc00530c.
 8. Alves, I.P. and Reis, N.M., Microfluidic smartphone quantitation of *Escherichia coli* in synthetic urine. *Biosens Bioelectron.*, 2019. 145: pp. 111624. DOI: 10.1016/j.bios.2019.111624.
 9. Huang, C., Ma, R., Luo, Y., Shi, G., Deng, J., and Zhou, T., Stimulus Response of TPE-TS@Eu/GMP ICPs: Toward Colorimetric Sensing of an Anthrax Biomarker with Double Ratiometric Fluorescence and Its Coffee Ring Test Kit for Point-of-Use Application. *Anal Chem.*, 2020. 92(19): pp. 12934-12942. DOI: 10.1021/acs.analchem.0c01570.
 10. Kathiravan, A., Khamrang, T., Dhenadhayalan, N., Lin, K.-C., Ramasubramanian, K., Jaccob, M., and Velusamy, M., Internet of Things-Enabled Aggregation-Induced Emission Probe for Cu²⁺ Ions: Comprehensive Investigations and Three-Dimensional Printed Portable Device Design. *ACS Omega*, 2020. 5(50): pp. 32761-32768. DOI: 10.1021/acsomega.0c05262.
 11. Wang, S., Zhao, X., Khimji, I., Akbas, R., Qiu, W., Edwards, D., Cramer, D.W., Ye, B., and Demirci, U., Integration of cell phone imaging with microchip ELISA to detect ovarian cancer HE4 biomarker in urine at the point-of-care. *Lab Chip*, 2011. 11(20): pp. 3411-3418. DOI: 10.1039/c1lc20479c.
 12. Shen, L., Hagen, J.A., and Papautsky, I., Point-of-care colorimetric detection with a smartphone. *Lab Chip*, 2012. 12(21): pp. 4240-4243. DOI: 10.1039/c2lc40741h.
 13. Oncescu, V., O'Dell, D., and Erickson, D., Smartphone based health accessory for colorimetric detection of biomarkers in sweat and saliva. *Lab Chip*, 2013. 13(16): pp. 3232-3238. DOI: 10.1039/c3lc50431j.
 14. Chen, A., Wang, R., Bever, C.R.S., Xing, S., Hammock, B.D., and Pan, T., Smartphone-interfaced lab-on-a-chip devices for field-deployable enzyme-linked immunosorbent assay. *Biomicrofluidics.*, 2014. 8(6): pp. 1-11. DOI: 10.1063/1.4901348.

15. Wang, R., Ongagna-Yhombi, S.Y., Lu, Z., Centeno-Tablante, E., Colt, S., Cao, X., Ren, Y., Cárdenas, W.B., Mehta, S., and Erickson, D., Rapid Diagnostic Platform for Colorimetric Differential Detection of Dengue and Chikungunya Viral Infections. *Anal Chem.*, 2019. 91(8): pp. 5415-5423. DOI: 10.1021/acs.analchem.9b00704.
16. Aydindogan, E., Ceylan, A.E., and Timur, S., Paper-based colorimetric spot test utilizing smartphone sensing for detection of biomarkers. *Talanta*, 2020. 208. DOI: 10.1016/j.talanta.2019.120446.
17. Kong, L., Gan, Y., Liang, T., Zhong, L., Pan, Y., Kirsanov, D., Legin, A., Wan, H., and Wang, P., A novel smartphone-based CD-spectrometer for high sensitive and cost-effective colorimetric detection of ascorbic acid. *Anal Chim Acta.*, 2020. 1093: pp. 150-159. DOI: 10.1016/j.aca.2019.09.071.
18. Wang, L.X., Fu, J.J., Zhou, Y., Chen, G., Fang, C., Lu, Z.S., and Yu, L., On-chip RT-LAMP and colorimetric detection of the prostate cancer 3 biomarker with an integrated thermal and imaging box. *Talanta*, 2020. 208. DOI: 10.1016/j.talanta.2019.120407.
19. Choi, C.K., Shaban, S.M., Moon, B.S., Pyun, D.G., and Kim, D.H., Smartphone-assisted point-of-care colorimetric biosensor for the detection of urea via pH-mediated AgNPs growth. *Anal Chim Acta*, 2021. 1170: pp. 338630. DOI: 10.1016/j.aca.2021.338630.
20. Lewińska, I., Speichert, M., Granica, M., and Tymecki, Ł., Colorimetric point-of-care paper-based sensors for urinary creatinine with smartphone readout. *Sens. Actuators B: Chem.*, 2021. 340. DOI: 10.1016/j.snb.2021.129915.
21. De Kock, J.H., Latham, H.A., Leslie, S.J., Grindle, M., Munoz, S.A., Ellis, L., Polson, R., and O'Malley, C.M., *A rapid review of the impact of COVID-19 on the mental health of healthcare workers: implications for supporting psychological well-being*. *BMC Public Health*, 2021. 21(1). DOI: 10.1186/s12889-020-10070-3.
22. Quigley, A.L., Stone, H., Nguyen, P.Y., Chughtai, A.A., and MacIntyre, C.R., *Estimating the burden of COVID-19 on the Australian healthcare workers and health system during the first six months of the pandemic*. *Int J Nurs Stud*, 2021. 114. DOI: 10.1016/j.ijnurstu.2020.103811.
23. Tohl, D., Teferra, M.N., Wallace, A., Pham, A.T.T., and Tang, Y., *Re-Referencing and Calibration for Robust Ratiometric Light Intensity Measurement*. *IEEE Trans. Instrum. Meas.*, 2022. 71: pp. 1-8. DOI: 10.1109/tim.2022.3194929.